Contribution of monocytes to immunopathology during influenza A virus infection

Suzanne Cole

St Edmund Hall

Nuffield Department of Clinical Medicine
University of Oxford



Submission for the degree of Doctor of Philosophy

Trinity Term 2014

Supervisor: Professor Ling-Pei Ho

Suzanne Cole
St Edmund Hall, University of Oxford
Thesis submitted for degree of Doctor of Philosophy, Trinity term 2014

Contribution of monocytes to immunopathology during influenza A virus infection

This thesis investigates the role of monocytes in mouse and human influenza A virus (IAV) infection and questions how they contribute to immunopathology. I first show in mice that Ly6C^{hi} monocytes are dominant immune cells in the lungs during severe IAV infection. Comparison of the gene expression profiles in lungs of severe or mild IAV infection revealed enrichment of genes related to monocyte recruitment in severe disease, which were more rapidly expressed than in mild infection. There was also less representation of M2 macrophage polarisation genes in lungs during severe disease.

In human IAV infection, inflammatory monocytes and neutrophilic MDSCs were higher in fresh blood samples in severe compared to mild disease; but only monocyte frequency was specific to IAV infection. There were less IL-10 producing monocytes and more IL-6^{+}TNFα^{-} producing monocytes in severe compared to mild infection, and HLA-DR was markedly reduced on these monocytes. Increase in monocytes, but not neutrophilic MDSC, was sustained throughout infection and into recovery. Frequency of monocytes correlated with differentiation states of CD8^{+} T cells, and there was a negative association between iNKT cells and inflammatory monocytes in blood.

Focusing on the interaction between iNKT cells and monocytes, I questioned if monocyte number and function were regulated by iNKT cells. Using iNKT deficient mice (Jα18$^{-/-}$) and deriving monocytes from blood and lungs following IAV infection and comparing to wild-type mice, I showed that iNKT cells influenced diverse monocyte characteristics including apoptosis, M1/M2 polarisation and inflammasome activation. Induction of monocyte apoptosis by activated iNKT cells was investigated *in vitro* as a possible mechanism by which activated iNKT cells controlled monocyte numbers.

This thesis established the role of monocytes in IAV immunopathology and provides a rationale for further studies in amelioration of monocyte number in severe IAV infection.

Acknowledgements

I would firstly like to thank my supervisor, Professor Ling-Pei Ho, for her encouragement and belief, and for constantly pushing me to stay focussed and reach my potential. I would also like to thank the Nuffield Department of Medicine and Medical Research Council for funding my DPhil research and making my studies possible.

I would like to thank current and past members of the Ho group – Anjali, Yvonne, Adel, Hong, Sharon, Laura, Wai-Ling and Kambez for their friendship and company, both in and out of the lab, over the past 4 years. Also to Beth, Rosie and Alba for being great housemates and friends along the way, as well as other friends from Teddy Hall and OUWLRC.

I would also like to thank Dr Jake Dunning and other MOSAIC investigators, Dr Tim Powell, Dr Persephone Borrow, Steve Taylor, Karene Argoud and all the blood donors for contributions and helpful discussions relating to this work, as well as Professor Sir Andrew McMichael and Professor Eddy Liew for enthusiastic, enjoyable and helpful discussions in my final viva examination.

Finally, I am extremely grateful to my family – Mum, Dad, Katherin and Christo for always being there for me, having confidence in my abilities, and being an incredible source of love. And Bodo, for the patience, encouragement and belief in me that far exceeded my own.

Publications arising from this thesis

Cole, S. L., K. H. Benam, A. J. McMichael, and L. P. Ho. 2014. Involvement of the 4-1BB/4-1BBL pathway in control of monocyte numbers by invariant NKT cells. *J Immunol* 192: 3898-3907.

Kok, W. L., L. Denney, K. Benam, **S. Cole**, C. Clelland, A. J. McMichael, and L.P. Ho. 2012. Invariant NKT cells reduce accumulation of inflammatory monocytes in the lungs and decrease immune-pathology during severe influenza A virus infection. *Journal of Leukocyte Biology* 91: 357-368.

Other related publications

Wegmann, F., K. H. Gartlan, A. M. Harandi, S. A. Brinckmann, M. Coccia, W. R. Hillson, W. L. Kok, **S. Cole**, L. P. Ho, T. Lambe, M. Puthia, C. Svanborg, E. M. Scherer, G. Krashias, A. Williams, J. N. Blattman, P. D. Greenberg, R. A. Flavell, A. E. Moghaddam, N. C. Sheppard, and Q. J. Sattentau. 2012. Polyethyleneimine is a potent mucosal adjuvant for viral glycoprotein antigens. *Nat Biotechnol* 30: 883-888.

Denney, L., W. L. Kok, **S. L. Cole**, S. Sanderson, A. J. McMichael, and L. P. Ho. 2012. Activation of invariant NKT cells in early phase of experimental autoimmune encephalomyelitis results in differentiation of Ly6C^{hi} inflammatory monocyte to M2 macrophages and improved outcome. *J Immunol* 189: 551-557.

Armitage, A. E., L. A. Eddowes, U. Gileadi, **S. Cole**, N. Spottiswoode, T. A. Selvakumar, L.-P. Ho, A. R. Townsend, and H. Drakesmith. 2011. Hepcidin regulation by innate immune and infectious stimuli. *Blood* 118: 4129-4139.

Contents

Abstract i

Acknowledgements ii

Publications arising from this thesis iii

List of figures x

List of tables xiv

List of abbreviations xv

Chapter 1: Introduction 1

1.1 Influenza A virus 1

1.1.1 Epidemiology & antigenicity 1

1.1.2 Virus structure 5

1.1.3 Virus replication 6

1.1.4 Pandemic H1N1 2009 virus properties 11

1.1.5 Determinants of pathogenicity in IAV infection 13

1.1.5.1 Susceptibility of the host 14

1.1.5.2 Virus factors in pathogenicity 15

1.1.6 Immune response to IAV infection 18

1.1.6.1 Adaptive immune response to IAV 18

1.1.6.2 Innate immune response to IAV 20

1.2 Monocytes 24

1.2.1 Background 24

1.2.2 Monocyte development and function 25

1.2.3 Monocyte differentiation 28

1.2.4 Monocyte response to inflammation 28

1.2.5 Fates of recruited monocytes 30

1.2.6 Monocytes in IAV infection 33

1.3 Myeloid-derived suppressor cells (MDSC) 35

1.3.1 MDSC origin and subsets 35

1.3.2 MDSC suppressive activity 36

1.3.3 MDSCs in disease settings 37

1.4 Invariant NKT cells **39**
1.4.1 iNKT cell biology and phenotype 39
1.4.2 iNKT cell development 40
1.4.3 iNKT cell activation 42
1.4.4 iNKT cell functions 45
1.4.5 iNKT cell interaction with APCs 46
1.4.6 iNKT cells in IAV infection 50
1.5 Project aims **52**

Chapter 2: Materials and Methods 53

2.1 Laboratory methods **53**
2.1.1 Cell culture and media 53
2.1.2 Isolation of human peripheral blood mononuclear cells (PBMCs) 53
2.1.3 Whole blood lysis 53
2.1.4 Cryopreservation and thawing of PBMCs 54
2.1.5 Magnetic isolation of cells using MACS beads 54
2.1.6 Flow cytometry 55
2.1.7 FACS sorting 58
2.1.8 iNKT cell clone 58
2.1.9 Monocyte-iNKT co-cultures 59
2.1.10 iNKT cell proliferation assay 59
2.1.11 Transwell experiments 60
2.1.12 *In vitro* IAV infection of monocytes 60
2.1.13 Enzyme-linked immunosorbent assay (ELISA) 61
2.1.14 Multiplex cytokine analysis 61
2.1.15 IFNγ Enzyme-Linked Immunosorbent Spot Assay (ELISpot) 62
2.1.16 Mixed leukocyte reaction (MLR) 63
2.1.17 HLA typing 63
2.1.18 RNA extractions 64
2.1.19 Agilent Bioanalyser 65
2.1.20 Gene expression profiling 65
2.1.20.1 Illumina Microarray 65
2.1.20.2 Affymetrix microarray 66
2.1.21 Interpretation of gene expression profiles 67

2.2 Human studies **68**
2.2.1 Patients and participants 68
2.2.2 Sample processing 69
2.3 Mouse studies **69**
2.3.1 Mouse strains 69
2.3.2 IAV inoculation 70
2.3.3 Preparation of cells from blood, BAL and bone marrow 70
2.3.4 iNKT cell adoptive transfer 71
2.3.5 Lung tissue digestion 72
2.3.6 αGC-loaded CD1d dimer 72
2.4 Statistics **73**
Chapter 3: Monocytes as dominant immune correlates to severe outcome in mouse influenza A virus infection **74**
3.1 Introduction **74**
3.2 Aims **75**
3.3 Methods **76**
3.3.1 Mouse IAV infection 76
3.3.2 Microarray analysis 77
3.4 Results **78**
3.4.1 Weight loss and mortality following X179A or H5N1 infection 78
3.4.2 Microarray quality control 79
3.4.3 Similarities in gene expression on day 3 and day 5 in lungs from H5N1 and X179A infected mice 82
3.4.4 Inflammatory genes increase more rapidly in lungs of H5N1 than X179A infected mice 83
3.4.5 Monocyte-associated cytokines and chemokines are higher in severe infection 93
3.4.6 Cellular immune changes following severe or mild IAV infection 97
3.5 Discussion **101**
3.6 Conclusions **109**

Chapter 4: Myeloid cell profile during acute influenza infection in humans 110

4.1 Introduction 110

4.2 Aims 112

4.3 Methods 112

4.3.1 Patient samples 112

4.3.2 Sample processing 114

4.3.3 Flow cytometry analysis and gating strategy for myeloid cells 116

4.4 Results 119

4.4.1 Neutrophilic MDSC and monocytes dominate cellular immune profile in blood during severe acute IAV infection 119

4.4.2 Differences in neutrophilic MDSC and monocytes post-freezing 126

4.4.3 Phenotypic and functional characterisation of monocytes 128

4.4.4 Monocyte frequency at different stages of disease 141

4.5 Discussion 145

4.6 Conclusions 153

Chapter 5: T cell response to influenza A virus in relation to high monocyte numbers 154

5.1 Introduction 154

5.2 Aim 155

5.3 Methods 156

5.3.1 Patient samples 156

5.3.2 Sample processing 156

5.3.3 Flow cytometry analysis and gating strategy of lymphocytes 156

5.4 Results 158

5.4.1 pH1N1-specific T cell response is higher in severe disease 158

5.4.2 Reduced $CD8^+$ T cell differentiation in severe disease is associated with high monocyte frequency 167

5.4.3 iNKT cells are lowest in pH1N1 patients with high $CD14^+CD16^+$ inflammatory monocytes 170

5.4.4 Magnitude of IAV-specific T cell responses, but not T cell frequency, increases with time from infection 173

5.5 Discussion 177

5.6 Conclusions 182

Chapter 6: The role of iNKT cells in regulating monocyte number and function during influenza A virus infection 183

6.1 Introduction 183

6.2 Aims 184

6.3 Methods 185

6.3.1 Mouse infection and sample preparation 185

6.3.2 Microarray analysis 186

6.4 Results 187

6.4.1 Monocyte frequency is higher in the lungs of iNKT deficient mice compared to wild-type 187

6.4.2 Phenotypic and functional profile of monocytes in wild-type and iNKT deficient mice following IAV infection 189

6.4.3 Microarray QC 192

6.4.4 Gene expression of monocytes from iNKT-deficient mice compared to wild-type is more variable in lungs than blood during IAV infection 194

6.4.5 Inflammatory processes are upregulated in monocytes from iNKT deficient mice compared to wild-type 196

6.4.7 Functional analysis of monocyte gene expression profiles 199

6.4.8 Characterisation of monocyte apoptosis 207

6.4.9 Adoptive transfer of iNKT cells to iNKT deficient mice reduces BAL monocytes 209

6.5 Discussion 210

6.6 Conclusions 215

Chapter 7: iNKT cells and apoptosis of human monocytes 216

7.1 Introduction 216

7.2 Aims 217

7.3 Methods 217

7.4 Results 219

7.4.1 iNKT-monocyte co-culture results in bi-directional activation 219

7.4.2 Activated iNKT cells induce monocyte apoptosis 222

7.4.3 Monocyte apoptosis does not involve TNFα 229

7.4.4 Expression of TNF receptor superfamily members in iNKT-monocyte co-cultures 231

7.4.5 4-1BB/4-1BBL co-stimulatory pathway maintains monocyte survival and iNKT cell proliferation 233

7.5 Discussion 236

7.6 Conclusions 241

Chapter 8: Final discussion and future directions 242

8.1 Main findings 242

8.2 Future work 247

8.3 Final conclusions 250

Appendix 1: ImmGen RNA extraction protocol 251

Appendix 2: GSE accession details for GSEA analysis 252

Appendix 3: Descriptions of differentially regulated genes in H5N1 and X179A infection 253

Appendix 4: Differentially regulated genes in Jα18$^{-/-}$ monocytes 254

References 255

List of figures

Figure 1.1	Structure of an influenza A virion	6
Figure 1.2	Influenza A virus life cycle	8
Figure 1.3	Lineage of the 2009 H1N1 pandemic virus	12
Figure 1.4	Monocyte differentiation pathway in mice	26
Figure 1.5	Activation of iNKT cells	43
Figure 1.6	Co-stimulatory and co-inhibitory interactions between iNKT cells and APCs	49
Figure 3.1	Weight loss and mortality of mice infected with mild or severe IAV	79
Figure 3.2	RMA-normalised microarray signal intensities from IAV infected mouse lungs	81
Figure 3.3	Common and unique genes upregulated in severe and mild IAV infection	83
Figure 3.4	Heat maps of immune response genes in severe and mild IAV infection	86
Figure 3.5	Kinetics of genes upregulated in both mild and severe IAV infection	88
Figure 3.6	Kinetics of genes upregulated only in severe IAV infection	90
Figure 3.7	Gene Set Enrichment Analysis of biological pathways enriched on day 3 or day 5 of IAV infection	92
Figure 3.8	Upregulation of monocyte-attracting chemokines in lungs is greater during severe than mild infection	93
Figure 3.9	Enrichment of inflammatory monocyte signature on day 3 of severe and mild infection	95
Figure 3.10	Enrichment of both inflammatory and regulatory monocyte signatures on day 5 of mild infection	96
Figure 3.11	Weight loss of X179A, H5N1, PR8 and uninfected mice over 3 days	97
Figure 3.12	Cellular immune change in BAL and blood during mild and severe infection	98
Figure 3.13	Early monocyte kinetics during severe IAV infection	99
Figure 3.14	Inflammatory M1 monocyte polarisation in severe IAV infection	101
Figure 4.1	MLR assay outline	116

Figure 4.2	Flow cytometry gating of myeloid cell populations	117
Figure 4.3	Flow cytometry of myeloid cell size and granularity	118
Figure 4.4	Altered immune cell profile in pH1N1 patients relative to ILI	119
Figure 4.5	High neutrophilic cells in PBMC samples during severe disease	121
Figure 4.6	Enrichment of neutrophilic MDSCs in PBMC samples compared to whole blood	122
Figure 4.7	High monocyte frequency is specific to severe IAV infection	124
Figure 4.8	Suppressive capacity of MDSCs in pH1N1 patients	125
Figure 4.9	Loss of neutrophilic cells from cryopreserved PBMC samples.	126
Figure 4.10	Changes in monocyte subsets from cryopreserved PBMC samples	127
Figure 4.11	Monocyte CD163 expression is increased in steroid-treated pH1N1 patients	129
Figure 4.12	Monocyte CCR7 expression is highest in pH1N1 patients	130
Figure 4.13	Monocyte HLA-DR expression is reduced in severe pH1N1 infection	132
Figure 4.14	Monocyte CD62L expression is lowest in pH1N1 subjects	133
Figure 4.15	IL-10 production by monocytes is reduced in severe pH1N1 infection	135
Figure 4.16	MCP-1 production by monocytes is lowest in steroid-treated pH1N1 subjects	136
Figure 4.17	Total IL-6 and TNFα production by monocytes is not altered in pH1N1 infection	137
Figure 4.18	IL-6^{+}TNFα^{-} producing monocytes are increased in severe pH1N1 infection	138
Figure 4.19	Cytokine levels in culture supernatant	140
Figure 4.20	Monocyte frequency correlates with days from first symptoms	142
Figure 4.21	Neutrophil frequency does not correlate with days from first symptoms	143
Figure 4.22	Monocytes remain high in convalescent samples	145
Figure 5.1	Flow cytometry gating of lymphocytes	157
Figure 5.2	Identification of effector and IAV-specific CD8^{+} T cells	158
Figure 5.3	T cell frequency and subsets during IAV infection	160
Figure 5.4	PD-1 expression is increased on CD4^{+} T cells during IAV infection	161

Figure 5.5	Identification of IAV-specific T cells in blood during pH1N1 infection	162
Figure 5.6	No association of IAV-specific T cells with monocyte frequency	163
Figure 5.7	IAV-specific IFNγ T cell responses are highest in severely infected pH1N1 infected patients	165
Figure 5.8	IAV-specific IFNγ T cell responses are low in ILI patients	166
Figure 5.9	Reduced $CD8^+$ T cell differentiation in severe pH1N1 infection	168
Figure 5.10	Reduced $CD8^+$ T cell differentiation correlates with high monocyte frequency	169
Figure 5.11	$CD4^+$ T cell differentiation in pH1N1 infection does not differ from healthy controls	170
Figure 5.12	Invariant NKT cells are low in IAV infection	171
Figure 5.13	Association between low iNKT cells and high $CD14^+CD16^+$ inflammatory monocytes	172
Figure 5.14	IAV-specific T cell responses correlate with symptom duration	174
Figure 5.15	T cell subsets in convalescent samples	176
Figure 5.16	Heightened IAV-specific IFNγ responses in convalescent samples	177
Figure 6.1	Flow cytometry gating strategy for analysis of mouse monocytes	186
Figure 6.2	Monocyte frequency in wild-type and iNKT deficient mice following IAV infection	188
Figure 6.3	iNKT deficient mice lose weight more rapidly than wild-type mice	189
Figure 6.4	Monocyte phenotype and function are altered upon PR8 infection but show little change between wild-type and iNKT deficient mice in blood	190
Figure 6.5	Monocyte phenotype in the lungs in wild-type and $Ja18^{-/-}$ mice	191
Figure 6.6	Microarray quality control	193
Figure 6.7	Unbiased clustering of $Ly6C^{hi}$ monocytes from wild-type and $Ja18^{-/-}$ mice	194
Figure 6.8	Number of differentially expressed genes in $Jα18^{-/-}$ mice between monocytes from blood and BAL	196
Figure 6.9	Enrichment of influenza virus life cycle in monocytes from wild-type mice	201
Figure 6.10	Enrichment of apoptosis induction in monocytes from wild-type mice	202

Figure 6.11	Enrichment of inflammasome activation in monocytes from iNKT deficient mice	203
Figure 6.12	M1 polarisation in monocytes from IAV infected iNKT deficient mice	204
Figure 6.13	M2 polarisation in monocytes from IAV infected wild-type mice	205
Figure 6.14	Enrichment of genes upregulated specifically to severe IAV in monocytes from iNKT deficient mice	206
Figure 6.15	Early monocyte apoptosis is reduced in the blood of IAV-infected iNKT deficient mice	208
Figure 6.16	Adoptive transfer of iNKT cells to iNKT deficient mice reduces BAL monocyte numbers	209
Figure 7.1	Gating strategy for monocyte identification in co-cultures	218
Figure 7.2	Cytokine production and cytotoxicity of αGC activated iNKT clones	220
Figure 7.3	Cytokine production by monocytes in αGC activated co-cultures	222
Figure 7.4	Monocyte apoptosis is induced following iNKT cell activation	223
Figure 7.5	Monocyte apoptosis is not induced by activated $CD8^+$ or NK cells	224
Figure 7.6	IL12/IL18 activate iNKT cells to secrete IFNγ but not to cause monocyte apoptosis	226
Figure 7.7	CD1d is partially involved in inducing monocyte apoptosis	227
Figure 7.8	Soluble factors induce monocyte apoptosis	228
Figure 7.9	Monocyte apoptosis is not caused by TNFα	230
Figure 7.10	Expression of co-stimulatory molecules on iNKT clones	232
Figure 7.11	Expression of co-stimulatory molecules on monocytes	233
Figure 7.12	Role of 4-1BB/L interactions in maintaining monocyte survival	234
Figure 7.13	4-1BB/L is required for iNKT proliferation and suppression of IL-4 production	235
Figure 7.14	4-1BBL and 4-1BB induction on monocytes and iNKT cells following *in vitro* PR8 infection	236

List of tables

Table 1.1	Mouse antibodies used in studies	56
Table 1.2	Human antibodies used in studies	57-8
Table 3.1	RNA quality for microarray	79
Table 3.2	Top 10 upregulated genes in severe or mild IAV infection on day 3 and day 5	82
Table 3.3	Biological Processes enriched upon IAV infection	84
Table 3.4	Significantly upregulated immune response genes in lungs on day 3 or day 5 of severe or mild IAV infection	85
Table 3.5	Pre-defined gene sets used in GSEA	91
Table 4.1	Input for logistical regression analysis of disease severity	113
Table 4.2	Demographics of all patients who provided blood samples during acute illness	114
Table 4.3	Classification of myeloid cell populations	118
Table 4.4	Demographics of patients from which cryopreserved samples were available.	128
Table 4.5	Normalised frequencies of cytokine-producing monocytes	139
Table 4.6	Demographics for patients from which acute and convalescent samples were received	144
Table 5.1	Classification of lymphocyte populations	158
Table 6.1	RNA quality for microarray	192
Table 6.2	Top 10 differentially expressed genes in blood and BAL monocytes from iNKT deficient mice	195
Table 6.3	Upregulated processes in blood of Jα18$^{-/-}$ mice compared to wild-type	197
Table 6.4	Downregulated processes in blood of Jα18$^{-/-}$ mice compared to wild-type	197
Table 6.5	Upregulated processes in BAL of Jα18$^{-/-}$ mice compared to wild-type	198
Table 6.6	Downregulated processes in BAL of Jα18$^{-/-}$ mice compared to wild-type	198
Table 6.7	Interferon regulated genes are upregulated in monocytes from both blood and BAL	199
Table 6.8	Pre-defined gene sets used in GSEA	200

List of abbreviations

αGalCer	α-galactosylceramide
Ag	Antigen
ANOVA	Analysis of variance
APC	Allophycocyanin
ARG1	Arginase 1
BAL	Bronchoalveolar lavage
BFA	Brefeldin A
BM	Bone marrow
BSA	Bovine serum albumin
BTLA	B and T lymphocyte attenuator
CCL	Chemokine ligand
CCR	Chemokine receptor
CD	Cluster of differentiation
cDC	Conventional dendritic cell
CFSE	Carboxyfluorescein succinimidyl ester
CLP	Common lymphoid progenitor
CMoP	Common monocyte progenitor
COPD	Chronic obstructive pulmonary disease
cRNA	Complementary RNA
CTL	Cytotoxic T lymphocyte
CTLA-4	Cytotoxic T-lymphocyte-associated protein 4
DAVID	Database for Annotation, Visualization and Integrated Discovery
DC	Dendritic cell
DMSO	Dimethyl sulphoxide
DNA	Deoxyribonucleic acid
EAE	Experimental autoimmune encephalomyelitis
EAE	Experimental autoimmune encephalomyelitis
EDTA	Ethylenediaminetetraacetic acid
ELISA	Enzyme-linked immunosorbent assay
ER	Endoplasmic reticulum
ES	Enrichment score
FACS	Fluorescence-activated cell sorting
FC	Fold change
Fc	Fragment, crystallisable
FCS	Foetal calf serum
FDR	False discovery rate
FITC	Fluorescein isothiocyanate
FoxP3	Forkhead box P3
FSc	Forwards Scatter
GITR	Glucocorticoid-Induced TNFR Family Related Gene
GM-CSF	Granulocyte-macrophage colony-stimulating factor
GMP	Granulocyte/macrophage progenitor
GO	Gene Ontology
GSEA	Gene Set Enrichment Analysis

HA	Hemagglutinin
HC	Healthy control
HIV	Human immunodeficiency virus
HLA	Human Leukocyte Antigen
HS	Human Serum
HSC	Hematopoietic stem cell
IAV	Influenza A virus
ICOS	Inducible T-cell costimulator
ICS	Intracellular cytokine staining
IFITM3	Interferon-induced transmembrane protein 3
IFN	Interferon
Ig	Immunoglobulin
iGb3	Isoglobotrihexosylceramide
IL	Interleukin
IMC	Immature myeloid cell
iNKT	Invariant natural killer T
iNOS	Inducible nitric oxide synthase
IRF	Interferon regulated factor
ISG	Interferon stimulated gene
LCMV	Lymphocytic choriomeningitis
Limma	Linear Models for Microarray Data
LN	Lymph node
LPS	Lipopolysaccharide
M	Matrix
M(1, 2, 2a, 2b, 2c)	Macrophage subsets
mAb	Monoclonal antibody
MACS	Magnetic-activated cell sorting
MCP	Monocyte chemoattractant protein
MDP	Macrophage dendritic cell progenitor
MDSC	Myeloid-derived suppressor cell
MHC	Major histocompatibility complex
MIP	Macrophage inflammatory protein
MLR	Mixed leukocyte reaction
mRNA	Messenger RNA
NA	Neuraminidase
NFκB	Nuclear factor kappa-light-chain-enhancer of activated B cells
NK	Natural killer
NLR	NOD-like receptor
NLS	Nuclear localisation sequences
NOD	Nucleotide-binding oligomerization domain-containing protein
NP	Nucleoprotein
NPC	Nuclear pore complexes
NS	Non-structural protein
PA	Polymerase acidic
PAMP	Pathogen-associated molecular pattern
PB	Polymerase basic
PBL	Peripheral blood lymphocytes

PBMC	Peripheral blood mononuclear cells
PBS	Phosphate buffered saline
PD-1	Programmed Death-1
pDC	Plasmacytoid dendritic cell
PE	Phycoerythrin
PerCP	Peridinin chlorophyll
pH1N1	Pandemic 2009 H1N1 (A/CA/04/2009)
PHA	Phytohemagglutinin
PMA	Phorbol 12-myristate 13-acetate
RdRP	RNA-dependent RNA polymerase
RIG-I	Retinoic acid-inducible gene 1
RMA	Robust Multi-array Average
RNA	Ribonucleic acid
ROS	Reactive oxygen species
SNP	Single nucleotide polymorphism
SSc	Side scatter
STAT	Signal Transducer and Activator of Transcription
TCR	T cell receptor
Th	T helper cell
TipDC	TNF and iNOS-producing dendritic cell
TLR	Toll-like receptor
TNF	Tumor necrosis factor
TNFRSF	Tumor necrosis family receptor superfamily
TNFSF	Tumor necrosis family superfamily
Treg	Regulator T cell
vRNP	Viral ribonucleoprotein
WT	Wild-type

Chapter 1: Introduction

1.1 Influenza A virus

1.1.1 Epidemiology & antigenicity

Human influenza A virus infection initiates in the respiratory tract and is a major cause of mortality. Seasonal epidemics affect 5-10% of adults and 20-30% of children and lead to an estimated 250,000 - 500,000 fatal cases annually (1). The high infection rate is due to failure of the host to generate long-term protective immunity as a result of genetic reassortment in the structural genes of the virus which allow it to evade pre-existing immunity, and frequent mutations introduced during virus replication that lead to generation of new strains (2). This is exemplified most clearly during pandemic infections where a new strain of the virus enters the human population and spreads on a worldwide scale. Influenza viruses are segmented, enveloped, negative-sense RNA viruses that belong to the *Orthomyxoviridae* family and can be classified into three types; A, B and C (3). Influenza A virus (IAV) infects humans and many animals and causes most of the annual epidemics and occasional pandemics in humans, while influenza B only infects humans and seals and only causes occasional epidemics (4). Influenza C can cause mild illness in humans but does not lead to epidemics.

HA and NA are the major viral glycoproteins of IAV that are detected by antibodies and are used to classify viruses into different subtypes (5). Avian species are a reservoir for diverse IAV subtypes. 16 HA and 9 NA subtypes have been isolated from birds, although most infections are asymptomatic or limited to the gastrointestinal and/or respiratory tract (6). New and unique influenza genomes have been isolated from bats, in 2012 when H17N10 was isolated from fruit bats and in 2013 when H18N11 was isolated from a Peruvian bat (7, 8). These are however thought to be distinct from the previous IAV strains as their HA molecules bind sialic acid differently (9).

It is mutations in the HA and NA proteins that lead to antigenic differences which allow viruses to escape existing antibody-mediated immune responses and ultimately result in the generation of new strains. Mutations occur via mechanisms described as antigenic drift and antigenic shift.

Antigenic drift occurs by accumulation of mutations throughout the genome, driven primarily by host immune pressure, and causes seasonal epidemics (10). The viral polymerase that copies the genome lacks proofreading function, resulting in high mutation rates of between $1x10^{-3}$ to $8x10^{-3}$ substitutions per site per year (11). Mutant viruses with amino acid substitutions in antigenic sites on the HA and NA glycoproteins are selected if they confer selective advantages to the virus. This is mainly via the ability to evade pre-existing humoral immunity from antibodies that were generated in response to a previous infection binding to the HA and preventing it from attaching to and infecting a host cell (12). Due to antigenic drift, the antigenicity of circulating IAV strains constantly changes and requires annual review and updating of vaccines to include current circulating strains, as limited cross-protection exists between immune responses to different strains (13).

Antigenic shift occurs when a virus with a new HA subtype to which the population has not recently been exposed is introduced into the human population and replaces the predominant circulating IAV subtype (14). This may occur by transmission of an animal IAV directly to humans without reassortment, or as a result of genetic reassortment of the RNA genome between animal and human IAV (13). Antigenic shift is the cause of pandemic IAV infections.

The majority of seasonal as well as pandemic IAV infections in humans are caused by H1, H2 or H3 and N1 or N2 subtypes (14) suggesting some inherent limitations in host adaptation. There have been three major IAV pandemics in the 20th century, each

differing in virus subtype, epidemiology and disease severity (15). The 1918 'Spanish flu' was the most devastating in documented history and was caused by direct transmission of an avian H1N1 virus (16). The 1957 'Asian flu' was caused by reassortment between the existing H1N1 virus and an avian H2N2 virus (17), and in 1968 the 'Hong Kong flu' emerged from another avian/human reassortment, and was identified as a novel H3N2 virus (18). All pandemic viruses since 1918 contain gene segments from the 1918 virus, which itself is thought to have been a new founding virus derived from an avian precursor that became adapted to mammals (19). The first pandemic of the 21st century was caused by an H1N1 virus, and will be discussed in detail later. A distinct difference in the distribution of IAV-related deaths is apparent in pandemics, as younger people <65 years old were shown to be 20 times more likely to succumb to IAV-related mortality during the three 20th century pandemics in the United States, whereas elderly individuals faced a similar risk as during inter-pandemic seasons (20). Autopsy of severe fatal cases in humans found consistent observations throughout different pandemics (21-24), including infection of the trachea, bronchi and pulmonary alveoli, as well as destruction and desquamination of the pseudostratified columnar epithelium of the trachea and bronchi, often leaving only a basal layer of epithelium (25, 26). IAV has been recovered from both upper and lower parts of the respiratory tract in human infections, with lower respiratory tract involvement and pneumonia being associated with higher morbidity and mortality (27).

Reports of human infection with avian-origin viruses H5N1, H7N9 and H7N7 demonstrates that influenza viruses are continually evolving ways to cross the species barrier to infect humans, and have caused considerably higher mortality than previous seasonal IAV strains (28-30). Since 2003, over 650 cases of H5N1 have been reported, most of which suffered from severe pneumonia and acute respiratory distress syndrome (ARDS). A fatality rate of over 59% has been reported for H5N1 infection (31), although this may be an overestimate due to asymptomatic and non-reported mild

cases (32, 33). A further strain, H9N2 which is thought to be rare but mild, has been detected in two individual cases in young children in Hong Kong, both of who recovered from the infection (34). These findings highlight the influenza virus's ability to evolve and spread into a human population, which if unexpected could lead to disastrous consequences, and necessitates the need for further understanding of the immune response to IAV infection.

High pathogenicity IAV strains such as H5N1 are a public health concern due to the lack of protective immunity. While human-to-human transmissions have not been reported for H5N1, a mutation in the virus which would enable this has the potential to cause a devastating pandemic. Two groups in 2012 demonstrated this by reporting that only a small number of mutations enabled airborne transmission of the virus in ferrets (35, 36). This work caused much concern, not only because of the potential emergence of a virus that could cause greater mortality than the 1918 H1N1 virus, which itself caused an estimated 50 million deaths, but also controversy over potential for bioterrorism. Publications from both groups were assessed by the US National Science Advisory Board for Biosecurity, who disallowed publication until methodologies were amended in order to avoid replication of experiments. (37). While both papers were eventually accepted with amended methodologies, this demonstrates the highly dangerous nature of the H5N1 virus.

The continued evolution of IAV causes challenges for vaccine development. The most successful vaccines against IAV generate a specific antibody response against the most variable viral protein, HA (38). This requires annual updates to vaccines and prediction of strains that will circulate in the upcoming season. The emergence of unexpected pandemic viruses or seasonal strains incorrectly predicted leads to incomplete protection from this vaccine. Development of a universal vaccine against IAV would overcome these issues, and work from many groups has focussed on

targeting highly conserved regions of the virus, such as the extracellular portion of the M2 protein (39) and HA stalk domain (40). Other work has focussed on inducing cytotoxic T lymphocyte (CTL) responses, as CTLs recognise conserved viral proteins, and thus may provide protection against a number of different variants of IAV (41). These CTLs could provide baseline immunity and may provide protection against newly emerging viruses which would reduce mortality, although most likely not prevent infection altogether.

Current treatment of those with severe IAV involves antiviral therapies that target the virus, such as Amantadine which targets and blocks the M2 ion channel and Oseltamivir and Zanamivir which inhibit the neuraminidase protein (42). Resistance to these has however been reported in the past, and the likelihood of further resistance developing is high (43, 44). Recently there have been developments in modulating the host response in order to target severity of infection, particularly for avian viruses whose high pathogenicity is partially driven by immunopathology caused by the host immune system. Using host transcriptional profiles, gene signatures shared between severe H5N1, H7N9 and H7N7 viruses were reported, and FDA-approved drugs able to target and dampen the pathologic cytokine response induced by the host in response to these severe viruses were identified (45).

1.1.2 Virus structure

The viral genome of IAV consists of eight single-stranded negative-sense segments that encode 11 proteins, each of which influence the complex pathogenicity of IAV infection (14). Segment 1 encodes polymerase basic protein 2 (PB2), segment 3 polymerase acidic protein (PA), segment 4 haemagglutinin (HA), segment 5 nucleoprotein (NP) and segment 6 neuraminidase (NA). Segment 2 encodes polymerase basic protein (PB1) as well as the small PB1-F2 by using alternative

translation initiation sites (46). Segment 7 encodes for matrix proteins M1 and M2 and segment 8 encodes for non-structural proteins NS1 and NS2, which are expressed by mRNA splicing (47).

The structure of an influenza A virion can be divided into an outer envelope consisting of HA, NA and M2 ion channels, the internal matrix consisting of M1, and the core which is made up of the 8 RNA segments that are individually packed and stabilised by multiple copies of NP into viral ribonucleoprotein (vRNP) complexes (48) (Figure 1.1).

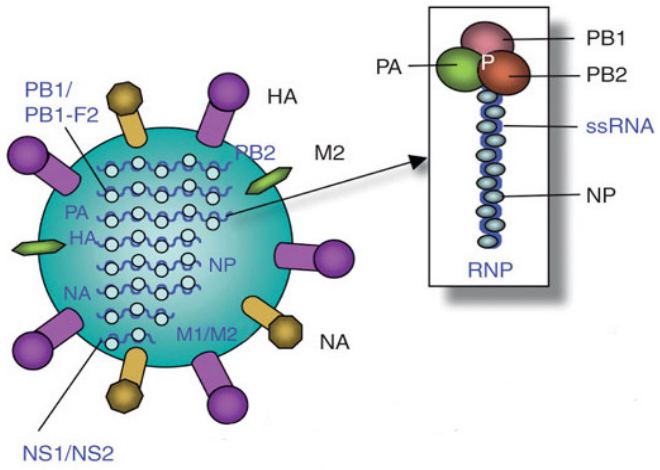

Figure 1.1: Structure of an influenza A virion. Virion made up of a lipid bilayer containing HA, NA and M2. Inside the virion are the eight RNA segments associated with the trimeric RNA polymerase (PB1, PB2, PA) and coated with NP to form vRNPs. vRNPs are attached to the inner layer by M1 which sits below the outer envelope. *Image adapted from (49)*.

1.1.3 Virus replication

The viral envelope is made up of a host-derived lipid bilayer consisting of roughly 80% HA and 17% NA, with M2 comprising a minor component of roughly 16-20 molecules per virion.

IAV infection begins with HA molecules binding to sialic acid receptors on the surface of host cells (50). The HA precursor, HA0, is made up of two chains, HA1 and HA2, which are covalently linked by a disulphide bond (51). HA1 forms the globular head containing a receptor-binding cavity, and HA2, which has a more conserved structure than HA1, makes up most of the stalk which anchors the molecule to the virus membrane, and contains a fusion peptide. The two-chain monomers associate non-covalently to form trimers at the surface of the virus membrane (52). Following sialic acid binding by HA1, the virus is endocytosed (Figure 1.2a). The endosome in which the virus is contained has a low pH of 5-6, which exposes the HA2 fusion peptide as a result of a loop-to-helix conformational change triggered by the low pH (53). The fusion peptide inserts into the endosomal membrane, fusing it with the viral membrane and enabling release of the viral genes (vRNP) into the cytoplasm (54) (Figure 1.2b). A further effect of the low pH is opening of M2 proton-selective ion channels, which acidify the viral core causing release of vRNPs from M1, which lies underneath the lipid bilayer membrane and enables the vRNPs to enter the cytoplasm (55).

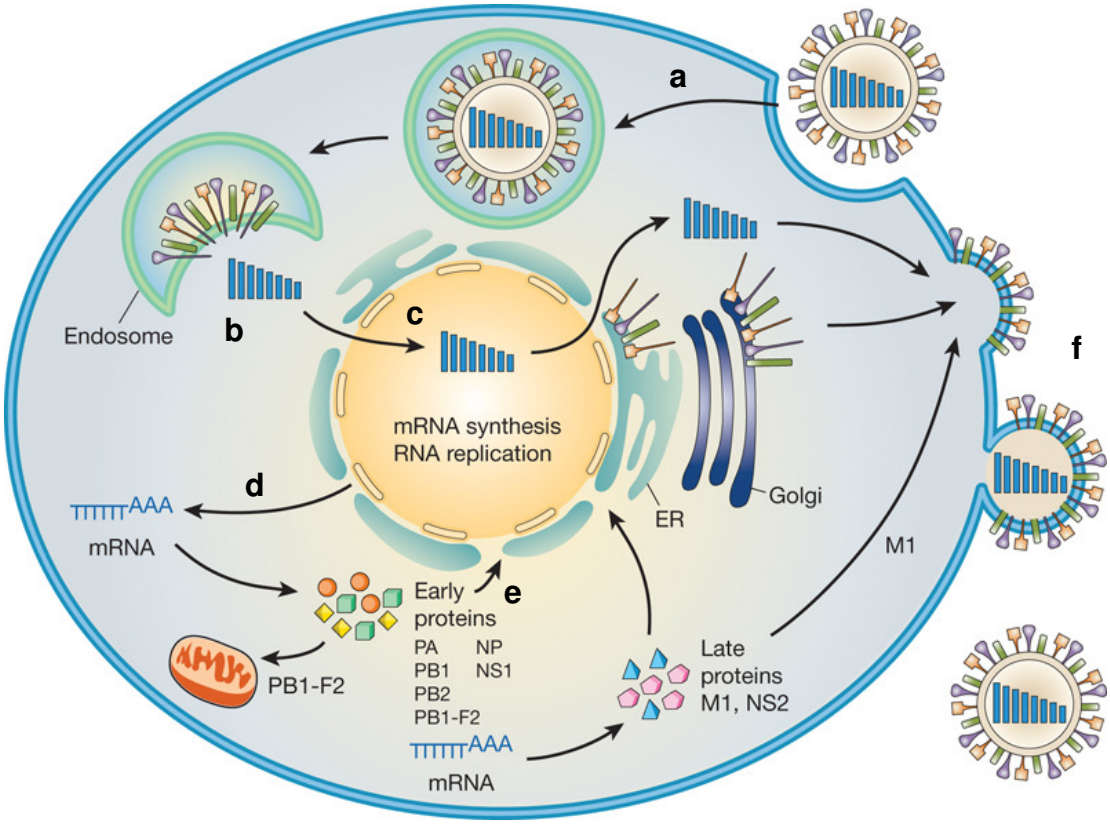

Figure 1.2: Influenza A virus life cycle. (a) IAV attaches to the host cell membrane via HA-sialic acid interactions and is endocytosed. **(b)** vRNPs are released into the cytoplasm and are transported to the nucleus. **(c)** Viral transcription is initiated in the nucleus. **(d)** Viral mRNAs are transported to the cytoplasm for translation into proteins. **(e)** Early viral proteins required for replication and transcription are transported back to the nucleus where unprimed replication of viral RNA by the viral polymerase takes place. **(f)** Assembled virions are released from the cell. *From* (56).

The vRNPs must reach the nucleus of the host cell in order to replicate. The virus polymerase proteins, which associate with each of the virus particles, contain nuclear localisation sequences (NLS) that mediate vRNP import into the nucleus by promoting binding to cellular nuclear import machinery (57). It is believed that while all polymerase proteins contain NLS, only NP mediates nuclear import (58). Once the vRNPs gain access to the nuclear import machinery (nuclear pore complexes; NPC), they are imported into the nucleus in an energy-dependent manner (59). This binding of NLS to NPC happens via two proteins, importin α and importin β. Importin α acts as

an adapter between the NLS-bearing protein (in this case the vRNP) and importin β, which is linked directly to the NPC (60).

Once inside the nucleus, transcription and replication of the virus are initiated (Figure 1.2c). The negative sense RNA is transcribed into positive-sense RNA for translation into proteins by the host ribosomes. Transcription is carried out by the RNA-dependent RNA polymerase (RdRP), which is a single trimeric polymerase complex (3P) consisting of PA, PB1 and PB2 and is encapsidated by multiple copies of NP (61). Transcription of mRNA from viral RNA is initiated by cap primers and terminated to form polyadenylated mRNA (62). As vRNPs do not contain 5' caps, they acquire them from nascent host pre-mRNAs via a 'cap-snatching' mechanism. This is facilitated by binding of the 5' caps by PB2 and cleavage of the pre-mRNA 10-13 nucleotides downstream from the cap by PA (63, 64). Viral mRNA transcription by the RdRP can then be initiated from the cleaved 3' end of the capped RNA fragment (65). Replication, via synthesis of cRNA and viral RNA, occurs without a primer, but requires viral polymerase proteins. During replication, nucleoprotein molecules are deposited on the cRNA and viral RNA, and the resulting vRNPs are transported to the cytoplasm (66).

Translation occurs in the cytoplasm of the cell by utilising host cytoplasmic ribosomes (67) (Figure 1.2d). The cap structure involved in transcription plays a critical role in recruitment of the ribosome to mRNA for translation (67). Internal proteins are synthesised in the cytosol, and are imported back to the nucleus for final stages of replication and vRNP assembly (Figure 1.2e). Final transport of assembled vRNPs to the cytoplasm is partially mediated by M1, which interacts with NS2. NS2 is associated with the rest of the vRNPs, and also contains known nuclear export signals (NES) (68). Hereby a M1-vRNP complex is formed which can be transported to the cytoplasm. Nuclear export is controlled by export receptors, most notably the highly conserved

CRM1 (chromosome region maintenance protein 1) which mediates export of the M1-vRNP complex through nuclear pores by associating with NES on NS2 (69).

In the nucleus, the non-structural protein NS1 plays an important role by suppressing the production of host mRNAs, and thereby shutting down host gene expression of antiviral factors such as interferon-β (70). It does this by inhibiting 3'-end cleavage and polyadenylation of host pre-mRNAs. Viral mRNAs do not require 3'-end processing, allowing their transport to the cytoplasm, while host mRNA synthesis is predominantly blocked (71).

Assembly and budding of virions occurs at the cell surface in lipid raft microdomains (72) and are the penultimate and final steps of virus replication (Figure 1.2f). The 8 gene segments must arrange themselves near the plasma membrane as all 8 segments must be present in the virus particle progeny in order for the virus to be infective. Over 90% of released virus particles do not contain all of the vRNPs and are therefore non-infectious (73). The envelope proteins HA, NA and M2 must all be present to form a viral particle. HA, NA and M2 are processed in the ER, glycosylated in the Golgi and transported to the apical plasma membrane. It is thought that the 8 genomic segments contain packaging signals that dictate which segments are to be packaged into the virions, and this enables their assembly (74, 75).

M1 is a crucial protein for virus budding, as it forms a bridge between the envelope proteins and vRNPs. Clustering of M1 on the inner lipid bilayer can cause membrane bending and initiation of bud formation (76). Buds are released by fusion of opposing membranes and splitting off of the virus particle. At this stage virus particles are generally filamentous (77) and may acquire a spherical shape at a later point. Release of the virus particle is mediated by NA, which acts as an exosialidase by removing sialic acid from virus particles and the infected cells (78). This is necessary as the

released particles may still re-attach to the infected cell, or self-aggregate, via sialic acid interactions. NA has also been proposed to facilitate spread of the virus by cleaving sialic acid residues from the respiratory tract mucins (79).

1.1.4 Pandemic H1N1 2009 virus properties

The first pandemic of the 21st century ('pH1N1') emerged in Mexico and the United States in 2009 and was labelled as 'swine flu' as it arose from two unrelated swine viruses (80). A Eurasian avian-like swine H1N1 virus contributed the NA and M gene segments to the 2009 pandemic strain. The remaining 6 segments arose from a North American triple reassortant swine influenza virus that emerged around 1998 by reassortment among human H3N2, North American avian and classical swine H1N1. The classical swine H1N1 virus is a descendant from the 1918 human H1N1 virus. (81, 82). The triple reassortant virus underwent further reassortment with classical H1N1 swine virus (83). Therefore the HA, NP and NS gene segments of pH1N1 were derived from the classical H1N1, the PB2 and PA segments arose from an avian IAV source, and PB1 arose from human H3N2 (84) (Figure 1.3).

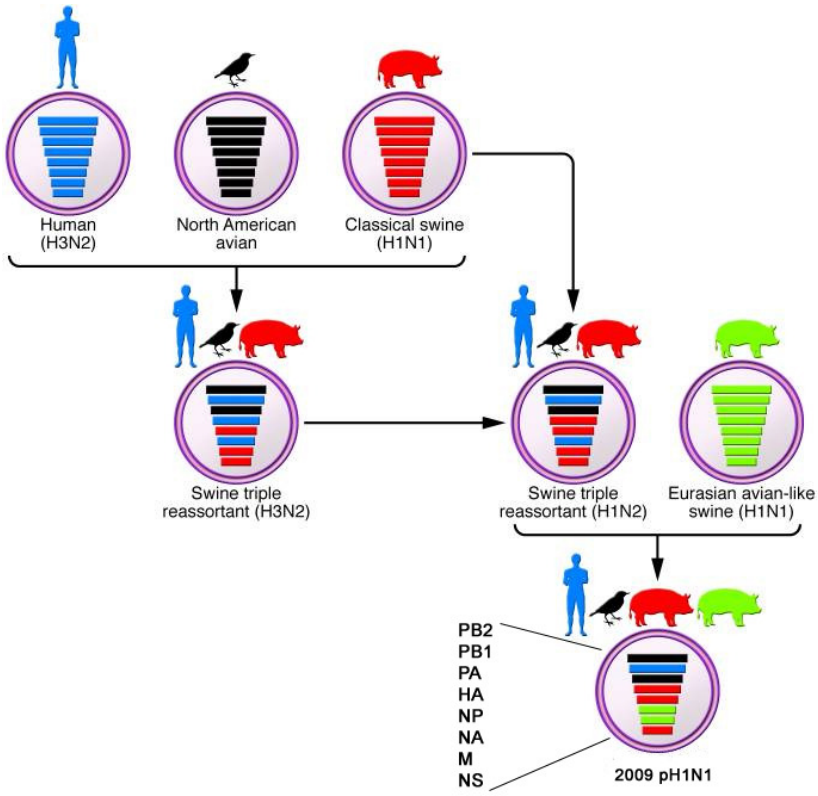

Figure 1.3: Lineage of the 2009 H1N1 pandemic virus. Reassortment of swine triple reassortant H3N2 virus and classical swine H1N1 with Eurasian avian-like H1N1 swine resulted in pH1N1. *Adapted from* (85).

Despite spreading rapidly to 30 countries within the first few weeks of surveillance and causing global health concern, pH1N1 only caused relatively mild disease in the majority of infected individuals (86). An early study looking at some of the first cases of infection in the United States found that only 9% of infected patients required hospitalisation, many of whom had pre-existing medical conditions that increased their susceptibility to infection (80). In previous pandemics and seasonal outbreaks, children and elderly individuals with weaker immune systems have suffered worse outcomes (87, 88). The pattern of the 2009 pandemic was however different, with only 2-3% of individuals over the age of 60 showing symptomatic infection. In younger children aged between 5-19, infection rates were highest at 34-43%, and infection in adults ranged from 9-10% (89, 90).

Sequence analysis of the pH1N1 2009 virus established that many viral proteins were more similar to the pandemic 1918 H1N1 strain than recent circulating seasonal H1N1 strains, and that this led to cross-reactive $CD8^+$ T cell immunity and antibody responses between the two strains (91, 92). Analysis of the cellular immune response to the 2009 pandemic found significant levels of cross-reactive T cells to pH1N1 in antibody-naïve healthy adults, and that individuals who had higher frequencies of pre-existing $CD8^+$ $IFN\gamma^+$ $IL2^-$ cross-reactive T cells to conserved $CD8^+$ epitopes developed less severe illness (93). These cross-reactive T cells recognised highly conserved epitopes from PB1, NP and M1 internal proteins that are conserved across viral subtypes, and provide a suggestion for the reasons behind the mild incidence of pH1N1 disease (94). Other reports support a role for antibody-mediated protection offered by previous infection with a different strain of IAV in reducing illness and susceptibility (95, 96). A significant number of older people were protected by neutralising antibodies that cross-reacted with pH1N1 (97-99). A study found that 34% of individuals born before 1950 had cross-reactive antibody titres of 80 or more, whereas only 4% of individuals born after 1980 had cross-reactive antibody titres of 40 or more (100), where a titre of 40 associates with 50% reduction in risk of infection. Cross-protective T cells and heterotypic immunity can only offer a limited amount of protection however, and therefore it is important to understand factors that may influence susceptibility to disease.

1.1.5 Determinants of pathogenicity in IAV infection

Outcome to IAV infection is dependent on host and virus factors. Infection with a particular strain of IAV can cause a range of outcomes in different individuals, ranging from mild disease to death. Reasons for these differences are not fully understood, but may be due to genetic differences in the host, as well as underlying medical conditions that affect the immune system. Different strains of IAV also lead to a range of

outcomes, for example the avian H5N1 and the 1918 H1N1 viruses caused a more severe clinical disease course and significantly higher death rates than most seasonal H1N1 and H3N2 viruses; partly due to genetic differences in the virus.

1.1.5.1 Susceptibility of the host

Studies have focussed on identifying host factors related to IAV disease susceptibility and severity. Underlying clinical conditions and comorbidities are a major correlate to developing severe disease, and include lung disease, heart disease, diabetes mellitus, malignancy, immune suppression and pregnancy (101). Obesity and pulmonary conditions such as COPD are amongst the most frequent comorbidities that cause severe complications (102).

Host genetic influence on susceptibility to IAV is apparent from the familial clustering of H5N1 cases among blood relatives (103). Identification of gene polymorphisms that impair the immune response or correlate with protection can help identify subject more vulnerable to severe infection (104). Examples identified from pH1N1 infection include the -238A SNP allele of TNF and the minor rs12252-C SNP allele of the interferon-induced transmembrane protein-3 (IFITM3) gene, both of which increased disease severity (105-107). The frequency of the -238A allele was significantly increased in pH1N1 patients compared to healthy controls, with enrichment in those developing viral pneumonia and acute lung injury (105). The role of IFITM3 in IAV infection is clear from IFITM3$^{-/-}$ mice that develop more severe disease than wild-type mice due to enhanced virus replication, suggesting that IFITM3 offers protection by restricting virus replication (106). In humans, the rs12252-C allele truncates the IFITM3 protein, thereby reducing restriction of virus replication. Monocyte chemoattractant protein-1 (MCP-1) levels were elevated in IFITM3$^{-/-}$ mouse lungs relative to wild-type and serum from humans with the homozygous CC genotype of the r12252 SNP in IFITM3, which caused most severe

disease, and suggests involvement of aberrant monocyte recruitment in worse outcome. Other identified gene polymorphisms that were found to correlate with severe disease include homozygosity of the CCR5Δ32 allele (108) and the rs1130866 allele of surfactant protein B (109). Mutations in the Mx1 gene, which encodes interferon (IFN) inducible proteins, have been associated with increased susceptibility to IAV infection in mice (110). Mice expressing Mx1 were shown to be better protected against the high mortality and lung pathology caused by H5N1 and the 1918 H1N1 IAV due to production of antiviral IFN-inducible proteins (111).

The HLA phenotype of individuals also plays a role in virus recognition and influences the magnitude and specificity of the cytotoxic T cell response to IAV infection. HLA molecules that bind virus antigen are recognised by T cells, and are very diverse. Early work identified that cell-mediated lysis of IAV-infected cells was found to be dependent on HLA specificities (112). Recently, it was shown that individuals with HLA A*24 alleles were associated with reduced virus clearance and increased severity of H1N1/09 infection (113).

Interplay between these host genetic differences and genetic differences of the infecting virus strain are likely to determine overall pathogenicity.

1.1.5.2 Virus factors in pathogenicity

As well as the continued rapid evolution of new IAV virus strains for which little pre-existing immunity is present and host factors described above, differences in virus pathogenicity can be caused by genetic differences in the infecting virus strains.

Infectivity of different IAV subtypes is partially due to differential expression of the HA receptor, sialic acid, in the respiratory tract of human and avian species. Sialic acid is associated with glycans that are linked to glycoproteins and glycolipids on the surface

of epithelial cells (114). The link between sialic acid and an underlying glycan can either form and α2,3 or an α2,6 glycosidic linkage (115) and the enzymes responsible for adding the sialic acid in a particular linkage, sialyltransferases, are differentially expressed in different species (116). In humans the respiratory tract consists of primarily α2,6-linked glycans, and therefore human IAV have developed a binding preference for these linkages, whereas avian IAV, such as H5N1, preferentially bind α2,3-linked sialic acids (117). Detailed analysis of the sialic acid linkages in the human respiratory tract revealed a prevalence of α2,6-linkages in the upper region of the respiratory tract, on epithelial cells in nasal mucosa, trachea and bronchi, while some α2,3-linkages were present lower down in type II alveolar cells (118), which have been shown to be infected with H5N1 in a patient (119). Infection of the lower respiratory tract is associated with pneumonia and a more severe infection, but lower transmissibility among individuals than viruses that infect the upper respiratory tract (120).

Adaptation of avian viruses to human transmission therefore relies heavily on a shift of the binding specificity from α2,3 to α2,6 (121). The switch in configuration of HA to bind α2,3 instead of α2,6-linked sialic acids requires only one amino acid change, E190D, which was found to have occurred in all 1918 H1N1 viruses that have been isolated and sequenced (122). Swine have been described as a good species for reassortment of IAV from different hosts, as their respiratory tract possesses both α2,3- and α2,6-linked sialic acids (123). With continued replication in pigs, avian-like swine viruses have been shown to develop the ability to recognise human receptors, enabling the possibility for direct transmission to humans (124).

Virus replication efficiency is another major driving force in determining outcome to infection, and can differ depending on the IAV strain (125). More pathogenic strains such as H5N1 have high replication rates, and suppression of early viral replication

was shown to improve outcome (126). In pH1N1 infected patients however, viral load was lower than in patients following seasonal infection, and did not correlate to concurrent illness (127). Use of a modified PR8 virus carrying a luciferase reporter gene allowed visualisation of bioluminescence in the lung and nasopharyngeal passage, representing viral load, and showed higher bioluminescence, weight loss and mortality as dose was increased (128).

Genetic differences in virus strains that influence pathogenicity have been identified for most of the IAV proteins, most notably PB1-F2, HA, NA and NS. The small pro-apoptotic PB1-F2 protein encoded by IAV causes virus-induced cell death by destabilising the mitochondrial membrane of innate immune cells, in an attempt to subvert host immunity (129, 130). PB1-F2 expression increased viral pathogenesis, immune pathology and secondary bacterial infection in mice (131, 132), but is not coded for by all IAV strains. pH1N1 for example differs from the previous pandemic viruses of the 20th century in that its genome does not code for this protein (133). Lack of PB1-F2 in pH1N1 has therefore been proposed as a reason for the low pathogenicity in relation to previous pandemics. Studies examining this directly however found that introduction of functional PB1-F2 into pH1N1 did not significantly enhance virulence in mice, ferrets or pigs, despite showing signs of increased proinflammatory gene expression and inflammatory cytokine production (134, 135). Therefore the exact contribution of this gene to virulence remains unclear.

The amino acid substitution D222G in the haemagglutinin (HA) protein of pH1N1 was associated with cases of severe disease and fatalities (136), and studies in mice showed that this mutation led to acquired specificity for both α2,3- and α2,6-linked sialic acids due to alterations in HA structure (137). Mutations in the NA protein have been identified in mice which allow the virus to replicate in many tissues outside of the respiratory tract. These mutations in a single codon, N146R or N146Y, have however

not been found in highly pathogenic human IAV such as the 1918 H1N1 virus, but show the potential of a single mutation in NA to cause a dramatic change in pathogenicity (138). The NS1 protein enables the virus to disable the host's type I IFN defence system, and the specific sequence of the NS1 gene can alter the cellular immune response to IAV infection by influencing the type and magnitude of IFN response. A virus containing the 1918 H1N1 NS1 protein was more efficient at blocking host IFN production than its parental influenza A/WSN/33 virus (139).

1.1.6 Immune response to IAV infection

Outcome to infection relies on reducing viral burden and/or reducing the negative impact of infection on host fitness (140). The immune response against IAV ultimately aims to abort virus replication in order to overcome infection, and induce immunological memory to protect against subsequent infections. The innate immune response is the rapid first line of defence, but lacks specificity. Adaptive immunity is slow to be initiated upon first encounter with a pathogen but is highly specific, consisting of virus-specific antibodies produced by B cells (humoral immunity) and virus-specific T cells (cellular immunity).

1.1.6.1 Adaptive immune response to IAV

Initiation of the adaptive immune response begins in the respiratory tract where antigen presenting cells (APC), most notably dendritic cells (DC), acquire antigen via direct infection or phagocytic engulfment of virions or infected cells. This leads to their maturation and activation and causes them to migrate to the draining lymph nodes along a CCR7 chemokine gradient. DC subsets in the non-inflamed lungs include conventional DCs (cDC) and plasmacytoid DCs (pDC). cDC can be further grouped into $CD103^{+}CD11b^{+/-}$ and $CD103^{-}CD11b^{hi}$. $CD103^{+}$ DC are the most potent APC following IAV infection for priming naïve T cells (141). In the draining LN, DCs induce

$CD4^+$ and $CD8^+$ T cell responses. Virus-specific $CD4^+$ helper cells and $CD8^+$ cytotoxic cells are generated upon recognition of MHC-II and MHC-I antigenic peptide complexes on APCs, respectively, and activated by cytokine and costimulatory molecule signals from APCs (142). Naïve T cells that interact with DCs in secondary lymphoid organs are sculpted to alter their transcriptional signature and activation profile and differentiate along the following axis; expansion, lineage commitment, effector phenotype, egress from draining LN to act at site of infection and survival of a small subset into memory (143). Protective immunity against subsequent infection relies on maintenance a small population of these memory T cells. In addition, memory T cells produced in response to one virus have been shown to protect against similar, but not identical strains of IAV (144). Presence, number and functionality of memory T cells have been shown to correlate with protection (94).

Depending on the cytokine milieu, $CD4^+$ T cells differentiate into T helper 1 cells (Th1) or Th2 cells (145). Th1 cells produce IFNγ and IL-2 and are involved in promoting CTL responses and induction of $CD8^+$ memory. Th2 cells produce IL-4, IL-5 and IL-13 and promote activation and differentiation of B cells, which are required for antibody production. $CD4^+$ T cells also induce antibody class switching, which is critical for the generation of long-term immunity to IAV. In the absence of $CD4^+$ T cells, initial virus-specific Ig antibody is produced, but virtually no IgG antibody-secreting B cells develop (146). In addition to helper cell functions, IAV-specific $CD4^+$ cells were also shown to have cytolytic functions in (147).

$CD8^+$ T cells activated upon viral antigen recognition differentiate into cytotoxic T lymphocytes (CTL) which migrate to the site of infection and cause apoptosis of IAV-infected cells via release of perforin and granzymes (148). FasL upregulation on CTL further promotes apoptosis of infected cells. Production of proinflammatory cytokines such as IFNγ and TNFα inhibit virus replication and enhance lytic activity (149). IAV-

specific CTLs are mainly directed against epitopes of highly conserved viral proteins such as M1, NP, PA and PB2, and therefore can provide cross-reactivity with different subtypes of IAV (150).

In addition to virus-specific $CD4^+$ and $CD8^+$ T cells, FoxP3 regulatory T cells (Tregs) and Th17 cells are also activated in response to IAV. Tregs limit $CD4^+$ and CTL responses to prevent immunopathology, while Th17 cells produce IL-6 which inhibits Tregs and thereby promotes $CD4^+$ and CTL responses (151).

B cells provide humoral immunity by producing strain-specific antibodies in response to IAV infection (152). Antibodies directed at viral HA and NA correlate with protective immunity. Antibody binding to the globular head of HA blocks virus attachment to host cells and receptor-mediated endocytosis (153). These antibodies are highly strain-specific due to the variability in the HA globular head between strains, however some protection is offered against strains that resemble, but are not identical to, the infecting strain. For example individuals exposed to H1N1 in the 1950s had antibodies which cross-reacted with pH1N1/09 and were protected against developing disease (100). Antibodies to NA inhibit the release and spread of newly formed virus from infected cells. Therefore they do not neutralise the virus, but shorten severity and duration of illness (154).

1.1.6.2 Innate immune response to IAV

The primary mechanism of defence following early onset of IAV infection is the innate immune response, the effectiveness and magnitude of which plays a major role in the resolution of infection (155). The innate immune system plays a critical role in early virus control and clearance, as virus-specific CTL do not appear in the lung until 5 days after infection (156). Recognition of IAV results in secretion of type I interferons (IFNs) and proinflammatory cytokines. Type I IFNs are produced primarily by tissue resident

macrophages and DCs and control viral replication through more than 300 interferon-stimulated genes (ISGs) (157). Recently it was however shown that high production of type I IFN (IFNα/β) caused more lung damage, morbidity and mortality in mice, due to the production of pro-inflammatory cytokines and recruitment of inflammatory cells to the lungs (158). Pro-inflammatory cytokines induce inflammation and fever and instruct the adaptive immune response, while chemokines recruit immune cells such as neutrophils, monocytes and NK cells to clear the virus by killing and phagocytosis of infected cells (159). Other less prevalent immune cell subsets, such as iNKT cells, innate lymphoid cells and γδ T cells, also have roles in the defence against IAV infection due to their residence in the lung (160). While an efficient innate immune response is necessary for effective virus clearance, over-exuberant activity can lead to pathology.

The innate immune response is not specific to a particular pathogen, and is therefore induced by recognition of pathogen-associated molecular patterns (PAMPs) which are different from self. At least 3 pattern recognition pathways exist whereby cells recognise IAV; Retinoic acid-inducible gene I (RIG-I), Toll-like receptors (TLRs) and nucleotide oligomerization domain (NOD)-like receptors (NLRs). The cytoplasmic RNA recognition protein RIG-I recognises 5'-capped RNA in the cytosol of infected cells which is revealed after virus fusion and replication, and leads to production of pro-inflammatory cytokines and type I IFN (161, 162). Toll-like receptors TLR3 and TLR7 recognise viral RNA in epithelial cells and DCs, respectively (163-165). TLR3 recognises double stranded RNA on the cell surface, while TLR7 recognises single stranded RNA in endosomes. As double stranded RNA is not generated by IAV infected cells, TLR3 is thought to recognise RNA in dying IAV-infected cells that have been phagocytosed (166). TLR3-mediated signals restrict viral replication but also lead to recruitment of immune cells that can cause damage to the host (167). TLR7 signals via MyD88 to activate NF-κB or IRF7, which stimulate the production of pro-

inflammatory cytokines and type I IFNs, respectively. H5N1 was also found to trigger TLR4 activation, leading to acute lung injury mediated by oxidised phospholipids (168). NLRs trigger the inflammasome pathway in macrophages and DCs leading to caspase-1 activation and IL1β and IL-18 production (169). Inflammasome activation has been shown to induce MIP-1α production by macrophages, mediating monocyte recruitment in early stages of infection (170), and to contribute to viral clearance in later stages of infection (171).

Epithelial cells are the first line of defence against invading pathogens in the lung, and can signal recruitment and activation of effector cells. As the primary targets of IAV are airway epithelial cells, infection is associated with significant pulmonary pathology and reduced respiratory functions (12). Infected epithelial cells undergo apoptosis within 24-48 hours due to membrane disruption caused by budding virus particles (172). Neutrophil infiltration is apparent as epithelial cells necrose as they are recruited to phagocytose apoptotic and necrosing IAV-infected cells. A large presence of neutrophils has been shown to occur in more severe infections, but is often also suggestive of coincident bacterial infection which is also most common in severe infection. Studies investigating the role of neutrophils in outcome to infection have yielded conflicting results and therefore their exact contribution is not fully established (173, 174). Following neutrophils, a larger mononuclear cell inflammatory infiltrate can often be seen in the walls of bronchi (175). The chemokines produced early during IAV infection in the lungs preferentially favour recruitment of blood mononuclear cells (176) and mononuclear cell influx is a well-established feature of host defence against viral infection (177). Epithelial cells produce large amounts of RANTES, MCP-1 and IL-8 (178, 179), while monocytes and macrophages secrete MIP-1α, MIP-1β, RANTES, MCP-1, MCP-3, MIP-3α and IP-10, all of which recruit circulating monocyte to the lungs (180). The role of monocytes in IAV infection is discussed in detail later (1.2.6).

Lung-resident macrophages and DCs are well-placed to respond to invading pathogens. They have roles in direct elimination of IAV-infected cells and priming of IAV-specific T cell responses. Alveolar macrophages become activated upon infection of the alveoli and phagocytose infected apoptotic cells, limiting viral spread (181). Phagocytosis correlates with viral clearance, and inhibition of phagocytosis augments inflammation and mortality (182). Alveolar macrophages infected with IAV do not release a large amount of infectious virus, but produce IFNα, pro-inflammatory cytokines and chemokines, and upregulate innate defence genes (183). Depletion of alveolar macrophages prior to infection led to increased viral replication and mortality, as well as reduced expression of cytokines and chemokines such as IFNα, TNFα and MIP-1α, suggesting a vital role for these cells in the early defence response (184-186). Production of pro-inflammatory mediators by alveolar macrophages has the potential to contribute to immune pathology in high pathogenicity IAV infections, but despite this their role in the early innate immune response is mostly protective. Depletion of alveolar macrophages prior to IAV infection led to a reduction in IAV-specific CTL responses post-infection (186).

Two main DC subsets, conventional DCs (cDC) and plasmacytoid DCs (pDCs) participate in early innate immune responses in the lung. cDCs capture antigen and mature in the presence of a danger signal (engagement of pattern recognition receptors (PRR)) which allows them to traffic to lymph nodes and initiate IAV-specific T cell responses (187). pDCs on the other hand are major producers of type I IFN and IL-12 and increase in number after infection (188). pDC have less of a direct role in stimulating naïve T cells, but can promote cDC maturation, and migration to lymph nodes is associated with modulation of the subsequent adaptive immune response (189). Both cDC and pDC produce distinct waves of cytokines and chemokines following infection that regulate recruitment of immune cell subsets to the lung, as

neutrophil and NK cell recruiting chemokines are produced earlier on, followed by chemokines involved in recruitment of effector memory T cells. (190).

A striking role of pulmonary endothelial cells during IAV infection was established in mice, demonstrating that these cells are major producers of pro-inflammatory cytokines and chemokines which drive the cytokine storm observed in severe infection and lead to increased mortality, as well as recruitment of activated monocytes/macrophages and NK cells to the lung (160, 191, 192). The role of NK cells in protection against IAV infection has been inferred by findings of increased morbidity and mortality and reduced viral clearance in mice with defected NK cells or none at all (193, 194). NK cells interact with IAV HA via the NKp46 (NCR1) receptor in a sialic acid dependent manner, leading to killing of IAV-infected cells (195). The CD16 receptor (FcγRIII) of NK cells can also bind the Fc portion of antibodies bound to IAV-infected cells and mediate lysis of these cells in a process known as antibody-dependent cell cytotoxicity (ADCC) (196).

Infection with IAV can therefore cause host injury in two different ways. Firstly, the virus itself causes direct injury by infection of target cells such as epithelial cells, and secondly injury caused by an over-exuberant immune response. Contribution from both of these ways is likely to determine outcome to infection in the end (197).

1.2 Monocytes

1.2.1 Background

The mononuclear phagocyte system was originally described in 1968 as a population of bone marrow-derived myeloid cells that circulate in blood as monocytes and populate tissues as macrophages (198). Monocytes are key players in inflammation

and pathogen challenge. They are present in all vertebrates, with different subsets being characterised by their location, morphology, phenotype and characteristic gene and microRNA expression signatures (199, 200).

Monocytes represent 4% and 10% of circulating cells in mice and humans, respectively. During inflammation this can rise as monocyte production in bone marrow increases, and they get recruited from sites such as the spleen which serves as a reservoir (201-204). Circulating monocytes have a short half-life of around 20 hours in mice and around 3 days in humans (205), after which they undergo spontaneous apoptosis or migrate to tissues if an inflammatory signal is sensed (206, 207). It was previously believed that because of this short half-life, monocytes under steady-state conditions continuously migrate to tissues to replenish resident macrophages (198). Recent studies have however established that many tissue macrophages and classical DCs originate from distinct embryonic precursors, and are maintained by self-renewal independently of monocyte input (208).

1.2.2 Monocyte development and function

Development and survival of monocytes is dependent on colony-stimulating factor 1 (CSF1/ M-CSF) and its receptor CSF1R (M-CSFR/ CD115) which is present on monocytes (209). Mice deficient in either have a severe deficiency in mononuclear phagocyte populations (210). Monocytes are produced in the bone marrow from hematopoietic stem cells (HSC) that initially follow the fate of granulocyte-macrophage progenitors (GMP) as opposed to common lymphoid progenitors (CLP). These then form macrophage and dendritic cell precursors (MDP) which are lineage negative but express CD117 (KIT), CD135 (FLT3) and CSF1R. Adoptive transfer of MDPs into bone marrow of mice depleted of mononuclear phagocytes show that they give rise to bone marrow and blood monocytes, as well as spleen cDC (211). An intermediate step in

monocyte development was identified recently by the discovery of the common monocyte progenitor (cMoP) which differs from the MDP by lack of CD135 and exists at four times the frequency of the MDP in bone marrow (212). The cMoP gives rise to monocytes and their descendants, but not cDC or pDC (Figure 1.4).

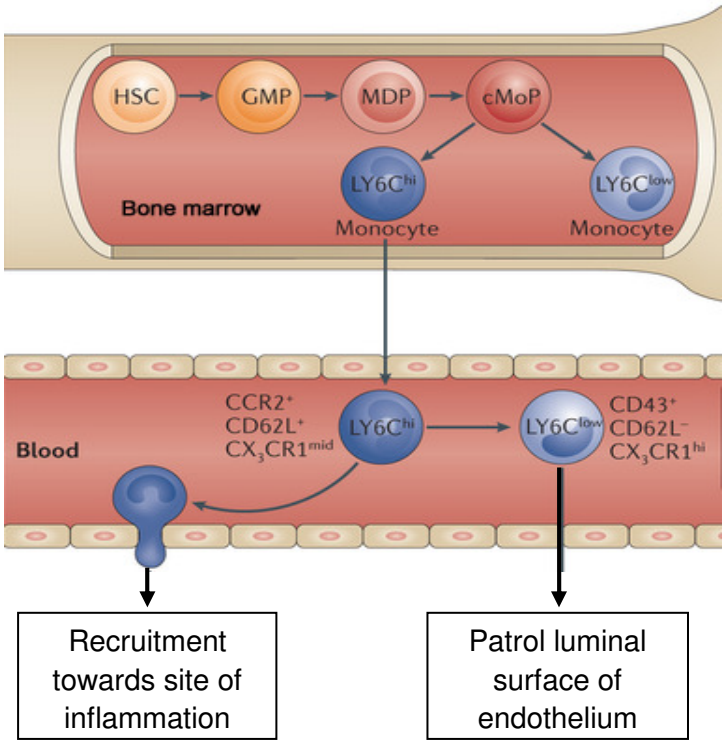

Figure 1.4: Monocyte differentiation pathway in mice. Monocytes are generated in bone marrow from hematopoietic stem cells (HSC) via macrophage DC precursors (MDP) and common monocyte progenitor (cMoP) intermediates. In steady state, Ly6C^{hi} and Ly6C^{low} subsets circulate in blood and take on different functions following inflammation. *Adapted from* (213).

In steady-state circulation, at least two distinct subsets of monocytes exist in mice and humans (214). Mouse monocyte subsets comprise a Ly6C^{hi} CX3CR1^{low} CCR2^{+} subset often referred to as 'inflammatory', and a Ly6C^{low} Cx3CR1^{hi} CCR2^{-} subset with patrolling behaviour (215). These phenotypes were identified by adoptive transfer of the two subsets, where transferred Ly6C^{low} monocytes patrolled blood vessels and migrated to non-inflamed tissues, whereas transferred Ly6C^{hi} monocytes trafficked to

sites of inflammation (214). Ly6C^{hi} monocytes can also give rise to Ly6C^{low} monocytes in the absence of inflammation (216). This has been shown in the blood of mice receiving Ly6C^{hi} grafted cells, and has been suggested to occur via re-entry into bone marrow and differentiation into Ly6C^{low} monocytes here which then re-enter the circulation and take up roles as the patrolling subset (211). Ly6C^{low} monocytes have a longer half-life than Ly6C^{hi} monocytes, at 2 days, which can be extended to 2 weeks in the absence of their renewal from Ly6C^{hi} monocytes (205).

Human monocytes are defined based on CD14 and CD16 expression (217) which identifies a CD14^{+} subset that can be further divided into 'classical' CD14^{+}CD16^{-} and 'intermediate' CD14^{+}CD16^{+} subsets, and a 'non-classical' CD14^{low}CD16^{+} subset (217, 218). Similarities have been found between the mouse and human subsets based on cell surface receptors as well as gene expression profiling (199). The mouse Ly6C^{hi} and human 'classical' monocyte subsets both express high CCR2 and CD62L (L-selectin) and low CX3CR1 and are recruited to sites of inflammation (219). The mouse Ly6C^{low} subset and the human 'non-classical' subset both display patrolling behaviour which may have a role in surveying endothelial integrity, and express high CX3CR1 and low CCR2 and CD62L (220, 221). The additional human 'intermediate' CD14^{+}CD16^{+} subset has also been labelled as 'pro-inflammatory' as they are capable of higher production of inflammatory cytokines such as TNFα and IL-12, and increased antigen presentation capacity (222). This subset has also been found to be increased in various diseases including rheumatoid arthritis, diabetes, bacterial sepsis, and HIV, to name a few (223-226).

While certain aspects of monocyte subsets are clearly conserved between mouse and human, some important distinctions exist, such as receptors involved in uptake of apoptotic cells, nucleic acid sensing via TLRs, and others (227) and therefore it is important to be cautious with any direct comparisons.

1.2.3 Monocyte differentiation

Monocytes differentiate into macrophages and DCs following inflammation, however they most likely do not readily give rise to tissue macrophages under steady state conditions. Mouse parabiosis experiments were carried out between wild-type and $CCR2^{-/-}$ mice, to identify whether the reduced number of monocytes in a $CCR2^{-/-}$ mouse could be replenished from the wild-type mouse (228). While blood monocytes from the $CCR2^{-/-}$ mouse were replenished, tissue macrophage chimerism remained negligible suggesting that peripheral blood monocytes do not give rise to tissue macrophages under these conditions. Depleted lung macrophages in this system were replenished primarily by in situ proliferation which was dependent on M-CSF and GM-CSF but not IL-4. Other work has found that tissue macrophage populations seem to be derived from embryonic progenitors that seed tissues before birth and maintain themselves by self-renewal (213). Development of these yolk sac-derived macrophages was independent of the transcription factor Myb, which on the other hand is needed for development of HSC and all $CD11b^{+}$ monocytes and macrophages in the adult (208). Langerhans cells of the epidermis were also found to be established during foetal development in a separate study (229), as were a subset of cardiac macrophages (230), and alveolar macrophages which was GM-CSF-dependent (231). Some degree of monocyte replenishment is however required to maintain macrophage populations in the uterus during murine pregnancy (232). Therefore the exact kinetics of monocyte and macrophage differentiation are likely to be tissue-specific.

1.2.4 Monocyte response to inflammation

During inflammation, monocytes form one of the first lines of defence. The bone marrow receives signals from pro-inflammatory cytokines and TLR ligands to increase monocyte production (233, 234). Activated monocytes also show increased resistance to apoptosis by downregulation of caspase-8/FLICE (235). This allows them more time

to home to the tissues to which they are recruited as a result of inflammatory stimuli, and to differentiate into macrophages or DCs which have a longer lifespan, and begin to target the infection (236).

Cytokines and chemokines are the main factors mediating effector cell recruitment to inflammatory sites (237). In the periphery, Ly6C^{low} monocytes can be recruited more quickly to a site of inflammation than Ly6C^{hi} monocytes, but despite this, the ensuing immune response is largely characterised by the Ly6C^{hi} inflammatory subset (221). Monocyte trafficking to sites of inflammation is largely dependent on the CCR2 receptor, and its ligands CCL2 (MCP-1) and CCL7 (MCP-3) (234). CCL2 in particular is induced as a result of many infections in serum and inflamed tissues, and most nucleated cells produce CCL2 upon receipt of a pro-inflammatory stimulus or microbial engagement of innate immune receptors (238, 239). Both CCL2 and CCL7 are however needed for appropriate monocyte recruitment during infection, evidenced by findings that CCL2$^{-/-}$ mice do not have as severe monocyte depletion as CCR2$^{-/-}$ mice in blood and spleen (240). A key role for monocyte-expressed CCR2 is mediating monocyte egress from bone marrow into the circulation during infection (234). Findings from *L. monocytogenes* infection show that CCL2 is released from bone marrow stromal cells in response to weak TLR or type I IFN signals, providing a mechanism whereby peripheral infections can induce bone marrow monocyte egress (241, 242).

Other chemokines and chemokine receptors also play a role in regulating monocyte trafficking and recruitment. CCR1 and CCR5 are expressed by monocytes and bind a variety of shared ligands including CCL3 (MIP1α), CCL4 (MIP1β), CCL5 (RANTES) and CCL7 (MCP-3) between the two of them (243, 244), many of which are induced in lungs of IAV-infected mice (180). CCR1 and CCR5 expression is upregulated upon monocyte differentiation to macrophages, with an associated chemotactic response to

MIP1α and reduced response to MCP-1, as CCR2 is downregulated on differentiated macrophages (243). CX3CL1 (fractalkine) primarily mediates the function of Ly6C^{low} monocytes by providing a survival signal as well as being necessary for patrolling during steady-state and tissue invasion following infection (221, 245)

The mechanism of trafficking employs use of integrins and adhesion molecules expressed on the cell surface in a process of rolling, adhesion and transmigration (246). CD62L has been identified as a major player in leukocyte recruitment, with findings that lack of cell-surface L-selectin reduced monocyte migration into inflamed peritoneum by 72-78% following an inflammatory stimulus (247). Monocyte-expressed LFA1 (lymphocyte function-associated antigen 1) and MAC1 (macrophage receptor 1) both recognise and bind to ICAM1 (intercellular adhesion molecule 1), but exhibit different crawling patters, likely due to differential expression of these receptors during steady state and inflammation, as well as on different monocyte subsets (221). Both contribute to monocyte crawling, particularly in the mouse Ly6C^{low} subset rather than the Ly6C^{hi} subset, however MAC1 plays the more prominent role in adhesion during inflammation (248, 249). Atherosclerosis has been used as a model used to identify much of what is known about leukocyte trafficking, and has identified roles for PECAM1 (platelet endothelial cell adhesion molecule 1), PSGL1 (P-selectin glycoprotein) and VLA4 (very late antigen 4) in monocyte adhesion, tethering and rolling (250, 251). Following recruitment to inflammatory sites, monocytes can differentiate into macrophages and DCs.

1.2.5 Fates of recruited monocytes

The plasticity of monocytes is apparent by their ability to differentiate into different types of macrophages and DCs following recruitment to tissues (252). In the tissues, macrophages contribute to degradation of apoptotic cells via phagocytosis, leukocyte

recruitment and instructing the adaptive immune response, depending on the functional phenotypes they acquire from the tissue and immunological environment (253).

Macrophages can be broadly grouped into M1 and M2 subsets, although in reality a continuum of differentiation exists of which these are the two opposite ends (254). M1 are the 'classically activated' subset that differentiate in response to IFN and TLR signalling and are associated with Th1 responses. M2 are 'alternatively activated' and further divided into M2a, M2b or M2c following exposure to IL-4/IL-13, immune complexes with IL1β or LPS, and IL-10, TGFβ or glucocorticoids, respectively, and mediate Th2-associated effector functions (255). An additional subset of suppressor macrophages has recently been identified in mycobacterial infection that are distinct from M1 and M2 subsets as they down-regulate T cell production of Th1 and Th2 cytokines while enhancing Th17 cytokines IL-17 and IL-22, and act as potent suppressors against T cell mitogenesis (256).

M1 macrophages express high levels of pro-inflammatory cytokines such as IL1β, TNFα, IL-6, IL-12 and IL-23, as well as toxic intermediates nitric oxide (NO) and reactive oxygen species (ROS) (257). They have high antigen presentation capacity and are implicated in initiating and sustaining infection. M1 macrophages are necessary for an appropriate immune response to *Listeria monocytogenes* and *Mycobacterium* tuberculosis as they kill the bacterium and activate adaptive immunity (254, 258). The inflammatory response must however be controlled by apoptosis of these macrophages, as the ensuing cytokine storm may be detrimental to the host.

M2 macrophages on the other hand are associated with resolution of inflammation by containing parasite infection and promoting tissue remodelling (259). They play important roles in suppressing inflammation in RSV-induced lung injury and fibrosis in severe acute respiratory syndrome (SARS) coronavirus infection (260, 261), controlling

parasite burden (262), and improving outcome to EAE (263). M2 macrophages are characterised by low level production of inflammatory cytokines IL-1, IL-6, TNFα and IL-12, but high IL-10 (252), and by overexpression of scavenger receptors (264). In mice, M2 macrophages can be distinguished from M1 by expression of markers such as FIZZ1 and Ym1 (265). Characteristic differences exist within this subset. M2a macrophages are involved in Th2 immune responses and are pro-fibrotic, while M2b macrophages are most similar to the M1 subset as they retain high IL-1, IL-6 and TNFα production, but with concomitant high IL-10 and low IL-12 (252). The M2c subset are induced by IL-10 and TGFβ and have roles in tissue repair and remodelling (266).

Most of the work differentiating M1 and M2 macrophages has been carried out in mouse models, with little known regarding translation to human macrophages. A transcriptional profiling study of human monocyte to macrophage differentiation identified that M-CSF-driven monocyte-to-macrophage differentiation is associated with expression of a large part of the M2 transcriptome, suggesting that a default shift towards M2 may occur under homeostatic conditions (267). Furthermore significant differences were identified in membrane receptor expression, while little difference was seen in nuclear factors. M1 macrophages had higher expression of apoptosis-related genes and molecules including TNF, CCR7 and TRAIL, whereas M2 macrophages were enriched for genes encoding TGFβ receptor II, Dectin 1, DCSIGN (CD209), and many more (267). Components of the pro-inflammatory IL-1 system are differentially expressed on M1 and M2 macrophages. IL-4 and IL-13, which polarise macrophages to an M2 phenotype, have been shown to increase the expression of the decoy receptor IL-1RII, induce IL-1 receptor antagonism and inhibit IL-1 (268, 269).

While monocytes do not tend to give rise to cDC or pDC, as discussed earlier, recruited monocytes may differentiate into inflammatory DCs during infection, most notably the TNFα/inducible nitric oxide synthase (iNOS)-producing DCs (TipDC) subset, which has

been identified in mice in a number of infections including IAV infection, bacterial *Listeria monocytogenes*, *Brucella melitenisis* and *Salmonella* infections, and parasitic infections including *Trypanosoma brucei*, *Leishmania major*, and *Toxoplasma gondii* (270-276). These cells have low-to-intermediate CD11c expression, and differentiate from Ly6C^{hi} monocytes. In the colon, monocytes differentiate into regulatory M2-like macrophages under steady-state conditions, but following colitis they differentiated into pro-inflammatory DCs and produced high levels of IL-12, IL-23, TNF and iNOS (277). TipDCs have been shown to contribute either positively or negatively to the outcome of different infections. They play a helpful role in limiting pathogen burden in the bacterial *L. monocytogenes* infection in the spleen while not being required for the initiation of an adaptive T cell response, whereas during parasitic trypanosome infection they represent a major pathogenic population that mediates necrosis in the liver (271, 274). In lethal IAV infection they are required for efficient IAV-specific T cell responses, but excessive TipDC recruitment to the lungs also contributes to pathogenicity (270). The type of infection, affected tissues, and magnitude of recruited cells all likely contribute to the protective versus pathogenic outcomes induced.

1.2.6 Monocytes in IAV infection

The role of monocytes recruited to the lungs during IAV infection is not straightforward, as some evidence points to them being protective, while others suggest they are harmful (278, 279). These differences partly come down to the number of monocytes recruited to the lungs, as a limited number offer protection while influx of large numbers induce lung pathology (280). Monocyte recruitment in IAV is largely mediated by CCL2 (MCP-1) production from inflamed lungs and CCR2 expression on monocytes. Alveolar epithelial cells infected with IAV elicited monocyte transepithelial migration *in vitro* via release of CCL2, and relied on monocyte CCR2 expression (281). Addition of IAV infected alveolar macrophages further enhanced monocyte transmigration.

Our group has previously published that monocyte influx to lungs during severe IAV infection is enhanced in the absence of iNKT cells, and that this leads to worse outcome due to excessive pulmonary inflammation (280). This is supported by work from others who found that monocytes recruited to the lung via CCR2 differentiated into inflammatory DCs that caused immune pathology, which was abrogated in the absence of CCR2 (279). $CCR2^{-/-}$ mice were also shown by another group to have a better outcome due to delayed monocyte recruitment, although an early increase in pulmonary viral titres was observed (282). A separate study also found that lack of CCR2 led to decreased immune pathology due to impaired monocyte recruitment to lungs, however this was also associated with diminished priming of virus-specific $CD8^+$ T cells and therefore delayed virus clearance (270). A partial diminution was found to be protective in this model. This supported early work showing that mice lacking MIP-1α (macrophage inflammatory protein-1α) had decreased pneumonitis, but also delayed virus clearance (283). Finally, circulating inflammatory monocytes were also shown to be recruited directly to lymph nodes where they differentiated into DCs and stimulated Th1 responses, which was dependent on CCR2 (284). This highlights a role for monocytes in initiating adaptive immune responses, which are necessary for effective IAV clearance. A protective role of monocytes during IAV infection was identified by their differentiation into type I IFN-producing DCs upon recruitment to lungs in mice (278). Depletion of monocytes reduced DC number and type I IFN responses in the lungs, causing an increase in virus titre and mortality in an IAV model that normally doesn't cause any death.

The roles of recruited monocytes in IAV pathology are therefore complex, and a fine balance exists between contributing to protective or pathological immune responses. This difference relies partly on the severity or pathogenicity of initial infection. Reduction, rather than complete elimination, of myeloid cells is likely to lead to a better outcome following severe infection (270). Outcome may also be determined by the

strain of infecting virus, as it was shown that, while less pathogenic human-adapted IAV strains do not replicate successfully in monocytes and macrophages, avian viruses such as the extremely virulent H5N1 strain, do (285). In keeping with this, analysis of gene transcription in H5N1-infected primary monocyte-derived macrophages showed higher proinflammatory gene expression of genes such as TNFα and IL1β when compared to infection with H3N2 or H1N1 viruses (286).

1.3 Myeloid-derived suppressor cells (MDSC)

1.3.1 MDSC origin and subsets

MDSCs are a heterogeneous population of myeloid progenitor cells and immature myeloid cells (IMC), comprising functionally distinct monocytic and neutrophilic subsets, which expand during acute and chronic inflammation (287). They are defined primarily by a remarkable ability to suppress T cell responses.

IMC are produced in the bone marrow (BM) and under normal non-inflammatory conditions differentiate into neutrophils, monocytes, macrophages and dendritic cells (DCs). In naïve mice, the BM contains 20-30% of IMCs, but these cells make up a tiny minority in circulation and tissues as they normally differentiate into mature cells before leaving the BM. A block in this differentiation however occurs in pathological conditions, which combined with increased myelopoiesis that occurs in response to many infections causes accumulation of IMCs. Increased myelopoiesis and expansion of MDSCs has been shown to involve hematopoietic growth factors G-CSF and GM-CSF, and is further potentiated by the inflammatory cytokine IL-6, linking inflammation to MDSC development (288, 289). Inflammatory signals ultimately activate transcription factors such as STAT3 and c/EBPβ, which are central players in MDSC generation (289). Overall, current data suggests that MDSCs are a heterogeneous population of

activated IMCs that have been prevented from fully maturing, rather than a defined subset of myeloid cells.

Attempts have been made to characterise MDSC surface marker expression, although it is difficult to differentiate them from mature neutrophilic or monocytic cells as they express similar markers, particularly in mice, and therefore the ability to suppress T cell activities is essential in MDSC characterisation. Mouse monocytic MSDCs have been characterised as being $CD11b^{+}Ly6C^{hi}Ly6G^{-}$ (identical to $Ly6C^{hi}$ inflammatory monocytes), and neutrophilic MDSC have been characterised as being $CD11b^{+}Ly6C^{int}Ly6G^{hi}$ (identical to neutrophils). Differences in classical and MDSC neutrophils have been identified by some groups, as MDSC expressed higher M-CSFR and CD244 (290). It is likely that more differences exist in both neutrophilic and monocytic MDSCs that require further characterisation. In humans, the basic characterisation of MDSCs is $CD33^{+}$ cells that lack markers of mature myeloid cells and HLA-DR, although many different phenotypic characterisations have been put forward in over 40 publications, most of which come from studies of cancer patients (291). Monocytic MDSCs are most widely characterised as $CD14^{+}HLA\text{-}DR^{low}$ or $CD11b^{+}CD14^{-}CD33^{+}CD15^{-}$ cells, and neutrophilic MDSC as $CD11b^{+}CD14^{-}CD33^{+}CD15^{+}$ in humans (288).

1.3.2 MDSC suppressive activity

The suppressive activity of activated MDSCs has been shown to require direct cell-to-cell contact, suggesting involvement of cell-surface receptors or short-lived soluble mediators. Arginase-1 (ARG1) and inducible nitric oxide synthase (iNOS) are expressed at high levels by MDSCs, and a direct role for both of these enzymes has been confirmed in mediating suppressive activity via metabolism of L-arginine, which acts as a substrate (292, 293). The metabolism of L-arginine by MDSCs depletes it

from the microenvironment, and shortage inhibits T cell proliferation through mechanisms including preventing upregulation of cell cycle regulators cyclin D3 and cyclin-dependent kinase 4 (294). iNOS generates nitric oxide (NO), which suppresses T cell functions through mechanisms involving inhibition of JAK3 and STAT5 function in T cells (295) and the induction of T cell apoptosis (296). Production of reactive oxygen species (ROS) is another characteristic mediating MDSC suppressive activity, as ROS inhibition from MDSCs isolated from cancer patients and tumor-bearing mice completely abrogated the suppressive effect of these cells *in vitro* (297, 298).

Monocytic and neutrophilic MDSCs were shown to suppress T cell functions via different mechanisms, although to similar extents as each other. While both expressed ARG1, the monocytic subset also expressed high NO and low ROS, whereas the neutrophilic subset expressed low NO and high ROS (299). Others found that the suppressive nature of the monocytic subset was due to STAT1 and iNOS, while suppression by the granulocytic subset depended more on ARG1 (300). The exact mechanisms and cell types involved will vary depending on the disease.

1.3.3 MDSCs in disease settings

MDSCs were first characterised in cancer patients and tumor-bearing mice. Up to a tenfold increase in MDSC has been detected in blood of patients with different types of cancer, with both monocytic and neutrophilic subsets having been identified (301, 302). The presence of MDSC is associated with poor prognosis in cancer, with reports of increased MDSCs correlating with reduced survival (303). In mice, MDSCs expand systematically upon inoculation with tumor cells. MDSCs were shown to accumulate well in the spleen, which were then amplified in this organ under the influence of angiotensin II to generate precursors for tumor-associated macrophages (304). Similar mechanisms were found by the same group in human cancer patients, where

proliferating monocytes with features of myeloid progenitors and T-cell tolerizing potential were found in splenic marginal zone of tumor-bearing patients (305).

MDSCs have since been identified in multiple other diseases including acute and chronic inflammation, sepsis, traumatic stress and bacterial and parasitic infections (287), with the majority of this work having been carried out in mice. In IAV infection, MDSCs were identified as $CD11b^{+}Gr1^{+}$ cells with ARG1 and iNOS activity which were expanded following infection (306). Frequency of MDSCs was higher in mice lacking iNKT cells, which had a poorer outcome to infection. In this model, iNKT cells abolished the suppressive activity of MDSCs and restored IAV-specific immune responses in a CD1d- and CD40-dependent manner. These results were mirrored in human IAV infection by identification of a subset of suppressive myeloid cells, whose suppressive activity could be reduced by iNKT cell activation. A separate study found accumulation of $CD11b^{+}Gr1^{+}$ MDSCs in $TLR7^{-/-}$ mice following IAV infection, which had increased weight loss and lung inflammation compared to wild-type mice (307). $CD11b^{+}Gr1^{+}$ MDSCs have been identified in other virus infections in mice, including hepatitis B virus infection and vesicular stomatitis virus (VSV) infection, where they caused impaired T cell functions (308, 309). In experimental autoimmune encephalomyelitis, a mouse model of multiple sclerosis, $Ly6C^{hi}$ monocytic MDSCs were expanded in spleen and blood and entered the central nervous system (310).

In humans, $CD15^{+}$ neutrophilic MDSCs have been identified from density-gradient separation of PBMCs. Neutrophils are normally excluded by this technique, however activated neutrophils and neutrophilic MDSCs have been shown to co-purify with PBMCs and associate with severe disease (311). In HIV and cancer, neutrophilic MDSC from PBMC suppressed T cell proliferation and showed impaired migration (312). Presence of activated neutrophils from PBMCs was found in systemic lupus erythematosus (SLE), which showed increased secretory capacity for type I IFNs, IFNγ

and TNFα but reduced phagocytosis (313). Identification of these cells is likely to be underestimated, due to their short-lived nature and high sensitivity to freezing, rendering them undetectable in analysis of defrosted cells, as is routinely performed in many laboratories.

1.4 Invariant NKT cells

1.4.1 iNKT cell biology and phenotype

Natural killer T (NKT) cells were first identified in 1987 in mice as a distinct subset of αβ-TCR T cells with a restricted TCR Vβ repertoire (314). Following this they were shown to express the NK cell marker NK1.1 (CD161) and to be a potent source of immunoregulatory cytokines such as IL-4, IFNγ and TNFα without the need for extensive cell division or differentiation (315, 316). Since then, NKT cells have been extensively characterised as CD1d-restricted lipid-reactive T cells, and can be separated into two groups, type I and type II NKT cells (317). Type I NKT cells are also known as invariant NKT (iNKT) cells and express an invariant TCR-α (Vα14Jα18 in mice; Vα24Jα18 in humans) combined with a limited TCR-β chain repertoire (usually Vβ8.2, Vβ8 or Vβ7 in mice; Vβ11 in humans) (317). This TCRαβ chain combination provides specificity for lipid antigen recognition presented by CD1d, with the prototypic antigen being the glycosphingolipid α-galactosylceramide (αGalCer) originally isolated from a marine sponge, although the original source is likely to be bacteria (318). More physiological glycolipids have since been identified from bacteria such as α-galacturonosylceramide, α- glucuronosylceramide and α- galactosyl-diacylglycerol (319, 320). Mammalian glycolipids have also been identified, including isoglobotrihexosylceramide (iGb3), β-galactosyleramide, β-glucosylceramide and the disialoganglioside GD3 (321-324). iNKT cells react very rapidly following antigenic stimulation as a result of pre-formed cytokine mRNA transcripts for IFNγ and IL4

facilitating a rapid Th1 or Th2 response, respectively (325). Hereby they are able to modulate the immune response to cancers, infection, asthma, allergy, diabetes and other diseases (326-329). iNKT cells play diverse roles in the immune response to different diseases, taking on either protective or pathogenic roles. They interact with APCs and influence the functions of many other immune cell types including NK cells, conventional T cells, neutrophils, macrophages and DCs, thereby acting as a bridge between innate and adaptive immune systems (330). Further understanding of iNKT cell dynamics has been aided by the recent use of intravital microscopy allowing the visualisation of iNKT cell interactions and trafficking in living mice (331). This has allowed identification of iNKT cells using *Cxcr6*$^{gfp/+}$ mice and showed that they crawl along sinusoidal endothelial cells independent of blood flow direction, and arrest almost immediately following αGalCer injection; a phenomenon which can be blocked with anti-CD1d (332).

The function of type II NKT cells is less well understood, although only one glycolipid antigen has been identified to date that activates these cells which is sulfatide; a mammalian sulphated β-GalCer analogue that promotes type II NKT cell immunosuppression (333). Non-glycolipid antigens such as lysophosphatidylcholine also activate type II NKT cells, as do non-lipidic small molecules (334). They seem to play a role in inhibiting tumor rejection and suppressing autoimmunity (333, 335). My studies focus on the type I invariant NKT cells, and therefore this subset will be discussed in further detail here.

1.4.2 iNKT cell development

iNKT cells represent a developmentally and functionally distinct rare cell subset, with numbers varying greatly between individuals although remaining stable over time (336). Peripheral blood iNKT cells range from 0.01 – 1% of total T cells in healthy

humans, but it is not fully understood what causes the different frequencies between individuals (337, 338). iNKT distribution in human tissues is not well studied, but they are thought to be around 10 times less frequent than in mice (317). In mice, iNKT cells represent around 0.5% of T cells in blood and peripheral lymph nodes, 5% of T cells in spleen, mesenteric and pancreatic lymph nodes and up to 30% of hepatic T cells (317).

iNKT cells constitute a separate lineage of cells based on their unique TCR repertoire, NK lineage marker expression, tissue distribution and functional properties. iNKT cells develop in the thymus after birth from the common lymphoid progenitor (CLP). At the double positive stage after TCR expression, the transcription factor RORγt indirectly induces expression of Bcl-xL to prolong thymocyte survival and allow rearrangement of Vα14 and Jα18 TCRα segments in mice (339). Following this stage, these double positive thymocytes that encounter CD1d expressed by cortical thymocytes become committed to develop into mature iNKT cells (340). This step is dependent on SLAM receptors that signal through SLAM-associated protein (SAP) and the tyrosine kinase Fyn to activate the NFκB signalling cascade, as mice and humans lacking SAP exhibit defective iNKT cell development (341, 342). Mouse iNKT cells downregulate CD8 following this step, although CD8 is expressed by some human iNKT cells, and begin the maturation process (343). iNKT cells undergo four stages of maturation; stages 0 – 3, which have been best characterised in mice (344). At stage 0 iNKT cells are $CD24^{+}CD44^{low}NK1.1^{low}$ and $CD4^{+}$. Cells at this stage are not proliferating and only represent 0.001% of total thymocytes (345). They downregulate CD24 to enter stage 1 and become highly proliferative, expanding the iNKT cell pool. Proliferating iNKT cells then upregulate CD44 as they enter stage 2, although apart from this change both stages 1 and 2 are mainly involved in expanding the population (346). At stages 1 and 2, iNKT cells are potent IL-4 and IL-10 producers, while producing little IFNγ. In stage 3, iNKT cells upregulate NK cell receptors such as NK1.1 (CD161) and undergo much less proliferation (347). Here they produce more IFNγ, less IL-4 and negligible IL-10

(348). iNKT cells can mature into stage 3 of development either in the thymus, or in the periphery, but this stage is CD1d-dependent (349). Emigration from the thymus is controlled by signalling through the lymphotoxin β receptor and the sphingosine 1-phosphate receptor (350).

In humans, iNKT cells in the thymus and cord blood of neonates are made up of 90% $CD4^+$ cells, which decreases to 40% $CD4^+$ in adult blood, although implications of this are unknown (351). Loss of CD4 expression happens between stages 1 and 2 in mice (352). Functional differences in $CD4^+$ and $CD4^-$ subsets, as well as the variation in ratios of these subsets in individuals suggests that this is an important differentiation step, although it is not clearly understood what factors regulate iNKT subset differentiation (336, 343).

In contrast to conventional thymocytes, iNKT cells are a mature, immune-competent population capable of producing IL-4, TNFα and IFNγ immediately after TCR stimulation, which may explain the complex genetic requirements in their development (346, 353). A large number of factors have been identified as being important for iNKT cell development including transcription factors, cytokines and cell surface molecules. These include, but are not limited to transcription factors RORγt, Egr2, c-Myc, Id2 and T-bet (354-356), the cytokine TGF-β in driving iNKT cell expansion and maintenance (357) and cell surface CD28 and ICOS in iNKT maturation in the thymus (358).

1.4.3 iNKT cell activation

Different means of iNKT activation have been identified as being either TCR-CD1d-mediated, cytokine-driven or both, and are summarised in Figure 1.5.

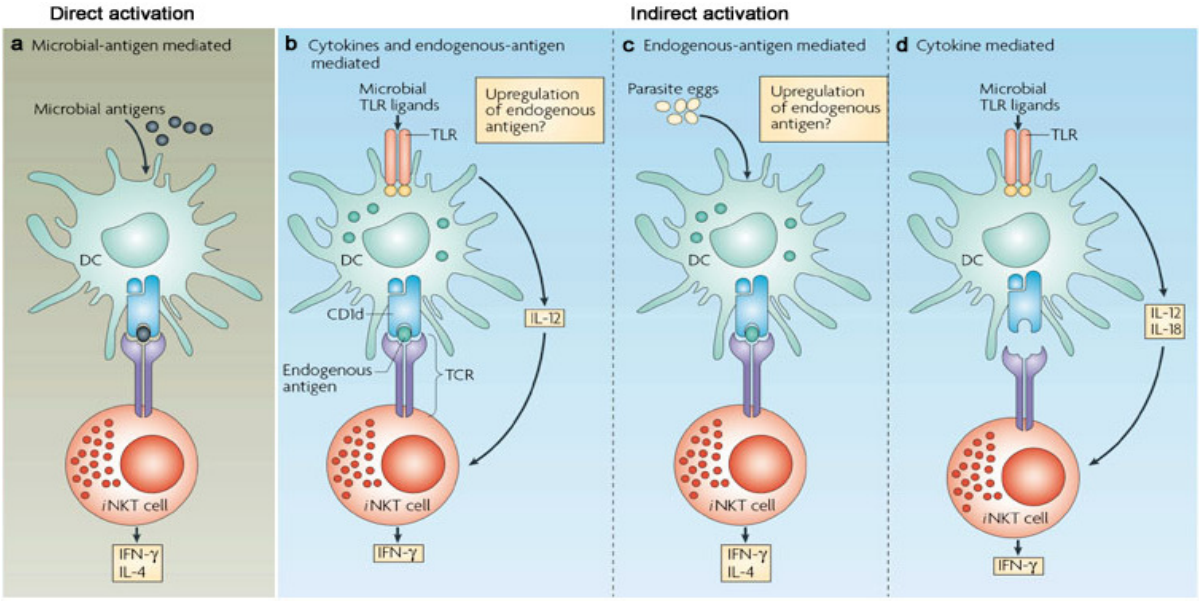

Figure 1.5: Activation of iNKT cells. (a) Direct activation following recognition of microbial derived antigens engaging the iNKT TCR. **(b)** Cytokine and endogenous antigen-mediated activation via IL-12 release from DC following TLR stimulation. **(c)** Endogenous antigen mediated activation following parasitic egg sensitisation of DCs. **(d)** Cytokine mediated activation following DC TLR ligation resulting in IL-12 and IL-18 release. *Adapted from* (359).

Direct activation (Figure 1.5a) physiologically occurs via uptake of microbial antigen such as glycosphingolipids from *Sphingomonas* species (360) and galactosyl-diacylglycerols from *Borrelia burgdorferi* (320). Purified glycosphingolipids from *Sphingomonas* can bind to CD1d and activate mouse and human iNKT cells, although the response is less potent than with αGalCer. Activation in this instance was IL-12 and TLR-independent, and also did not require the self-ligand iGb3 (360). Mice deficient in iNKT cells had higher disease burdens following low dose *Sphingomonas* infection, however following a high dose of infection iNKT-deficient mice were protected, whereas those with iNKT cells died of shock. This shows how the iNKT cell response can be either helpful or detrimental, depending on severity of infection. Activation by *B. burgdorferi* glycolipids is also TLR-independent and induced iNKT cell proliferation and activation in mice, as well as IFNγ and IL-4 production by human iNKT cell lines (320).

iNKT cells are also activated in response to lipid antigens from house dust extract or pollen (361, 362).

Indirect activation of iNKT cells was identified by findings that iNKT cells influence outcome to many infections where microbial antigen is not present. In these circumstances, activation is instead dependent on endogenous lipid presentation by CD1d and/or cytokine production by APCs (Figure 1.5b-d).

Indirect iNKT cell activation was first shown by findings that LPS from *Salmonella typhimurium* engages TLRs and induces IL-12 production from DCs, which amplifies weak endogenous CD1d-presented antigens and led to iNKT cell IFNγ production (363) (Figure 1.5b). The mechanism was identified since DCs from $CD1d^{-/-}$ mice or mice unable to synthesise iGb3 ($Hexb^{-/-}$) did not induce iNKT IFNγ production (321). CD1d expression on APCs can be upregulated following bacterial infections such as *S. typhimurium*, *M. tuberculosis* or *L. monocytogenes* as well as by TLR stimulation with LPS or Pam_3Cys (364-366). The consequence of this is increased CD1d-dependent cytokine production by iNKT cells, even in the absence of endogenous antigen.

iNKT cells were shown to be activated by endogenous antigen iGb3, without the requirement for TLR signalling or IL-12 production from the APC in *Schistosoma mansoni* infection (367) (Figure 1.5c). The effect on CD1d expression levels or cytokines other than IL-12 in mediating this activation is not known.

Finally, iNKT cells can also be activated by cytokines such as IL-12 and IL-18 in the absence of endogenous cytokine presentation by CD1d using LPS stimulation (368) (Figure 1.5d). *In vitro*, iNKT cells can be activated by addition of physiological levels of IL-12 and IL-18 even in the absence of DCs. Intravital microscopy showed that IL12 and IL18 can also activate iNKT cells *in vivo* independently of CD1d, causing iNKT cell

arrest within liver sinusoids (331). IL-12 and IL-18 are often produced as response to infections, which provides a mechanism for iNKT cell activation in situations where glycolipids and TLR stimulation do not play a role, such as in response to viruses that do not encode glycolipid antigens.

1.4.4 iNKT cell functions

Upon activation, iNKT cells are capable of rapid Th1, Th2 or Th17 cytokine production as well as cytotoxicity. The type and magnitude of response can be either beneficial or detrimental, which is likely to be dictated by disease setting, microenvironment, type of APC, strength of TCR signal, iNKT cell subset, or a combination of these (352, 369, 370). A huge list of cytokines has been identified to date that can be produced by iNKT cells, including IL-2, IL-4, IL-5, IL-6, IL-9 IL-10, IL-13, IL-17, IL-21, IL-22 TNFα, IFNγ, TGFβ, GM-CSF, and undoubtedly others (317, 371-373). Cytotoxic functions have been shown to be mediated by perforin and granzymes, or upregulation of FasL and TRAIL (343). iNKT cell cytotoxicity is positively correlated with CD1d expression by target cells, as well as TCR affinity for the target antigen (374).

iNKT cell subsets consist of $CD4^+CD8^-$, $CD4^-CD8^-$ (DN) and in humans also $CD4^-CD8^+$ although this subset does not exist in mice (375). These subsets represent functionally distinct lineages based on their cytokine profiles. $CD4^-$ iNKT cells produce predominantly Th1 cytokines, whereas $CD4^+$ iNKT cells show more of a Th2 bias, but are also capable of Th1 cytokine production (343). Within the $CD4^-$ subset, both $CD8^+$ and $CD8^-$ share similar cytokine profiles, however the human $CD8^+$ subset is associated with more cytotoxic functions, and is able to suppress proliferation of activated T cells in vitro (376, 377). As well as CD4 and CD8 expression, cell surface receptors such as CD40 and PD-1 have been shown to influence cytokine responses (378, 379).

Different synthetic analogues of αGalCer were also able to bias cytokine production, mostly in mouse models, depending on the composition of their lipid tails (380, 381). Two prototypic lipid antigens with Th2-biasing ability have been documented, OCH and C20:2, which have shortened unsaturated tails, increased polarity and reduced hydrophobicity compared to αGalCer (382). Treatment of mice with these Th2-biased compounds is beneficial in the control of Th1-driven autoimmune diseases. OCH was associated with suppression of experimental autoimmune encephalomyelitis (EAE) (383) while C20:2 reduced the incidence of diabetes (384). C20:2 is also a more potent activator of human iNKT cells than αGalCer. Th1-biased analogues, such as the C-glycoside analogue, α-C-GalCer, bind more tightly to CD1d and are able to facilitate a sustained, although weak, interaction with the iNKT TCR (385). α-C-GalCer led to better protection against malaria and melanoma metastases; two diseases that are known to require Th-1 type responses for effective control (386). This outcome in Th1-driven responses is thought to be partially due to transactivation of NK cells through IFNγ (387). Other important differences in establishing either a Th1 or Th2 response were identified from findings that Th1-biasing antigens have to be loaded in the endosome and require presentation by DCs which also secrete IL-12, whereas Th2-binding antigens are loaded at the cell surface of more diverse APCs including macrophages and B cells (388). These findings show the plasticity of iNKT cell function and ability to modulate outcome to disease in response to activation with different compounds and APCs.

1.4.5 iNKT cell interaction with APCs

Direct contact between iNKT cells and APCs is mediated by lipid antigen presented on CD1d binding to the iNKT TCR. CD1d is expressed by a variety of cell types including epithelial cells, DCs, monocytes, macrophages and B cells (389).

Activation of conventional T cells is driven by two signals; first a specific signal involving peptide presentation by MHC molecules on APCs binding to the TCR, and a second non-specific costimulatory signal, or signals (390). This costimulatory signal was originally identified as CD28 which binds to its ligand B7-1 (CD80) or B7-2 (CD86) on APCs, although it is now known that a more diverse repertoire of costimulatory molecules exist which can transduce signals to T cells to either positively or negatively modulate TCR signalling (391). It is believed that this second costimulatory signal is not an entirely separate signal, but feeds into downstream signalling pathways by virtue of multiple costimulatory signals (392). Most costimulatory molecules are members of the immunoglobulin or tumor necrosis factor receptor superfamilies (IgSF or TNFRSF). As well as acting as the second signal to activate T cells, signals through these molecules may either positively or negatively regulate cytokine production or cytotoxicity.

Costimulatory molecules are expressed by iNKT cells and play an important role in modulating function following binding of a particular ligand (393). Differences exist between T cell costimulation and iNKT cell costimulation, determined largely by the differences in effector state of naïve cells. In T cells, the costimulatory signal provided by CD28 binding its ligand B7 is required to initiate cytokine gene transcription, whereas iNKT cells constitutively express cytokine mRNAs and can synthesise cytokines in response to TCR ligation without CD28 signals, suggesting that iNKT cells may have a lower threshold for activation (394). CD28 is however required for proper iNKT cell development, particularly in young mice, and for optimal cytokine responsiveness (378, 395). Furthermore anergy is defined differently in T versus iNKT cells, as a single dose of αGalCer induces long-term anergy in iNKT cells following their rapid cytokine secretion and proliferation, evidenced by their inability to respond to αGalCer re-challenge (396). αGalCer-induced anergy in iNKT cells is mediated by PD-1/PD-L1 interactions (397, 398). T cells on the other hand are able to maintain long-term memory in response to specific peptide antigens, and become anergic in the

absence of appropriate costimulatory signals (399). Cytokine secretion and cytotoxic functions of CD1d-activated iNKT cells is likely to depend on the balance of costimulatory and coinhibitory molecules.

As well as CD28 and PD-1 which belong to the IgSF, other members of this family which have a role in regulating iNKT cell function include ICOS, which is important for normal homeostasis and peripheral survival of iNKT cells (400) and BTLA which regulates cytokine production, as $BTLA^{-/-}$ mice mount a much more vigorous cytokine response than wild-type mice (401). The final member of this family is CTLA-4, which has not been detected on iNKT cells (378).

Members of the TNF superfamily also have roles in iNKT cell costimulation (Figure 1.6). TNF superfamily receptors are type I transmembrane proteins, and while some ligands can be secreted, they are also expressed as type II transmembrane proteins on the cell surface of many APCs. Ligation of receptor-ligand pairs enables bidirectional signalling to occur, which influences the function of the receptor-bearing cell and the ligand-bearing cell. As displayed in Figure 1.6, members with roles in mediating iNKT cell function include but are not limited to CD40, OX40, 4-1BB and GITR.

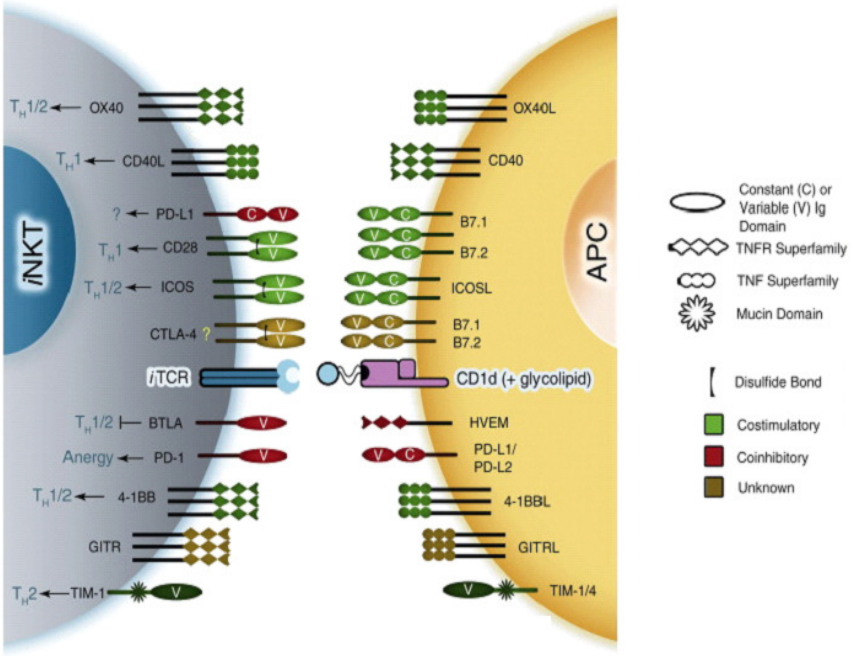

Figure 1.6: Co-stimulatory and co-inhibitory interactions between iNKT cells and APCs. iNKT cells recognise glycolipid presented by CD1d expressed on APCs. Responses are regulated by costimulatory (green) and coinhibitory (red) molecules. *Adapted from* (393).

CD40L is expressed on activated iNKT cells following αGalCer stimulation, which crosslinks with CD40 on DCs. This interaction is necessary for IL-12 production by DCs, which in turn stimulates iNKT cell IFNγ production, skewing iNKT cell responses to a Th1 phenotype, with functional consequences in metastasis and EAE (378, 402, 403). The ability of iNKT cells to link innate and adaptive immunity by maturing DCs in order to elicit effective T cell immunity was shown to be dependent on CD40 and CD40L interactions, CD80/CD86 costimulation and antigen presentation (404).

Consequences of OX40 expression by iNKT cells have been shown to vary in different settings. Interaction with OX40L on pDCs promoted crosstalk and type I IFN production by pDCs, which controlled tissue damage and CD8 T cell response to LCMV (405). Th2 cytokine responses and eosinophilic inflammation were also dependent on OX40 stimulation on $CD4^+$ T cells and iNKT cells in house dust mite-induced allergy (406).

4-1BB plays a role in iNKT cell development as 4-1BB$^{-/-}$ mice have decreased frequencies of CD3^{+}DX5^{+} NKT cells in their thymus, spleen and liver (407). 4-1BB was found to be upregulated on iNKT cells upon αGalCer stimulation, and an agonistic antibody increased IL-4, IL-13 and IFNγ secretion which was associated with more aggravated airway hyper-responsiveness (AHR) and lung inflammation (408). This was dependent on IL-4Rα, as αGalCer-mediated AHR was not developed in IL-4Rα$^{-/-}$ mice, but was exacerbated in IFNγ$^{-/-}$ mice. These findings suggest that 4-1BB functions in maintaining IL-4 and Th2 responses, however αGalCer and the same 4-1BB agonistic antibody eradicated established tumors in mice in an IFNγ-dependent manner (409). Therefore outcome may vary depending on the experimental model.

GITR (Glucocorticoid-induced TNFR) has been shown to lead to both costimulatory and coinhibitory regulation of iNKT cell responses. Agonistic GITR mAb augmented iNKT cytokine responses in one study, but inhibited αGalCer induced proliferation and cytokine production in another study (410). GITR$^{-/-}$ mice given αGalCer had higher cytokine responses and increased survival in a metastatic tumor model compared to wild-type mice, favouring a coinhibitory role in iNKT activation (411).

1.4.6 iNKT cells in IAV infection

iNKT cells have been shown to be largely protective in the outcome to IAV infection, although difference exist in the proposed mechanisms of protection, most likely due to the use of different strains of virus, as well as methods of infection. Viral genomes do not encode lipid molecules, and therefore iNKT activation must use either host lipids presented on CD1d or be entirely TCR-independent (412).

In IAV infection using the H1N1 PR8 strain (A/Puerto Rico/8/34), activation of iNKT cells by intraperitoneal αGalCer administration was found to reduce viral titres in the

lungs and enhanced early innate immune responses, without affecting the virus-specific $CD8^+$ T cell response (413). Further investigation found that mice deficient in iNKT cells ($J\alpha18^{-/-}$) have more inflammatory monocytes infiltrating the lungs, which was driven by MCP-1, and led to increased lung injury and mortality when compared to wild-type mice (414). A separate study also using PR8 also showed higher mortality in $J\alpha18^{-/-}$ mice, but found that this was driven by an increase in myeloid-derived suppressor cells (MDSC) which expressed ARG1 and iNOS and suppressed IAV-specific immune responses (306). Adoptive transfer of iNKT cells to $J\alpha18^{-/-}$ mice in this model offered protection, but not when transferred to $CD1d^{-/-}$ mice, demonstrating that the protective effect is CD1d-dependent. This suggests that iNKT cells during IAV infection are activated in a CD1d-depenedent manner, rather than cytokine driven. Another study using PR8 found that IFNγ produced by iNKT cells enhanced NK cell and $CD8^+$ T cell cytotoxicity which helped eliminate the virus and enhanced survival (415). Infection of mice with an H3N2 IAV strain also saw $J\alpha18^{-/-}$ mice develop an accelerated fatal outcome due to severe bronchopneumonia, which could be reversed by adoptive transfer of iNKT cells prior to infection (416). In contrast to the previously mentioned study, the fatal outcome in this instance was due to a reduced IAV-specific $CD8^+$ T cell response, which correlated with accumulation of $CD103^+$ DCs in mediastinal lymph nodes. A further study provided insight into how iNKT cells may be exerting their protective roles by finding that IAV-infected DCs activate iNKT cells to produce IL-22, which reduces lung epithelial damage (417).

The use of αGalCer as a vaccine adjuvant has mostly shown positive results, primarily through boosting T and B cell responses and enhancing pathogen clearance (418, 419). αGalCer was found to act as a potent mucosal adjuvant to trigger long-term protective mucosal and systemic immunity against lethal IAV infection (420). A separate study found that intranasal administration of αGalCer enhanced a protective

immune response against different IAV strains, including H5N1 by increasing the mucosal iNKT population by a partly CXCL16/CXCR6 dependent mechanism (421).

Only a couple of studies have identified iNKT cells not being directly helpful in protection against IAV infection. Heterosubtypic immunity was not found to be affected by lack of NKT cells in CD1d$^{-/-}$ mice, suggesting that they are not required in this type of protection (422). In a further study looking at iNKT cell receptors PD-L1 and PD-L2 and using adoptive transfer of iNKT cells from PD-L1$^{-/-}$ and PD-L2$^{-/-}$ mice, lack of PD-L1 on iNKT cells improved outcome to IAV, whereas lack of PD-L2 was associated with increased weight loss and pulmonary inflammation (423).

1.5 Project aims

Studies investigating the response to IAV infection have received attention in the last few years, particularly since the emergence of the H1N1 pandemic in 2009. Despite this, immune-mediated factors leading to severe disease are still not fully established; particularly when I started this project. The aims of my project were to:

1. Compare the immune response to IAV in the lungs following severe or mild infection to identify components unique to severe infection.
2. Characterise the innate immune response to IAV infection in humans with severe or mild disease, focusing on the roles of myeloid-derived cells in influencing disease severity.
3. Examine the role of iNKT cells in regulating monocyte number and function during severe IAV infection.

Chapter 2: Materials and Methods

2.1 Laboratory methods

2.1.1 Cell culture and media

Cells were cultured in sterile tissue culture flasks or plates in an incubator at 37°C with 5%CO_2. Isolated primary cells from human and mouse were cultured in RPMI-1640 (Sigma Aldrich) supplemented with 10% foetal calf serum (FCS), 2mM L-Glutamine and 50U/ml Penicillin-Streptomycin ('R10'). Media without FCS is 'R0'. Human iNKT clones were grown in 'H10' which contained human serum (HS) (First Link; batches HUT5726/HUT5141) instead of FCS. The THP-1 cell line was maintained in R10 and split twice weekly.

2.1.2 Isolation of human peripheral blood mononuclear cells (PBMCs)

Mononuclear cells were separated from whole blood using density gradient centrifugation. Blood was collected directly in heparin-containing polypropylene tubes. After mixing with an equal volume of R0, diluted blood was layered onto Lymphoprep™ (Axis-Shield) solution at a 2:1 ratio. This was centrifuged at 850xg for 25 minutes with no brake and the interface containing PBMCs harvested with a Pasteur pipette. The cells were washed twice in R10 for 10 minutes at 300xg and then re-suspended in R10 to be counted and used.

2.1.3 Whole blood lysis

Whole blood was incubated with Red Blood Cell Lysis Solution ('RBC lysis'; Qiagen) at a 1:4 ratio for 5-10 minutes at room temperature in a 15ml Falcon tube. Cells were then washed by topping up tube with R10 and centrifuging for 5 minutes at 300xg. The

supernatant was discarded and a second RBC lysis step was performed by resuspending the pellet in 3ml of RBC lysis and incubating for another 5-10 minutes at room temperature. Following another wash, cells were resuspended in R10 and counted.

2.1.4 Cryopreservation and thawing of PBMCs

PBMCs were pelleted by centrifugation at 300xg for 5 minutes. The supernatant was removed and cells were resuspended at 5-10x10^6 cells/ml freezing media (10% Dimethyl sulphoxide (Sigma Aldrich) in FCS). Cells were frozen in 1ml aliquots in labelled cryovials for storage at -80°C in a Nalgene freezing container (Thermo Scientific). For long-term storage, cells were transferred to liquid nitrogen.

Cells were thawed by placing cryovials in a 37°C pre-heated water bath. Thawed cells were transferred to a 50ml Falcon tube already containing 37°C pre-warmed R10 and washed twice in R10 by centrifugation at 300xg for 5 minutes. Cells were then counted and used.

2.1.5 Magnetic isolation of cells using MACS beads

All magnetic isolations of cells were carried out using kits from Miltenyi Biotec, according to the manufacturer's protocols (available at www.miltenyibiotec.com). Single cell suspensions were obtained by passing cells through a 30µm filter (Partec). The following isolation kits were used: human $CD14^+$ microbeads (130-050-201), human NK cell negative selection kit (130-092-657), human $CD8^+$ T cell isolation kit (130-096-495), human $CD11b^+$ microbeads (130-049-601), $CD15^+$ microbeads (130-046-601) and mouse $NK1.1^+$ iNKT cell isolation kit (130-096-513).

2.1.6 Flow cytometry

Monoclonal antibodies (mAbs) used in this thesis are listed in Table 1.1 for mouse and Table 1.2 for human studies. All mAbs were titrated to optimise intensity for staining of 200,000 cells in 30µl of FACS buffer (PBS containing 10% FCS and 1% BSA) by staining with varying concentrations of mAb. All flow cytometry samples were acquired on a 3 laser, 9 colour, CyAn^{TM} ADP Flow Cytometer and analysed using Summit 4.3^{TM} (both Dako).

Surface antigen staining: Cells were incubated for 20 minutes at 4°C in the dark with panels of fluorochrome conjugated mAbs in 96 well plates in FACS buffer. Cells were then washed twice in FACS buffer and re-suspended in a total of 400µl FACS buffer for acquisition. If primary and secondary mAbs were used, cells were first stained with primary mAb as described above, washed twice in FACS buffer, and stained with the secondary mAb for another 20 minutes as described above.

Intracellular cytokine staining (ICS): $2x10^5$ PBMCs were incubated in round bottomed 96-well plates in a total volume of 200µl culture media with 1µg/ml *Escherichia coli* lipopolysaccharide (LPS) (Sigma Aldrich) for 6 or 18 hours, and 10µg/mL Brefeldin A (Sigma Aldrich) was added for the last four hours of stimulation. For CD107a staining, 0.1µg of anti-human CD107a was added at the start of the stimulation period to $2x10^5$ cells in 200µl. Surface antigens were stained as described above, after which cells were fixed in 1% paraformaldehyde diluted in PBS (Sigma Aldrich) for 15 minutes at room temperature. Cells were then washed and re-suspended in 30µl of FACS buffer containing 0.5% Saponin (Sigma Aldrich) with conjugated mAbs. Cells were washed twice, fixed as described above and re-suspended in 400µl FACS buffer for acquisition.

For apoptosis studies, surface antigens were first stained as described above. Cells were then washed once in FACS buffer and once in 'binding buffer' (eBioscience). Cells were re-suspended in 50µl binding buffer containing Annexin V and left for 10 minutes in the dark at room temperature. Cells were washed and re-suspended in 200µl binding buffer, to which 0.2µg of 7AAD, a fluorescent DNA intercalator which marks dead cells, was added. Following a 15 minute incubation, samples were acquired immediately on a flow cytometer.

For detection of IAV-specific T cells, an MHC-I tetrameric complex (HLA-A*0201) loaded with peptide (GILGFVFTL) derived from the conserved M (Matrix M58-66) virus protein, and conjugated to PE was employed (424, 425). When used, cells were incubated with 20ng of tetramer for 15 minutes at 37℃ in a 96-well plate in R10. Following this, cells were washed twice and stained with surface antigens as described above.

Antibody	Conjugate	Clone	Host & Isotype	Supplier	Cat. Number
CCR2	APC	475301	Rat IgG2B	R&D	FAB5538A
CCR7 (CD197)	APC	4B12	Rat IgG2a, κ	eBioscience	17-1971
CD115	PE	AFS98	Rat IgG2a	Miltenyi	130-096-308
CD3	APC-eFluor780	145-2C11	Armenian Hamster IgG	eBioscience	47-0031
CD206	PE-cy7	C068C2	Rat IgG2a, κ	BioLegend	141719
CD45 (B220)	FITC	RA3-6B2	Rat IgG2a, κ	BD	553088
Ly6C	eFluor450	HK1.4	Rat IgG2c, κ	eBioscience	48-5932
Ly6G	FITC	1A8	Rat IgG2A	Miltenyi	130-093-138
Ly6G	APC	1A8	Rat IgG2a, κ	BioLegend	127614
IL-12	PE	C17.8	Rat IgG2a, κ	eBioscience	12-7123
TNF-a	APC	MP6-XT22	Rat IgG1, κ	eBioscience	17-7321
HA primary	Unconjugated	(H26-E33)	Mouse IgG	In house	n/a
HA secondary	Alexa Fluor 488	n/a	Goat IgG	Life Technologies	A-11001

Table 2.1: Mouse antibodies used in studies

Antibody	Conjugate	Clone	Host & Isotype	Supplier	Cat. Number
Annexin V	PE	n/a	n/a	eBioscience	88-8102
7AAD	n/a	n/a	n/a	eBioscience	00-6993
CCR7	PB	G043H7	Mouse IgG2a, κ	BioLegend	353210
CD11b	APCe-fluor780	ICRF44	Mouse IgG1, κ	eBioscience	47-0118
CD134 (OX40)	PE	ACT34	Mouse IgG1, κ	BD	555838
CD134 (OX40L)	APC	ACT35	Mouse IgG1, κ	BD	563473
CD137 (41BB)	FITC	4B4	Mouse IgG1, κ	eBioscience	11-1379
CD137 (41BB)	APC	4B4-1	Mouse IgG1, κ	BioLegend	309809
CD137L (41BBL)	PE	5F4	Mouse IgG1, κ	BioLegend	311503
CD14	PEcy7	61D3	Mouse IgG1, κ	eBioscience	25-0149
CD15	APC	HI98	Mouse IgM, κ	BioLegend	301907
CD15	PERcP	W6D3	Mouse IgG1, κ	BioLegend	323018
CD16	eFluor450	CB16	Mouse IgG1, κ	eBioscience	48-0168
CD16	PE	B73.1	Mouse IgG1, κ	BioLegend	360704
CD163	PE	GHI/61	Mouse IgG1, κ	BioLegend	333606
CD163	PERcP	215927	Mouse IgG1	R&D	FAB1607C
CD178 (FasL)	PE	NOK-1	Mouse IgG1, κ	eBioscience	12-9919
CD27	FITC	M-T271	Mouse IgG1, κ	BioLegend	356404
CD28	APC	CD28.2	Mouse IgG1, κ	BioLegend	302912
CD3	APC-eFluor780	UCHT1	Mouse IgG1, κ	eBioscience	47-0038
CD3	FITC	UCHT1	Mouse IgG1, κ	eBioscience	11-0038
CD3	PEcy7	UCHT1	Mouse IgG1, κ	BioLegend	300420
CD38	APC	HIT2	Mouse IgG1, κ	eBioscience	17-0389
CD4	PB	RPA-T4	Mouse IgG1, κ	BioLegend	300521
CD4	PEcy7	RPA-T4	Mouse IgG1, κ	eBioscience	25-0049
CD56	PEcy7	HCD56	Mouse IgG1, κ	BioLegend	318318
CD62L	PE	DREG56	Mouse IgG1, κ	eBioscience	12-0629
CD62L	APC	DREG-56	Mouse IgG1, κ	BioLegend	304810
CD8a	eFluor450	RPA-T8	Mouse IgG1, κ	eBioscience	48-0088
CD8a	PERcP	HIT8a	Mouse IgG1, κ	BioLegend	300922
CD95 (Fas)	eFluor450	DX2	Mouse IgG1, κ	eBioscience	48-0959
HLA-DR	FITC	L243	Mouse IgG2a, κ	BioLegend	307603
PD-1	APC	MIH4	Mouse IgG1, κ	eBioscience	17-9969
Vα24 Jα18 TCR	FITC	6B11	Mouse IgG1, κ	BD	558371
Vα24 Jα18 TCR	APC	6B11	Mouse IgG1, κ	eBioscience	17-5806
CD107a	FITC	eBioH4A3	Mouse IgG1, κ	eBioscience	11-1079
IFNγ	APC-cy7	4S.B3	Mouse IgG1, κ	BioLegend	502529
IL-10	PE	JES3-9D7	Rat IgG1, κ	eBioscience	12-7108
IL-10	APC	JES3-9D7	Rat IgG1, κ	BioLegend	501410
IL-12	eFluor660	eBioHP40	Mouse IgG1, κ	eBioscience	50-7235
IL-17	APC-cy7	BL168	Mouse IgG1, κ	BioLegend	512320
IL-6	FITC	MQ2-13A5	Rat IgG1, κ	BioLegend	501104
MCP-1	FITC	2H5	Armenian Hamster IgG	eBioscience	11-7096
TNFα	eFluor450	Mab11	Mouse IgG1, κ	eBioscience	48-7349
4-1BB	Unconjugated	4B4-1	Mouse IgG1, κ	BD	555955
4-1BBL	Unconjugated	C65-485	Mouse IgG1, κ	BD	559445

CD1d	Unconjugated	CD1d42	Mouse IgG1, κ	BD	550254
FasL	Unconjugated	NOK-1	Mouse IgG1, κ	eBioscience	16-9919
IL-12	Unconjugated	C8.6	Rat IgG	Thermo Scientific	M121
TNFR	Unconjugated	H398	Mouse IgG2a	eBioscience	BMS106
NKp46	Unconjugated	9 E 2	Mouse IgG1, κ	eBioscience	16-3359
Fixable viability dye	eFluor780	n/a	n/a	eBioscience	65-0865

Table 2.2: Human antibodies used in studies

2.1.7 FACS sorting

Samples for FACS sorting were stained in FACS buffer (Methods 2.1.6) and resuspended at a density of between $1x10^7$ and $5x10^7$ cells/ml. Samples were kept on ice before, during and after the sort. Sorting was carried out using a MoFlo^{TM} XDP (Beckman Coulter) sorting machine with assistance from Craig Waugh and Kevin Clark at the WIMM Flow Facilities.

2.1.8 iNKT cell clone

Vα24$^+$ Vβ11$^+$ iNKT clones LH22 was used in these studies, which were characterised and derived as previously described (426). Briefly, iNKT clones were generated by positively selecting Vα24$^+$ T cells from PBMCs using MACS beads (Miltenyi Biotec). These were then seeded onto 96-well plates together with gamma-irradiated allogeneic feeders from three donors and cultured in H10 with PHA. Three days later, IL-2 was added (200U/ml, Peprotech). After 15-20 days, cells were screened for Vα24$^+$ Vβ11$^+$ CD1d tetramer$^+$ cells which were expanded with irradiated feeders and PHA as above.

iNKT cell clones stored in liquid nitrogen were thawed in warm H10 and maintained in H10 by stimulating with allogeneic feeders and 45μg/ml PHA (Remel) every 14 days. 200U/ml IL-2 (Peprotech) was added every 3-4 days and media was changed every 3-4 days or when necessary.

2.1.9 Monocyte-iNKT co-cultures

$2x10^5$ $CD14^+$ positively selected monocytes were plated in round-bottom 96-well plates at differing ratios to iNKT clones and incubated for either 6 or 24 hours at 37℃ in 5%CO_2. Co-cultures were set up in 200µl H10 media. Where indicated in the text, 4-1BB blocking antibody (4B4-1; BD), and 4-1BB ligand blocking antibody (C65-485; BD) (427) were added at the beginning of the co-culture at 5µg/ml each. CD1d blocking antibody (CD1d42; BD) was added at 10 or 25µg/ml. 10µg/ml TNFR1 blocking antibody (H398; eBioscience) and 2, 5 or 10µg/ml TNFα neutralisation antibody (MAb1; eBioscience) were used. Recombinant human TNFα (Peprotech) was added at varying concentrations from 5-500ng/ml. When used, α-GC ($C_{50}H_{99}NO_9$; Enzo Life Sciences) was added after addition of any blocking antibodies at 0.4µg/ml. Prior to use, αGalCer was heated at 80℃ for 5 minutes and sonicated for 3x1 minute.

For monocyte:NK and monocyte:CD8 T cell co-cultures, monocytes were co-cultured with NK cells or CD8 T cell clones as described above at differing ratios. NK cells were negatively isolated using MACS beads according to manufacturer's protocol and activated with 5µg/ml anti-NKp46 (9E2; eBioscience). Nef-specific $CD8^+$ T cell clones isolated from an HIV patient with delayed disease progression and clone-specific peptide (FLKEKGGL) were a kind gift from Professor Tao Dong (University of Oxford) (428).

2.1.10 iNKT cell proliferation assay

iNKT cell proliferation was measured using a standard Carboxyfluorescein succinimidyl ester (CFSE) fluorescence assay (Invitrogen). iNKT clones were prepared by incubating with CellTrace™ CFSE (C34554) according to the manufacturer's protocol. Briefly, cells were washed in R0 and re-suspended in warm PBS supplemented with 1% BSA (Sigma Aldrich) at a concentration of $1x10^6$ cells/mL. 10mM of CFSE was

added to the cell suspension which was mixed thoroughly and incubated for 10 minutes at 37℃ in the dark. After incubation, 10mL of ice cold R10 was added to the cells followed by a 10 minute incubation on ice. Cells were then washed three times with R10. To induce proliferation, $2x10^5$ CFSE labelled cells were incubated with $5x10^4$ monocytes and αGC (0.4μg/mL) in round bottomed 96 well plates in 200μl. After five days of co-culture, fluorescence was measured using a flow cytometer. Reduction in CFSE staining indicates cells that have divided, which was measured against a sample of CFSE-labelled iNKT cells that were fixed immediately after the point of CFSE labelling on day 0.

2.1.11 Transwell experiments

Separation of cells in culture was performed using Transwell® inserts (Corning) with a 0.4μm pore diameter for a 24 well plate. $CD14^+$ isolated monocytes were first added to a 24 well plate in 600μl of media (H10). The transwell insert was then placed in the well, and 100μl of monocytes and iNKT cells ± αGC were added in the insert in H10. All cells were seeded at $1x10^6$ per ml. The 0.4μm pore size of the transwell allowed diffusion of soluble factors but prevents direct cell contact through the membrane.

2.1.12 *In vitro* IAV infection of monocytes

Primary $CD14^+$ positively selected monocytes from human blood were infected with A/PR/8/34/H1N1. $2x10^6$ monocytes were cultured with 40 hemagglutination units (HAU)/ml of PR8 in 400μl R0 containing 2μg/ml trypsin (Sigma Aldrich) in a 15ml Falcon tube for 2 hours at 37℃ and 5% CO_2 to allow for virus adsorption. Cells were then washed twice and plated out in 6-well plates for 18 hours. Infection was confirmed with HA expression by flow cytometry (as in 2.1.6). The HA antibody was a kind gift from Professor Alain Townsend.

2.1.13 Enzyme-linked immunosorbent assay (ELISA)

Cytokine concentration in culture supernatant or mouse BAL fluid was measured by ELISA. All samples were stored at -20℃ prior to analysis. Human IL-12 and TNFα and mouse IL-6 were measured using Ready-SET-Go! kits from eBioscience, human IL-8 was measured using ELISA MAX^{TM} kit from BioLegend and human Perforin was measured using ELISA^{PRO} kit from Mabtech. ELISA wash buffer was prepared as PBS+0.05% Tween-20 (Sigma-Aldrich) according to manufacturer's instructions. 96-well flat bottom plates (Maxisorp immunoplate, Nunc-Thermofischer) were coated with 100µl capture antibody and incubated overnight at 4℃. Plates were then washed 5 times in ELISA wash buffer and blocked for 1 hour using assay diluent provided. Standards were prepared with the top concentration as described on the Certificate of Analysis and eight 1:2 serial dilutions were prepared to produce a standard curve. Plates were washed again prior to addition of samples for an overnight incubation at 4℃. Plates were then washed 5 times and 100µl/well detection antibody added and incubated for 1 hour at room temperature. Following this plates were washed 5 times and 100µl/well Avidin-HRP was added and plates incubated for 30 minutes at room temperature. After a further 5 washes, 100µl/well substrate solution was added and incubated in the dark at room temperature for 15 minutes. 50µl/well 2M H_2SO_4 was added to stop the assay. Plates were read at 450nm, subtracting background values at 570nm, on the 6800 plate reader (Bio-Rad) using microplate manager 5.2.1 software.

2.1.14 Multiplex cytokine analysis

Cytokine concentrations in culture supernatant were measured by a bead cytokine assay using the Bio-Plex^{TM} 200 system (Bio-Rad) according to the manufacturer's instructions (http://www.bio-rad.com/webroot/web/pdf/lsr/literature/10014905.pdf). This procedure utilises the same principle as an ELISA but allows for the detection of

multiple proteins in one sample due to the use of uniquely identifiable beads, created by the use of two fluorescent dyes at distinct ratios.

2.1.15 IFNγ Enzyme-Linked Immunosorbent Spot Assay (ELISpot)

Following PBMC extraction, ex vivo ELISpot assays were performed on fresh cells using methods described previously (429). For this, plates were coated the day before with 50µl of IFNγ capture antibody (1-D1K; MabTech) at 10µg/ml, and blocked with 100µl R10. $2x10^5$ total PBMC were added in duplicate to each well with peptides at a final concentration of 2µg/ml in a total volume of 100µl. Plates were incubated for 18-20 hours at 37℃. R10 was used as a negative control and 1µg/ml PHA was used as a positive control.

Plates were developed the following day by first washing six times with PBS-Tween, and then adding 50µl of 1µg/ml detector antibody (7-B6-1-Biotin; Mabtech). 50µl of 1/1000 Steptavidin conjugated to alkaline phosphatase was added following another wash with PBS-Tween. The plates were developed with a precipitating substrate ALP kit (Bio-Rad) according to manufacturer's instructions. Plates were dried and read using an ELISPOT Plate Reader (CTL). Results are expressed as spot-forming units (SFU) per 10^6 PBMCs after background subtraction.

For stimulation with pH1N1 specific peptides, sequences from the full A/CA/04/2009 proteome were split into overlapping peptides of 18-20 mers and divided into pools comprising HA, NA, NP, NS, PA, PB and M. Overlapping peptides spanning the entire length of HA were split into two pools (SO-HA1 and SOHA2).

2.1.16 Mixed leukocyte reaction (MLR)

MLRs were used to measure proliferation of T cells following addition of the following cell populations harvested following standard PBMC extraction: (a) $CD15^+$ MDSCs from the mononuclear cell layer isolated by $CD15^+$ MACS bead positive selection, (b) $CD15^-CD11b^+$ cells from the mononuclear cell layer isolated from the negative fraction from $CD15^+$ MACS bead selection, and further purified by $CD11b^+$ MACS bead positive selection, and (c) classical granulocytes harvested from above the red cell pellet,. Gamma irradiated allogeneic DCs were added to peripheral blood lymphocytes (PBL) as an activating stimulus to induce proliferation at a 1:4 ratio, and cell populations (a), (b) or (c) added at a 1:1 ratio to PBL.

After 5 days of culture at 37℃ in 5%CO_2, 1µCi of tritiated thymidine [3H-TdR] (Perkin Elmer) and 25µl media were added and incubated for a further 15-18 hours in a designated radiation incubator. Cells were then harvested on a filter mat and amount of [3H]-thymidine incorporated into DNA measured with a scintillation counter.

Percentage suppression of proliferation was calculated as amount of PBL proliferation driven by allogeneic irradiated DCs in the presence of cell subsets (a), (b) or (c) compared with alloreactive PBL proliferation in the absence of (a), (b) or (c) (100%).

2.1.17 HLA typing

HLA-type of IAV infected patients was carried out to determine HLA-A*0201 status with the help of Tim Rostron and the DNA Sequencing/MiSeq laboratory at the WIMM. For this, DNA from 1ml of whole blood was extracted using the Gentra Puregene Blood Kit (Qiagen) according to manufacturer's instructions. Briefly, blood was lysed with 3ml RBC lysis buffer, washed in 15ml R10 and the pellet resuspended in cell lysis buffer. Cells were stable in cell lysis buffer for at least two years, so DNA extractions were

carried out together after all samples had been received. RNase A was added to cell lysis to remove RNA, and proteins were precipitated. Following centrifugation to pellet proteins, DNA was precipitated by mixing the supernatant with isopropanol. Following a wash in 70% ethanol, samples were centrifuged to pellet DNA, which was then resuspended in 100µl DNA hydration solution. Samples were incubated at 65°C for 5 minutes and left overnight with gentle shaking before quantifying DNA using a NanoDrop. All reagents from Qiagen.

2.1.18 RNA extractions

Total RNA was extracted from FACS-sorted Ly6C^{hi} monocytes using TRIzol® reagent (Ambion). FACS sorting was carried out directly into 1.5ml Eppendorf tubes containing 500µl TRIzol, shaken to ensure mixing of cells and TRIzol solution, and each sample was frozen at -80°C within 20 minutes of the FACS sort being complete. For lung samples, whole lung tissue was homogenised in TRIzol using glass homogenisers. After incubating for 5 minutes at room temperature, the whole sample was passed through a QIAshredder (Qiagen) for simple and rapid homogenisation. The lysate that passed through was then used for RNA extraction. RNA extraction was carried out following a protocol from the Immunological Genome Project (ImmGen) (Appendix 1). Briefly, following thawing of TRIzol samples at room temperature, 200µl Chloroform was added, tubes were shaken for 15 seconds and incubated for 3 minutes. Samples were then centrifuged for 15 minutes at 12,000g at 4°C, following which the aqueous phase containing RNA was transferred to a new tube on ice. 50ng Glycoblue (Invitrogen) was added which acts as a carrier to enable detection of low amounts of RNA. 500µl Isopropanol was then added to precipitate RNA, and samples were stored again overnight at -80°C. The following day, samples were centrifuged for 20 minutes at 12,000g at 4°C, and the pellet was washed twice in 75% ethanol at 7,400g at 4°C, before resuspending in 15µl Nuclease-free water (Qiagen). Sample quantity and quality

were measured using Nanodrop and Agilent 2100 Bioanalyser instruments, and intact, non-degraded RNA was stored at -80℃ until further processing.

2.1.19 Agilent Bioanalyser

The integrity of total isolated RNA was assessed with RNA 6000 Nano or Pico Reagents kits (Agilent) depending on quantity, and analysed with Agilent 2100 Bianalyser. This evaluated the electrophoretic trace of RNA to determine sample integrity and provides an RNA Integrity Number (RIN) which was marked on a scale of 1 to 10; 10 representing completely intact RNA. Values above 7 are considered high enough quality for hybridisation to gene expression chips and further analyses.

2.1.20 Gene expression profiling

2.1.20.1 Illumina Microarray

Ly6C^{hi} monocytes were FACS sorted from blood and BAL of A/PR/8/34/H1N1-infected wild-type and Jα18$^{-/-}$ mice as Ly6C^{hi}Ly6G^{-}CD3^{-} single cells, directly into 500µl TRIzol. RNA extraction was carried out as described above. Samples for Microarray were hybridized on Illumina MouseWG-6 v3.0 in collaboration with the High-Throughput Genomics Group at the Wellcome Trust Centre for Human Genetics, Oxford.

RNA preparation was carried out using the Illumina® TotalPrep™ RNA Amplification Kit (Ambion). Briefly, RNA samples were first subjected to reverse transcription to synthesise first strand cDNA, and then second strand cDNA. Following cDNA purification, cRNA is amplified by *in vitro* transcription (IVT), which is carried out for 14 hours, to synthesise cRNA. cRNA size distribution was measured using an Agilent 2100 Bioanalyser to ensure that the majority of fragments are in the expected size

range of 850-1500nt. Labelled cRNA was then hybridised onto the gene chips for 18 hours, after which chips were washed and scanned to detect probe intensities. Initial analysis was carried out using the Illumina BeadStudio software, and further detailed analysis was carried out with the help of Stephen Taylor from the WIMM.

2.1.20.2 Affymetrix microarray

Whole lungs from mice were first cut into 2mm pieces and placed in RNA-later. RNA extraction was performed within one week. Lung tissue was homogenised in 1ml TRIzol using glass homogenisers and RNA extractions were performed as mentioned above. Following TRIzol RNA extraction, samples were cleaned up by passing through a Qiagen mini spin column following the manufacturer's protocol. Samples for microarray were hybridised onto Affymetrix Mouse Gene 1.0 ST Array chips.

For this, GeneChip® whole-transcriptome (WT) target preparation was performed using the WT PLUS Reagent Kit (Affymetrix), which uses a reverse transcription priming method that primes the entire length of RNA, including both poly(A) and non-poly(A) mRNA to provide complete unbiased coverage of the transcriptome. 100ng input RNA was used for this purpose. Under the standard protocol, double stranded cDNA was synthesised using random hexamers attached to a T7 promoter sequence. The ds-cDNA was used as a template for T7 RNA polymerase to produce multiple copies of antisense cRNA. Following cRNA purification and quantitation, second-cycle cDNA synthesis was carried out using random hexamers containing dUTP to yield single-stranded cDNA copies. The ss-cDNA was then treated with uracil DNA glycosylase (UDG) and (APE) for fragmentation, and labelled by terminal deoxynucleotide transferase (TdT) with biotin. The fragmented, labelled samples were hybridised onto Mouse Gene 1.0 ST Array chips, stained and washed using GeneChip Fluidics Station

450, and the fluorescent signals were captured as data image files for analysis with Affymetrix Gene Expression Console.

2.1.21 Interpretation of gene expression profiles

Interpretation of microarray data was performed using the Database for Annotation, Visualisation and Integrated Discovery v6.7 ('DAVID'; NIAID, NIH) (430, 431), MetaCore™ (Thomson Reuters) and Gene Set Enrichment Analysis ('GSEA'; Broad Institute) (432).

DAVID was used for functional annotation of significant gene lists ($p \leq 0.05$). It works by using an enrichment analytic algorithm with annotations covering Gene Ontology (geneontology.org) terms, protein-protein interactions, protein functional domains, bio-pathways and over 40 more annotation categories to group genes from the input list into groups associated with a common biological process.

Metacore is a knowledge-based package used to decipher functional information from lists of genes in order to identify pathways, networks and processes associated with genes of interest. It is based on high-quality manually-curated data of protein-protein, protein-DNA and protein-RNA interactions. Fold changes and p values from microarray data are entered to identify relevant biological networks associated with these genes, enabling visualisation of networks based on fold change and significance. For analyses performed as part of this thesis, only genes with a p value ≤ 0.05 were included.

GSEA is a powerful analytical tool which was used to evaluate microarray data to determine whether pre-defiled sets of genes, grouped together by biological processes, showed statistically significant, concordant differences between two phenotypes. The entire gene list is ranked so that genes expressed highly in one group are at the top,

and genes expressed highly in the other group are at the bottom. GSEA is then used to determine whether members of a particular gene set occur towards the top or bottom of the list in order to see which phenotype that particular gene set is associated with. Pre-ranked gene lists which were generated according to the moderate t-statistic computed by limma were input for this purpose. Gene lists were filtered so that very lowly expressing transcripts were removed. No significance cut-off was applied, and therefore these lists contain a larger cohort of genes to test against. The output includes an enrichment score (ES) which reflects the degree to which a gene set is overrepresented at the top or bottom of the ranked list of genes. The higher the ES, the greater the enrichment is of the particular gene set towards the top of the ranked list and the lower the score, the greater the enrichment is towards the bottom of the list. The normalised enrichment score (NES) is the primary statistic for examining gene set enrichment results as it normalises the enrichment score for gene set size and correlations between gene sets and expression dataset. The nominal p value estimates the statistical significance of the enrichment score for a particular gene set.

2.2 Human studies

2.2.1 Patients and participants

Patients with pandemic influenza A pH1N1 (A/CA/04/2009) infection who required hospitalization in England between November 2010 and February 2011 were recruited via MOSAIC (Mechanism of Severe Acute Infection Consortium). All patients with influenza-like illness were recruited from Brompton Hospital and Royal Liverpool Hospital and clinical data collected at point of recruitment. Blood samples were collected in sodium heparin tubes and placed in a BioJar with cool gel packs for all patients and sites, and transported by courier immediately to Oxford where they were received and processed within 4-6 hours of venesection. The MOSAIC study was

approved by the NHS National Research Ethics Service, Outer West London REC (09/H0709/52, 09/MRE00/67). Blood from age- and sex-matched healthy controls was also received for comparison in this study which underwent identical transport and processing procedures. Detailed inclusion and exclusion criteria, clinical data analyses and categorisation of patients are placed in the Methods section of Chapter 4. Consent was obtained directly from competent patients, and assent from relatives/friends/ welfare attorneys of incapacitated patients.

All samples from MOSAIC were tested for pH1N1/09 by PCR. Acute samples were obtained within 48-72 hours of hospitalisation and convalescent samples were obtained 4-6 weeks after acute sampling.

2.2.2 Sample processing

Samples were processed immediately upon receipt. A 2ml aliquot of blood was subjected to whole blood lysis using RBC lysis solution (2.1.3) for HLA typing (2.1.17) and LPS stimulation for flow cytometry analysis (2.1.6). Supernatants from LPS stimulated samples were stored at -20℃ for multiplex cytokine analysis (2.1.14). Peripheral blood mononuclear cells (PBMCs) were extracted using density gradient separation from the remaining blood (2.1.2) for same day flow cytometry analysis and IFNγ ELISpot assay (2.1.15). Leftover PBMCs were cryopreserved.

2.3 Mouse studies

2.3.1 Mouse strains

C57BL/6 mice were obtained from breeding pairs originally purchased from The Jackson Laboratory. Jα18$^{-/-}$ mice were kindly provided by Professor Masaru Taniguchi (RIKEN, Japan) and have been backcrossed at least 12 times with the C57BL/6 wild

type mice. All mice were maintained at the Biomedical Services Unit at the John Radcliffe Hospital, Oxford and were used according to established institutional guidelines under the authority of a UK Home Office project licence. Female mice were used between 6-9 weeks old.

2.3.2 IAV inoculation

IAV was administered intra-nasally to mice that had been anaesthetised with Isoflurane (IsoFlo®; Abbott Laboratories). Diluted virus was administered to each mouse in a total volume of 40µl; 20µl per nostril. Weight change was monitored over the course of the experiment. Virus stock was stored in liquid nitrogen prior to use, and thawed on ice and diluted over multiple dilutions in PBS on the day of the experiment. The 'PR8' virus (A/PR/8/34/H1N1) was titrated to cause high pathogenicity and used at a final dose of 0.1 HAU per mouse, diluted from a stock of 1000HAU/50µl. The final dose of 'X179A' (NYMC-X179A) used was 10^5 EID50/ml, diluted from a stock of $10^{8.3}$ EID50/ml.

2.3.3 Preparation of cells from blood, BAL and bone marrow

Mice were sacrificed by CO_2 asphyxiation and blood, BAL and bone marrow cells obtained. Euthanized mice were pinned to a cork board and sprayed with isopropanol. The chest cavity was opened by cutting through the rib cage to expose lungs and heart using sterile, sharp scissors. Blood was collected following cardiac puncture and 200µl blood placed in 200µl of 10mM EDTA which was then treated with 1ml RBC lysis solution.

BAL cells were obtained by lavaging lungs via the exposed trachea. For this, the trachea was exposed and a small lateral incision was made using a sterile disposable scalpel (Swann-Morton). Portex fine-bore polyethylene tubing (0.76mm ID, 1.22mm

OD; Smiths Medical) was attached to a 2ml syringe which was filled with 2ml R10 and inserted delicately into the incision in the trachea. The syringe was depressed so 1ml of R10 entered and inflated the lung cavity, and was taken back up. This process was repeated three times. Return of BAL fluid was 1.8-2ml, which was placed in a 15ml Falcon tube on ice until all mice had undergone the procedure. Samples were centrifuged at 300xg before treatment with 500µl RBC lysis solution. BAL fluid supernatant was stored at -20℃.

Bone marrow was obtained from the femur and tibia of mice by firstly isolating these bones and removing the ends using sterile scissors. Bone marrow was flushed out using a 26 gauge needle attached to 10ml syringe filled with PBS directly into a 50ml Falcon tube on ice by inserting the needle into one end of the bone and depressing syringe. Cells were passed through a 70µm strainer, centrifuged at 300xg and treated with 1ml RBC lysis solution.

All samples were treated with RBC lysis solution for 10 minutes and then washed in R10 by centrifuging at 300xg for 5 minutes. If red cells were still present, RBC lysis step was repeated. Following this, cells were resuspended in R10 and counted.

2.3.4 iNKT cell adoptive transfer

For iNKT cell transfer, cells were isolated from spleens of PR8-infected C57BL/6 mice on day 3, using NK1.1$^+$ NKT isolation kit (Miltenyi Biotec) according to manufacturer's instructions. iNKT cells were prepared at a concentration of 1.5 x10^4 purified iNKT cells in 20ul PBS per mouse. PR8 was diluted to 0.1HAU in 20µl, which was mixed with iNKT cells and immediately used to inoculate mice intra-nasally so that the final infectious dose was 0.1HAU per mouse in 40µl volume, containing 1.5x10^4 purified iNKT cells

2.3.5 Lung tissue digestion

For lung homogenate studies, lungs from euthanized WT and Jα18$^{-/-}$ mice were first perfused with PBS. The chest cavity was opened by cutting through the rib cage to expose lungs and heart. Thread was used to tie ligatures on superior and inferior vena cavae to prevent backflow of PBS during perfusion. An incision was made in the left ventricle of the heart to allow PBS to exit following perfusion. A 10ml syringe was filled with PBS and a 26 gauge needle attached. The needle was inserted into the right ventricle of the heart and the syringe depressed to push PBS into the pulmonary circulation until lungs appeared white. Perfused lungs were then removed, cut into pieces and incubated with Collagenase A (Roche) (1mg/mL in 10mL PBS) and DNAse I (Sigma-Aldrich) (200ug/lung) for 1 hour at 37℃ on a shaking platform. The resulting suspension was then passed through a 23G needle and a 70μm filter. Cells were treated with RBC lysis solution before FACS staining.

2.3.6 αGC-loaded CD1d dimer

Mouse iNKT cells were detected using an α-Galactosyl Ceramide (αGC)-loaded CD1d-IgG1 dimer protein (BD Pharmingen) conjugated with PE anti-mouse IgG1 (BD Pharmingen). Prior to use, αGC was heated at 80℃ for 5 minutes and sonicated for 3x1 minute. The dimer was generated by mixing 0.2μg of αGC with 3μg of soluble divalent human CD1d-IgG1 protein and incubating at 37°C overnight on a rotating tube rotator. The CD1d dimer was conjugated with anti-mouse PE IgG1 at a 2:1 *wt:wt* ratio by incubating at room temperature for 1 hour, and then stored at 4℃.

2.4 Statistics

All statistical analysis was performed using GraphPad Prism 5.01 (GraphPad). Normality of data distribution was first tested using the D'Agostino & Pearson omnibus normality test. Normally distributed data sets were compared using Student t test; where comparisons included data not normally distributed, the Mann-Whitney test was used to compare data sets. To compare multiple, normally distributed data sets simultaneously, one-way ANOVA with Tukey post-test analysis was used. Where multiple data sets included data that were not normally distributed, Kruskal-Wallis with Dunn's multiple comparison post-test analysis was performed. A p value of less than 0.05 was considered significant. Error bars on graphs represent SEM unless otherwise stated.

Chapter 3: Monocytes as dominant immune correlates to severe outcome in mouse influenza A virus infection

3.1 Introduction

The cause of poor outcome to severe influenza A virus (IAV) infection has not been fully elucidated, although both viral and host factors are likely to contribute. Variations in IAV severity in humans have been linked to virulence of different strains or the immune status of the individual. Recently, gene polymorphisms have been identified that predispose infected individuals to a worse outcome, such as the minor rs12252-C allele of the IFITM3 gene (106, 433). Familial clusters of severe H5N1 infection furthermore suggest host-dependent susceptibility in humans (103).

Most evidence points towards an aberrant immune response following infection with highly pathogenic viruses as being the cause of mortality, linked with severe pneumonia and impaired virus clearance in the lungs (434). In mice, a very recent study identified that the worse outcome of 129 mice compared to C57BL/6 mice following infection with the same dose and strain of IAV was attributed to higher levels of type I interferons (IFN), which led to increased inflammatory cell infiltrate and lung pathology (158). Although IFNs are long-established antiviral mediators, the implication of a pathogenic role highlights the dysregulated immune response in the lungs during severe IAV infections. In humans, severe IAV infection induced a 45-fold increase in IAV-specific $CD8^+$ T cells in lungs compared to blood, highlighting the importance of investigating the immune response at the site of infection (435).

Highly pathogenic avian viruses such as H5N1 infect cells in the lower respiratory tract due to their preference for α2,3-sialic acid receptors which localise there, and cause

severe pneumonia and respiratory failure (117). H5N1 has a 59% mortality rate in officially confirmed human cases and remains a global health concern (436). A better understanding of the immune response to highly pathogenic viruses is necessary in order to target the infection, however since patients present upon symptom acquisition it is not possible to obtain pre-infection samples or to track very early immune responses to highly pathogenic IAV infection. Furthermore, it is difficult to identify what dose of H5N1 causes severe disease in humans as this depends on antigen exposure and is not controlled between individual cases. Experimentally, a dose-dependent increase in weight loss and mortality is observed in mice and ferrets, following infection with different virus strains (128). In addition to antigenic exposure, subsequent viral load is linked to replication efficiency of the virus (125, 437). H5N1 has been shown to replicate well in immune cells compared to less pathogenic viruses, facilitating virus spread.

In this chapter, I examined the immune response in the lungs of C57BL/6 mice infected with the same dose of IAV, but using a highly pathogenic and low pathogenic strain. The study controlled for host susceptibility and infecting viral dose, and allowed the examination of immune responses in the lungs at different time points which is often difficult to achieve in humans. Gene expression profiling provided insights into the global changes induced in the lungs by these two different viruses.

3.2 Aims

The aim of this chapter was to identify features of the early immune response in the lungs during severe IAV infection caused by a high-pathogencity strain of IAV.

3.3 Methods

3.3.1 Mouse IAV infection

C57BL/6 mice were infected with 10^5 EID50/ml of either VN/1203/04/H5N1 (H5N1) or the reassortant virus NYMC-X179A (X179A) in a total volume of 40µl and sacrificed on days 3 and 5. Uninfected mice were used for comparison. At these time points, whole lungs were removed, immediately dissected into 2mm pieces and placed in RNA-later at 4℃ for RNA extraction within a week (Methods 2.1.20.2). X179A was chosen as a mild virus to act as a suitable comparison for H5N1, as both are human viruses, unlike the more commonly used highly mouse-adapted A/PR/8/34/H1N1 (PR8). Both viruses were gifts from Dr John McCauley, NIMR, Mill Hill. The H5N1 strain was isolated from a patient during the lethal human outbreak in Vietnam from 2003-2005 and causes severe disease in mice (438). X179A is a low-pathogenicity H1N1 IAV which contains the HA and NA genes of the pandemic CA/7/09/H1N1 virus and the internal genes of PR8.

H5N1 infections were carried out at Mill Hill, London in a Category IV laboratory. Due to high virus pathogenicity and constraints of Category IV requirements, only weight loss profiles and RNA samples were obtained. X179A infections were carried out in Oxford. Weight loss profile and RNA samples were obtained, as well as FACS analysis of the cellular immune profile in blood and bronchoalveolar lavage (BAL) at the same time points.

As a comparison for cellular immune response, the high-pathogenicity PR8 virus was used. The caveat when comparing to X179A is that it adds an additional contributing factor to the worse outcome as this virus is adapted to mice and therefore infects more easily.

3.3.2 Microarray analysis

Gene expression profiling was carried out using Affymetrix Mouse ST1.0 arrays. For H5N1 samples, low quantities of RNA were derived from each mouse, possibly due to the extent of lung injury. Therefore RNA samples in each group were pooled and hybridised onto one cartridge. For X179A samples, enough RNA was obtained to hybridise each biological replicate separately, and therefore 3 cartridges were hybridised per time point.

Quality control of microarray samples was carried out using the Affymetrix® Expression Console™ (http://www.affymetrix.com/estore/browse/level_seven_software_products_only.jsp?productId=131414#1_1). Samples were normalised using Robust Multi-array Average (RMA) normalisation.

For analysis of H5N1 samples, due to pooling of samples there were no p values to determine significance of up- or down-regulated genes. Therefore a log2FC cut off of 1.5 was applied (FC of 2.8) and no genes with a lower fold-change were included in analysis. For X179A samples, a log2FC of 1.5 was also applied in order to be comparable. Within this group, significant genes at an adjusted P value≤0.05 were used for analysis. The adjusted p value is the p value adjusted for multiple testing.

Then, two main comparisons were made. Firstly, genes on day 3 or day 5 of infection were compared to uninfected mice to identify differentially expressed genes at either time point for both H5N1 and X179A separately. These gene lists were compared to each other to identify common and unique genes comparing H5N1 and X179A on either day 3 or day 5. The online bioinformatics tool DAVID (Methods 2.1.21) was used to identify the biological processes related to these differentially expressed gene lists, and the kinetics of these identified genes were explored over the course of infection.

Secondly, Gene Set Enrichment Analysis (GSEA) (Methods 2.1.21) was applied to whole genome data to test for enrichment of pre-defined gene sets. Comparisons were made for i.) day 3 vs. day 0, ii.) day 5 vs. day 0 and iii.) day 3 vs. day 5, for both mild and severe infection, creating six ranked lists in total.

Pre-defined gene sets used in GSEA were derived from the Molecular Signatures Database (MSigDB) available from the Broad Institute as part of the GSEA program (http://www.broadinstitute.org/gsea/msigdb), or were custom made based on published gene array data identified using keyword searches from NCBI (National Centre for Bioinformatics Information) GEO (Gene Expression Omnibus) Datasets. Gene array data were analysed with GEO2R; a web-based program that tests for significant differences between groups defined by the user using the bioinformatics package limma. The output is a list of significantly differentially expressed genes, which can be input into GSEA and tested for enrichment at either end of ranked gene lists. Details of custom-made gene sets are in Appendix 2.

3.4 Results

3.4.1 Weight loss and mortality following X179A or H5N1 infection

Weight loss of H5N1 (severe) and X179A (mild) infected mice was tracked over 7 days and compared to uninfected mice. H5N1 mice showed the most dramatic weight loss profile, losing 35.8%±4.2 SEM of body weight by the 7th day (Figure 3.1A). X179A mice lost very little weight during the course of infection, until the 7th day where there was 3.9%±1.59 weight loss (Figure 1A) and did not appear unwell. 100% of uninfected and X179A infected mice survived over 7 days, whereas H5N1 infection caused 15.3% mortality by day 5, 72.56% mortality by day 6, and all mice succumbed to infection by day 7 (Figure 3.1B).

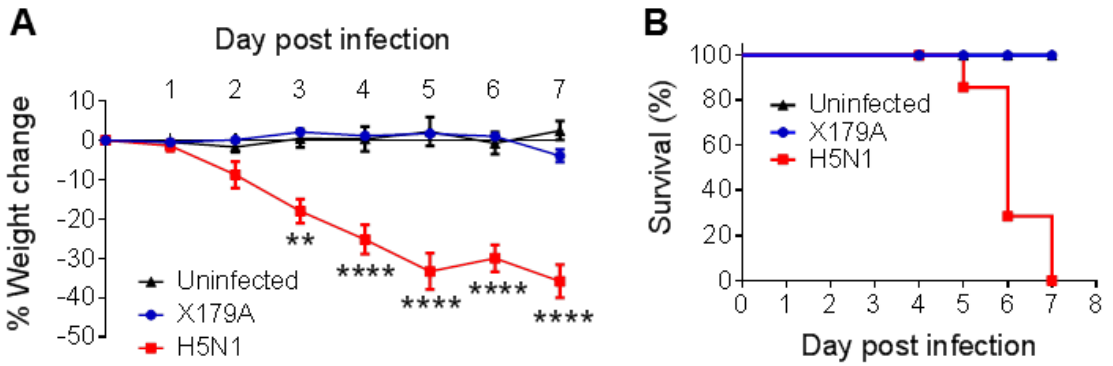

Figure 3.1: Weight loss and mortality of mice infected with mild or severe IAV. (A) Weight loss profiles and **(B)** survival curves of uninfected mice or mice infected with 10^5 EID50/ml of X179A (mild) or H5N1 (severe). Black triangle= uninfected, blue circle= Z179A, red square= H5N1. Difference between groups in (A) analysed using two-way ANOVA with repeated measures on different days. **p≤0.01, ****p≤0.0001

3.4.2 Microarray quality control

Following RNA extraction and prior to hybridisation, sample quality was assessed using the Agilent™ Bioanalyzer (Methods 2.1.19). The RIN values for all mouse lung samples from both H5N1 and X179A experiments are shown in table 3.1. Two H5N1 samples had undetectable RIN values (Day 0c and Day 3c); a likely consequence of low RNA quantities below what the Bioanalyser was able to interpret, and were therefore not included in further processing. All X179A samples had high quality RNA.

	Day 0			Day 3			Day 5		
	(0a)	**(0b)**	**(0c)**	**(3a)**	**(3b)**	**(3c)**	**(5a)**	**(5b)**	**(5c)**
H5N1	8.9	9.1	N/A	9.6	9.2	N/A	9.3	9.2	9.4
X179A	8.7	8.7	8.6	8.8	8.6	8.9	8.4	8.5	8.6

Table 3.1: RNA quality for microarray. RIN values for RNA extracted from lungs of X179A and H5N1 infected mice. Quality ranked on a scale of 1-10 (1=poor, 10=excellent). (a), (b) and (c) represent replicates within a group.

Following hybridisation using standard protocols, RMA normalisation was carried out to adjust for background signals and non-specific binding between arrays, and RMA-normalised data were compared to examine for unintended bias. A histogram of intensity values (Figure 3.2A) and box plots showing the median and 25th and 75th percentiles (Figure 3.2B) demonstrated that expression signals were comparable across all samples.

To provide a view of the natural grouping of samples based on RMA-normalised signal intensity without a priori hypothesis, values were first assessed using Principal Component Analysis (PCA). This reduces a large number of variables (as is the case with large numbers of genes) into a smaller number of principal components (artificial variables) that account for most of the variance in the observed variables (439). The data is transformed by 'orthogonal linear transformation' so that the greatest variance is defined by the first component (PC1), the second greatest variance by PC2 and so on. In H5N1 samples, each experimental group clustered away from the others, although there were only three samples to compare due to the pooling of RNA, and it was not possible to show the variance within these groups for this data set (Figure 3.2C). In X179A samples, the most distinct cluster was formed between infected samples from day 3 and two of the day 5 samples. One of the day 5 samples (5B) showed greater variance than the others for an unknown reason. The day 0 samples clustered away from the group of infected samples (Figure 3.2D). This showed that there was variance in the data, providing a robust basis to address further questions.

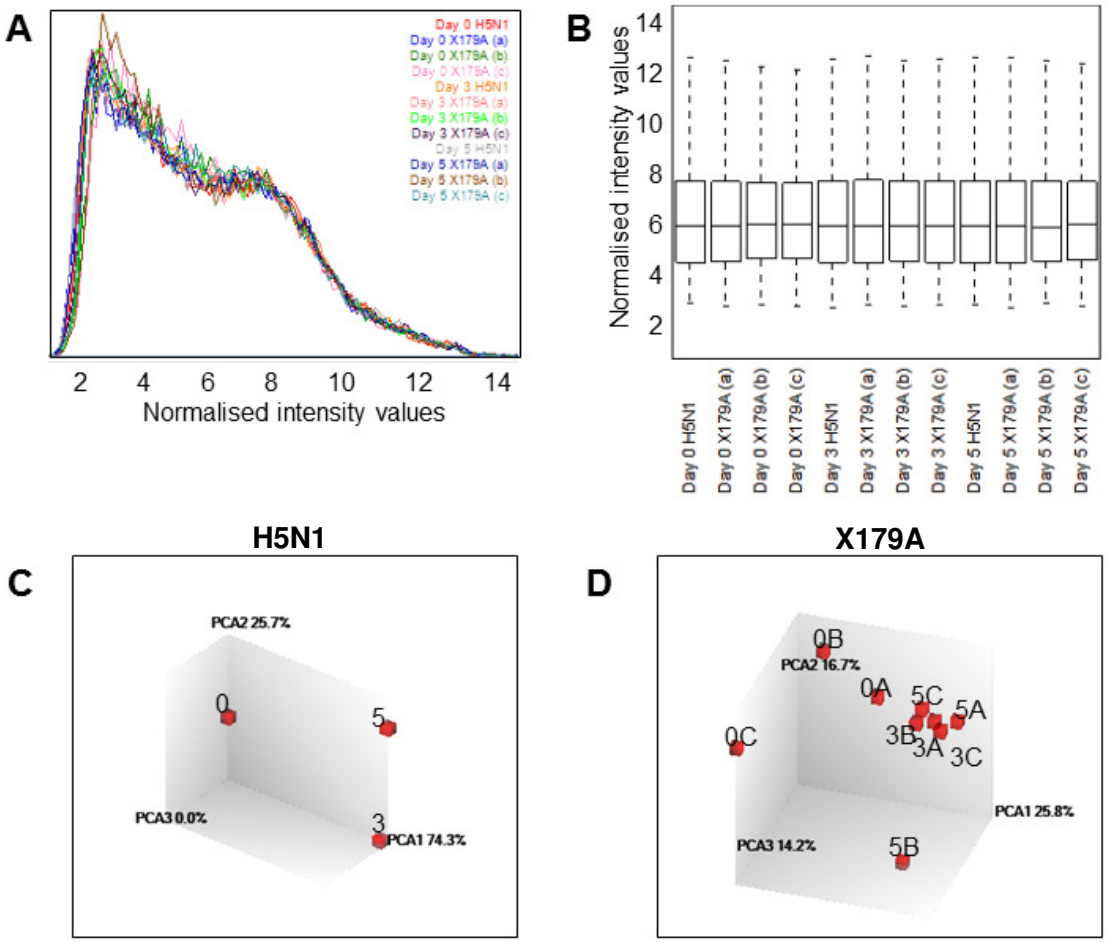

Figure 3.2: RMA-normalised microarray signal intensities from IAV infected mouse lungs. Expression distribution of all genes from all samples after RMA-normalisation as **(A)** histograms or **(B)** box plots. Box plots are drawn between 25th and 75th percentile of normalised data with the median represented by the middle horizontal line. Comparable unimodal distribution patters of expression intensities were evident. **(C)** Principal component analysis of samples from H5N1 or **(D)** X179A infected mice.

3.4.3 Similarities in gene expression on day 3 and day 5 in lungs from H5N1 and X179A infected mice

Differences in gene expression following infection with H5N1 or X179A were first analysed by comparing day 3 samples to uninfected controls and day 5 samples to the uninfected controls within each virus group. Using a log2 fold change (FC) cut off of 1.5 (absolute FC of 2.8), 421 and 445 genes were identified as being differentially expressed on day 3 and day 5 of H5N1 infection, respectively. Of these differentially expressed genes, 348 were upregulated and 73 downregulated on day 3, while 362 were upregulated and 82 downregulated on day 5. With a log2FC cut off of 1.5 and adjusted p ≤0.05 in X179A infection, 44 and 86 differentially expressed genes were identified on day 3 and day 5, respectively. In X179A infection no significantly downregulated genes were detected and therefore analysis focussed on upregulated genes. The top 10 genes of known function upregulated in either infection on day 3 or day 5 are shown in Table 3.2. Genes that appear in both H5N1 and X179A at either time point are highlighted in grey. Full descriptions of genes are in Appendix 3.

Day 3 H5N1		**Day3 X179A**		**Day 5 H5N1**		**Day 5 X179A**	
Gene	**Log2FC**	**Gene**	**Log2FC**	**Gene**	**Log2FC**	**Gene**	**Log2FC**
Slfn4	6.34346	Cxcl10	4.073257	Slfn4	6.04552	Cxcl10	5.22217
Cxcl10	5.78079	Ly6i	3.53972	Ifi205	5.91477	Saa3	4.71356
Ifi205	5.66317	Irf7	3.21832	Saa3	5.68556	Slfn4	4.06299
Saa3	5.61736	Isg15	3.21184	Cxcl10	5.62808	Cxcl9	4.006473
Irg1	5.14436	Apod	3.091097	Ms4a4c	5.43413	Rsad2	3.886137
Timp1	5.10918	Rsad2	2.994207	Ccl2	5.15553	Irf7	3.484003
Ms4a4c	4.99255	BC023105	2.967807	Ccl7	5.15509	Ly6i	3.470463
Ccl2	4.94014	Ifi205	2.943133	Cxcl9	5.13375	Timp1	3.426647
Rsad2	4.89944	Zbp1	2.920057	Timp1	5.00086	Ifi205	3.397337
Ccl7	4.8507	Gm5431	2.7466	Irg1	4.95016	Isg15	3.263883

Table 3.2: Top 10 upregulated genes in severe or mild IAV infection on day 3 and day 5. Top 10 genes upregulated in IAV infected mice ordered by fold change relative to uninfected controls. Common genes upregulated in both H5N1 and X179A are highlighted in grey. Full descriptions of genes are in Appendix 3.

The analysis identified a large overlap in genes expressed between mild and severe IAV infections, in particular CXCL10 (IP-10) and the IFN inducible protein IFI205, which were highly upregulated in both infections at both time points. Many genes upregulated on day 3 of either infection were also still upregulated on day 5 of that infection.

3.4.4 Inflammatory genes increase more rapidly in lungs of H5N1 than X179A infected mice

To elucidate differences between mild and severe infection, the number of genes upregulated at log2FC>1.5 on day 3 (Figure 3.3A) or day 5 (Figure 3.3B) of infection are shown, comparing H5N1 to X179A. The majority of genes upregulated in mild infection were also upregulated in severe infection (43/44 on day 3, 81/86 on day 5). Genes unique to mild infection are listed in Figure 3.3, the relevance of which will be discussed later.

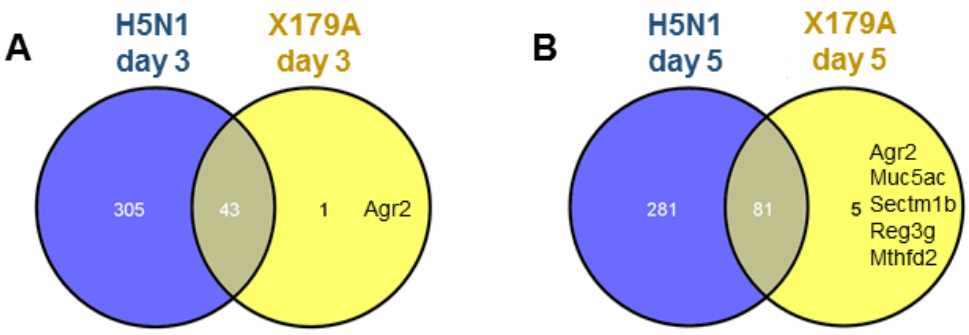

Figure 3.3: Common and unique genes upregulated in severe and mild IAV infection. (A) Venn diagram displaying number of differentially expressed genes upregulated in H5N1 infection or X179A infection relative to uninfected mice at log2FC>1.5 (adj p≤0.05) on day 3 or **(B)** day 5. The names of X179A unique genes are displayed.

Genes unique to H5N1 infection or common to both infections were first analysed using DAVID to group genes within these by similar biological processes ('clusters') (Table 3.3).

	Cluster	Count	P value	FDR
Day 3 H5N1 specific	Immune response	67	5.1E-47	7.0E-44
	Inflammatory response	40	6.0E-31	4.1E-28
Day 3 H5N1/X179A overlapping	Immune response	13	1.2E-12	1.5E-10
	Response to virus	6	1.2E-7	7.1E-6
Day 5 H5N1 specific	Immune response	64	1.1E-45	1.5E-42
	Inflammatory response	34	7.3E-25	5.0E-22
Day 5 H5N1/X179A overlapping	Immune response	23	1.2E-21	4.5E-19
	Defence response	15	3.3E-11	6.1E-9

Table 3.3: Biological Processes enriched upon IAV infection. Gene Ontology (GO) Biological Processes identified using DAVID enriched in lists of H5N1 specific genes or H5N1/X179A overlapping genes from Figure 3. Count refers to the number of genes from the input list involved in the cluster, p value≤0.05 signifies significant result, FDR= false discovery rate; expected proportion of false positives among discoveries.

Not unexpectedly, 'immune response' was the top category identified in all cases, with further immune related mechanisms following. The 'immune response' cluster identified the most genes ('count' column in Table 3.3) and therefore genes in this cluster were used for further analysis. Pathway analysis in DAVID identified four main biological pathways that encompassed the majority of genes in the 'immune response' cluster for each of the time points analysed - 'cytokines & chemokines' 'toll-like receptors (TLR)' 'defence response' and 'interferon regulated'. It is of note that some genes in the 'defence response' cluster are also regulated by interferons, however the 'interferon regulated' cluster includes genes that were not classified as 'defence response' genes by DAVID. Table 3.4 shows genes upregulated by log2FC>1.5 on day 3 or day 5, relative to uninfected mice, for both H5N1 and X179A. Full descriptions of genes are in Appendix 3.

Gene ID	up d3 X179A	up d5 X179A	up d3 H5N1	up d5 H5N1
Chemokines & cytokines				
Ccl2			x	x
Ccl3		x	x	x
Ccl4			x	x
Ccl5			x	x
Ccl7		x	x	x
Ccl8	x		x	x
Ccl9			x	x
Ccl12		x	x	
Ccl19			x	
Ccl20			x	x
Cxcl2			x	x
Cxcl3				x
Cxcl5			x	x
Cxcl9		x	x	x
Cxcl10	x	x	x	x
Cxcl11			x	x
Cxcl13		x	x	x
Il1a				x
Il1b			x	x
Il6		x	x	x
Il7r				x
Il15				x
Il18bp			x	x
Tnf			x	x
Ccr1			x	x
Ccr2			x	x
Ccr5			x	x
Cxcr2			x	x
TLRs				
TLR1			x	x
TLR3			x	x
TLR7			x	x
TLR9			x	x
TLR13			x	x

Gene ID	up d3 X179A	up d5 X179A	up d3 H5N1	up d5 H5N1
Defence response				
Bcl3				x
Fcgr1		x	x	x
Fcgr2b			x	x
Fcgr3			x	
H2-Q6			x	x
H2-Q8			x	x
Ido1			x	x
Mx1		x	x	x
Mx2	x	x	x	x
Myd88			x	x
Rsad2	x	x	x	x
Saa1			x	
Saa3		x	x	x
Samhd1			x	x
Interferon regulated				
Ifi203			x	x
Ifi204	x		x	
Ifi205	x		x	
Ifi27l2a	x		x	
Ifi35			x	x
Ifi44	x	x	x	
Ifi47			x	x
Ifih1			x	x
Ifit1	x	x	x	x
Ifit2		x	x	x
Ifit3	x	x	x	x
Ifitm3			x	x
Iigp1	x	x	x	x
Irf1			x	x
Irf7	x	x	x	x
Isg20			x	
Irgm1	x	x	x	x
Irgm2			x	x

Table 3.4: Significantly upregulated immune response genes in lungs on day 3 or day 5 of severe or mild IAV infection. Genes from the 'immune response' Gene Ontology cluster were grouped into genes involved in 'cytokines & chemokines', 'TLRs', defence response' or 'interferon regulated' using DAVID Pathway Analysis. 'x' represents a gene that was significantly upregulated by log2FC>1.5. Full descriptions of genes are in Appendix 3.

For visualisation of fold changes within these clusters between infections, heatmaps were created (Figure 3.4).

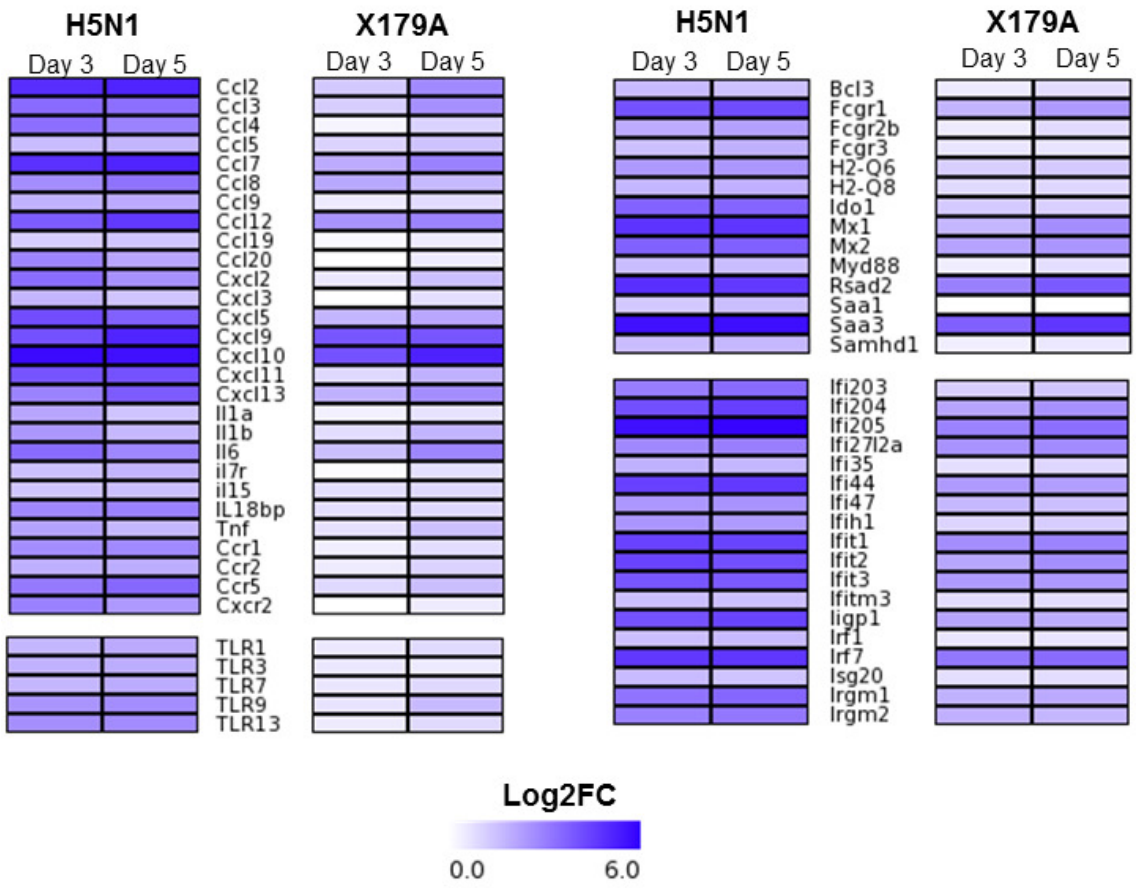

Figure 3.4: Heat maps of immune response genes in severe and mild IAV infection. Log2FC values on day 3 and day 5 relative to uninfected mice are displayed on a gradient of white to dark blue. White= not expressed, darker colour represents higher fold change.

The kinetics of gene upregulation over the course of infection were next investigated for the transcripts in Table 3.4. All genes chosen were significantly increased upon infection relative to uninfected mice at a log2FC>1.5 in at least one of the time points per infection. Comparison of each gene was made relative to expression values of uninfected mice, in order to identify relative changes on day 3 and day 5 of infection. Transcripts that were common to both infections were first compared.

Upregulation of genes in H5N1 and X179A infection followed different kinetics, as genes in H5N1 infection generally rose sharply on day 3 but remained unchanged on

day 5, while in X179A infection there was a more gradual increase to day 3 but a continued increase on day 5 for many genes analysed. Cytokine and chemokine genes showed no significant change in expression from day 3 to day 5 in H5N1 infection (Figure 3.5A), but increased from day 3 to day 5 in X179A infection ($p=0.017$) (Figure 3.5B). The genes with the highest increase between days in X179A infection were IL-6, CCL3 (MIP1α), CXCL10 (IP-10) and CCL7 (MCP-3). These genes have known roles in monocyte recruitment and were also expressed highly in H5N1 infection. Magnitude of fold change relative to uninfected mice on day 3 was higher for H5N1 than X179A infection ([mean log2FC±SEM]: 3.9±0.36 vs 2.4±0.38).

A similar trend was observed in the defence response gene group, where there was no significant change in expression from day 3 to day 5 in H5N1 infection (Figure 3.5C) but there was a significant increase from day 3 to day 5 in X179A infection ($p=0.0041$). The genes with the highest increase in X179A infection were Saa3 (serum amyloid A 3) (absolute FC on day 3: 13.39 to day 5: 26.24, Rsad2 (Radical S-Adenosyl methionine domain-containing protein 2) (FC 7.97 to 14.79) and Mx1 (myxovirus (influenza virus) resistance 1) (3.32 to 6.49) (Figure 3.5D). Magnitude of fold change relative to uninfected mice on day 3 was higher for H5N1 than X179A infection (4.6±0.33 vs 2.5±0.4).

Interferon regulated genes remained unchanged between day 3 and day 5 in both H5N1 and X179A infection (Figure 3.5E-F). The magnitude of fold change on day 3 in H5N1 infection was again higher than in X179A infection (4.2±0.25 vs 2.4±0.13), and unlike the previous gene groups, the interferon genes in X179A infection did not continue to increase on day 5.

The lower expression of genes in all clusters analysed in X179A infection, and the trend for continued increase in many cytokine and defence genes, suggests slower kinetics of inflammatory gene expression in mild infection.

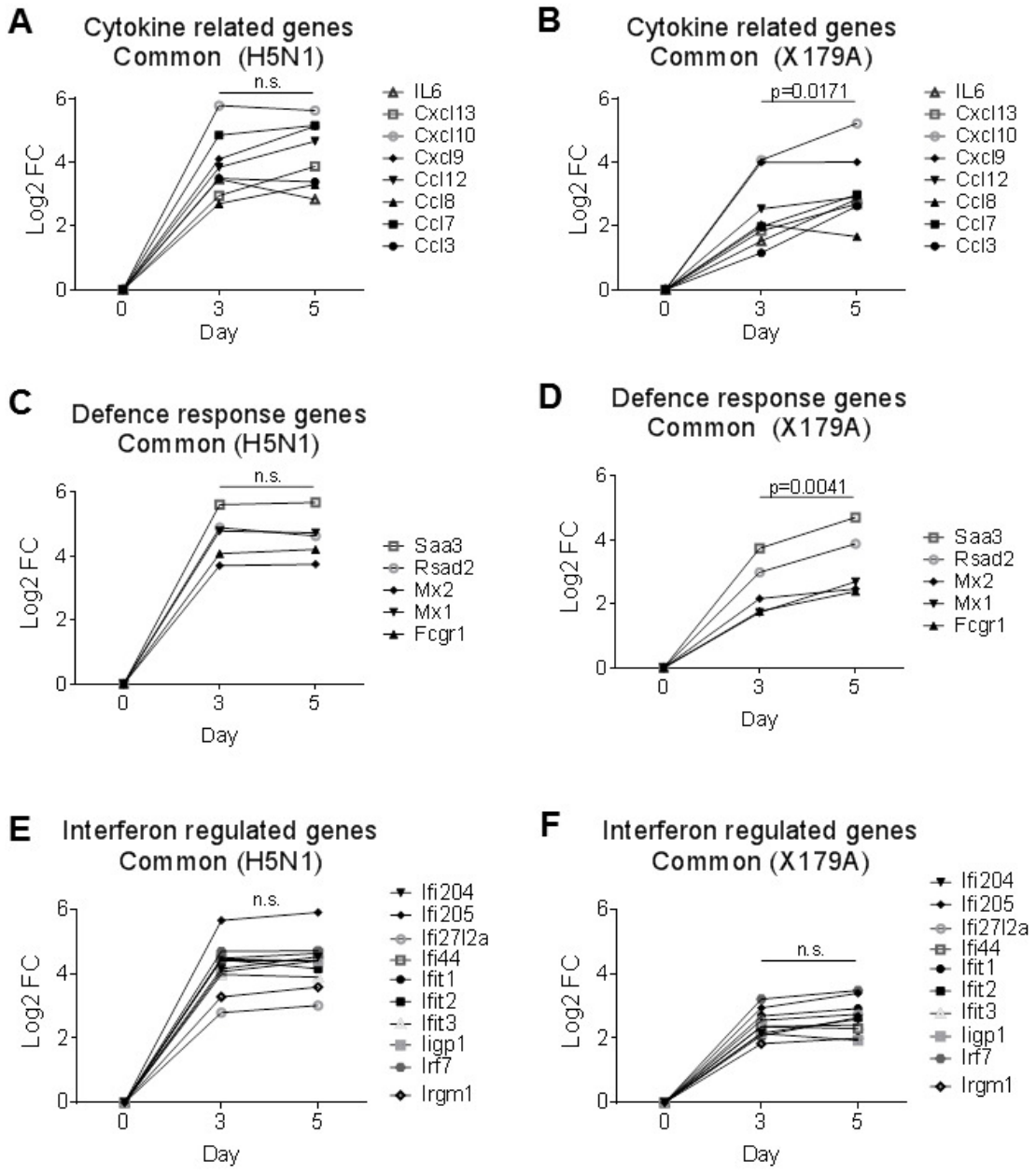

Figure 3.5: Kinetics of genes upregulated in both mild and severe IAV infection. **(A)** Cytokine related genes common to both infections in H5N1 and **(B)** X179A infection. **(C)** Defence response genes common to both infections in H5N1 and **(D)** X179A infection. Interferon regulated genes common to both infections in H5N1 **(E)** and X179A infection. Paired t-test between day 3 and day 5 used to determine significant change in gene expression. (Log2FC of 0= FC of 1; Log2FC of 6= FC of 64).

Genes unique to severe infection rose sharply on day 3 but did not change significantly to day 5 in any group of genes analysed. Cytokine genes were split into two groups for better visualisation due to a large number of genes; one containing chemokine ligands and the other chemokine receptors and cytokines. No significant changes were found from day 3 to day 5 in either group (chemokine: 2.9±0.41 to 2.7±0.40, cytokine: 3.2±0.19 to 2.2±0.23), and many of these genes had started to decrease by day 5 relative to day 3 (Figure 3.6A-B). This suggests a rapid cytokine storm that dominates the early stages of severe infection.

Defence response genes remained unchanged from day 3 (1.9±0.25) to day 5 (2.0±0.23) (Figure 3.6C), interferon regulated genes remained unchanged from day 3 (2.2±0.23) to day 5 (2.2±0.28) (Figure 3.6D) and TLR genes remained unchanged from day 3 (2.1±0.20) to day 5 (2.3±0.18) (Figure 3.6E).

The magnitude of fold change on day 3 in defence and interferon gene groups was low compared to the magnitude of fold change in genes from these groups identified in the previous figure (common to H5N1 and X179A). This suggested that within a biologically common cluster of genes, the most highly upregulated genes in severe infection were those upregulated in response to both severe and mild infection. Severe infection induced expression of additional genes, but at a lower magnitude.

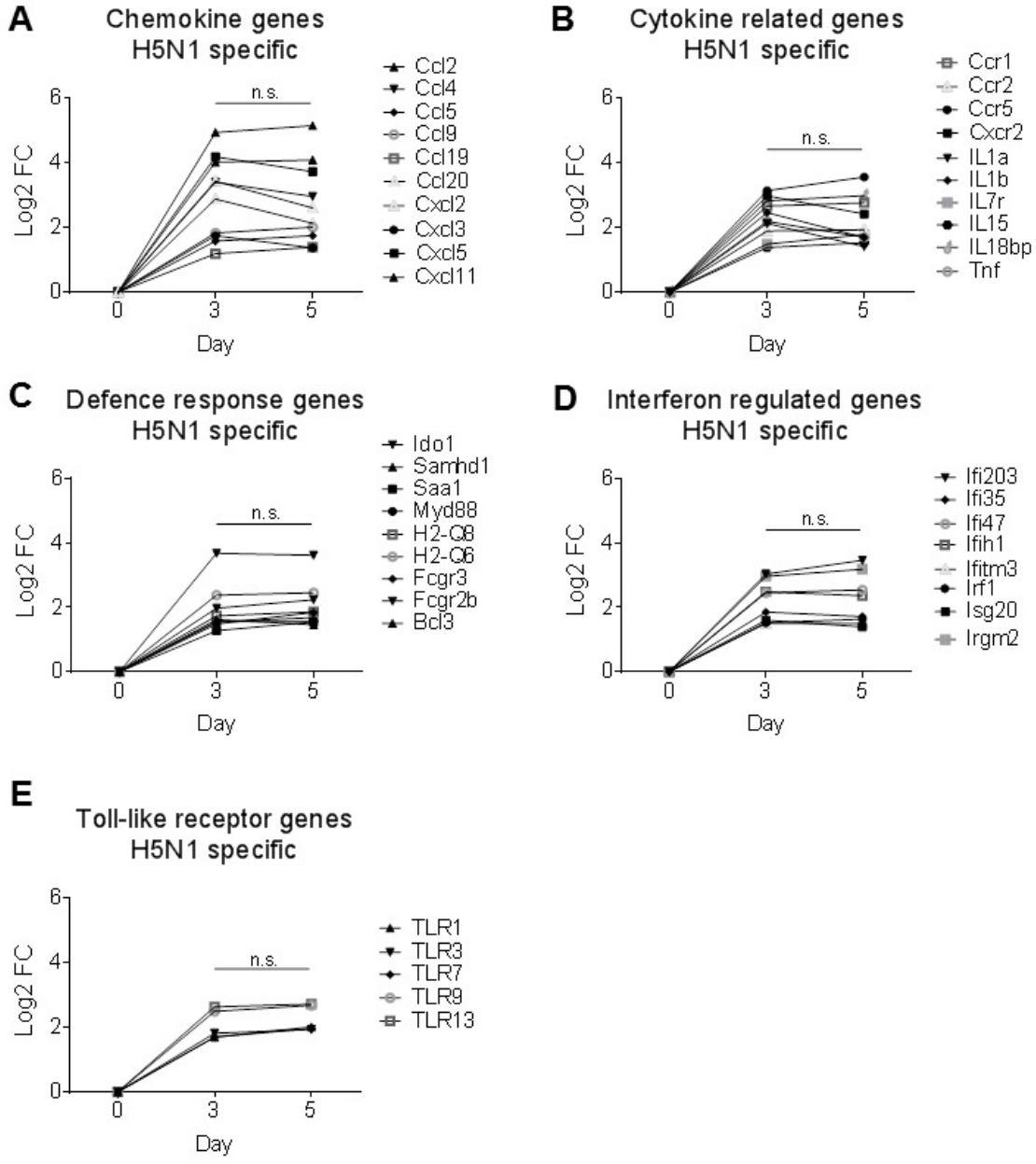

Figure 3.6: Kinetics of genes upregulated only in severe IAV infection. Fold change of genes unique to H5N1 infection on day 3 and day 5 relative to uninfected samples analysed by clusters of **(A)** Chemokine genes, **(B)** Cytokine genes, **(C)** Defence response genes, **(D)** Interferon-regulated genes and **(E)** Toll-like receptor genes. Paired t-test between day 3 and day 5 used to determine significant change in gene expression. (Log2FC of 0= FC of 1; Log2FC of 6= FC of 64).

These results were next interrogated using GSEA, which scrutinises gene expression patterns of the whole genome. For this purpose, gene lists comparing day 3 to day 5 of infection were used to create a ranked list where genes highly expressed on day 5 were at the top of the list, and genes highly expressed on day 3 were at the bottom of the list. Pre-defined gene sets were then tested for enrichment in both H5N1 and X179A lists in order to identify whether genes in these lists were higher on day 3 or day 5 within each group. Gene lists were chosen based on biological processes identified in table 3.4. Details of the gene sets used for analysis are shown in table 3.5.

Gene Set Name	Source	No. genes in set
Cytokine_Cytokine_Receptor_Interaction	KEGG	267
Chemokine_Receptors_Bind_Chemokines	Reactome	57
Defense_Response	Gene Ontology- BP	270

Table 3.5: Pre-defined gene sets used in GSEA. Gene sets openly available from the Broad Institute Molecular Signatures Database (MSigDB).

The ‘cytokine-cytokine receptor interaction’ group was enriched on day 3 in H5N1 lungs ($p=0.005$), while the same list of genes was enriched on day 5 in X179A lungs ($p\leq0.001$) (Figure 3.7A). The ‘chemokine receptors bind chemokines’ group was also enriched on day 3 in H5N1 ($p=0.017$) and on day 5 in X179A ($p\leq.0001$) infection (Figure 3.7B). Genes involved in the defence response were not significantly enriched in H5N1 infection on either day ($p=0.259$), as many genes were expressed on both days. In X179A infection however, enrichment was once again observed on day 5 of infection ($p\leq0.001$) (Figure 3.7C). These findings confirm the earlier observations of a continued increase in expression of immune response genes in mild infection over the course of 5 days, whereas expression peaks around day 3 in severe H5N1 infection.

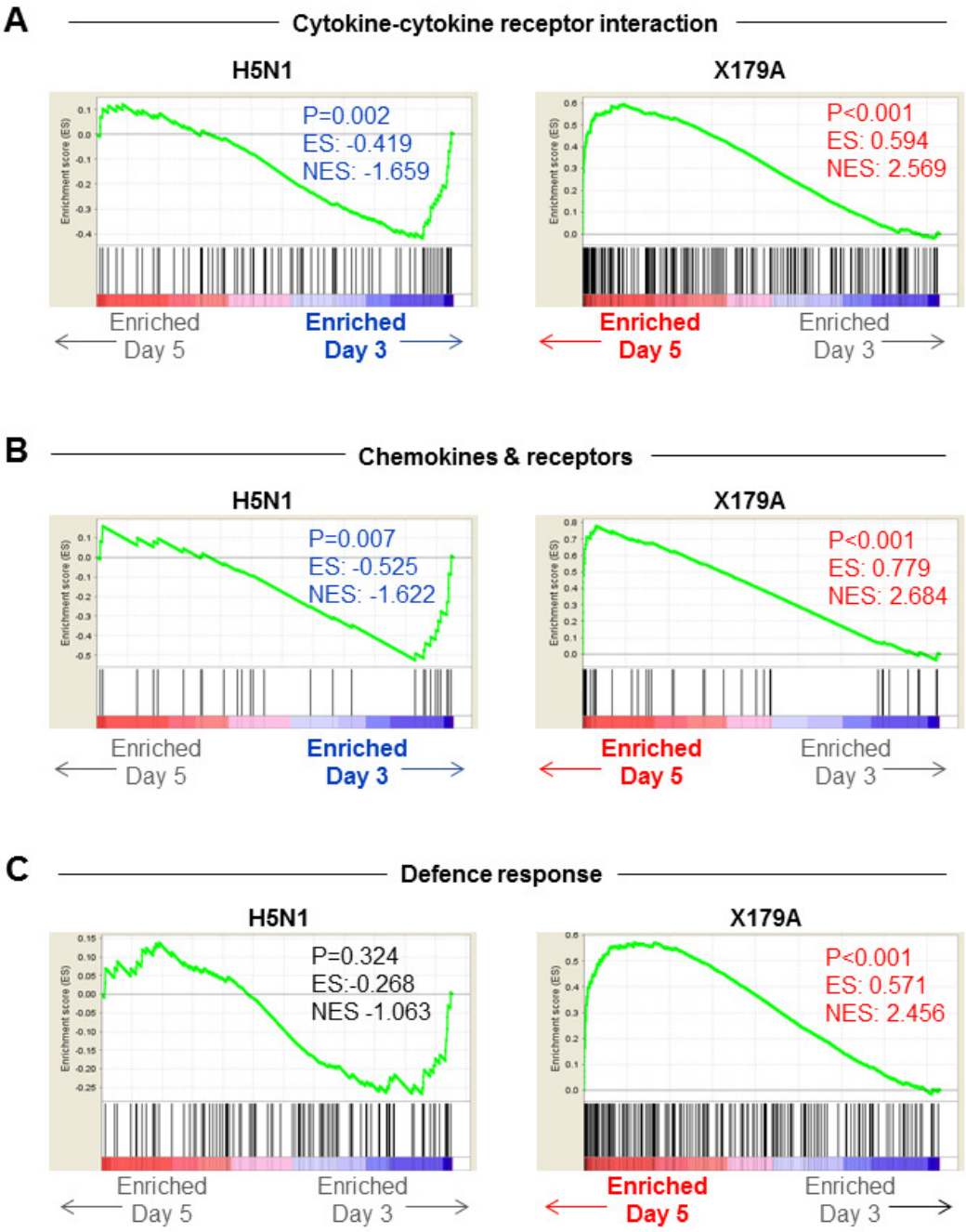

Figure 3.7: Gene Set Enrichment Analysis of biological pathways enriched on day 3 or day 5 of IAV infection. GSEA plots of gene sets involved in **(A)** Cytokine-cytokine receptor interactions, **(B)** Chemokines and receptors and **(C)** Defence response genes. Genes are ranked from day 5 (left) to day 3 (right) in order of expression values. Significant enrichment on day 3 is displayed in blue text and significant enrichment on day 5 is displayed in red text. Grey text= no enrichment. ES: enrichment score (scale -1 to 1), NES: nominal enrichment score (ES normalised for gene set size). P value is significance of the ES.

3.4.5 Monocyte-associated cytokines and chemokines are higher in severe infection

As identified in Figure 3.5A-B, genes encoding chemokines involved in monocyte recruitment were highly expressed early in H5N1 infection, while only becoming upregulated on day 5 in X179A infection. Genes in table 3.4 were therefore scrutinised to identify all transcripts with known roles in monocyte recruitment for further investigation. On day 3 of H5N1 infection, a large number of mononuclear cell-recruiting chemokines were expressed, whereas only CXCL10 (IP-10) and CCL8 (MCP-2) were expressed on day 3 in X179A (Figure 3.8A). On day 5, genes expressed in H5N1 showed comparable expression to day 3. In X179A, further monocyte-attractant chemokines CCL3 (MIP-1α), CCL7 (MCP-3) and CCL12 (MCP-5), as well CCR2, the CCL2 (MCP-1) receptor were expressed (Figure 3.8B). Other monocyte chemoattractant proteins that were upregulated during severe H5N1 infection were however not upregulated in mild infection.

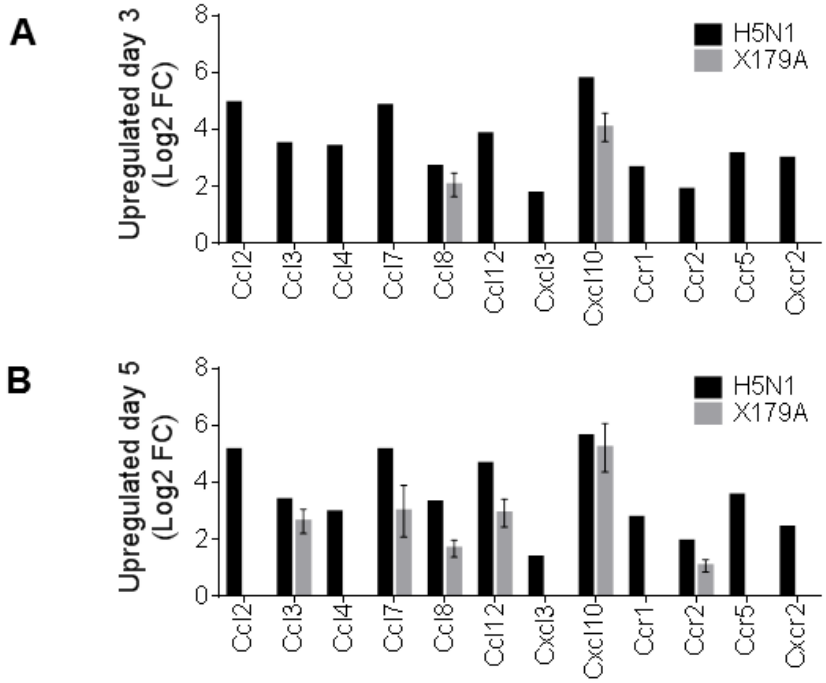

Figure 3.8: Upregulation of monocyte-attracting chemokines in lungs is greater during severe than mild infection. Log2FC of chemokines involved in monocyte recruitment significantly upregulated on **(A)** Day 3 or **(B)** Day 5 of either H5N1 infection (black) or X179A infection (grey).

One hypothesis therefore could be that an overwhelming monocyte infiltration to the lungs during severe IAV infection could be partly responsible for the immune pathology and worse outcome to infection. After entry to tissues, monocytes can differentiate into macrophages which take on either an inflammatory 'M1' phenotype or a regulatory 'M2' phenotype. To test whether either of these phenotypes was enriched in lungs during severe or mild infection, genes that were upregulated in M1 or M2 polarised macrophages were identified (440) (Chapter 3.3.2, Appendix 2) and tested for enrichment. This would not only identify the presence of monocytes/macrophages in the lungs and determine on which day they were most enriched, but also examine the polarisation towards inflammatory or regulatory functions.

On day 3, the inflammatory M1 phenotype was strongly enriched in both infections ($p \leq 0.001$) (Figure 3.9A). The regulatory M2 phenotype was enriched in uninfected mice relative to day 3 of H5N1 infection, whereas no enrichment was observed in the M2 phenotype in X179A infection (Figure 3.9B).

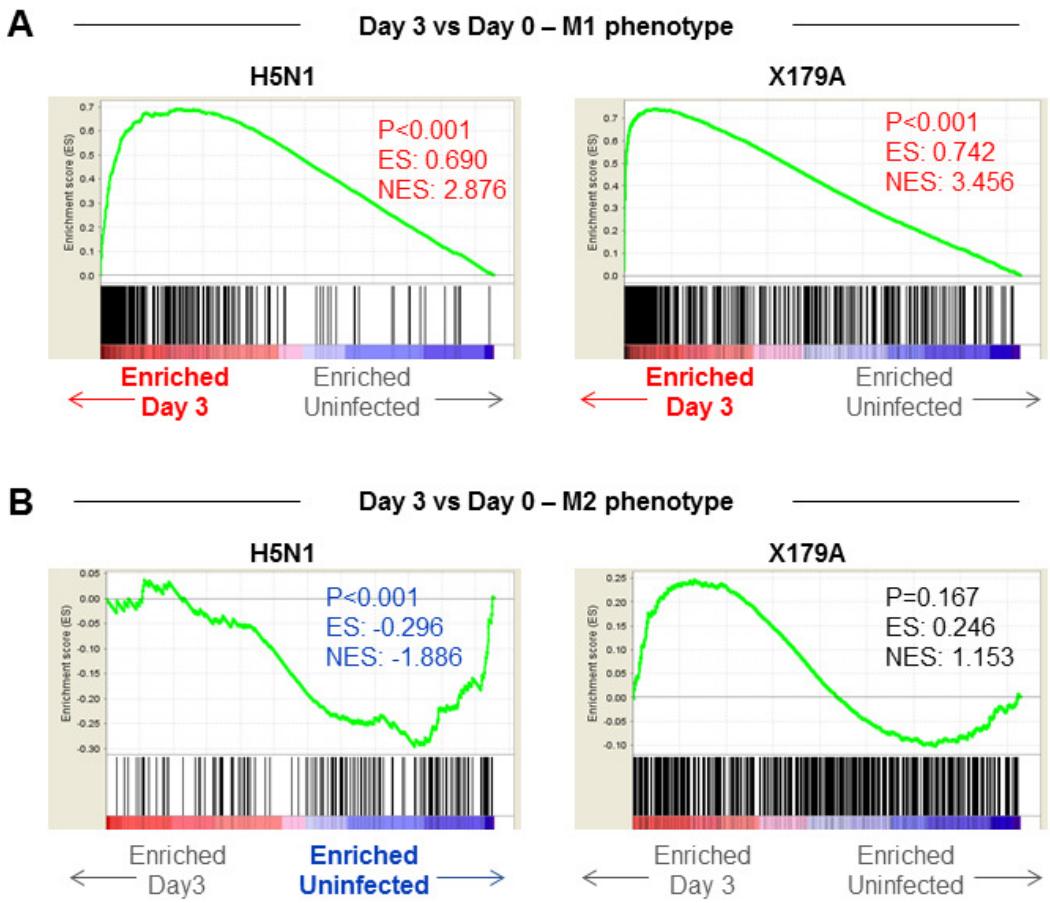

Figure 3.9: Enrichment of inflammatory macrophage signature on day 3 of severe and mild infection. GSEA plots of gene sets involved in **(A)** M1 polarisation or **(B)** M2 polarisation. Genes are ranked from day 3 (left) to uninfected (right) in order of expression values. Significant enrichment in uninfected mice is displayed in blue text and significant enrichment on day 3 is displayed in red text. Grey text= no enrichment. ES: enrichment score (scale -1 to 1), NES: nominal enrichment score (ES normalised for gene set size). P value is significance of the ES.

On day 5 there was still enrichment of M1 in both infections (Figure 3.10A). As well as this, the M2 phenotype was significantly enriched in X179A but not H5N1 infected mice on day 5 (Figure 3.10B). This suggests that H5N1 infection induces a purely inflammatory macrophage profile, whereas in a milder infection such as X179A, the inflammatory macrophage profile predominates early in infection on day 3, but by day 5 the additional presence of a more regulatory M2 subset may be beneficial in the outcome to less pathogenic virus strains.

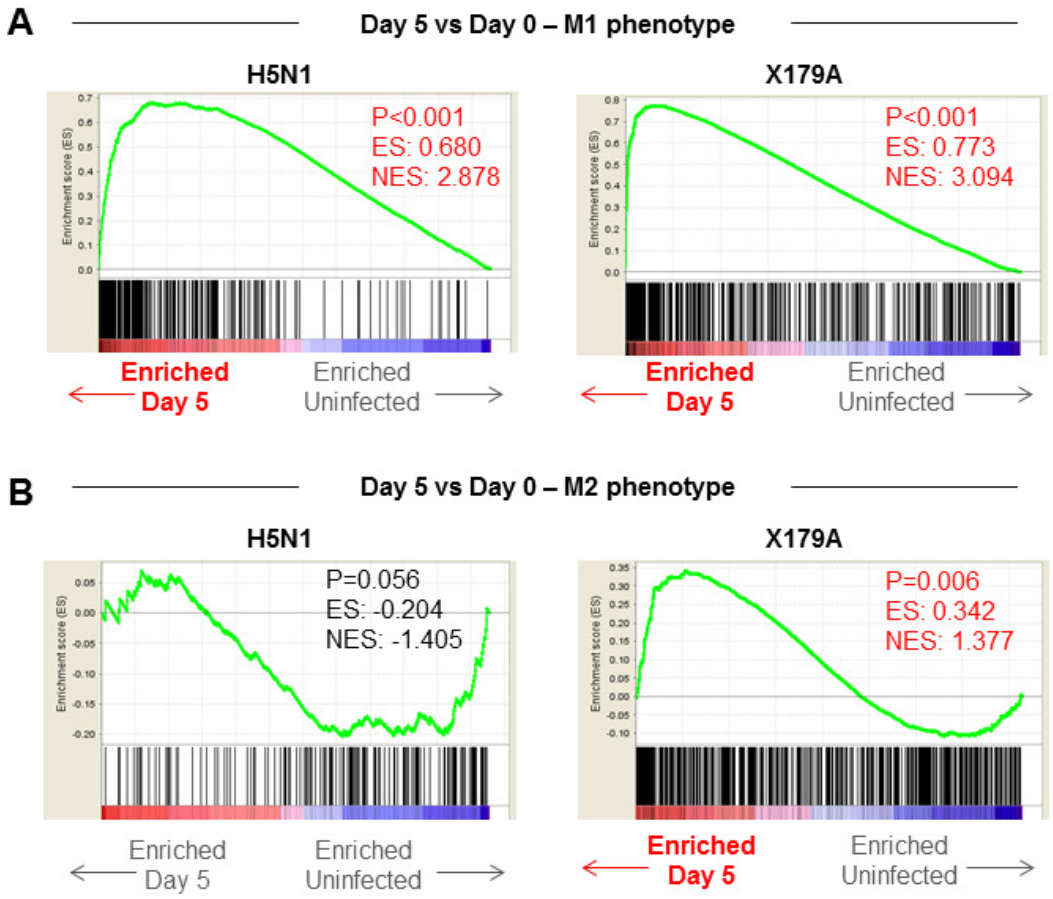

Figure 3.10: Enrichment of both inflammatory and regulatory macrophage signatures on day 5 of mild infection. GSEA plots of gene sets involved in **(A)** M1 polarisation or **(B)** M2 polarisation. Genes are ranked from day 5 (left) to uninfected (right) in order of expression values. Significant enrichment on day 5 is displayed in red text. Grey text= no enrichment. ES: enrichment score (scale -1 to 1), NES: nominal enrichment score (ES normalised for gene set size). P value is significance of the ES.

3.4.6 Cellular immune changes following severe or mild IAV infection

The changes in gene expression profile were next examined at a cellular level. Due to the virulence and pathogenicity of the H5N1 virus, its use was restricted to Category IV laboratory use, and could thus not be used for this purpose. Therefore the PR8 strain was titrated to cause similar weight loss (Figure 3.11). Experiments were terminated before mice lost 20% of their initial weight, and the early immune response analysed on day 3.

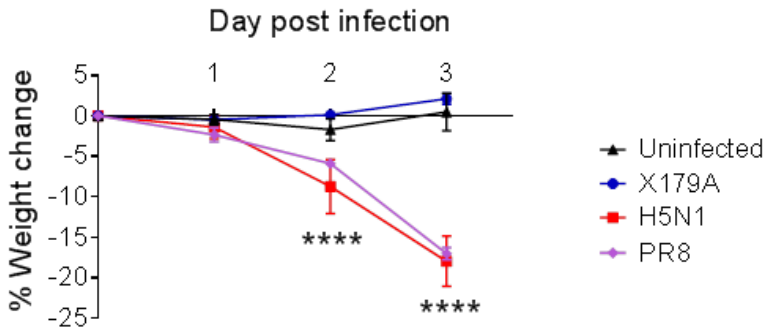

Figure 3.11: Weight loss of X179A, H5N1, PR8 and uninfected mice over 3 days. Percentage weight loss relative to initial weight as measured every 24 hours over 3 days of infection with either 10^5 EID50/ml X179A, 10^5 EID50/ml H5N1, 0.1HAU PR8 or uninfected mice. N=5-7 mice per group. Difference between groups analysed using two-way ANOVA with repeated measures on different days. ****p≤0.0001.

The immune profile in lungs and blood on day 3 post infection was compared between X179A and PR8 (Figure 3.12A). In the lungs, Ly6C^{hi} monocytes were highly elevated in PR8 infected mice (31.59%±2.88 SEM). Significantly fewer monocytes were present in X179A infection (5.68%±1.84). Ly6G neutrophils were present at lower frequencies than monocytes in both infections and were again higher in PR8 infection (13.5%±1.1) than X179A (2.51%±0.33). T cells were significantly higher in X179A infection (6.46%±1.71) than in PR8 infection where they remained minimal (1.4%±0.15).

In the blood, no significant changes were observed in monocyte or neutrophil frequency in X179A infected mice (M: 2.51%±0.45, N: 4.22%±0.22) relative to uninfected mice (M: 2.2%±0.37, N: 5.33%±0.33), unlike in PR8 infection which caused increase in both monocytes (9.24%±1.26) and neutrophils (15.81%±1.14) by day 3 (Figure 3.12B). T cells were reduced in both mild (18.46%±4.06) and severe (12.45%±1.34) IAV infections relative to uninfected mice (25.54%±2.45), with the greatest reduction in PR8 infected mice.

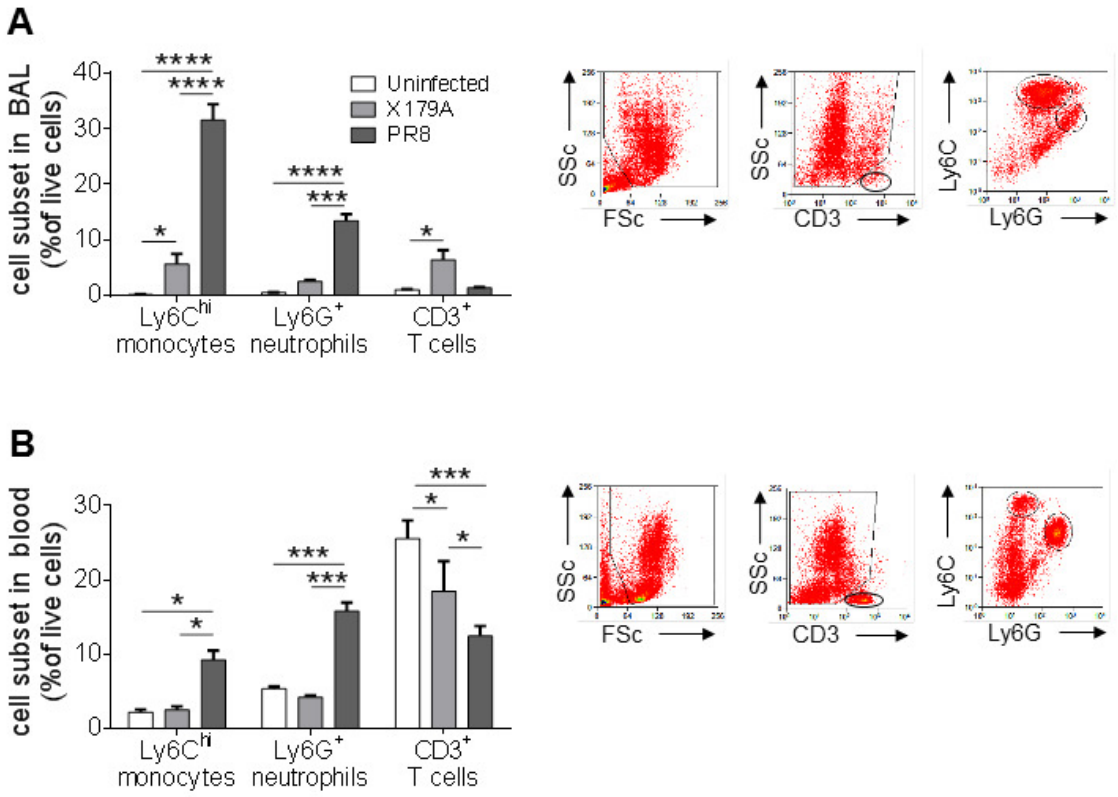

Figure 3.12: Cellular immune change in BAL and blood during mild and severe infection. Percentages of Ly6C^{hi} monocytes, Ly6G^{+} neutrophils and CD3^{+} T cells in **(A)** BAL and **(B)** blood of mice either uninfected or infected with X179A or PR8 viruses on day 3. Representative flow cytometry plots show identification of cell populations. N=3 mice per group. Two-way ANOVA with repeated measures used to determine differences between infections. *p≤0.05, ***p≤0.001, ****p≤0.0001.

Due to the significant increases in monocyte frequency on day 3 of infection, kinetics of monocyte localisation over the first 3 days of infection were analysed in paired bone marrow (BM), blood and BAL samples in severe PR8 infection (Figure 3.13). No changes were found in absolute number of monocytes in BM over the first three days. In the blood, monocyte frequency was the most variable, increasing from $1.7x10^5$/ml in uninfected mice to $9.3x10^5$/ml on day 2, and decreasing to $4.5x10^5$/ml on day 3. In the BAL, uninfected mice had no cellular influx, but as infection progressed, results mirrored what was seen in the blood. A 6-fold increase in monocyte numbers was observed between days 2 and 3 ($0.6x10^5$ to $3.7x10^5$).

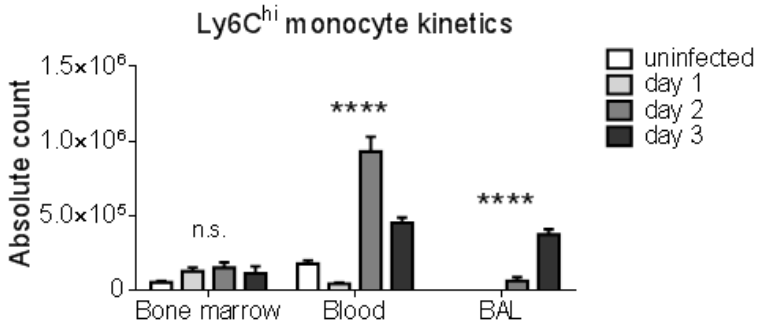

Figure 3.13: Early monocyte kinetics during severe IAV infection. Absolute number of Ly6C^{hi} monocytes, over 3 days of infection with PR8. BM absolute count per tibia, Blood absolute count per ml whole blood, BAL absolute count per whole BAL (2ml BAL fluid). n=4-5 mice; 2 experiments. One-way ANOVA between timepoints in each compartment. ****p≤0.0001.

As gene expression analysis identified an inflammatory M1 polarised monocyte profile as being enriched in severe compared to mild IAV infection in lungs, expression of M1 or M2 markers on Ly6C^{hi} monocytes during severe and mild infection in whole lung digests were examined using CCR7 to identify inflammatory M1 and CD206 to identify regulatory M2 polarisation; markers which have been used by others (441). The percentage of CCR7 expressing monocytes increased 2.2-fold upon severe infection compared to uninfected mice, but did not change in mild infection (Figure 3.14A). MFI revealed a reduction in CCR7 expression in mild infection (20.32±1.35) as well as an increase in severe infection (34.37±0.77) relative to uninfected mice (24.39±0.45) (Figure 3.14B), confirming an inflammatory M1 phenotype in severe infection.

The percentage of CD206 expressing monocytes was low in uninfected mice (8.43%±0.6) and did not significantly change in mild (10.42%±1.16) or severe (11.2%±0.6) infection (Figure 3.14D). There was however a difference in MFI, as monocytes from severely infected mice downregulated CD206 in comparison to monocytes from mild infection (15.9±0.86 vs 22.93±1.98) (Figure 3.14E), further supporting a lack of regulator M2 polarisation in severe infection.

As IL-6 was identified as being more highly upregulated in severe compared to mild infection on day 3, and is associated with an inflammatory monocyte/macrophage phenotype, IL-6 production was measured following *in vitro* LPS stimulation of cells from lung digests, to show the capacity of monocytes to produce IL-6 on day 3 of IAV infection. An increase in IL-6 producing monocytes was found in severe (10.39%±0.9) compared to mild (7.16%±0.42) and uninfected (5.89%±0.58) mice, supporting an inflammatory phenotype and confirming the gene expression results on day 3 of higher IL-6 in severe infection (Figure 3.14G).

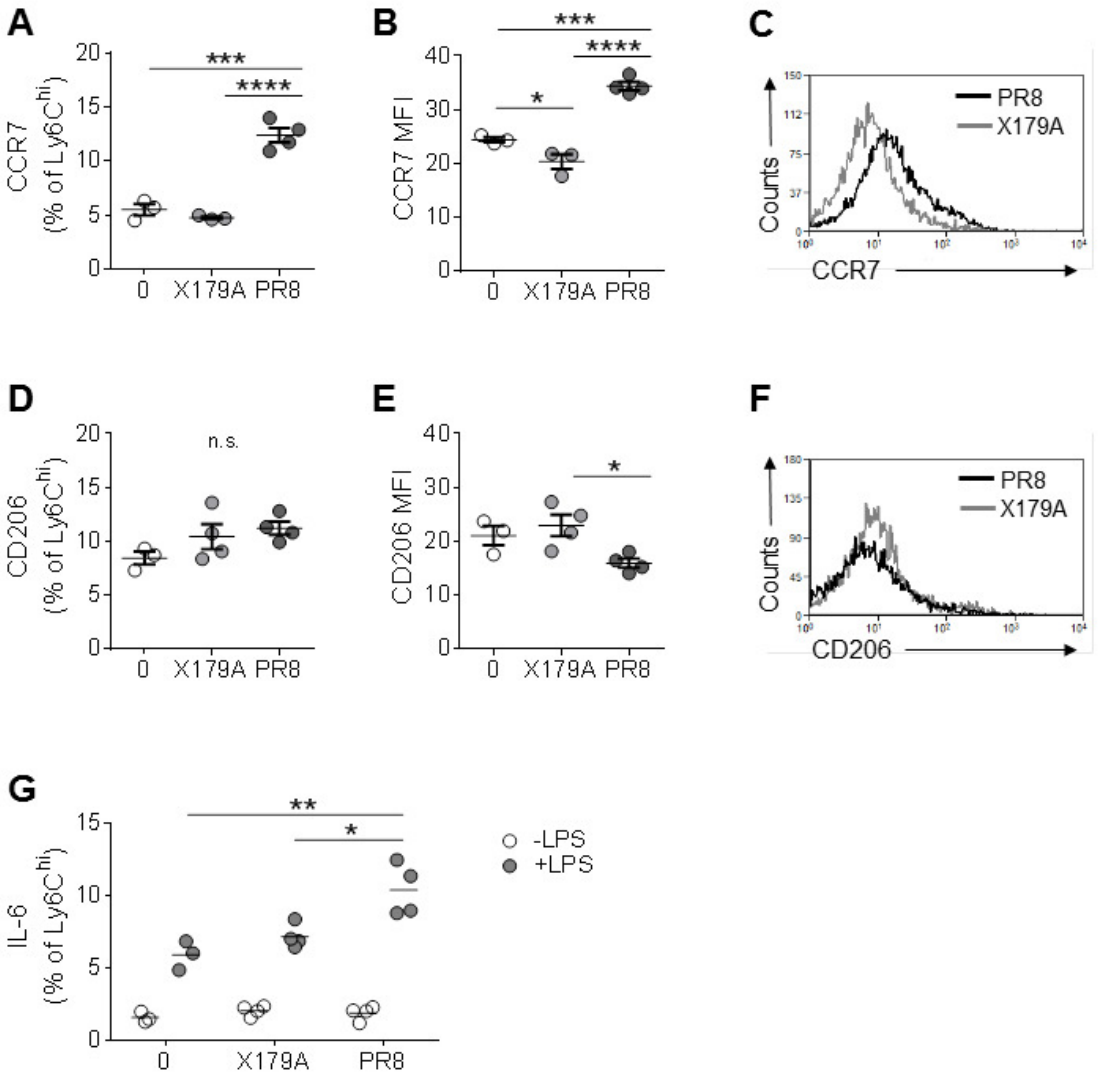

Figure 3.14: Inflammatory M1 monocyte polarisation in severe IAV infection. Expression of CCR7 on Ly6C^{hi} monocytes as **(A)** percentage, **(B)** MFI and **(C)** representative histograms. Expression of CD206 on Ly6C^{hi} monocytes as **(D)** percentage, **(E)** MFI and **(F)** representative histograms. One-way ANOVA used to test for significance **(G)** Percentage of IL-6 production by monocytes stimulated ± 1µg/ml LPS for 18 hours with BFA for the last 4 hours. Two-way ANOVA used to test for significance. N=3-4 mice per group.

3.5 Discussion

In this chapter I showed that severe IAV infection is associated with unique changes in gene expression not observed following infection with a milder strain at the same dose, which were induced rapidly following onset of infection. The number of immune response genes differentially expressed in the lungs in severe infection was much

higher than in mild infection, as was the magnitude of induction for many genes, suggesting a heightened immune response early in severe infection. Significant differences between severe and mild infection with potential implications towards outcome were observed for monocyte-recruiting chemokines and cytokines, interferon and antiviral defence genes.

While viral load was not measured, precluding the ability to compare and determine differences in viral replication between the mild and severe strains, administration of the same dose of either virus to mice did offer some insight into the pathogenicity induced by a standardised dose of virus. The H5N1 virus was much more virulent than X179A at the same dose. Reasons for the higher pathogenicity of H5N1 may lie in the virus's ability to replicate, or mutations in particular viral genes altering the immune response. In humans infected with H5N1, the virus was found to disseminate beyond the respiratory tract, with viral antigen being detected in neurons of the brain and epithelial cells of intestines (442). Detection of viral RNA in blood samples of several H5N1 patients always resulted in fatality (443). The replication efficiency of H5N1 in the lungs was found to be much greater than milder influenza viruses, with highest viral loads correlating with worse outcome (444). The cause of this virulence is likely to reside in the genetic makeup of the virus. Many genes of H5N1 differ from milder H1N1 or H3N2 seasonal virus strains. Early stages of replication involve fusion of the viral membrane with the endosomal membrane via a fusion peptide in the HA molecule. For exposure of the fusion peptide to occur, HA needs to be cleaved into two subunits; HA1 and HA2, and it has been established that the level of cleavability determines virulence. Virulent strains, such as H5N1, have multiple residues at the cleavage site that can be activated by ubiquitous intracellular proteases, potentially leading to systemic infection (445). A number of H5N1 strains were also reported to be resistant to neuraminidase inhibitor treatment (oseltamivir) as a result of a histidine to tyrosine substitution at position 274 of NA (446). Polymerase complex genes PB1, PB2 and PA have been

shown to account for the high virulence of H5N1 strains, even more than HA or NA genes. Lysine, instead of glutamic acid, at position 627 of PB2 confers high pathogenicity due to the ability to replicate better in a wider range of cell types, and has been detected in several H5N1 viruses (447). Perhaps the best known proteins that influence virus pathogenicity are the NS proteins which inhibit antiviral responses mediated by type I IFNs. The NS genes of some H5N1 viruses confer resistance to antiviral effects of TNFα and IFNs due to a glutamic acid at position 92 of NS1 (448). Virulence appears to be determined by several genes acting together, rather than only one of these substitutions.

In this study, cytokine gene expression in severe infection peaked on day 3, with some genes even decreasing by day 5, whereas in mild infection most genes continued to increase from day 3 to day 5, as shown by differences in fold change and GSEA analysis. IL-6 was the gene with the greatest reduction from day 3 to day 5 in severe infection (FC 11.08 to FC 7.16). In mild infection on the other hand, only a 2.89 FC was observed on day 3 but this increased to 7.21 by day 5. IL-6 is noteworthy as others have shown that high expression in lungs and serum from IAV infected mice and humans associates with inflammation, but the exact functional relevance of this is not clear (449, 450). Recent studies have demonstrated that IL-6 actually plays a role in protection against fatal IAV-induced lung pathology. One study found that mice lacking IL-6 were less able to control virus spread, and had enhanced inflammatory monocyte infiltration to the lungs (451). A second study also showed that loss of IL-6 resulted in IAV persistence, leading to lung damage and death. IL-6 protected neutrophils from virus-induced death, which went on to mediate viral clearance (452). These findings fit with the current results as IL-6 was reduced on day 5 compared to day 3 in severe infection, while still increasing in mild infection. Loss of IL-6 later in severe infection may enhance monocyte recruitment and lung damage. IL-6 has also been implicated in regulating the balance between regulatory T cells (Treg) and Th17 cells by suppressing

Tregs and inducing Th17 cells. (453). Suppression of virus-specific Tregs is beneficial by preventing their ability to down-modulate the immune response, suggesting that IL-6 may be beneficial to the host during the adaptive immune response (454). Presence of Tregs however reduced monocyte influx during the early innate response and delayed mortality, which would depend on lower IL-6 levels that do not suppress Treg function (455). The kinetics of IL-6 expression may therefore impact Treg activity differently in innate and adaptive immune responses. CCL8 was the only gene showing a reduction on day 5 in mild infection, while still increasing on day 5 in severe infection. This gene, also known as MCP-2, recruits monocytes to the lungs during IAV infection (455). Out of the three primary monocyte chemoattractant proteins (MCP), MCP-2 has the least potent effect in monocyte recruitment, followed by MCP-3 and then MCP-1 which has the highest activity (456). Lower expression of CCL8 by day 5 in mild infection may contribute to a more regulated recruitment of fewer monocytes, while higher expression in severe infection, along with other monocyte chemoattractants, induces continued monocyte recruitment, which may be driving immune pathology.

Genes within the ‘defence response’ cluster showed the most striking and consistent kinetics over the course of 5 days. In severe infection, a sharp increase was observed in all common ‘defence response’ genes on day 3, which were sustained but not increased on day 5. In mild infection however, a more gradual increase was seen in the same genes on day 3, but expression of all genes continued to increase by day 5. This was most apparent for Saa3, Rsad2 and Mx1. Saa3 has long been recognised as being secreted by the liver during the acute phase of many infections, including IAV (457). It is used as an inflammatory marker, although its exact functions in virus defence are not fully understood. Its expression can be modulated by IL-6, and therefore the continued IL-6 upregulation over the course of mild infection may influence Saa3 upregulation on day 5 (451). Rsad2 is induced by IFNs in airway epithelial cells and is an antiviral mediator (458). It encodes the protein viperin which in

IAV infection has been shown to inhibit budding of the virus from the plasma membrane by disturbing lipid rafts (459). The continued increase in expression may therefore contribute significantly to the milder disease course in X179A infection. Mx1 is another IFN-inducible antiviral gene that functions by blocking viral transcription and replication via inhibiting the PB2-NP interaction (460). These results suggest that an increase in relative expression of interferon-stimulated antiviral genes in mild infection may play an important role in regulating the outcome to infection.

IFNs and IFN-induced genes are primary antiviral agents in IAV infection that function by killing virus-infected cells, upregulating MHC molecules, activating other immune cells, and more. A study in macaques that were infected with H5N1 viruses of differing pathogenicity found that lower expression of IFN-induced genes caused severe infection due to inability to effectively suppress viral replication (434). This was despite comparable upregulation of IFNs themselves in mild and severe cases. A separate study in ferrets also found reduced IFN production to correlate with a more severe outcome to IAV infection (461). In contrast, a study in mice identified that higher morbidity and mortality were caused by higher IFNα/β levels inducing inflammatory cell recruitment and pulmonary damage (158). In the current study, higher expression of IFN-regulated genes were identified in severe compared to mild infection when analysing genes common to both infections. IFN-regulated genes unique to severe infection alone however showed lower expression relative the subset of genes common to both mild and severe infection. This suggests that IFN-regulated genes induced specifically in severe infection are relatively low compared to those induced by IAV infection in general, supporting published findings of low IFN-regulated genes in severe infection. It does however also add a new dimension by showing that there is high expression of some IFN-regulated genes in severe infection which are expressed at low levels in mild infection. This is also supported by studies that identified high IFNα/β levels being causative of severe outcome. Outcome is likely reliant on differential

expression of host IFN associated genes, thresholds of which differ between mild and severe infection. All IFN-regulated genes in this study reached their peak production on day 3 and remained stable on day 5, supporting a role for them in the early innate immune response.

A large number of differentially expressed cytokine genes unique to severe infection were associated with monocyte recruitment. Driven by the observations in IL-6 expression discussed earlier, which has been shown to regulate monocyte infiltration to IAV-infected lungs, a group of chemokines with known roles in myeloid cell recruitment were further analysed. This included the classic monocyte chemoattractant proteins CCL2 (MCP-1), CCL7 (MCP-3), CCL8 (MCP-2) and CCL12 (MCP-5), macrophage inflammatory proteins CCL3 (MIP1α), CCL4 (MIP1β) and CXCL3 (MIP2β) and the IFNγ-inducible cytokine CXCL10 (IP-10). Receptors expressed on myeloid cells or involved in their recruitment were also detected and included CCR1, CCR2, CCR5 and CXCR2 (IL8Rβ). All of these were enriched in the lungs in severe infection on day 3 supporting a role for early monocyte influx, however only IP-10 and CCL8 were expressed in mild infection at this early timepoint. IP-10 is a proinflammatory cytokine which upon binding to CXCR3 induces not only monocyte chemotaxis, but also T cell activation and attraction (462). This early production of IP-10 may preferentially induce T cell trafficking and activation, which was confirmed by the FACS data of X179A infected BAL, showing higher T cells in BAL on day 3 of infection compared to severe infection. However, increased serum IP-10 measurement has also been associated with more severe outcome in humans, and therefore whilst being associated with better outcome in the current study, the exact role of this multifarious cytokine in the outcome to IAV infection is not entirely clear (463).

By day 5, MIP1α, MCP-3 and MCP-5 had become upregulated in mild infection, as well as the MCP-1 receptor CCR2, however there was a trend for levels to be lower than in

severe infection, and on top of this the main monocyte attractant protein MCP-1 was not significantly expressed. This reduction in number and levels of chemokines detected could partially be because monocytes themselves are producers of many of the proteins mentioned, including MCP-1, and therefore lower numbers of monocytes do not have the capacity to produces as many mediators as the large influx seen in more severe infections (464). IAV infection of MCP1$^{-/-}$ mice with a non-lethal dose led to a worse outcome, showing that a regulated influx of monocytes is required for effective clearance of the virus, but if too high can cause pulmonary damage (465). The finding that CCL8 was reduced on day 5 compared to day 3 supports a regulated monocyte recruitment in mild infection. The reduced levels of monocyte associated genes in conjunction with the findings mentioned above regarding sustained IL-6 and antiviral gene expression in mild compared to severe infection supports a vital role for these cells in determining immune pathology and outcome to infection.

Of the chemokine receptors analysed, only CCR2 expression was enhanced on day 5 in mild infection. As well as being the receptor for MCP-1, CCR2 also acts as a receptor for CCL7 (MCP-3). It is also a receptor for CCL11, CCL13 and CCL16, although these cytokines bind other receptors too. CCR2 is expressed highly on inflammatory monocytes, so detection of this gene could be a sign of monocyte recruitment to the lungs by day 5 in mild infection.

The identification of a dominant M1 inflammatory macrophage phenotype in severe infection but both inflammatory M1 and regulatory M2 genes being enriched in mild infection suggests that differences in myeloid subset polarisation may influence outcome to different influenza viruses. The regulatory M2 subset has not been well characterised in IAV infection as most evidence points towards an inflammatory monocyte/macrophage phenotype in driving pathology. One report found that natural bacteria protect against IAV-mediated lung injury by polarising lung-recruited

monocytes to M2 macrophages, dependent on TLR2 signalling, and suggested that iNKT cells were the main source of IL-13 that promote this priming (466). The confirmation of gene expression results by FACS analysis of CCR7 and CD206 add further weight to these findings. While expression was measured on monocytes rather than macrophages, transcriptional profiling of monocyte to macrophage differentiation in humans identified an increase in CCR7 transcript expression on monocytes differentiating to M1 macrophages (267).

The fact that it takes longer in X179A infection to mount a similar magnitude of response as in H5N1 infection in certain cytokines and defence genes could explain why this virus is less harmful to the host. Severe infection in humans is associated with increased serum levels of inflammatory mediators including IL-6, IL-8, TNFα, IFNγ, IP-10 and MCP-1 which is associated with higher viral loads, suggesting that hypercytokinemia drives pathogenicity of severe infection (444, 467). Therefore a more gradual induction of inflammatory mediators may be less destructive to lung epithelial cells that are already damaged by the virus.

A potential limitation in this work was the need to pool the RNA samples for gene chip hybridisation in H5N1 infection, and therefore the lack of p values for analysis. This makes the interpretation difficult when it comes to the genes that were identified as being ‘unique’ to mild infection, which may have been significantly differentially expressed in severe infection but at a lower fold change. Genes unique to mild infection were however very limited. Agr2 was the only gene upregulated on both day 3 (FC 3.89) and day 5 (FC=4.38) in mild infection that was not upregulated in severe infection. This gene is also known as Anterior Gradient protein 2 and is expressed in tissues that secrete mucus, including the lungs. Agr2 was found to be induced in asthma and promoted mucin overproduction (468). Interestingly, Agr2 associates with

the mucin Muc5ac which promotes mucin secretion and was also unique to mild infection on day 5 (FC=4.14) (469). Agr2$^{-/-}$ mice show 50% reduction in Muc5a expression following allergen challenge showing a link between these two proteins (468). Mucus production protects against virus and bacterial infections by providing a barrier, however overproduction can impede comfortable breathing. As the IAV infected X179A mice did not appear to suffer from respiratory impairment, it is likely that the increase in these genes leads to more mucus production which protected against infectivity by trapping the virus. While the NA protein of IAV is specialised for degrading mucus barriers, more mucus production will make this harder to do. The other unique genes to mild infection, Sectm1b (Secreted and Transmembrane 1B), Reg3g (Regenerating islet-derived 3 gamma) and Mthfd2 (Bifunctional methylenetetrahydrofolate dehydrogenase/cyclohydrolase) did not show any links or relevance to these findings.

3.6 Conclusions

Monocyte processes dominate the early immune response to severe IAV infection in the lungs. The induction of monocyte-specific genes in severe infection is more rapid and of a greater magnitude than during mild infection, where fewer monocyte related genes are upregulated. The later induction of monocyte-recruiting genes during an asymptomatic mild disease, and presence of both M1 and M2 polarisation, supports the hypothesis that recruitment of a limited number of monocytes is important for defence against IAV infection, but that an overwhelming number of inflammatory monocytes may contribute towards the pulmonary damage and inflammation observed in severe infection.

Chapter 4: Myeloid cell profile during acute influenza infection in humans

4.1 Introduction

Having established that high monocytes correlated with severe disease in mouse Influenza A virus (IAV) infection in the previous chapter, the immune cell phenotype during acute IAV infection in humans was next examined in order to determine if the findings in mice were reflected in human disease. In this chapter I focused on the hypothesis generated from Chapter 3; that monocytes are a major determinant of pathology and outcome during severe IAV infection.

The 2009 H1N1 pandemic ('pH1N1'; A/CA/04/2009) provided a unique opportunity to study immune cell responses to a virus not previously encountered by the population. Pandemic IAV strains have the ability to transmit rapidly and cause severe illness. The contribution of the innate immune response to pathology during human IAV infection has however not been widely studied, despite its importance in a situation where limited or no specific pre-existing adaptive immunity exists. In particular, monocyte contribution to immune pathology in severe human IAV infection was under-studied at the start of my project. This is partly because innate cells have been less well characterised in humans during inflammation, and because of the requirement of fresh samples for accurate identification and profiling of these cells.

The majority of pH1N1 infected individuals only suffered mild symptoms, however a subset required hospitalisation. Analysis of the lungs in fatal cases of pH1N1 infection revealed similar pathological findings as past pandemics comprising severe alveolar damage compatible with the generic, most severe form of lung injury - acute respiratory distress syndrome (ARDS). Influenza viral antigen was detected in bronchiolar

epithelium and alveolar macrophages, and histopathological changes were apparent in the upper and lower respiratory tract (470). Obesity, chronic lung disease, pregnancy and immunosuppression were identified as clinical correlates to poor outcome (102).

Circulating monocytes display high plasticity and appear to have contrasting functions upon recruitment to IAV infected lungs in different models. In mouse IAV infection, monocytes recruited to lungs were shown to differentiate into antiviral type I IFN-producing DCs which improved outcome in one study (278), inflammatory DCs that drove pulmonary immune pathology in a separate study (279) or TNFα and iNOS producing DCs (TipDC) which were required for an appropriate $CD8^+$ effector T cell response for virus control, but led to pulmonary pathology and lethal outcome if recruited in excessive numbers in another study (270). Alveolar macrophages were crucial for protection against IAV infection in one study as ablation increased viral load and airway inflammation (471), however in another study inflammatory monocytes recruited to the lungs that differentiated into macrophages caused lung injury (282).

Understanding the role of myeloid-lineage cells in human IAV infection will depend in part on detailed phenotypic and functional characterisation of these cells *ex vivo* and the accompanying innate and adaptive immune response. If indeed there is a role for monocytes in causation of pathology in severe IAV, then these cells are an attractive drug target since they are circulating, can be clearly identified, and targeting these cells peripherally may well modulate the ultimate type of macrophage or Tip-DC response in the lungs. In addition, monocytic profiling could provide a biomarker for identification of patients with poorer outcome to IAV infection.

4.2 Aims

The aims of this chapter were to characterise the myeloid cell response in the blood of patients with severe IAV infection to identify immune cell correlates to disease outcome, and to explore the correlation of monocyte frequency, phenotype and function with severity of IAV infection.

4.3 Methods

4.3.1 Patient samples

Hospitalised patients with influenza-like illness were recruited as part of the MOSAIC study and pH1N1/09 infection was confirmed by viral PCR (Methods 2.2.1) (472).

76 samples were received from acutely infected patients. Blood was obtained 48-72 hours after hospitalisation regardless of PCR status, co-infection, co-existing illness and medication. Of these, 34 patients provided a “convalescent” sample, obtained 4-6 weeks after acute sampling. Blood from healthy controls was also sent in identical conditions from London. Blood was processed and analysed immediately for all samples (Methods 2.2.2).

Patient disease severity was based on respiratory score at the time of sampling and formed two final groups for analysis:

- Mild: no respiratory compromise (O_2 saturation > 93% on room air)
- Severe: respiratory compromise (O_2 saturation 93% or less, on room air with or without assisted ventilation (non-invasive or mechanical ventilation)).

Maximum severity score during hospitalisation was also recorded, and has been used to identify whether predictive markers of severity could be identified in this analysis.

At the point of analysis, all samples with confirmed pH1N1 infection were first subjected to ordered logistic regression analysis performed in R statistical programming environment (www.r-project.org) using the function polr (package MASS (473)) in collaboration with our biostatistician, Emmanouela Repapi, to first identify if any confounding clinical factors (Table 4.1) associated with disease severity. Only pregnancy had a significant association with severity at the point of admission (p value ≤0.001) and at any point during hospitalisation (p value 0.020). In order to identify potential associations with immune response markers an analysis was performed for each immune marker in table 4.1 (including pregnancy in the models) using an ordered logistic regression with disease severity as the outcome. No associations were shown to be significant (p value≤0.05) in this analysis.

Confounding clinical factors	**Immune response markers**

• Asthma
• Diabetes mellitus
• Current cancer
• Pregnancy
• Bacterial co-infection within 48 hours of sampling
	• T cell ELISpot(1) (SFU/10^6 PBMC)
	  ○ pH1N1/09 HA peptide pool 1
	  ○ pH1N1/09 HA peptide pool 2
	  ○ pH1N1/09 NA peptide pool
	  ○ pH1N1/09 NP peptide pool
	  ○ pH1N1/09 NS peptide pool 1/2
	• Absolute number of PBMC/ml blood
	• Neutrophilic MDSC (as % of all FACS events)(2)
	• Monocytes (as % of all FACS events)(3)
	• $CD14^+CD16^-$ (as % total monocytes)
	• $CD14^{mid}CD16^+$ (as % total monocytes)
	• $CD14^{mid}CD16^+$ (as % total monocytes)
	• CD3 (as % of all FACS events)(4)
	• Neutrophilic MDSC (as ratio to CD3)
	• Total monocytes (as ratio to CD3)
	• Activated effector CD8 (as % of CD8)(5)

Table 4.1: Input for logistical regression analysis of disease severity. (1)IFNγ ELISPOT of fresh PBMC stimulated with peptide pools spanning the pH1N1 proteome, as described in Methods 2.1.15. (2)Percentage of neutrophilic MDSC, as defined in Figure 4.2C, in PBMC samples. (3)Percentage of total monocytes and monocyte subsets, as defined in Figure 4.2F, in PBMC samples. (4)$CD3^+$ T cells, as defined in Chapter 5 Figure 1A and (5)Activated effector $CD8^+$, as defined in Chapter 5 Figure 2A as $CD38^+HLA\text{-}DR^+$ cells. MDSC= myeloid-derived suppressor cells

As a result of this, exclusions were applied to provide analysis of patients without unordered confounding factors. Patients with the following conditions were excluded:

- Pregnancy
- Subjects with haematological malignancies, and any current known cancers
- Subjects with formal non-malignant immune-deficient states e.g. HIV infection, previous organ transplant and immunosuppressant use

Of the pH1N1 patients, a subset was treated with oral or parenteral corticosteroids at or before the point of sampling. These were grouped separately for analysis. Those who were classified as having influenza clinically at the point of sampling and latterly shown to be H1N1 negative by PCR were classified as having influenza-like illness (ILI).

Following application of these criteria, details of number and demographics of MOSAIC patients used in this study for analysis are displayed in table 4.2.

	Severity	Number	Age (mean)	Male n (%)	Asthma n (%)	BMI>30 n (%)
pH1N1	Mild Severe	7 14	42.4 41.7	3 (42.9%) 8 (57.1%)	3 (42.9%) 0	2 (28.6%) 7 (50%)
pH1N1 (steroids)	Mild Severe	5 7	36.1 50.9	0 6 (85.7%)	5 (100%) 3 (42.9%)	2 (40%) 1 (14.3%)
pH1N1$^-$ (ILI)	Mild Severe	10 7	50.1 51.3	4 (40%) 4 (57.1%)	5 (50%) 1 (14.3%)	4 (40%) 5 (71.4%)

Table 4.2: Demographics of all patients who provided blood samples during acute illness. Number of patients with mild or severe disease in each group, further characterised by age, sex, asthma status and BMI (BMI>30: obese).

4.3.2 Sample processing

Samples were processed immediately upon receipt (Methods 2.2.2). Whole blood was divided into two aliquots; one small 2ml aliquot for whole blood lysis, while PBMCs were extracted from the remaining blood by layering over Ficoll. Surface antigen staining for phenotyping of immune cells by flow cytometry was carried out on PBMC and lysed blood samples immediately. For detection of cytokines by multiplex analysis, whole lysed blood samples were stimulated with LPS for 18 hours or left unstimulated

and supernatants collected at the end of stimulation. Absolute counts of immune cells were calculated based on starting volume of blood, PBMC count following isolation and frequency of immune cell subset determined by flow cytometry, by using the following formula:

$$\text{Cells/ml blood} = \frac{\textit{PBMC count}}{\textit{ml blood}} \times \frac{\textit{population of interest (event count)}}{\textit{live cells (event count)}}$$

Further monocyte characterisation was carried out on cryopreserved PBMCs which had been frozen immediately after PBMC extraction and initial analyses had been carried out. PBMCs were thawed, rested for 1 hour and counted. Surface antigen staining was carried out on cells immediately following thawing, and intracellular cytokine staining was carried out following 6 hours of *E. Coli* LPS stimulation (Methods 2.1.6).

Mixed leukocyte reactions (MLR) were carried out to determine the suppressive effect of (a) neutrophilic MDSC, (b) monocytes and (c) classical neutrophils on T cell proliferation, as summarised in Figure 4.1 and detailed in Methods 2.1.16. Following Ficoll density gradient separation, the PBMC layer was extracted. From this, MACS beads were used to isolate $CD11b^+$ cells and then $CD15^+$ cells (Methods 2.1.5). $CD11b^+CD15^+$ cells were neutrophilic MDSC and the remaining $CD11b^+CD15^-$ cells were monocytes. Cells isolated from immediately on top of the red blood cells represented classical neutrophils. Peripheral blood lymphocytes (PBL) from the $CD11b^-$ fraction were stimulated with allogeneic irradiated DCs at a 4:1 ratio, and cell subsets (a), (b) or (c) were added at a 1:1 ratio to PBL. Proliferation was measured over 5 days by thymidine incorporation.

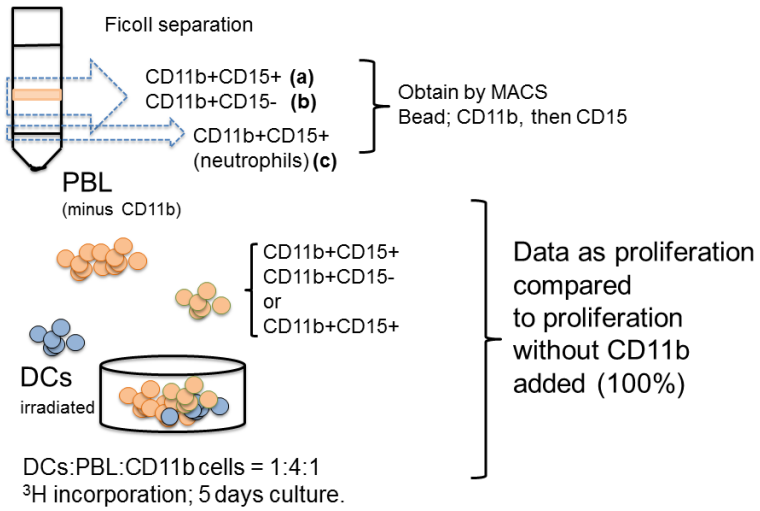

Figure 4.1: MLR assay outline. Myeloid cells derived from PBMC or red blood cell layer; PBL derived from PBMC layer. Allogeneic irradiated DCs co-cultured with PBL and myeloid populations for 5 days and proliferation measured by thymidine incorporation.

4.3.3 Flow cytometry analysis and gating strategy for myeloid cells

Following compensation and doublet exclusion, autofluorescent cells were excluded from the FSc/SSc profile (Figure 4.2A) and the remaining leukocytes gated to analyse CD14 and CD15 expression (Figure 4.2B). Neutrophilic MDSCs were gated from the $CD15^{hi}$ cells, while monocyte populations were gated from $CD15^{low}$ cells. $CD15^{hi}$ cells were gated to analyse CD16 expression (Figure 4.2C). $CD16^{-}CD11b^{+}CD15^{hi}$ cells were characterised as neutrophilic MDSC, while $CD16^{+}CD11b^{+}CD15^{hi}$ were characterised as activated neutrophils. Further analysis of neutrophilic MDSC revealed high CD66, variable CD62L (Figure 4.2D), and low HLA-DR expression (Figure 4.2E).

For gating of monocyte populations, all except the $CD15^{hi}$ cells were gated to show CD14 against CD16 (Figure 4.2F). This allowed identification of the three well characterised monocyte subsets (474): (i) $CD14^{+}CD16^{-}$ classical, (ii) $CD14^{+}CD16^{+}$ inflammatory and (iii) $CD14^{mid}CD16^{+}$ patrolling monocytes. The combination of these three subsets is referred to as 'total monocytes'. Positive HLA-DR staining for

monocytes is shown (Figure 4.2G) as comparison for low HLA-DR staining identified in neutrophilic MDSCs in Figure 4.2E.

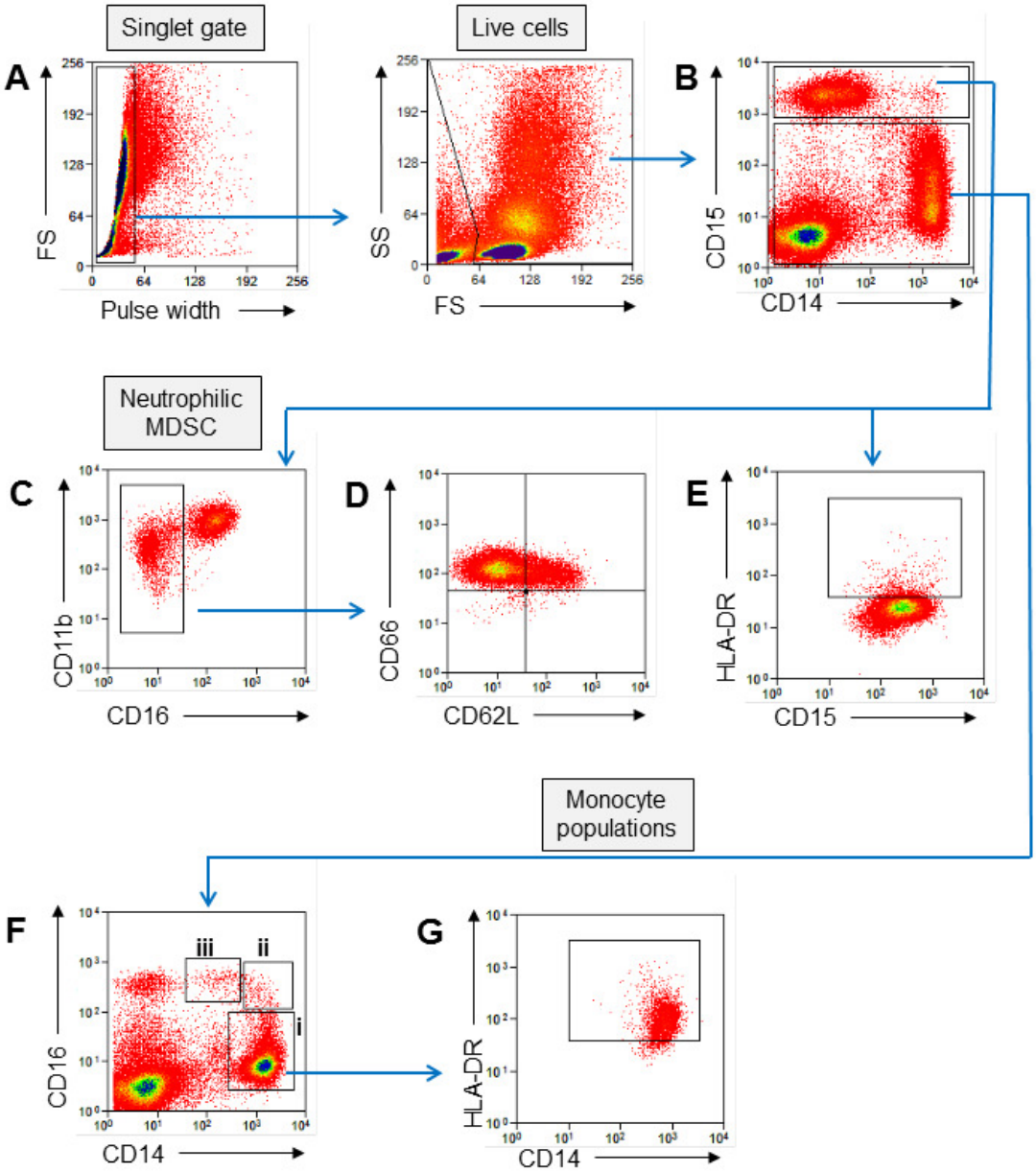

Figure 4.2: Flow cytometry gating of myeloid cell populations. (A) Singlets were selected based on pulse width (top left) and gated onto FSc/SSc. Autofluorescent cells were excluded to provide a 'live cell' gate, which was applied to a plot of **(B)** CD14 against CD15. **(C)** $CD15^{hi}$ neutrophils were divided based on CD16 expression to distinguish activated neutrophils and neutrophilic MDSCs, both expressing CD11b. **(D)** Neutrophilic MDSC expressed high CD66, variable CD62L and **(E)** low HLA-DR. **(F)** $CD15^{low}$ cells from **(B)** were gated onto CD14/CD16 plot to identify monocyte populations: (i) classical monocytes, (ii) inflammatory monocytes, (iii) patrolling monocytes). **(G)** HLA-DR expression of classical monocytes. Blue arrows depict application of gate from plot that arrow originates from onto plot at which arrow is pointing.

$CD14^{hi}(CD15^{low})$ and $CD15^{hi}$ cells gated from all live cells were coloured green and blue, respectively, and gated back on the FSc/SSc profile to display size and granularity of monocytes (green) and neutrophils (blue) (Figure 4.3A). Hoechst staining was used to identify dead cells which were routinely no more than 0.5%-1.5% of the 'live cell' gate (Figure 4.3B).

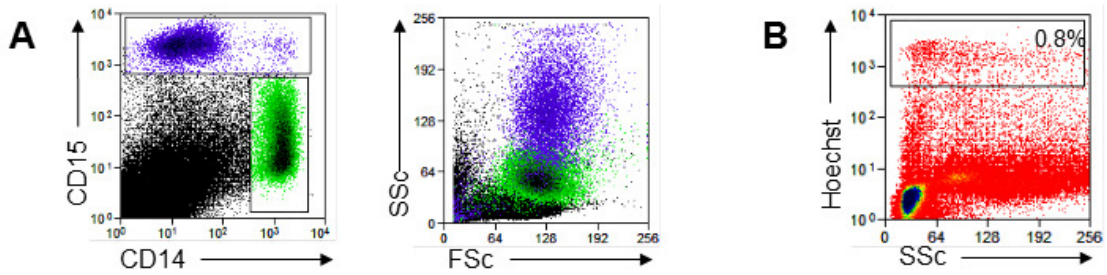

Figure 4.3: Flow cytometry of myeloid cell size and granularity (A) $CD14^{hi}$ monocytes (green) and $CD5^{hi}$ neutrophils (blue) analysed for size and granularity by FSc/SSc. **(B)** Dead cell analysis using Hoechst staining showed that only a small minority of cells were $Hoechst^{+}$ (gated from all singlets in Figure 4.2A).

Details of gating and identification of myeloid subsets are outlined in Table 4.3.

Cell population	Gating strategy	Figure reference
Activated neutrophils	Live cells, $CD15^{hi}$, $CD11b^{+}$, $CD16^{+}$	Figure 2B
Neutrophilic MDSC	Live cells, $CD15^{hi}$, $CD11b^{+}$, $CD16^{-}$ $CD66^{+}$, $CD14^{+/-}$, $CD62L^{+/-}$, HLA-DR^{low}	Figure 2C
Total monocytes	Live cells, CD15low, $CD14^{+/mid}$, $CD16^{+/-}$	Figure 2F
• Classical monocytes	Live cells, $CD15^{low}$, $CD14^{+}$, $CD16^{-}$	Figure 2F (i)
• Inflammatory monocytes	Live cells, $CD15^{low}$, $CD14^{+}$, $CD16^{+}$	Figure 2F (ii)
• Patrolling monocytes	Live cells, $CD15^{low}$, $CD14^{mid}$, $CD16^{+}$	Figure 2F (iii)

Table 4.3: Classification of myeloid cell populations. Populations of myeloid cells used for phenotyping analyses.

4.4 Results

4.4.1 Neutrophilic MDSC and monocytes dominate cellular immune profile in blood during severe acute IAV infection

Frequencies of immune cell subsets in pH1N1 patients ('pH1N1'), pH1N1 patients treated with corticosteroids ('pH1N1 steroids'), patients with influenza-like illness ('ILI') and healthy controls ('HC') were analysed first. Percentage and absolute counts of neutrophils, neutrophilic MDSCs and monocytes were determined (as described in 4.3.3) and grouped by mild or severe disease within each patient group. The analysis first questioned if there was a difference between severe and mild disease in pH1N1 patients and pH1N1 steroid-treated patients. Then the uniqueness to pH1N1 was questioned by examining if the differences were also observed in ILI patients. Values from mild and severe pH1N1 infection were then compared to healthy controls.

The most striking finding was the presence of large high granularity cells in the FSc/SSc profiles of pH1N1 patients. These were not expected in PBMCs extracted by Ficoll density gradient separation and not observed to the same extent in ILI samples which were sampled, transported and processed in the same manner (Figure 4.4). Others have identified these lower-density neutrophilic cells as either being activated neutrophils or MDSCs with T cell suppressive effects (475).

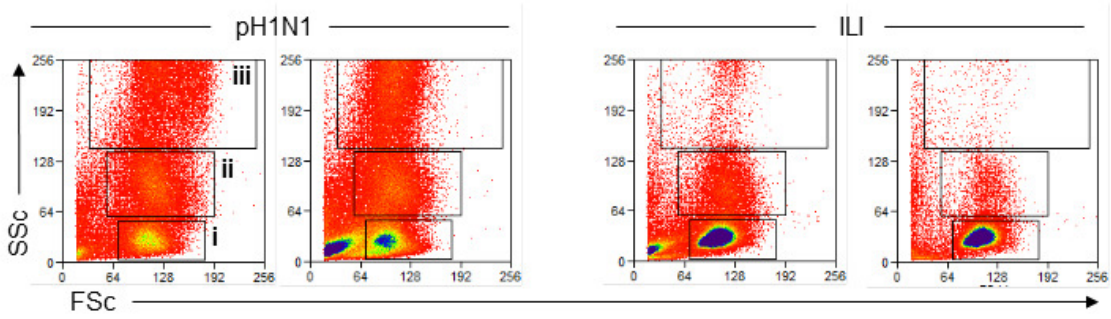

Figure 4.4: Altered immune cell profile in pH1N1 patients relative to ILI. Representative flow cytometry plots from two severe pH1N1 subjects and 2 mild ILI subjects to demonstrate over-representation of populations (ii) and (iii) in severe pH1N1 patients compared to ILI. Populations refer approximately to (i) lymphocytes, (ii) monocytes, (iii) neutrophils.

The total frequency of these large granulocytic cells was first evaluated (Figure 4.5A). Absolute numbers per ml blood of $CD15^{hi}$ neutrophils were higher in severe compared to mild pH1N1 patients ([mean±SEM] 861,687±208,076 vs 174,840±108,335). There was no change in severe compared to mild pH1N1 steroid-treated patients (179,067±60,979 vs 246,748±131,095). ILI patients also showed an increase in severe compared to mild disease (432,932±263,371 vs 67,063±24,087), although numbers were 2-fold lower than in pH1N1 infection. HC had very low numbers of $CD15^{hi}$ cells in PBMC (18,462± 5,639); significantly lower than severe pH1N1 patients.

The frequency of total $CD15^{hi}$ neutrophils as a percentage of live cells was not significantly different between severe and mild pH1N1 patients (24.61±4.18 vs 16.89±6.57) or pH1N1 steroid-treated patients (29.51±15.86 vs 22.19±8.129), but was significantly higher in severe ILI patients compared to mild (16.76±7.58 vs 4.804±0.94) (Figure 4.5B). Comparison of pH1N1 patients to healthy controls showed a higher percentage of $CD15^{hi}$ neutrophils in severe pH1N1 disease compared to HC (6.32±2.30).

As these neutrophilic cells were not expected in PBMC, they were further characterised using CD16, by enumerating $CD15^{hi}CD16^{-}$ cells ('neutrophilic MDSC'; defined in 4.3.3.) The absolute value of neutrophilic MDSCs/ml blood was significantly higher in severe compared to mild pH1N1 patients (451,839±141,332 vs 38,209±14,137) (Figure 4.5C). No difference between severe and mild disease was found in steroid-treated pH1N1 patients (100,810±51,961 vs 122,761±84,976). ILI patients showed an increase in neutrophilic MDSCs in severe compared to mild disease (289,364±180,478 vs 10,955±5,080). Comparison of pH1N1 patients to healthy controls revealed significantly more neutrophilic MDSCs in severe disease (HC: 849±103).

Similar results were found when analysing neutrophilic MDSCs as a percentage of live cells, with an increase in severe pH1N1 patients compared to mild (11.94±3.21 vs 3.62±1.53) (Figure 4.5D). No significant difference was found between severe and mild steroid-treated pH1N1 patients (11.44±7.40 vs 14.02±6.82), but an increase in severe disease compared to mild was found in ILI patients (7.10±4.12 vs 0.86±0.26). Healthy controls had less neutrophilic MDSCs as a percentage of live cells than severe pH1N1 patients (0.89±0.21).

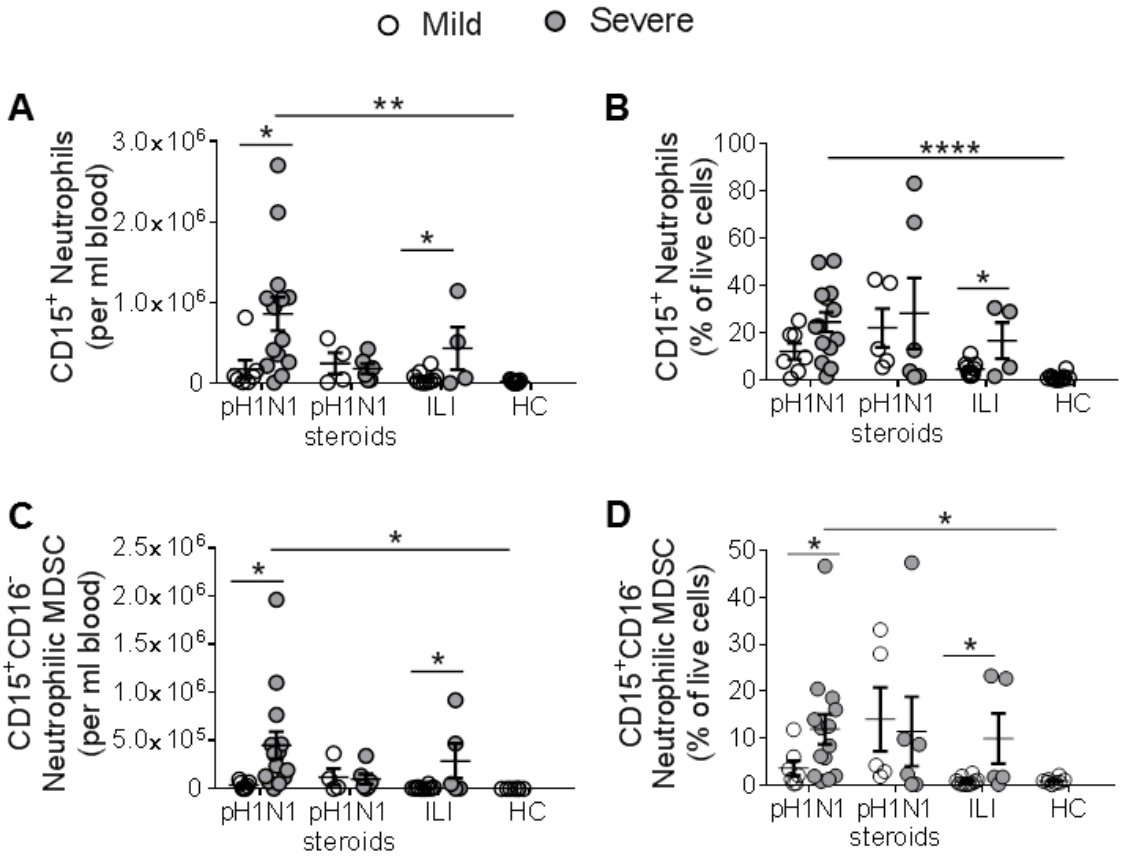

Figure 4.5: High neutrophilic cells in PBMC samples during severe disease. Neutrophil frequency as **(A)** absolute count/ml blood or **(B)** percentage of live cells from flow cytometry analysis in pH1N1 subjects (n=7 mild, n=14 severe), pH1N1 steroid-treated subjects (n=5 mild, n=6 severe), ILI subjects (n=10 mild, n=5 severe) and healthy controls (n=8). Neutrophilic MDSC frequency as **(C)** absolute count/ml blood or **(D)** percentage of live cells in the same patients as (A)-(B). Significance determined by t-tests within groups and one-way ANOVA between pH1N1 patients and HC.*p≤0.05, **p≤0.01, ****p≤0.0001.

Whole lysed blood samples, which were available for a subset of patients from Figure 4.5, were next analysed for total neutrophil frequency and compared between severe and mild pH1N1 patients and HC (Figure 4.6A). Severe pH1N1 patients had significantly more $CD15^{hi}$ neutrophils compared to healthy controls (67.77±4.28 vs 44.01±2.56).

In order to determine the relative proportion of neutrophilic MDSC in PBMC samples, comparisons between whole lysed blood and PBMC samples were made for $CD16^-$ neutrophils as a percent of $CD15^{hi}$ cells. In severe pH1N1 disease, significantly more neutrophils were $CD16^-$ in PBMC than in lysed blood (44.92±11.36 vs 11.52±2.44), suggesting that the presence of $CD15^{hi}$ cells in PBMC is largely due to an enrichment of the $CD16^-$ subset; neutrophilic MDSCs (Figure 4.6B).

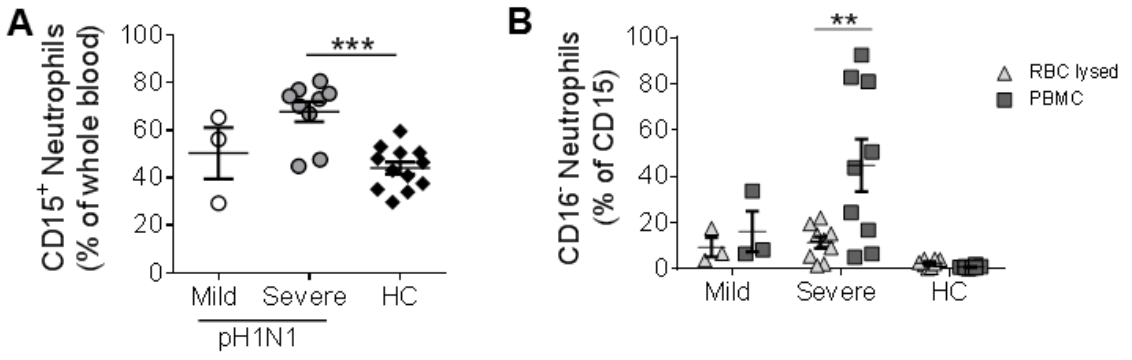

Figure 4.6: Enrichment of neutrophilic MDSCs in PBMC samples compared to whole blood. (A) Percentage of total $CD15^+$ neutrophils in whole lysed blood samples from mild pH1N1 (n=3), severe pH1N1 (n=9) and HC (n=12). **(B)** Comparison of neutrophilic MDSC ($CD15^+CD16^-$) as percentage of total neutrophils between PBMC and whole lysed blood samples from the same patients as (A). Significance in (A) determined using one-way ANOVA and in (B) using two-way ANOVA **p≤0.01, ***p≤0.001.

Absolute number of total monocytes (as defined in 4.3.3) were higher in severe compared to mild pH1N1 patients (441,275±102,865 vs 88,127±755,135) (Figure 4.7A). There was no difference between severe and mild disease in pH1N1 steroid-treated patients (167,629±42,695 vs 188,815±108,366), or severe and mild disease in ILI patients (276,397±146,937 vs 89,491± 34,914). Comparison of pH1N1 patients to healthy controls found a significant increase in monocyte number in severe disease compared to HC (67,840±15,329). Two outliers in mild disease were identified; one in the pH1N1 group (431,783 monocytes/ ml blood) and one in the steroid-treated group (617,543 monocytes/ ml blood), both of who went on to develop severe disease during hospitalisation, suggesting that increased monocyte frequency may be predictive of a worse outcome.

Total monocytes as a percentage of live cells were increased in severe compared to mild disease in pH1N1 patients (13.57±2.63 vs 5.06±1.59) but no significant differences between severe and mild disease were found in steroid-treated pH1N1 patients (12.05±5.45 vs 8.96± 2.85) or ILI patients (9.57±4.06 vs 6.55±1.22), or between pH1N1 infection and healthy controls (7.16±2.08) (Figure 4.7B). The patients with the highest monocyte frequency in the mild pH1N1 and steroid-treated pH1N1 groups were the same as identified in the previous graph that went on to develop severe disease.

Monocyte subsets from pH1N1 patients were next analysed to identify percentage of classical ($CD14^{+}CD16^{-}$), inflammatory ($CD14^{+}CD16^{+}$) and patrolling ($CD14^{mid}CD16^{+}$) monocytes (gated and defined as in 4.3.3). In severe disease compared to mild, there was a reduction in classical monocytes (90.79±1.4 vs 96.5±0.9) (Figure 4.7C) and an increase in inflammatory monocytes (5.3±0.7 vs 2.3±0.3) (Figure 4.7D). No significant changes were observed in patrolling monocytes (2.5±0.6 vs 1.6±0.6) (Figure 4.7E).

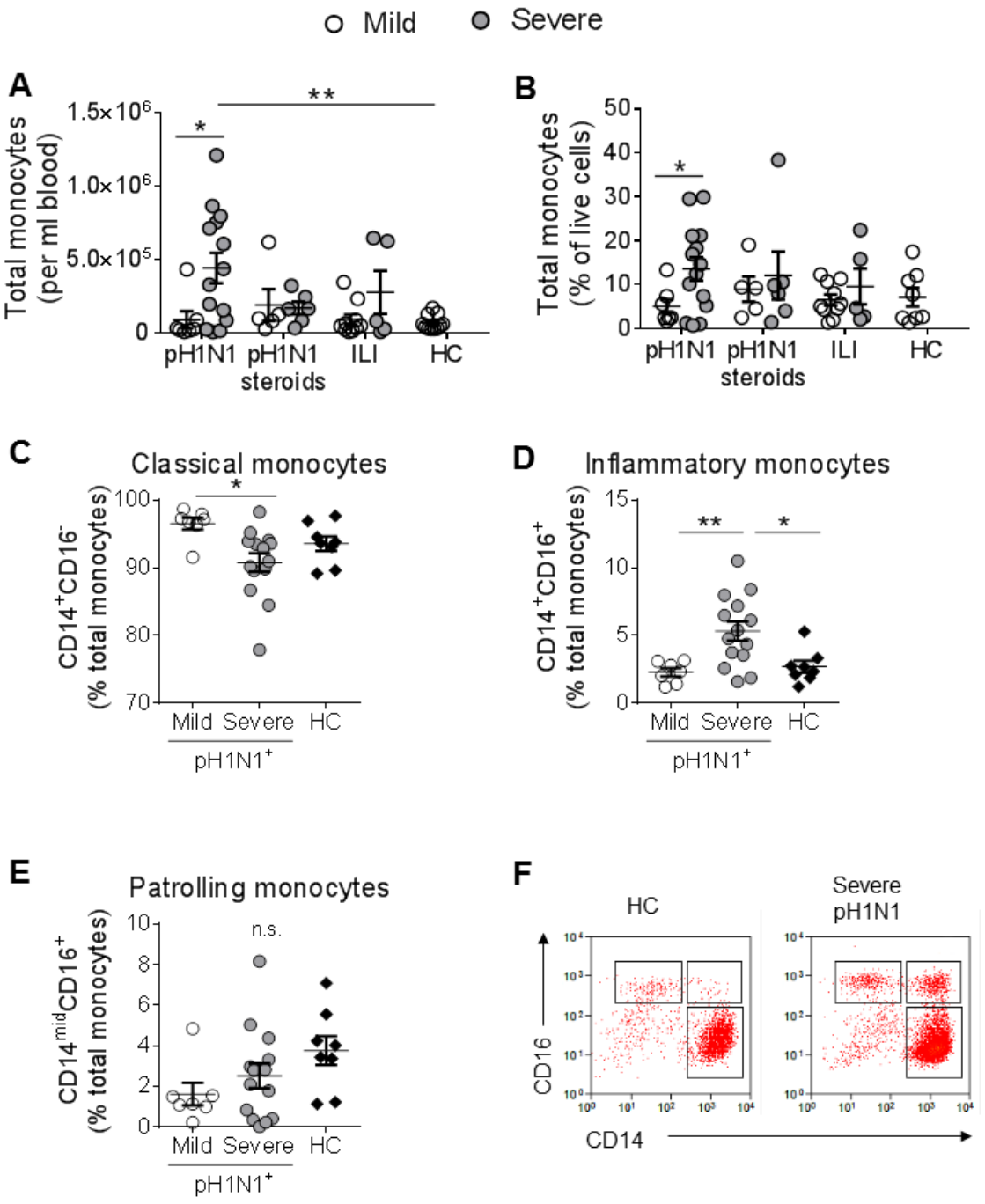

Figure 4.7: High monocyte frequency is specific to severe IAV infection. Monocyte frequency as **(A)** absolute count per ml blood or **(B)** percentage of live cells from flow cytometry analysis in pH1N1 subjects (n=7 mild, n=14 severe), pH1N1 steroid-treated subjects (n=5 mild, n=6 severe), ILI subjects (n=10 mild, n=5 severe) and healthy controls (n=8). Monocyte subsets identified as **(C)** classical monocytes ($CD14^+CD16^-$), **(D)** inflammatory monocytes ($CD14^+CD16^+$) and **(E)** patrolling monocytes ($CD14^{mid}CD16^+$) calculated as a percentage of total monocytes for mild pH1N1 patients (n=7), severe pH1N1 patients (n=14) and healthy controls (n=8). **(F)** Flow cytometry analysis of monocyte subsets in a representative HC and severe pH1N1 patient. Significance determined by t-tests within groups and one-way ANOVA between pH1N1 patients and HC.*p≤0.05, **p≤0.01.

To determine the suppressive nature of MDSCs, a mixed leukocyte reaction (MLR) was used to investigate T cell proliferation (TCP) following addition of classical neutrophils, neutrophilic MDSC or monocytes (isolated as in 4.3.2) for pH1N1 and ILI patients. In pH1N1 patients, classical neutrophils were poor at suppressing T cell proliferation (74%±7.8 TCP). Both neutrophilic MDSC and monocytes were suppressive, and more so than classical neutrophils (53.64±8.71 and 34.64±9.01 % TCP, respectively) (Figure 4.8A). This confirmed the suppressive nature of neutrophilic MDSCs, and furthermore identified a monocytic MDSC population, although the assay was unable to differentiate between classical monocytes (characterised in Figure 4.7) and monocytic MDSC. In ILI patients, there was no difference in the ability of classical neutrophils, neutrophilic MDSC or monocytes to suppress T cell proliferation (65.5±12.66, 70.25±10.29 and 55.75±21.51 % TCP, respectively) (Figure 4.8B). This suggests that innate cells with suppressive capacities were found only in IAV-infected patients.

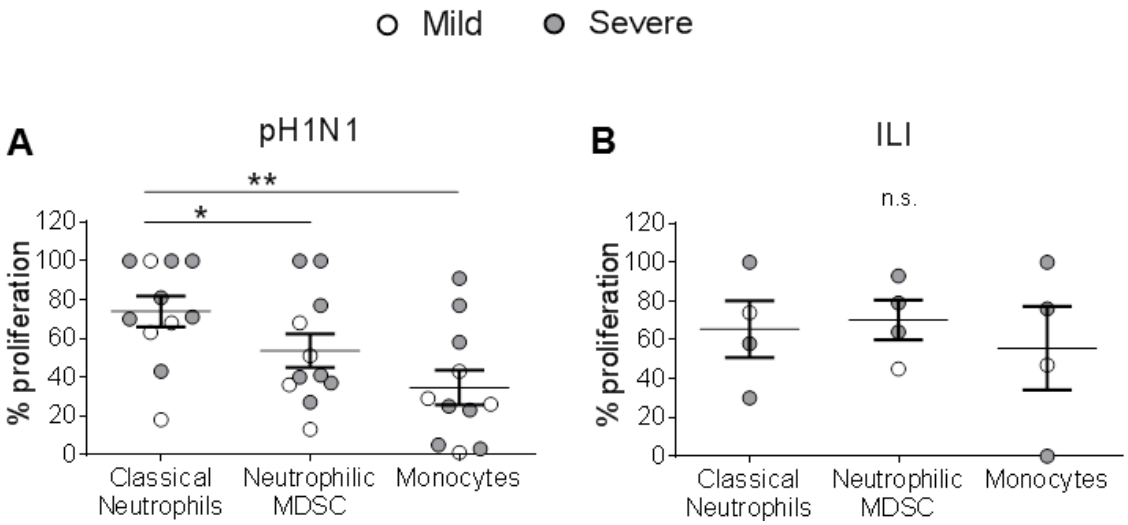

Figure 4.8: Suppressive capacity of MDSCs in pH1N1 patients. Percentage of T cell proliferation in response to allogeneic DCs following addition of classical neutrophils, neutrophilic MDSC or monocytes. pH1N1: n=4 mild, 7 severe; ILI: n=1 mild, 3 severe. One-way ANOVA between groups *p≤0.05, **p≤0.01.

4.4.2 Differences in neutrophilic MDSC and monocytes post-freezing

This study so far identified monocytes and neutrophilic MDSCs as major cellular components in severe IAV infection. This is one of few studies on innate cells in human cohorts where samples had not been frozen and thawed before analysis. PBMCs that had been frozen and later thawed from this study revealed a near complete loss of $CD15^{hi}$ neutrophils, identifiable in flow cytometry FSc/SSc profiles (Figure 4.9A) and as quantification of total $CD15^{hi}$ cells as a percentage of live cells (Figure 4.9B). Total monocyte frequency was not significantly altered following freezing, although an increase in some cases is due to the loss of large quantities of $CD15^{+}$ neutrophils, causing the remaining cells to account for a larger proportion of live cells (Figure 4.9C). T cell frequency was unaltered following freeze-thawing (Figure 4.9D). This identified the importance of analysing fresh samples, as further characterisation of neutrophilic MDSCs was no longer possible post-freezing.

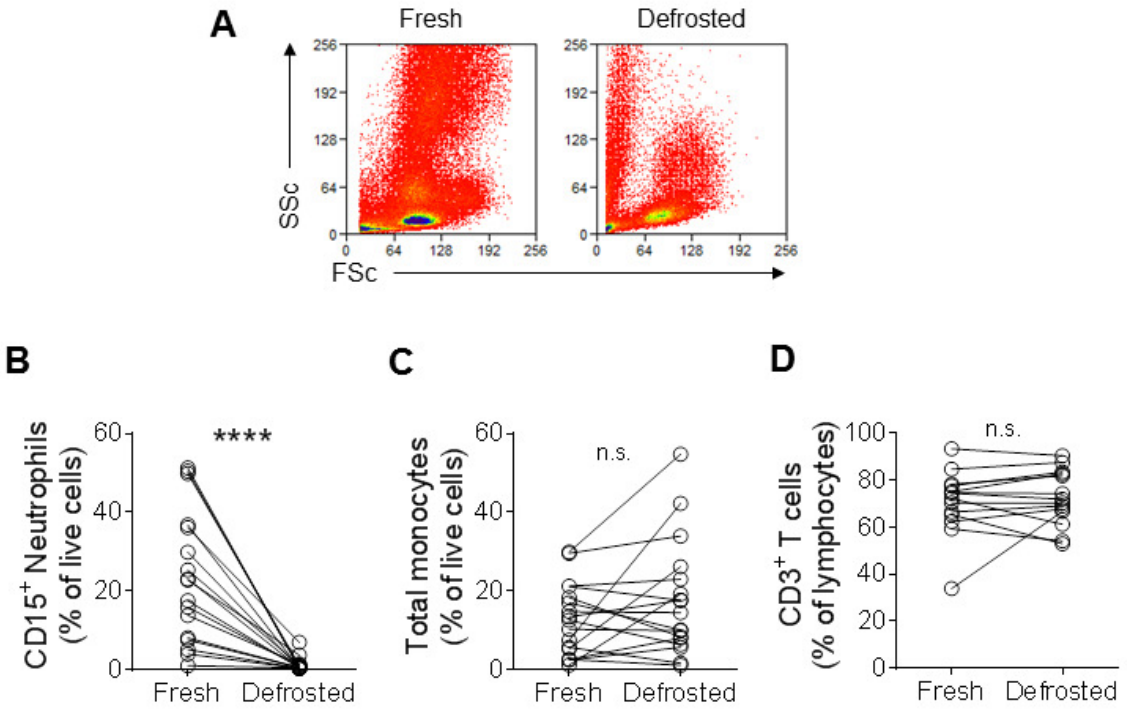

Figure 4.9: Loss of neutrophilic cells from cryopreserved PBMC samples. (A) Flow cytometry FSc/SSc profiles depicting loss of large, granulocytic cells in defrosted sample. **(B)** Frequency of total neutrophils is reduced in defrosted samples. **(C)** Monocytes as percentage live cells and **(B)** T cells as a percentage lymphocytes were unchanged in fresh and defrosted samples. Paired t-test between groups ****p≤0.0001.

Although total monocyte frequency remained unchanged, a selective loss was observed in $CD14^{+}CD16^{+}$ inflammatory (Figure 4.10A) and $CD14^{mid}CD16^{+}$ patrolling (Figure 4.10B) monocytes in thawed samples from pH1N1 patients. $CD14^{+}CD16^{-}$ classical monocytes as percentage of total monocytes were significantly increased as a consequence (Figure 4.10C). This meant that further study of monocyte phenotype had to be directed solely at the classical monocyte subset.

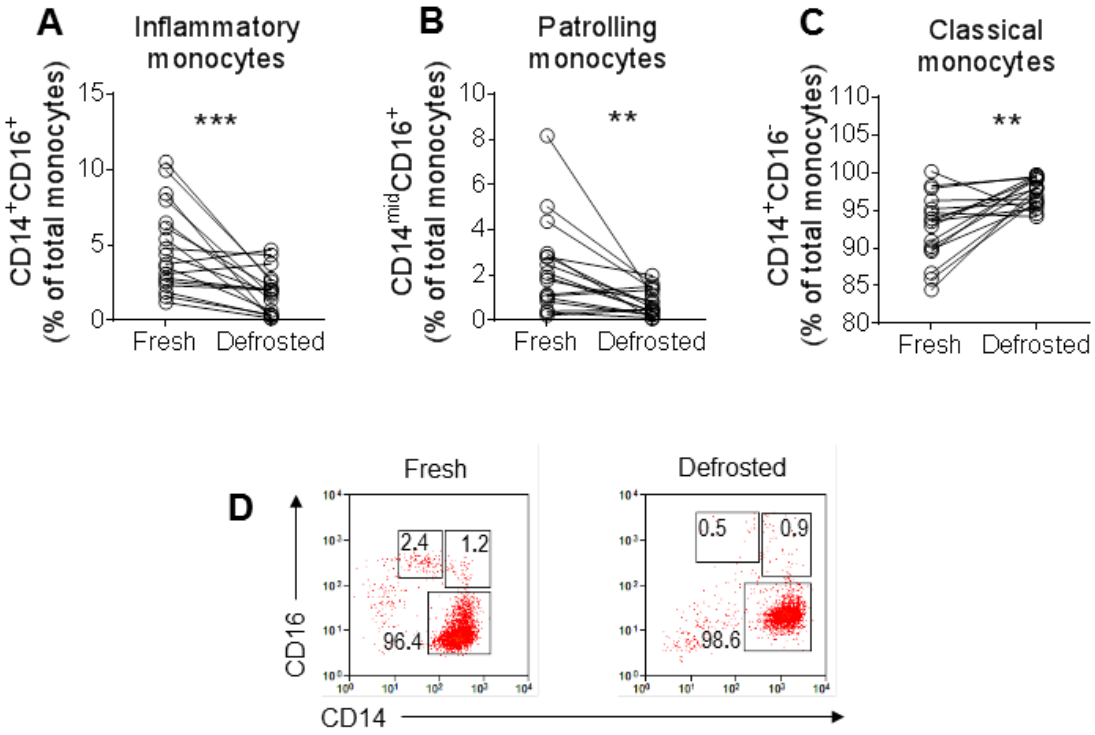

Figure 4.10: Changes in monocyte subsets from cryopreserved PBMC samples. Reduction in **(A)** inflammatory monocytes and **(B)** patrolling monocytes, and increase in **(C)** classical monocytes in defrosted samples. **(D)** Flow cytometry depiction of monocyte subsets from fresh or defrosted PBMC. Paired t-tests between groups in (A)-(C). **p≤0.01, ***p≤0.001.

4.4.3 Phenotypic and functional characterisation of monocytes

In view of findings from the previous chapter where acquisition of M1 and lack of M2 polarisation in monocytes correlated with severe IAV, further phenotypic and functional characterisation of monocytes was carried out in severe and mild pH1N1 infection. This involved examining M1/M2 polarisation using CD163 and CCR7, maturity and activation state of monocytes using HLA-DR and CD62L, and cytokine response to LPS stimulation measuring IL-6, TNFα, IL-10 and MCP-1 production. To identify IAV-specific changes in monocytes, comparisons were first made between pH1N1, steroid-treated pH1N1, ILI samples and healthy controls with no division of mild or severe disease, as the number of subjects for which cryopreserved PBMCs were available was too low to gain statistical significance. Demographics are shown in Table 4.4. Comparisons were then made between severe and mild disease in the pH1N1 group.

	Severity	Number	Male n (%)	Age (mean)	Asthma n (%)	BMI>30 n (%)
pH1N1	Mild	6	1 (16.7%)	46.1	2 (33.3%)	1 (16.7%)
	Severe	12	8 (66.7%)	39.9	0	5 (41.7%)
pH1N1 (steroids)	Mild	4	0	34.4	4 (100%)	2 (50%)
	Severe	7	4 (57.1%)	51.7	3 (42.9%)	1 (14.3%)
pH1N1$^-$ (ILI)	Mild	4	3 (75%)	43.5	1 (25%)	0
	Severe	3	2 (66.7%)	51.6	0	1 (33.3%)

Table 4.4: Demographics of patients from which cryopreserved samples were available. Number of patients with mild or severe disease in each group, further characterised by age, sex, asthma status and BMI (BMI>30: obese).

The percentage of monocytes expressing CD163 were highest in steroid-treated pH1N1 patients (70.1±4.97) compared to pH1N1 (40.38±3.25), ILI (42.66±6.56) and HC (44.06±6.09), suggesting a regulatory M2 monocyte phenotype in steroid-treated patients (Figure 4.11A). Similar results were revealed by MFI as CD163 expression was highest in steroid-treated pH1N1 patients (57.43±6.14) compared to pH1N1 (25.81±2.14), ILI (26.86±4.49) and HC (31.49±5.29) (Figure 4.11B). Comparison of

mild and severe disease in pH1N1 infection showed no significant changes in percentage of CD163 expressing monocytes (39.07±6.44 vs 41.04±3.87) (Figure 4.11C) or MFI (22.60±3.42 vs 27.42±2.69) (Figure 4.11D).

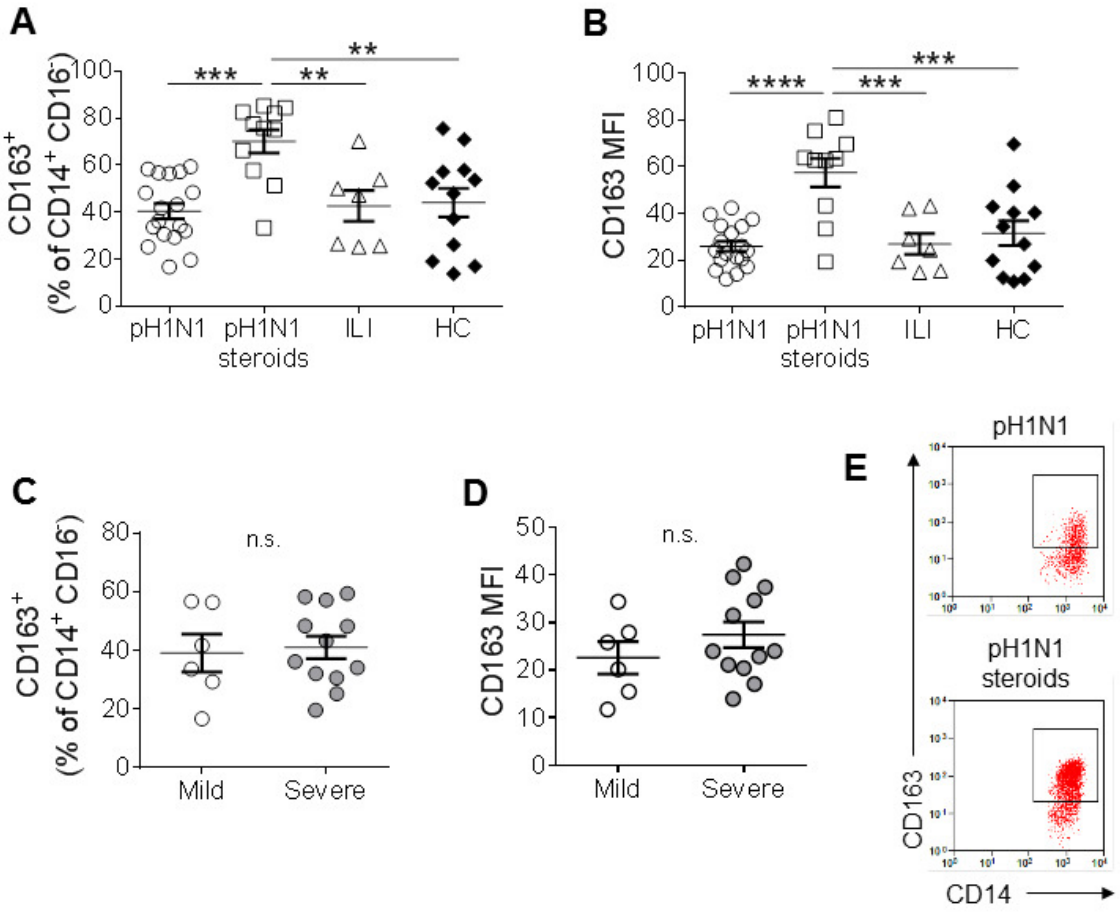

Figure 4.11: Monocyte CD163 expression is increased in steroid-treated pH1N1 patients. Expression of CD163 on classical monocytes as **(A)** percentage and **(B)** MFI in pH1N1 subjects (n=18), pH1N1 steroid-treated subjects (n=11), ILI subjects (n=7) and healthy controls (n=12). CD163 expression on monocytes from pH1N1 subjects grouped into mild (n=6) and severe (n=12) disease as **(C)** percentage and **(D)** MFI showed no significant changes between groups. **(E)** Flow cytometry plots of lower CD163 expression in a pH1N1 subject and higher CD163 expression in a pH1N1 steroid-treated subject gated on $CD14^{+}CD16^{-}$ monocytes. One-way ANOVA between groups in (A)-(B), t-test in (C)-(D). **p≤0.01, ***p≤0.001, ****p≤0.0001.

The percentage of monocytes expressing CCR7 was highest in pH1N1 patients (93.67±1.07) compared to steroid-treated pH1N1 patients (80.41±4.91) and healthy controls (78.47±2.67), while no significant differences were found when comparing to

ILI patients (89.28±5.05), suggesting an inflammatory M1 phenotype in pH1N1 infection (Figure 4.12A). CCR7 expression as MFI was highest in pH1N1 (26.28±1.62) and ILI (30.05±3.79) patients and low in steroid-treated pH1N1 patients (17.96±1.11) and HC (17.43±0.74) (Figure 4.12B). Comparison of mild and severe disease in pH1N1 infection showed no significant changes in percentage of CCR7 expressing monocytes (91.92±2.51 vs 94.54±1.02) (Figure 4.12C) or MFI (27.92±3.67 vs 25.47±1.69) (Figure 4.12D).

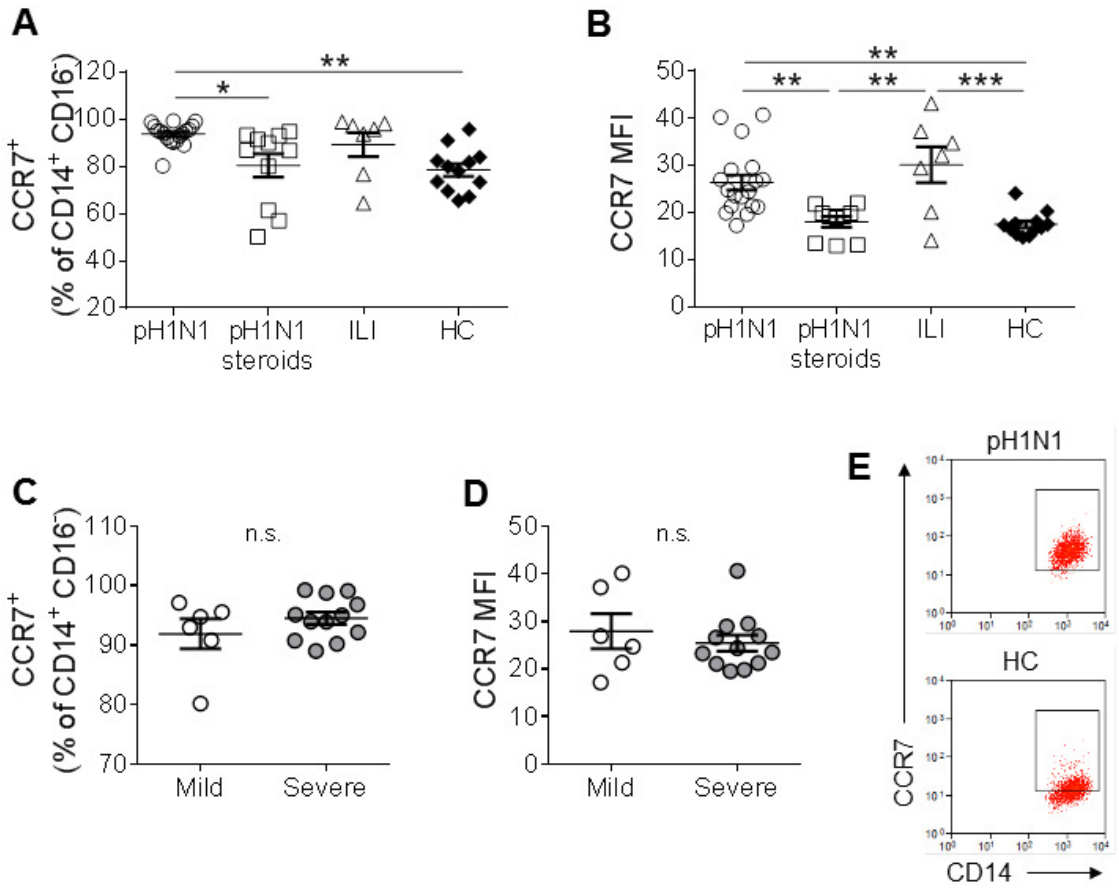

Figure 4.12: Monocyte CCR7 expression is highest in pH1N1 patients. Expression of CCR7 on classical monocytes as **(A)** percentage and **(B)** MFI in pH1N1 subjects (n=18), pH1N1 steroid-treated subjects (n=11), ILI subjects (n=7) and healthy controls (n=12). CCR7 expression on monocytes from pH1N1 subjects grouped into mild (n=6) and severe (n=12) disease as **(C)** percentage and **(D)** MFI showed no significant changes between groups. **(E)** Flow cytometry plots of higher CCR7 expression in a pH1N1 subject and lower CCR7 expression in a healthy control gated on $CD14^{+}CD16^{-}$ monocytes. One-way ANOVA between groups in (A)-(B), t-test in (C)-(D). *p≤0.05, **p≤0.01, ***p≤0.001.

HLA-DR expression was measured as a marker of monocyte maturity and because HLA-DR has been shown to be pathologically reduced on monocytes in several diseases (476). The percentage of monocytes expressing HLA-DR was reduced in pH1N1 infection (88.73±3.21) compared to healthy controls (99.59±0.13) (Figure 4.13A). Monocytes from steroid-treated pH1N1 and ILI patients had high HLA-DR expression (96.01±2.04 and 96.76±2.07, respectively). HLA-DR expression on monocytes determined by MFI was lowest in pH1N1 (147.3±26.04) and steroid-treated pH1N1 (116.2±24.28) patients compared to healthy controls (393±40.55) (Figure 4.13B). HLA-DR on monocytes from ILI patients (281.8±47.28) was higher than steroid-treated pH1N1 patients but not significantly different from healthy controls. Comparison of mild and severe pH1N1 disease revealed a reduction in HLA-DR expression on monocytes from severe patients compared to mild (83.63 ± 4.10 vs 98.95 ± 0.40) (Figure 4.13C). This was also seen as MFI (259.9±47.70 vs 90.91±13.76) (Figure 4.13D) and associated a reduction in monocyte HLA-DR with severe disease, specific to IAV infection, regardless of steroid treatment

The mild pH1N1 patient with highest monocyte frequency identified in Figure 7 who went on to develop severe disease had the lowest HLA-DR expression (MFI 109.9) in the mild group in Figure 4.13D, suggesting that reduced monocyte HLA-DR could be a predictor for severe disease.

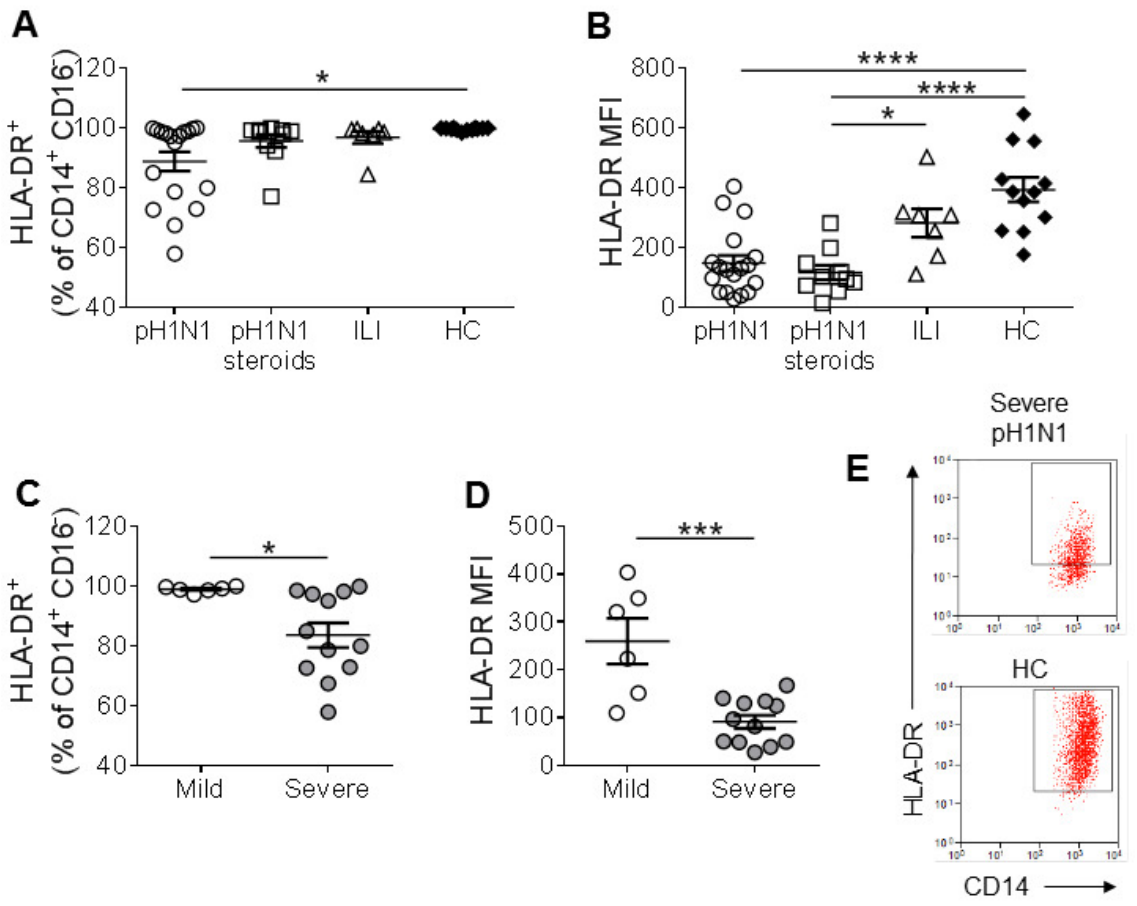

Figure 4.13: Monocyte HLA-DR expression is reduced in severe pH1N1 infection. Expression of HLA-DR on classical monocytes as **(A)** percentage and **(B)** MFI in pH1N1 subjects (n=18), pH1N1 steroid-treated subjects (n=11), ILI subjects (n=7) and healthy controls (n=12). HLA-DR expression on monocytes from pH1N1 subjects grouped into mild (n=6) and severe (n=12) disease as **(C)** percentage and **(D)** MFI showed significant HLA-DR reduction in severe patients. **(E)** Flow cytometry plots of reduced HLA-DR expression in a pH1N1 subject and higher HLA-DR expression in a healthy control gated on $CD14^{+}CD16^{-}$ monocytes. One-way ANOVA between groups in (A)-(B), t-test in (C)-(D). *p≤0.05, ***p≤0.001, ****p≤0.0001.

CD62L expression on monocytes was examined as CD62L shedding has been associated with an activated monocyte phenotype. The percentage of monocytes expressing CD62L was lowest in pH1N1 patients (21.56±2.67) compared to ILI patients (37.81±6.24) suggesting that monocytes were more activated in IAV infection (Figure 4.14A). CD62L expression in steroid-treated pH1N1 patients (34.27±4.0) and HC

(25.92±4.51) did not significantly differ from the other disease groups. There were no significant differences in CD62L as MFI on monocytes from pH1N1 (23.47±2.91), steroid-treated pH1N1 (36.49±5.22), ILI (44.83±12.14) or HC (34.46±5.94) groups (Figure 4.14B). Comparison of mild and severe disease in pH1N1 infection showed no significant changes in percentage of CD62L expressing monocytes (19.78±5.310 vs 22.45±3.124) (Figure 4.14C) or MFI (20.26±3.845 vs 25.08±3.953) (Figure 4.14D).

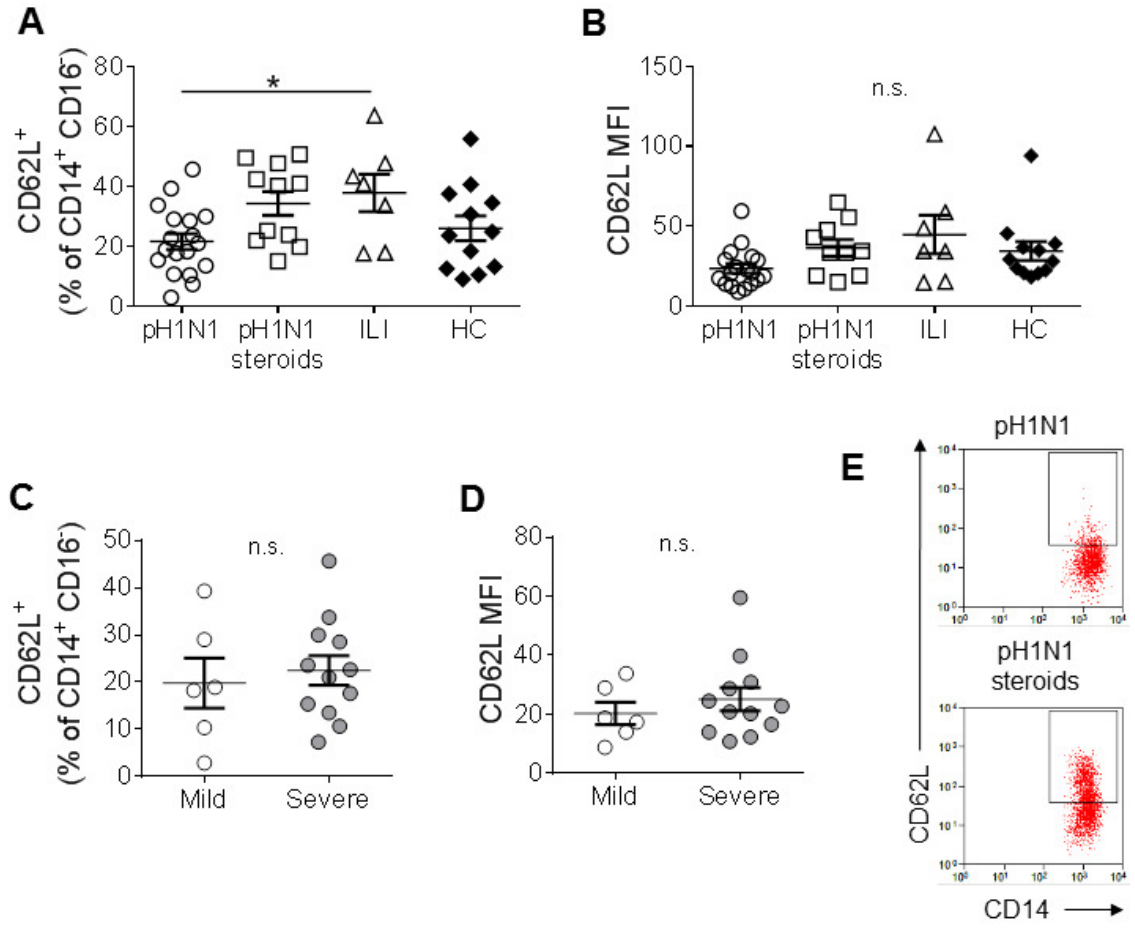

Figure 4.14: Monocyte CD62L expression is lowest in pH1N1 subjects. Expression of CD62L on classical monocytes as **(A)** percentage and **(B)** MFI in pH1N1 subjects (n=18), pH1N1 steroid-treated subjects (n=11), ILI subjects (n=7) and healthy controls (n=12). CD62L expression on monocytes from pH1N1 subjects grouped into mild (n=6) and severe (n=12) disease as **(C)** percentage and **(D)** MFI showed no significant changes between groups. **(E)** Flow cytometry plots of lower CD62L expression in a pH1N1 subject and higher CD62L expression in a pH1N1 steroid-treated subject gated on $CD14^{+}CD16^{-}$ monocytes. One-way ANOVA between groups in (A)-(B), t-test in (C)-(D). *p≤0.05.

Monocyte cytokine and chemokine production was examined by ICS following 6 hours of LPS stimulation from defrosted samples, and as total concentration in supernatants following 18 hours of LPS stimulation from fresh samples. IL-10 was examined as our lab previously identified a link between low monocyte IL-10 production and higher disease activity in sarcoidosis (477). MCP-1 is a major monocyte chemoattractant; high levels of which have been implicated in more severe outcome to IAV infection. IL-6 was found in the previous chapter to be highly expressed early in severe infection and later in mild infection, and therefore its production in severe and mild disease was further explored here. TNFα has been reported to have antiviral effects, although production by Tip-DC has also been implicated with worse outcome to IAV in mice (270, 478), warranting further study.

The percentage of monocytes producing IL-10 was lowest in pH1N1 (3.02±0.21) and steroid-treated pH1N1 patients (3.25±0.24) compared to healthy controls (7.24±1.54) but not ILI patients (4.61±0.65) (Figure 4.15A). Furthermore, IL-10 producing monocytes were lowest in severe pH1N1 patients compared to mild (2.698 ± 0.2016 vs 3.662 ± 0.3551) (Figure 4.15B), implicating low monocyte IL-10 production with more severe disease and strengthening previous work from our lab (477). The mild pH1N1 patient with highest monocyte frequency identified in Figure 4.7 who went on to develop severe disease had the lowest IL-10 production (2.46%) in the mild group in Figure 4.15B, suggesting that reduced ability of monocytes to produce IL-10 could be a predictor for severe disease.

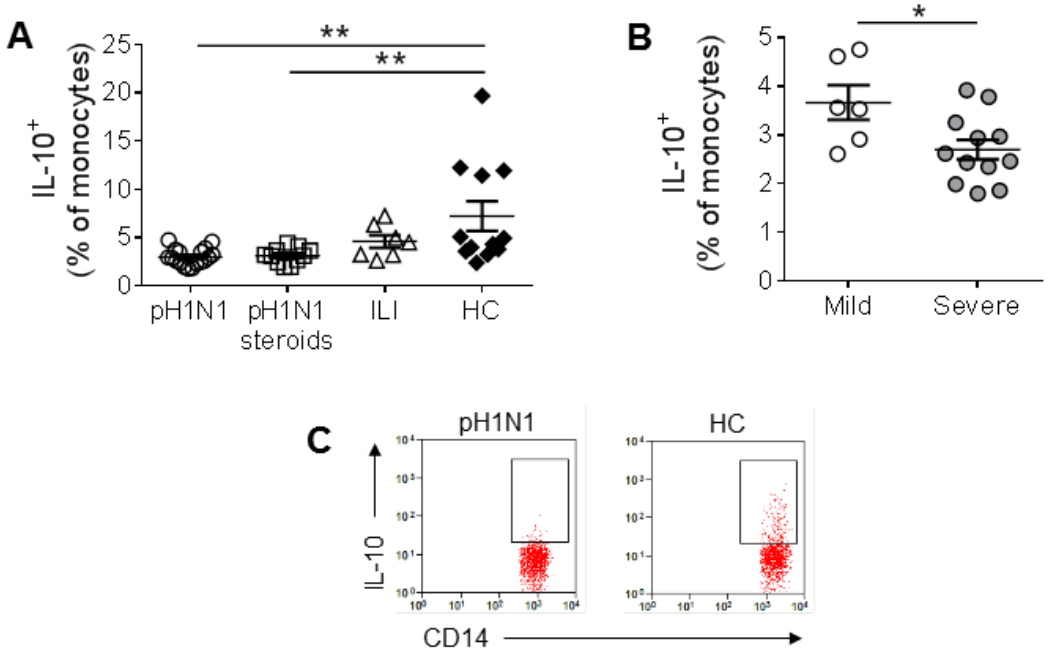

Figure 4.15: IL-10 production by monocytes is reduced in severe pH1N1 infection. (A) Percentage of monocytes producing IL-10 following 6 hour LPS stimulation with BFA for the last 4 hours in pH1N1 subjects (n=18), pH1N1 steroid-treated subjects (n=10), ILI subjects (n=7) and healthy controls (n=12). **(B)** IL-10 production by monocytes from pH1N1 subjects grouped into mild (n=6) and severe (n=12) disease. **(C)** Flow cytometry plots of reduced IL-10 production in a pH1N1 subject and higher IL-10 production in a healthy control gated on $CD14^{+}CD16^{-}$ monocytes. One-way ANOVA between groups in (A), t-test in (B). *p≤0.05, **p≤0.01.

The percentage of monocytes producing MCP-1 was lowest in steroid-treated pH1N1 patients (5.82±1.37) compared to healthy controls (11.61±0.94), while no significant differences were found in pH1N1 (10.3±1.41) and ILI (9.79±1.60) patients compared to the other groups (Figure 4.16A). MCP-1 producing monocytes were not significantly different in severe pH1N1 patients compared to mild (10.27 ± 1.786 vs 10.37 ± 2.470) (Figure 4.16B).

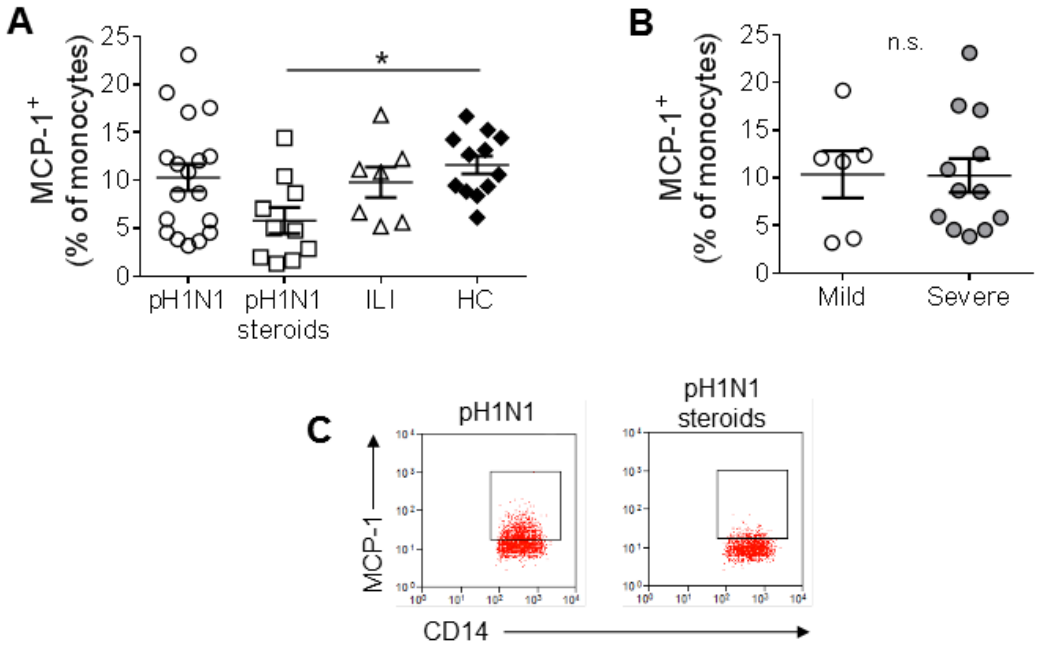

Figure 4.16: MCP-1 production by monocytes is lowest in steroid-treated pH1N1 subjects. (A) Percentage of monocytes producing MCP-1 following 6 hour LPS stimulation with BFA for the last 4 hours in pH1N1 subjects (n=18), pH1N1 steroid-treated subjects (n=10), ILI subjects (n=7) and healthy controls (n=12). **(B)** MCP-1 production by monocytes from pH1N1 subjects grouped into mild (n=6) and severe (n=12). **(C)** Flow cytometry plots of higher MCP-1 production in a pH1N1 subject and reduced MCP-1 production in a pH1N1 steroid-treated subject gated on $CD14^{+}CD16^{-}$ monocytes. One-way ANOVA between groups in (A), t-test in (B). *p≤0.05.

The percentage of monocytes producing IL-6 or TNFα were high following LPS stimulation, with no significant differences between pH1N1 (IL6: 70.29±3.48, TNFα: 68.2±2.97), steroid-treated pH1N1 (IL6: 66.45±4.91, TNFα: 70±5.08), ILI (IL6: 65.26±6.17, TNFα: 72.54±5.92) or HC (IL6: 76.75±5.16, TNFα: 81.01±4.38) (Figure 4.17A-B). Comparison of severe and mild pH1N1 groups found no difference in IL-6 (70.50±4.76 vs 69.86±4.92) or TNFα (66.47±3.87 vs 71.68±4.51) production by monocytes (Figure 4.17C-D).

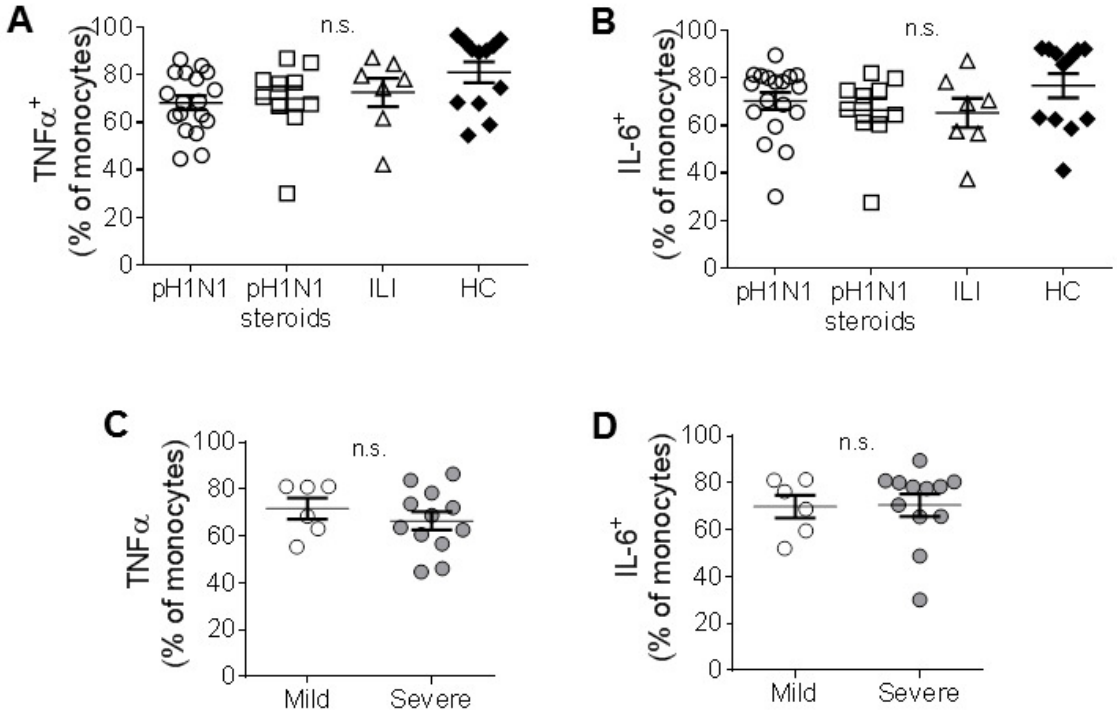

Figure 4.17: Total IL-6 and TNFα production by monocytes is not altered in pH1N1 infection. Percentage of monocytes producing **(A)** TNFα or **(B)** IL-6 following 6 hour LPS stimulation with BFA for the last 4 hours in pH1N1 subjects (n=18), pH1N1 steroid-treated subjects (n=10), ILI subjects (n=7) and healthy controls (n=12). **(C)** TNFα and **(D)** IL-6 production by monocytes from pH1N1 subjects grouped into mild (n=6) and severe (n=12) disease. Gated on $CD14^{+}CD16^{-}$ monocytes. One-way ANOVA between groups in (A)-(B), t-test in (C)-(D).

Monocyte IL-6 and TNFα production were further analysed to determine single or double cytokine-producing monocytes, and found a greater proportion of IL-6^{+}TNFα^{-} producing cells in pH1N1 infected patients (9.20±1.61) than healthy controls (3.25±0.52) (Figure 4.18A). IL-6 single-producing monocytes were also higher in severe compared to mild pH1N1 infection (11.43±2.081 vs 4.730±1.189) (Figure 4.18B).

The mild pH1N1 patient with highest monocyte frequency identified in Figure 4.7 who went on to develop severe disease had the highest IL-6^{+}TNFα^{-} production (10.23%) in the mild group in Figure 4.19B.

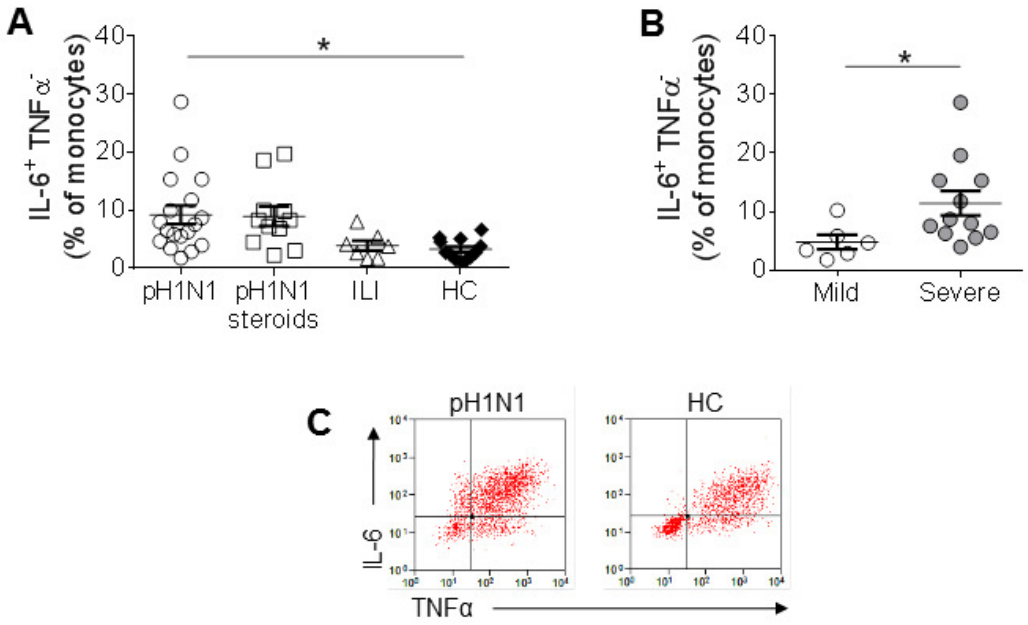

Figure 4.18: IL-6^{+}TNFα^{-} producing monocytes are increased in severe pH1N1 infection. (A) Percentage of total monocytes producing only IL-6 but not TNFα following 6 hour LPS stimulation with BFA for the last 4 hours in pH1N1 subjects (n=18), pH1N1 steroid-treated subjects (n=10), ILI subjects (n=7) and healthy controls (n=12). **(B)** IL-6^{+}TNFα^{-} production by monocytes from pH1N1 subjects grouped into mild (n=6) and severe (n=12) disease. **(C)** Flow cytometry plots of IL-6 and TNFα producing monocytes, gated on total monocytes, showing more IL-6 single producing cells in a pH1N1 subject compared to a healthy control. One-way ANOVA between groups in (A), t-test in (B). *p≤0.05.

In order to take into account the differences in monocyte frequency in each of the groups identified earlier in this chapter, the percentage of cytokine producing monocytes were normalised to the absolute monocyte number per ml blood. This identified the number of cytokine producing monocytes per ml of blood for IL-10, MCP-1, IL-6 and TNFα, and revealed that numbers were highest in the pH1N1 group for all cytokines, as could be expected from the high absolute number of monocytes in this group. Results are displayed in Table 4.5.

	Cytokine production (% of monocytes)	Total monocytes per ml blood	Normalised cytokine producing monocytes (per ml blood)
IL-10			
pH1N1	3.02+0.21	348270+80981	10,517.8
pH1N1 steroids	3.25+0.24	192385+54325	6,252.5
ILI	4.61+0.65	143701+101143	6,624.6
HC	7.24+1.54	67840+15329	4,911.6
MCP-1			
pH1N1	10.3+1.41	348270+80981	35,871.8
pH1N1 steroids	5.82+1.37	192385+54325	11,196.8
ILI	9.79+1.60	143701+101143	14,068.3
HC	11.61+0.94	67840+15329	7,876.2
IL-6			
pH1N1	70.29+3.48	348270+80981	244,799.0
pH1N1 steroids	66.45+4.91	192385+54325	127,839.8
ILI	65.26+6.17	143701+101143	93,779.3
HC	76.75+5.16	67840+15329	52067.2
TNFα			
pH1N1	68.2+2.97	348270+80981	237,520.1
pH1N1 steroids	70+5.08	192385+54325	134,669.5
ILI	72.54+5.92	143701+101143	104,240.7
HC	81.01+4.38	67840+15329	54,957.2

Table 4.5: Normalised frequencies of cytokine-producing monocytes. The average percentages of IL-10-, MCP-1-, IL-6- and TNFα-producing monocytes in from pH1N1, pH1N1 steroids, ILI and HC groups were multiplied by the total monocytes per ml blood identified in Figure 4.7, to determine frequency of cytokine producing monocytes per ml blood.

Cytokine levels were measured in culture supernatants by multiplex cytokine analysis following 18 hours of stimulation with LPS or unstimulated cells, in order to determine total amount of monocyte cytokine production and proof of secretion of IL-10, MCP-1, IL-6 and TNFα. There was significantly less IL-10 production following LPS stimulation in both pH1N1 (28.87pg/ml±7.9) and steroid-treated pH1N1 (32.8±10.5) compared to ILI (234.3±90.9) patients (Figure 4.19A). MCP-1 production did not increase after LPS stimulation, and did not differ between patient groups (Figure 4.19B). IL-6 was produced in high quantities relative to other cytokines following LPS stimulation, but no difference was found between patient groups (Figure 4.19C). TNFα production was induced upon LPS stimulation with no significant differences across groups, although with a trend for lower quantities in pH1N1 compared to ILI patients (Figure 4.19D).

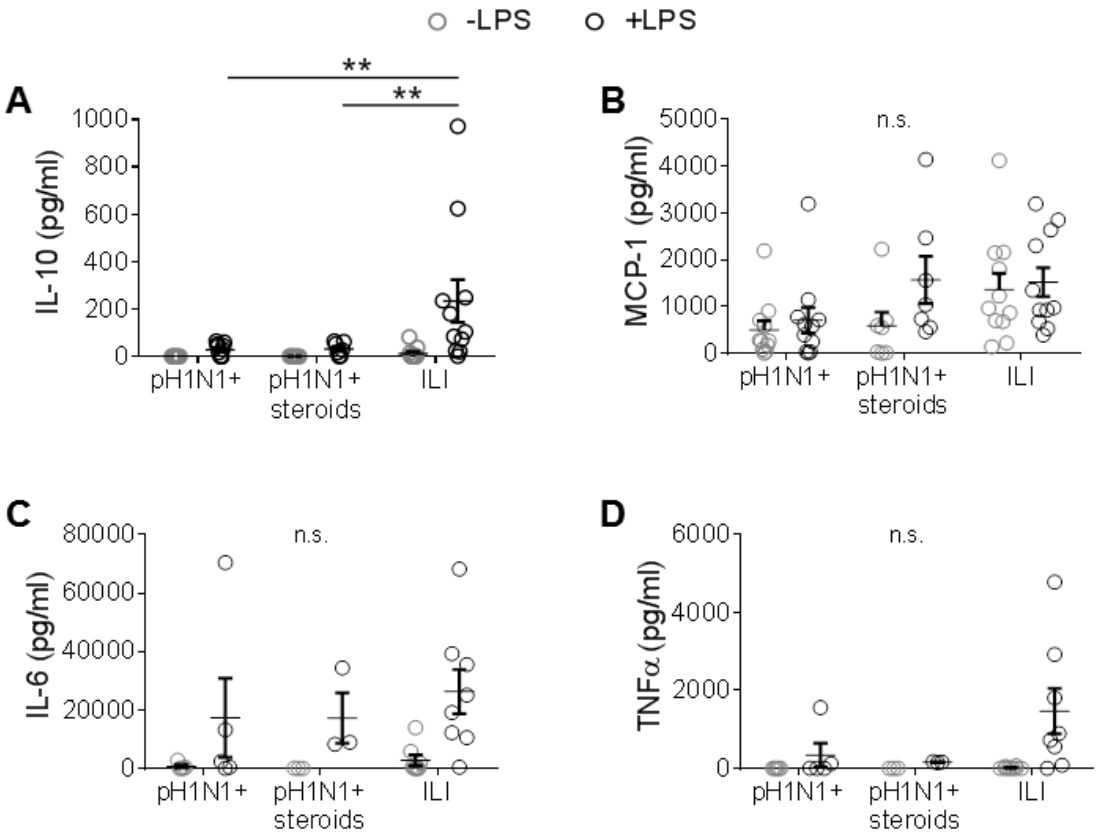

Figure 4.19: Cytokine levels in culture supernatant. Multiplex analysis of cytokine levels in supernatants of 200,000 whole blood lysed cells ± 18 hours of LPS stimulation for **(A)** IL-10, **(B)** MCP-1, **(C)** IL-6 and **(D)** TNFα comparing pH1N1 subjects (n=5-11), pH1N1 steroid-treated subjects (n=3-7) and ILI subjects (n=8-11). Two-way ANOVA **p≤0.01.

4.4.4 Monocyte frequency at different stages of disease

Blood samples were obtained during acute infection, which was within 48-72 hours of hospital admission for all patients analysed. A second sample was obtained 4-6 weeks later for a subset of these patients. At the time of acute sampling, patients were at different stages of disease, as symptoms had started anywhere from five to 26 days earlier. This was partly because Royal Brompton was a tertiary referral centre for IAV during the pandemic, and patients who had severe disease requiring tertiary care had often spent some time in other hospitals. This provided the opportunity to examine frequency of monocytes at different stages of disease, although not in the same individual. Neutrophils and neutrophilic MDSCs were also analysed.

There was no significant difference in days from first symptoms in mild or severe pH1N1 groups, so these were grouped together into one pH1N1 group for subsequent analysis (Figure 4.20A). PBMC count per ml blood correlated positively with days from first symptoms (Figure 4.20B), and therefore subsequent analysis was carried out on percentage of live cells, as absolute counts of cell subsets may have led to false positive correlations since the absolute number of total PBMCs themselves increased with days from first symptoms. Percentage of monocytes in PBMC samples correlated positively with days from first symptoms in pH1N1 patients (Figure 4.20C) but not ILI samples (Figure 4.20D). This revealed a pH1N1 specific correlation that associated monocyte frequency with duration of illness.

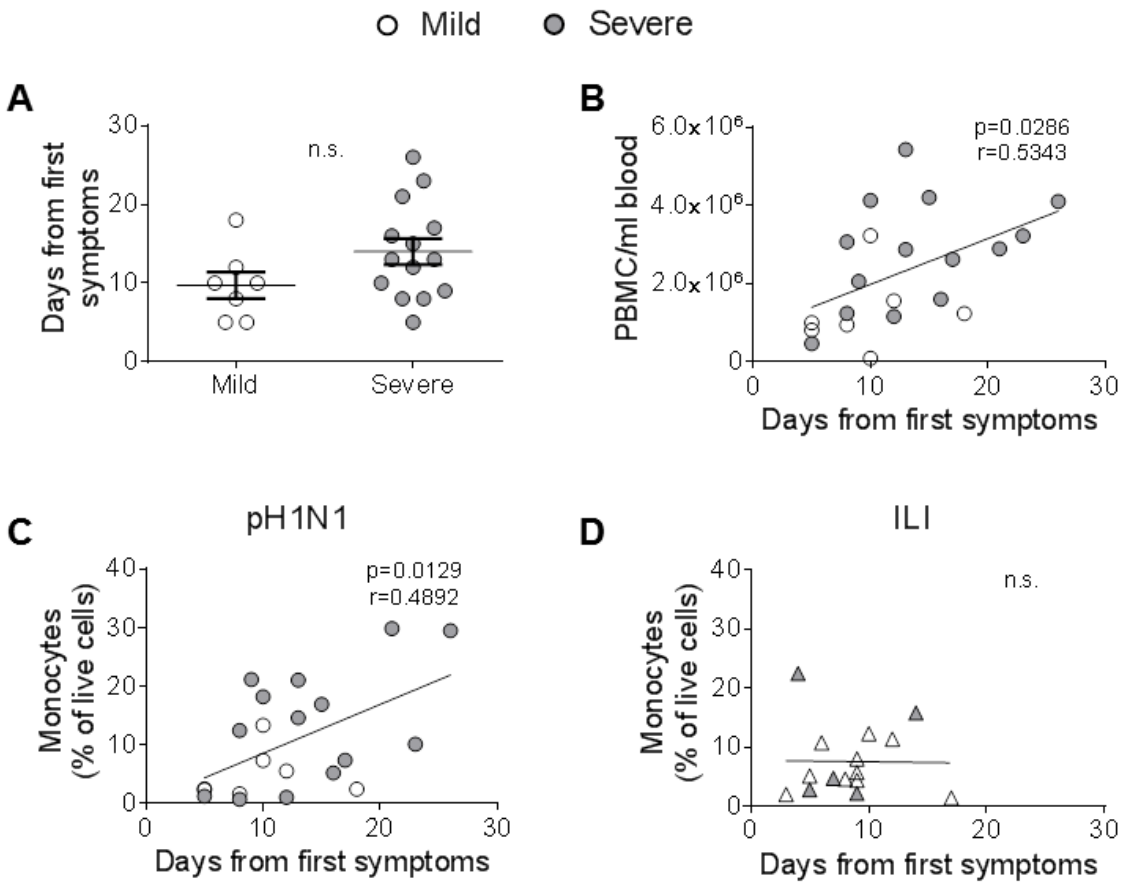

Figure 4.20: Monocyte frequency correlates with days from first symptoms. (A) Days from first symptoms in mild (n=7) or severe (n=14) pH1N1 patients. **(B)** Correlation between days from first symptoms and absolute PBMC count/ml blood. Days from first symptoms correlated against monocyte percentage in **(C)** pH1N1 patients or **(D)** ILI patients. Correlations determined using Spearman's rank.

No significant correlations against days from first symptoms were observed for total $CD15^{hi}$ neutrophils in PBMC in pH1N1 (Figure 4.21A) or ILI (Figure 4.21B) patients, or $CD15^{hi}CD16^{-}$ neutrophilic MDSC in pH1N1 (Figure 4.21C) or ILI (Figure 4.21D) patients.

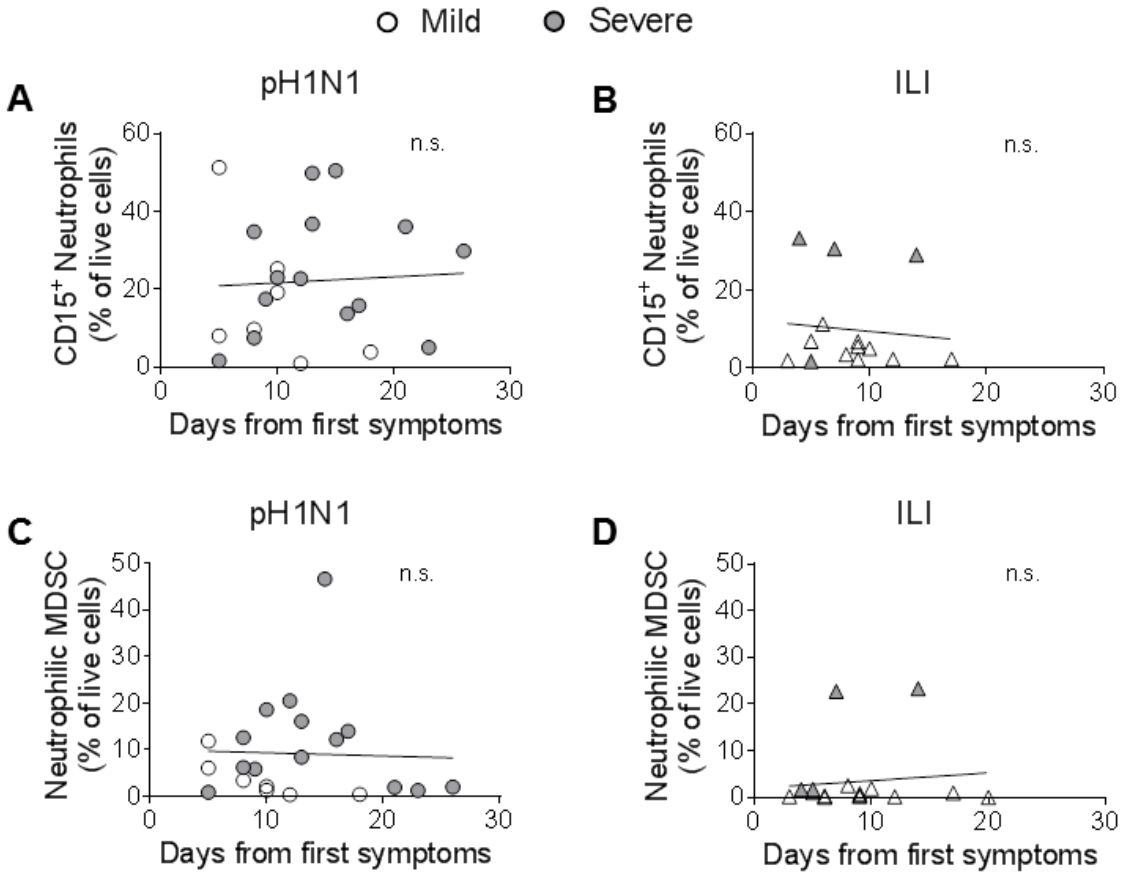

Figure 4.21: Neutrophil frequency does not correlate with days from first symptoms. Correlations between days from first symptoms and total $CD15^{hi}$ neutrophils in **(A)** pH1N1 or **(B)** ILI patients, or $CD15^{hi}CD16^{-}$ neutrophilic MDSCs in **(C)** pH1N1 or **(D)** ILI patients. Correlations determined using Spearman's rank.

Acute and convalescent samples were next compared. Paired convalescent samples were received for a subset of patients (details in Table 4.6). Due to low numbers in the mild and severe groups, patients were not split into severity for analysis, but instead analysed as pH1N1, pH1N1 (steroids) and ILI, with comparisons made between acute to convalescent samples in each group.

	Severity	Number	Male n (%)	Age (mean)	Asthma n (%)	BMI>30 n (%)
pH1N1	Mild	3	1 (33.3%)	45.7	1 (33.3%)	2 (66.7%)
	Severe	6	5 (83.3%)	41.4	0	3 (50%)
pH1N1 (steroids)	Mild	3	0	44.1	3 (100%)	1 (33.3%)
	Severe	6	4 (66.7%)	51.3	2 (33.3%)	0
pH1N1$^-$ (ILI)	Mild	3	2 (66.7%)	56.9	0	2 (66.7%)
	Severe	1	1 (100%)	45.5	1 (100%)	1 (100%)

Table 4.6: Demographics for patients from which acute and convalescent samples were received. Number of patients with mild or severe disease in each group, further characterised by age, sex, asthma status and BMI (BMI>30: obese).

The percentage of monocytes was unchanged in convalescent compared to acute samples in pH1N1 (13.67±2.19 vs 14.24±5.31), steroid-treated pH1N1 (14.55±4.87 vs 9.51±3.82) and ILI (9.14±4.18 vs 7.86±2.21) patient groups (Figure 4.22A). The percentage of CD15^{hi} neutrophils in PBMCs was reduced in convalescent compared to acute samples in pH1N1 (5.36±1.26 vs19.33±4.26) and steroid-treated pH1N1 (6.21±2.15 vs 32.03±10.18) patients, but was not significantly changed in ILI patients (1.966±0.5659 vs 5.926±1.987) (Figure 4.22B). The percentage of CD15^{hi}CD16$^-$ neutrophilic MDSCs in PBMCs was also reduced in convalescent compared to acute samples in pH1N1 (0.53±0.11 vs 5.88±1.84) and steroid-treated pH1N1 (3.54±1.9 vs 15.65±5.51) patients, but was not significantly changed in ILI patients (0.69±0.51 vs 1.05±0.45) (Figure 4.22C).

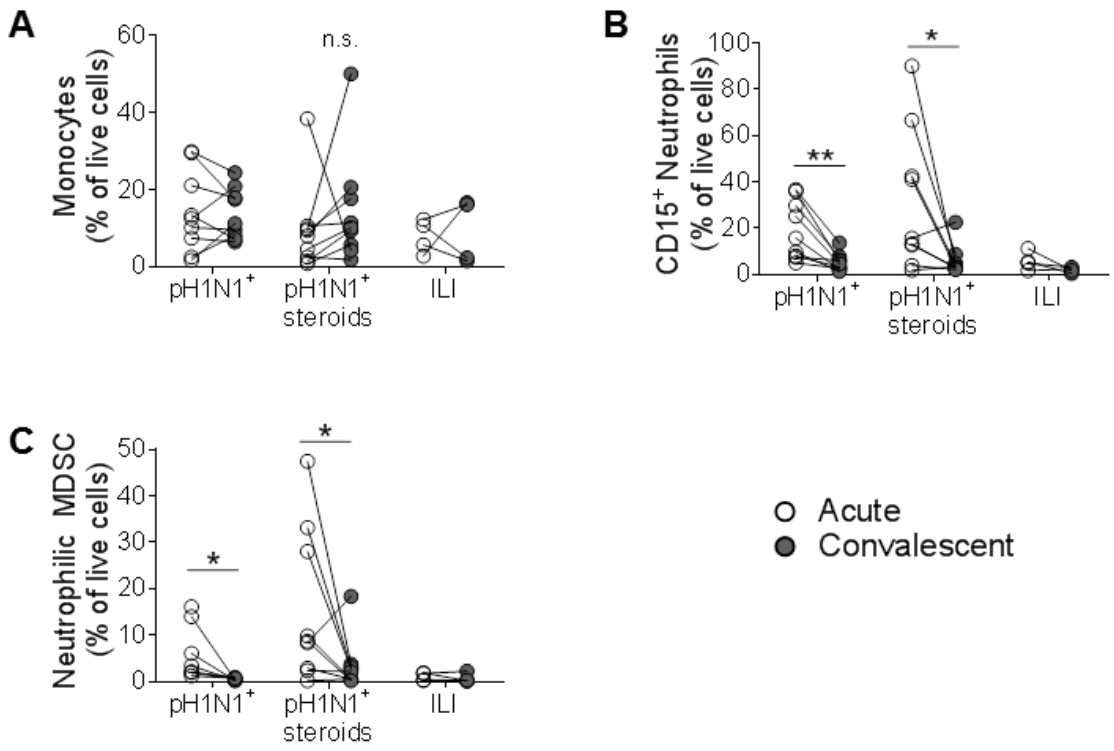

Figure 4.22: Monocytes remain high in convalescent samples. Percentage of **(A)** monocytes, **(B)** neutrophils and **(C)** neutrophilic MDSC in paired acute and convalescent PBMC samples from pH1N1 (n=9), pH1N1 steroid-treated (n=9) and ILI (n=4) subjects. Paired t-tests within groups used to determine significance. *p≤0.05.

4.5 Discussion

The findings in this chapter underlined the prominence of monocytes in human IAV infection and reflect results from the murine studies. $CD14^{+}CD16^{+}$ inflammatory monocytes were increased in blood of patients with severe IAV infection, and monocytes from severely infected patients produced less IL-10 after LPS stimulation and had strikingly lower HLA-DR than during mild disease, and when compared to ILI and HC groups. Patients on corticosteroid treatment had fewer circulating monocytes, with a bias towards an M2 phenotype. While neutrophilic MDSCs were also increased in severe pH1N1 patients compared to mild, this was also observed in severe compared to mild ILI patients, albeit at lower levels. This is unlike monocytes, which

were increased in severe pH1N1 patients, but did not differ between severity in ILI patients. Two-point longitudinal data for individual patients and overall correlation to days from first symptoms suggest that the increase in monocytes is sustained over a long period of time, unlike that of neutrophils. Furthermore, the one pH1N1 patient who had mild disease at the point of sampling but went on to develop severe disease had the highest number of monocytes, and lowest IL-10 and HLA-DR levels of the mild group, suggesting that the dysregulated monocyte phenotype may influence severe disease.

The selective increase in the $CD14^{+}CD16^{+}$ subset of monocytes in the severe pH1N1 group has also been reported for other inflammatory and infectious conditions such as HIV/AIDS, dengue virus, asthma and bacterial sepsis (479). Inflammatory monocytes are a small but distinct subset of total monocytes in blood that have been reported to be capable of higher proinflammatory cytokine production, in particular TNFα and IL-6, and better antigen presentation capacity as a result of higher MHC surface density compared to other monocyte subsets (217, 480). Expression of adhesion molecules LFA-1 and ICAM-1 are also higher in $CD14^{+}CD16^{+}$ monocytes, which are involved in cell-cell interactions (481). *In vitro* culture of blood monocytes with MCP-1 expanded the inflammatory monocyte subset (482), which could explain the increase in this subset, as MCP-1 levels are known to be high in both serum and lungs in IAV infection. Unfortunately further phenotypic characterisation of this subset was not possible in this study due to depletion post thawing. It would have been interesting to determine if the $IL\text{-}6^{+}TNF^{-}$ phenotype following LPS stimulation identified in classical monocytes would have differed in this subset, and whether HLA-DR expression was also reduced in inflammatory monocytes similarly to the reduction in classical monocytes during severe infection, despite higher reported HLA-DR expression on this subset.

While bronchoalveolar lavage (BAL) samples were not obtained in this human study, it can be postulated from the mouse studies that monocytes are being recruited to the lungs. Monocyte frequency was high throughout the course of disease as measured on different days for different patients, which questions the characterisation of monocytes as 'early' innate effector cells. As monocytes do not divide outside of the bone marrow, an increase in peripheral blood suggests continuous production and recruitment from bone marrow (483). Monocyte production in bone marrow increases upon sensing of inflammatory stimuli; in monkey SIV infection, an increased rate of monocyte recruitment from bone marrow correlated with rapid disease progression and severity, linked to more inflammatory macrophages in CNS (484). Monocyte emigration from bone marrow is driven by CCR2 signalling in response to MCP-1; levels of which are high during IAV infection in lungs and serum (485). IFN-I signalling was found to trigger hematopoietic stem cell proliferation, and was specifically required for Ly6C^{hi} monocyte differentiation in a mouse model of IAV infection (486). Recently IL-6 was found to play a role in promoting myeloid differentiation from hematopoietic stem cells, which were themselves triggered by IFNγ secretion by CTL in the response to intracellular pathogens (487). High expression of IL-6 and IFN-inducible genes were found in the previous chapter in severe, and to a lesser extent mild IAV infection, in mouse lungs. It is possible that signals from IL-6 and IFNs are sensed by the bone marrow to stimulate myelopoiesis, causing the high levels of circulating monocytes observed here.

HLA-DR has been shown to be low on immature myeloid cells released early from the bone marrow before fully differentiating (488). It is possible that high HLA-DR expressing monocytes are recruited to the lungs where IAV antigens are found, and that circulating monocytes in this study are therefore representative of an immature pool of monocytes. Reduced monocyte HLA-DR has been shown in other diseases to indicate immune dysfunction that occurs as a protective response against harmful inflammatory bursts, such as with cytokine storms in severe IAV infection. Mechanisms

and reasons for downregulation have been identified in different diseases, but in all cases low monocyte HLA-DR associated with adverse outcome. Downregulated monocyte HLA-DR correlated with disease severity in acute liver failure (489), and predicted longer post-surgery recovery rates due to bacterial sepsis in multiple surgical situations (490-492). In human CMV infection, the virus caused degradation of HLA-DR molecules, thereby inhibiting peptide presentation of viral antigens, allowing virus-infected cells to resist recognition by T cells (493). It is possible that this could happen in IAV infection, as IAV infects monocytes, although the direct effect on HLA-DR degradation has not been examined in IAV infection. The consequences of reduced HLA-DR in IAV infection have not been widely studied. One group examining the immune response to H7N9 infection identified reduced HLA-DR expression on monocytes from patients with severe infection, although in contrast to the current study, monocyte numbers were also decreased in severe H7N9 infection (494). The reduced HLA-DR in this context decreased antigen-presenting capacity and led to an impaired T cell response. The fact that the one pH1N1 patient from the mild group who went on to develop severe disease had the lowest monocyte HLA-DR expression in the mild group suggests that low HLA-DR may be indicative of developing severe disease.

HLA-DR expression has also been used to characterise MDSCs; many reports describe MDSC in humans as $CD33^{+}HLA\text{-}DR^{-/low}$ and lineage negative (i.e. $CD3^{-}$, $CD19^{-}$, $CD56^{-}$ and $CD14^{-}$). CD33 is expressed on myeloid lineage cells, and while not determined in this study, CD66 was found to be highly expressed by neutrophilic MDSCs, and has a similar expression pattern as CD33 on myeloid cells (495). Neutrophilic MDSCs in this study were characterised as $CD15^{hi}CD16^{-}$ cells which co-localised with mononuclear cells during PBMC extraction and had low HLA-DR expression. High frequencies of $CD15^{hi}CD16^{-}$ suppressive granulocytes were associated with reduced survival in a mixed population of patients suffering from terminal cancer (496). A further subset of $CD15^{hi}CD16^{+}$ cells was identified in some

patients in the current study, which likely represents an activated neutrophil subset, as neutrophils with both suppressive and activated phenotypes have been shown to localise with mononuclear cells by others (291). Activated neutrophils were found in PBMCs from patients with systemic lupus erythematosus (SLE) and were associated with more severe disease. The activated neutrophils in SLE secreted more type I IFN and inflammatory cytokines but had reduced phagocytosis (475). The activated nature of $CD15^{hi}CD16^{+}$ neutrophils from IAV patients in this study was unfortunately not further explored at the time, unlike the suppressive functions. Neutrophilic MDSC were found to suppress T cell proliferation to a greater extent than classical neutrophils from the same patients. It is likely that the amount of suppression identified in the MLR assays is in fact an under-representation of actual suppressive capacities of neutrophilic MDSCs, as MLRs contained all $CD15^{hi}$ cells from PBMC extraction, including both $CD16^{-}$ and $CD16^{+}$ subsets. The presence of neutrophilic MDSCs in PBMC samples has been shown in patients with cancer and HIV, and correlate with severe disease (311, 497). T cell suppressive functions have been shown by others to involve hydrogen peroxide and Mac-1 expression by neutrophilic MDSCs (498). This is the first characterisation of neutrophilic MDSCs in human acute IAV infection, although monocytic MDSCs were previously identified in human and mouse (306). These were characterised in humans as $CD11b^{+}$ cells isolated from PBMCs which suppressed T cell proliferation through ARG1 and iNOS. In the current study, monocytes with the ability to suppress T cell proliferation were also identified. Naïve monocytes from healthy individuals are however known to suppress T cell proliferation, shown by our group and others (477, 499). As there were only four ILI patients for comparison, and inhibition of T cell proliferation in these samples ranged from 0% to 100%, it was not possible to accurately identify whether the suppressive nature of monocytes was altered in IAV infection. This was in contrast to data from neutrophilic MDSCs, which could be compared to classical neutrophils from the same patient due to differences in density gradient separation.

LPS stimulation to activate monocytes identified significantly low IL-10 production as being characteristic of pH1N1 patients, both by intracellular cytokine staining and quantification in supernatants. IL-10 has shown to both contribute to immune pathology by suppressing Th17 and IAV-specific cells in the lungs (500, 501), or protection by regulating excessive injury when produced by $CD8^+$ effector T cells (502) during IAV infection. The origin of IL-10 during IAV infection has not been widely explored, although monocyte IL-10 production is low in relation to both $CD8^+$ and $CD4^+$ effector T cells, which are thought to be the main IL-10 producing cells in IAV infected mouse lungs (500). Whether IL-10 from monocytes contributes protection or pathogenicity cannot be determined by this study. In other diseases, reduced monocyte IL-10 was found to associate with higher disease activity in sarcoidosis (477) whereas increased monocyte IL-10 led to immunodeficiency in HIV which was harmful to the host (503). Therefore the effects of monocyte IL-10 are likely to be disease-specific and would require further investigation in the context of IAV. The kinetics of when IL-10 is produced may influence subsequent immune regulation, as high IL-10 early during infection when immune cell influx and consequent lung damage are high could be protective against tissue injury, whereas high IL-10 in lungs later when IAV-specific effector T cells are present could be harmful due to suppressed virus-specific T cell functions. This is however difficult to establish as there is not a clear-cut line between innate and adaptive immunity in natural human IAV infection.

While total frequency of IL-6 or TNFα producing monocytes were unchanged in pH1N1 infection, the percentage of $IL\text{-}6^+TNF\alpha^-$ producing monocytes were increased in pH1N1 patients following LPS stimulation, with percentage highest in the severe group. This shows that a subset of monocytes in severe pH1N1 infection have the capacity to produce only IL-6, whereas in mild infection and ILI or HC the majority of IL-6 producing monocytes are also TNFα producing. Enrichment in the severe group and the one mild patient who went on to develop severe disease suggests that this might

contribute to worse outcome. IL-6 and TNFα were shown to synergistically induce T cell proliferation, while stimulation with either cytokine alone led to less proliferation (504). The fact that more monocytes from patients with severe infection produced only IL-6 may lead to reduced stimulation of IAV-specific T cell proliferation, leading to a worse outcome. IL-6 levels in serum of pH1N1 infected patients were shown to associate with severity and predict fatal outcomes, suggesting a harmful role of IL-6 in the immune response to pH1N1 infection (449). On the other hand IL-6 in the lung promoted neutrophil survival and thereby led to protection against pH1N1 infection in mice (452). The protective effect of neutrophil survival is however dependent on disease severity as neutrophils have been implicated in both protective and pathological responses (505). While the results in the current study do not reflect *in vivo* cell functions due to the *ex vivo* LPS stimulation, it allows identification of increased or decreased capability of cytokine production.

As monocytes differentiate into macrophages they can take on inflammatory M1 or anti-inflammatory M2 phenotypes which may contribute to tissue injury or repair, respectively. As M1 macrophages upregulate CCR7 and M2 macrophages upregulate CD163 (441), expression of these markers on monocytes may be an early sign indicative of differentiation to either phenotype. The upregulation of CCR7 on monocytes from pH1N1 steroid-naïve patients suggests an M1 phenotype, which supports previous findings from this thesis which identified an M1 phenotype to be highly enriched during severe IAV infection in mice. CD163 expression was unchanged in this group relative to HC or ILI, unlike CD163 expression in steroid-treated pH1N1 patients, which was significantly upregulated. CD163 expression has previously been shown to be induced by corticosteroids, and an M2 phenotype is apparent in lungs during asthma infection (506). A large proportion of steroid-treated patients in this study had asthma (66.7%), and therefore whether the M2 phenotype is associated with steroid treatment or asthma is unclear. The reduction in MCP-1 producing monocytes

in the steroid-treated pH1N1 group does however support a less inflammatory monocyte phenotype in this group. A similar proportion of steroid-treated (58%) and non-steroid treated pH1N1 (67%) patients however had severe disease, and therefore it is not clear whether the differentiation of circulating monocyte to M1 or M2 phenotypes associates with outcome. Analysis of this is further confounded by the fact that higher numbers of M2 macrophages exacerbate airway inflammation in asthma (507), which could have contributed to increased disease severity in steroid-treated patients where 66.7% were asthmatic, compared to only 14.3% of steroid-naïve patients.

These results also show that steroid-treatment at or before the point of sampling did not influence development of mild or severe disease. Using an established susceptible pH1N1 mouse model, it was shown that steroid treatment ameliorated acute lung injury and improved survival rate (508). However this is unlikely to be a realistic representation of human infection, as the majority of subjects who are hospitalised from IAV suffer from other co-morbidities which are confounding factors that may be affected by steroid treatment. A larger cohort of patients would be required to control for these confounding factors in order to identify true correlates of disease severity related to steroid treatment.

Convalescent samples taken 4-6 weeks after acute samples showed loss of neutrophilic MDSCs, but the high monocyte frequency remained unchanged. It is not known what the immune cell compartment of these patients was prior to infection, and therefore whether the convalescent samples reflect baseline levels of cells in healthy patients. It is possible that a subset of patients with high monocyte frequency is pre-disposed to more severe infection, although this cannot be concluded from these data. It could also be that certain immune cell types take longer to recover to baseline levels, in which case a second convalescent sample longer after recovery would be useful, but

was not part of this human study. It is also possible that monocytes are still participating in an immune response at this time point. Antibody production in response to IAV occurs within 2 weeks of infection, peaks between 4-7 weeks and remains for years (509). Induction of adaptive IAV-specific T cells requires antigen presentation by myeloid cells such as DCs in draining lymph nodes. Prior to recruitment to lymph nodes, DCs acquire antigen in the lungs either through infection or phagocytosis of infected cells (510). In mice, circulating monocytes recruited to the lungs contributed to the initiation of adaptive immune responses to IAV infection (270). It is possible that monocytes are still receiving signals that stimulate their production in bone marrow 4-6 weeks after acute infection, suggesting why their frequency is still high at this time point.

4.6 Conclusions

The myeloid cell compartment is significantly altered in acute pH1N1 infection in humans, characterised by an increase in the number of monocytes, which are phenotypically distinct in severe disease, and share features from severe IAV infection in mice such as inflammatory M1 polarisation. The presence of MDSCs with the ability to suppress T cell proliferation suggests pathogenic implications for T cell functions.

Chapter 5: T cell response to influenza A virus in relation to high monocyte numbers

5.1 Introduction

Having identified that high monocyte frequency during pandemic H1N1 2009 ('pH1N1'; A/CA/04/2009) infection was associated with severe disease in the previous chapter, I next evaluated the T cell response, including the invariant natural killer T (iNKT) cell subset, and examined these responses in relation to high monocyte frequency during influenza A virus (IAV) infection. Monocytes have the ability to influence the polarisation and expansion of T cells (511). While generation of a memory immune response takes weeks, the optimal programming of $CD8^+$ and $CD4^+$ T cells occurs during the acute phase of IAV infection (512) at a time when monocytes are known to dominate. In mouse IAV infection, inflammatory monocytes from the blood can be recruited to lungs where they differentiate into DCs, acquire antigen, and migrate to lymph nodes (LN) to stimulate naïve T cells (270), or directly to LN to become $CD11c^+CD11b^+Gr1^+$ inflammatory DCs which stimulate Th1 responses (284).

T cells play an important role in controlling IAV replication and mediating clearance in the lungs. The virus-specific $CD8^+$ T cell response is initiated in lung draining lymph nodes after antigen encounter, following which activated IAV-specific cells infiltrate the lung and destroy IAV-infected cells by secreting perforin and granzymes or mediating Fas/FasL apoptosis following TCR engagement (513). While IAV-specific $CD8^+$ CTL are required for virus clearance, they can also contribute to pathology and mortality in highly pathogenic virus infections (514), through the production of pro-inflammatory mediators such as IFNγ, TNFα and IL-17 (151). IFNγ from $CD8^+$ T cells was shown to cause monocyte differentiation into Tip-DCs, which cased lung pathology in a model of

severe IAV infection (270, 515). The primary role of $CD4^+$ cells during IAV infection has been ascribed to promoting antibody production by B cells and the generation of memory $CD8^+$ T cells (516). Cytotoxic IAV-specific $CD4^+$ T cells have been shown to be induced in the lungs during IAV infection in mice (517), and levels of pre-existing IAV-specific $CD4^+$ T cells with cytotoxic activity correlated with disease protection in a mild human IAV challenge study (144). Analysis of IAV-specific T cells in severely infected pH1N1 infected patients however identified that high levels of circulating IAV-specific $CD4^+$ cells predicted worse outcome (435), making the T cell response to IAV infection multidimensional and complex. Little is known about the kinetics of IAV-specific T cell responses following recovery from severe infection in humans, although in mild infection responses had returned to baseline by day 28 (144).

iNKT cells have immune regulatory roles and are beneficial during IAV infection as identified in mouse IAV infection models (280, 306, 413, 417). Data from human IAV infection is however lacking, with most studies relying on *in vitro* experiments. Our group showed that iNKT cells lysed IAV-infected human monocytes better than uninfected monocytes (280), and others have shown that iNKT cells reduced the immunosuppressive properties of monocytic MDSCs isolated from IAV-infected patients (306), providing evidence for iNKT cell-monocyte cross-talk during IAV infection.

5.2 Aim

The aim of this chapter was to evaluate the response of T cells to pH1N1 infection and to determine the influence of high monocyte frequency on T cell numbers and function.

5.3 Methods

5.3.1 Patient samples

Hospitalised patients with influenza-like illness were recruited as part of the MOSAIC study and pH1N1/09 infection was confirmed by viral PCR (Methods 2.2.1) (472). Study inclusion criteria and patient severity assessment is outlined in Chapter 4.3.1.

5.3.2 Sample processing

Blood samples were processed immediately upon receipt, as described in Chapter 4.3.1. Fresh PBMC samples were used in an IFNγ ELISpot assay (Methods 2.1.15) and stained for flow cytometry analysis of T cell frequencies and subsets, as detailed below.

For the ELISpot assay, the number of IFNγ secreting IAV-specific T cells were detected for each patient during acute infection, and for a subset of patients at convalescence (4-6 weeks after acute sampling) using peptide pools spanning the entire pH1N1 proteome. Pools were divided into HA, NA, NP, M, NS, PB1, PB2 and PA and results displayed as spot-forming units (SFU) per 10^6 PBMC.

5.3.3 Flow cytometry analysis and gating strategy of lymphocytes

Following compensation and doublet exclusion, $CD3^+$ cells were backgated to the FSc/SSc profile to identify the lymphocyte population, and a gate drawn around this (Figure 5.1A). This population is from here on referred to as the lymphocyte gate. All singlets were then gated onto the FSc/SSc profile with the lymphocyte gate as identified in Figure 5.1A. The lymphocyte gate was then applied to new plots to identify CD3 (B), CD4 (C), CD8 (C), and Vα24Jα18 (D) expressing cells in Figure 5.1. Back-gating was regularly carried out to ensure accurate gating of lymphocyte populations.

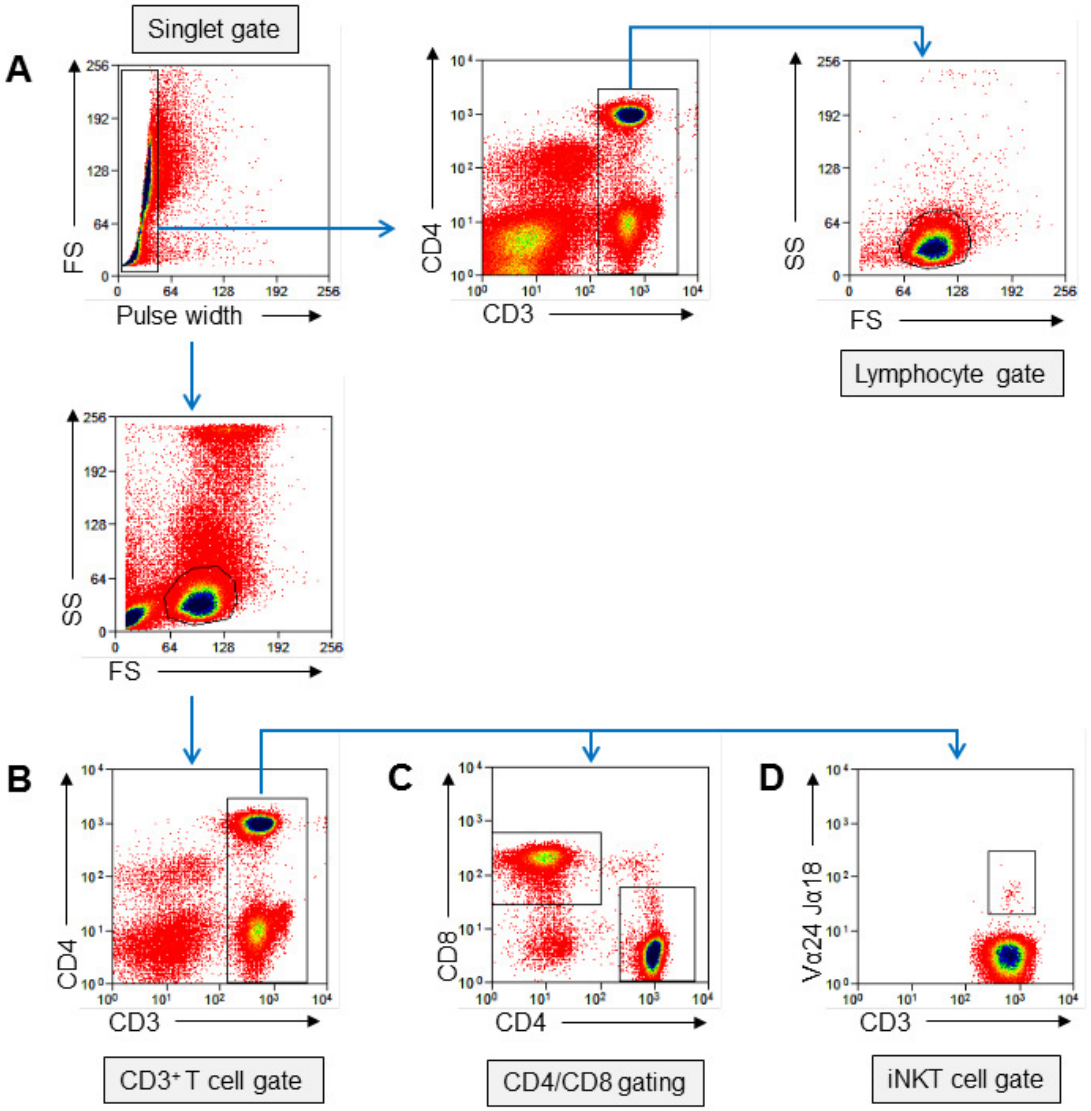

Figure 5.1: Flow cytometry gating of lymphocytes. (A) Singlets were selected based on pulse width (top left) and gated to identify $CD3^+$ T cells (top middle), which were gated onto FSc/SSc to identify the lymphocyte population (top right). All singlets were gated onto FSc/SSc and the lymphocyte population applied to the plots shown in order to identify **(B)** $CD3^+$ T cells, **(C)** $CD4^+$ and $CD8^+$ T cells and **(D)** iNKT cells. Blue arrows depict application of gate from plot that arrow originates from onto the plot at which the arrow is pointing.

Activated effector $CD8^+$ T cells were defined at $CD38^+HLA\text{-}DR^+$, gated from the $CD8^+$ T cell gate (Figure 5.2A). IAV-specific $CD8^+$ T cells were identified by employing an MHC-I tetrameric complex (HLA-A*0201) loaded with peptide (GILGFVFTL) derived from the conserved M (Matrix $M1_{58\text{-}66}$) virus protein, and conjugated to PE (424, 425) (Methods 2.1.6) (Figure 5.2B).

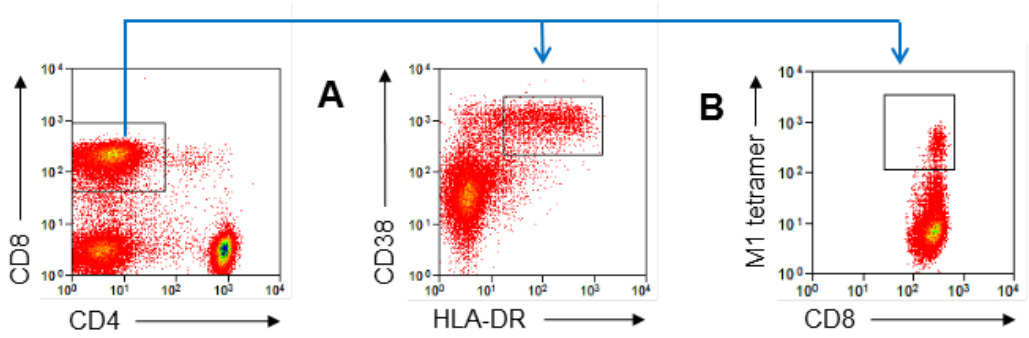

Figure 5.2: Identification of effector and IAV-specific CD8⁺ T cells. CD8⁺ T cells were analysed for expression of **(A)** CD38 and HLA-DR to identify activated effector CD8⁺ T cells, and **(B)** IAV matrix-loaded tetramer to identify matrix-specific T cells.

Lymphocyte populations were defined as detailed in table 5.1:

Cell population	Gating strategy	Figure reference
Total T cells	Lymphocytes, $CD3^+$	Figure 1B
$CD4^+$/$CD8^+$ T cells	Lymphocytes, $CD3^+$, $CD4^+CD8^-$ or $CD8^+CD4^-$	Figure 1C
iNKT cells	Lymphocytes, $CD3^+$ Vα24Jα18$^+$	Figure 1D
Activated effector $CD8^+$	Lymphocytes, $CD3^+$, $CD8^+$, $CD38^+HLA\text{-}DR^+$	Figure 2A
M1 $tetramer^+$	Lymphocytes, $CD3^+$, $CD8^+$, M1 $tetramer^+$	Figure 2B

Table 5.1: Classification of lymphocyte populations. Populations of lymphocytes used in immune cell phenotyping analysis.

5.4 Results

5.4.1 pH1N1-specific T cell response is higher in severe disease

T cell frequency (as defined in 5.3.3) was first examined in the blood of patients with pH1N1 infection ('pH1N1'), pH1N1 infected patients on corticosteroid treatment ('pH1N1 steroids'), patients with influenza-like illness ('ILI') and healthy controls ('HC'). Comparisons were made between mild and severe disease within each patient group to determine if there was a difference depending on disease severity, and whether this difference was specific to pH1N1 infection. Values from pH1N1 patients were then compared to healthy controls.

Absolute number of $CD3^+$ T cells was not significantly different between severe and mild disease in pH1N1 patients ([cells/ml blood±SEM]: 590,246±99,317 vs 647,986± 196,809), steroid-treated pH1N1 patients (666,858±184,518 vs 149,124±42,395) or ILI patients (368,243±104,606 vs 565,962±153,857) (Figure 5.3A). There was a large range of values within each group. There was no significant difference in absolute number of $CD3^+$ T cells between pH1N1 patients and HC (679,861±50,839).

Percentage of $CD3^+$ T cells was again not significantly different between severe and mild disease in pH1N1 patients (57.91±6.86 vs 68.0±7.99), steroid-treated pH1N1 patients (41.05 ±10.79 vs 58.19±6.62) or ILI patients (48.81±9.78 vs 64.15±4.16) (Figure 5.3B). There was no significant difference between percentages of $CD3^+$ T cells in severe or mild pH1N1 patients to HC (67.01±3.20).

The ratio of $CD4^+$ to $CD8^+$ cells was next determined in order to identify changes in T cell subsets between severe and mild disease compared to healthy controls. Severe pH1N1 patients had a significantly higher CD4:CD8 ratio compared to HC (5.53±0.96 vs 2.44±0.31) (Figure 5.3C). The CD4:CD8 ratio in mild patients (4.52±1.34) was not significantly different from HC or severe patients.

To further examine the T lymphocyte profile, the proportion of activated effector $CD8^+$ and $CD4^+$ T cells were determined using a combination of CD38 and HLADR mAbs, as described previously by our laboratory and others (518, 519) to represent effector T cells. Comparisons were made between severe and mild pH1N1 disease and to HC. There was an increase in the proportion of activated effector $CD8^+$ T cells in both mild and severe pH1N1 disease relative to HC (13.36±3.05, 11.56±2.81 and 2.75±0.65, respectively) (Figure 5.3D). No changes were found in frequency of activated effector $CD4^+$ T cells in severe disease (3.33±0.66), mild disease (4.61±1.86) and HC (1.75±0.21) (Figure 5.3E).

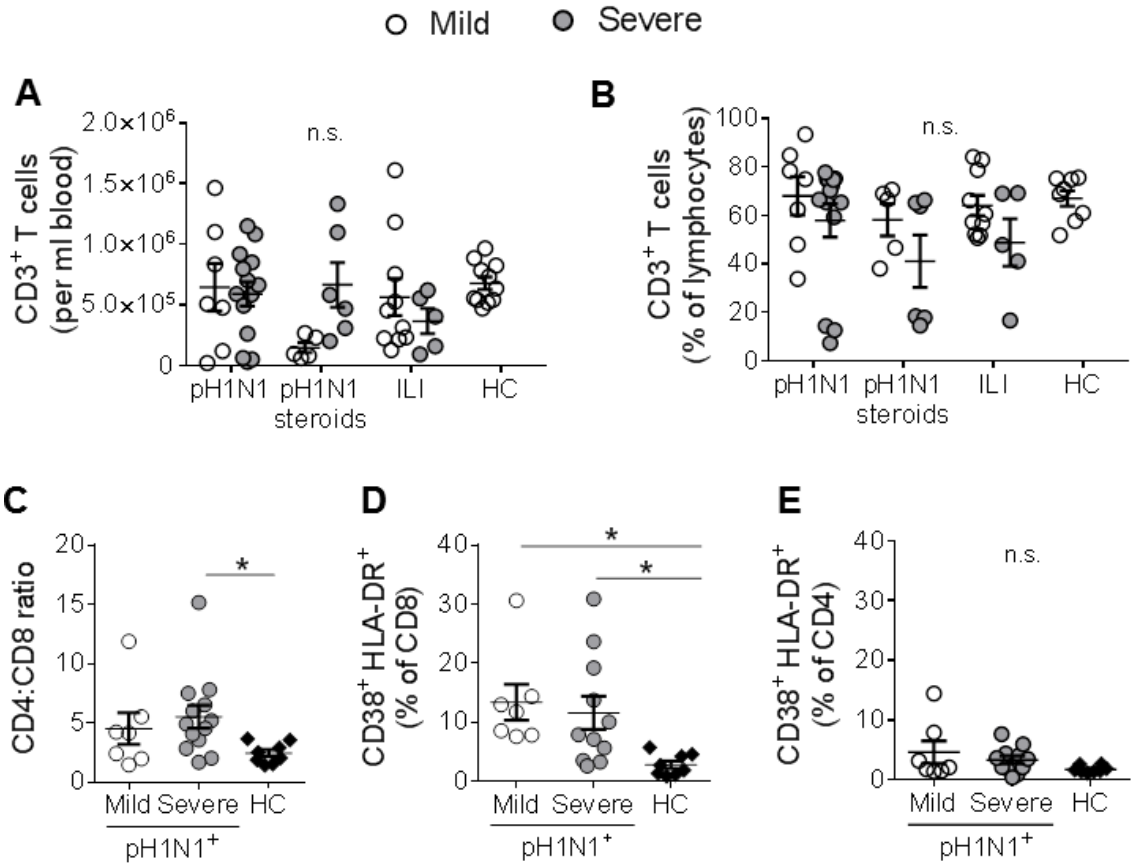

Figure 5.3: T cell frequency and subsets during IAV infection. T cell frequency as **(A)** absolute count per ml of blood or **(B)** percentage of live cells in pH1N1 (n=7 mild, n=14 severe), pH1N1 steroid-treated (n=5 mild, n=6 severe), ILI (n=10 mild, n=5 severe) and HC (n=8). **(C)** CD4:CD8 ratio in pH1N1 patients compared to healthy controls. **(D)** Percentage of activated effector $CD8^+$ and **(E)** $CD4^+$ T cells in pH1N1 patients compared to healthy controls, identified as $CD38^+HLA\text{-}DR^+$ cells. Significance determined by t-tests within groups and one-way ANOVA between pH1N1 patients and HC.*$p \leq 0.05$.

PD-1 expression on CD4 and CD8 T cells was investigated as it has been identified as an exhaustion marker which associates with worse outcome as a result of functionally suboptimal IAV-specific T cell responses (520). PD-1 expression on $CD4^+$ T cells was increased as a percentage in both severe (17.42±1.48) and mild (18.35±3.1) pH1N1 patients compared to HC (7.85±1.23) (Figure 5.4A) and as MFI in severe (17.83±1.49) and mild (14.42±2.75) disease compared to HC (8.04±0.65) (Figure 5.4B). No changes were found in $CD8^+$ PD-1 expression comparing severe and mild pH1N1 disease to HC as percentage (21.65±3.77, 22.69±5.18 and 19.15±3.36, respectively) (Figure 5.4C) or MFI (19.41±3.57, 15.05±3.54 and 11.09±1.4, respectively) (Figure 5.4D).

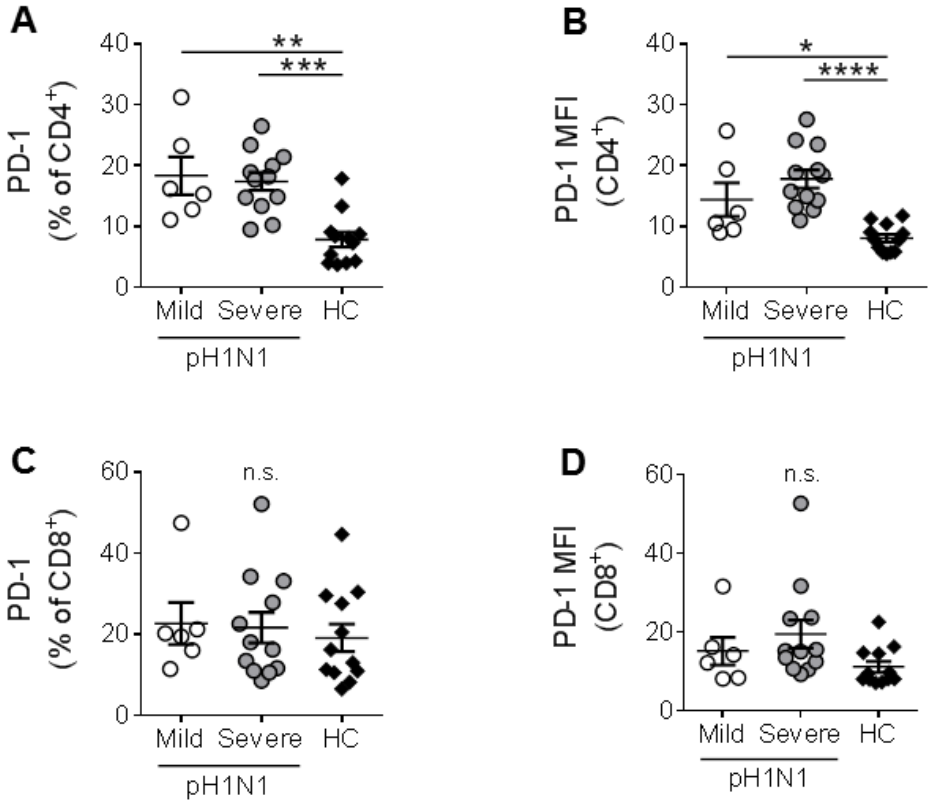

Figure 5.4: PD-1 expression is increased on $CD4^+$ T cells during IAV infection. PD-1 expression on $CD4^+$ T cells as **(A)** a percentage of total $CD4^+$ T cells and **(B)** MFI shows an increase in pH1N1 infection. PD-1 expression on $CD8^+$ T cells was unchanged in pH1N1 infection and in HC as **(C)** percentage of total $CD8^+$ T cells and **(D)** MFI. Significance determined by one-way ANOVA between groups.*p≤0.05, **p≤0.01, ***p≤0.001, ****p≤0.0001.

Frequency of IAV-specific CD8$^+$ T lymphocytes in peripheral blood were next determined using an HLA-A*0201 tetrameric complex loaded with peptide derived from the conserved M (Matrix M_{58-66}) virus protein (424, 425). HLA typing of patients identified eight out of 21 pH1N1, three out of 12 steroid-treated pH1N1 and three out of 17 ILI patients who were HLA-A*0201. Due to these limited numbers, patients were not divided by mild or severe disease. Tetramer$^+$ cells as a percentage of CD8$^+$ were identified in pH1N1 patients (median [range]: 0.205 [0.02-2.26]), steroid-treated pH1N1 patients (1.8 [0.14-4.57]), and to a lesser extent in one of the three ILI patients (0.07 [0-0.33]) (Figure 5.5A). Positive Tetramer staining is depicted in Figure 5.5B.

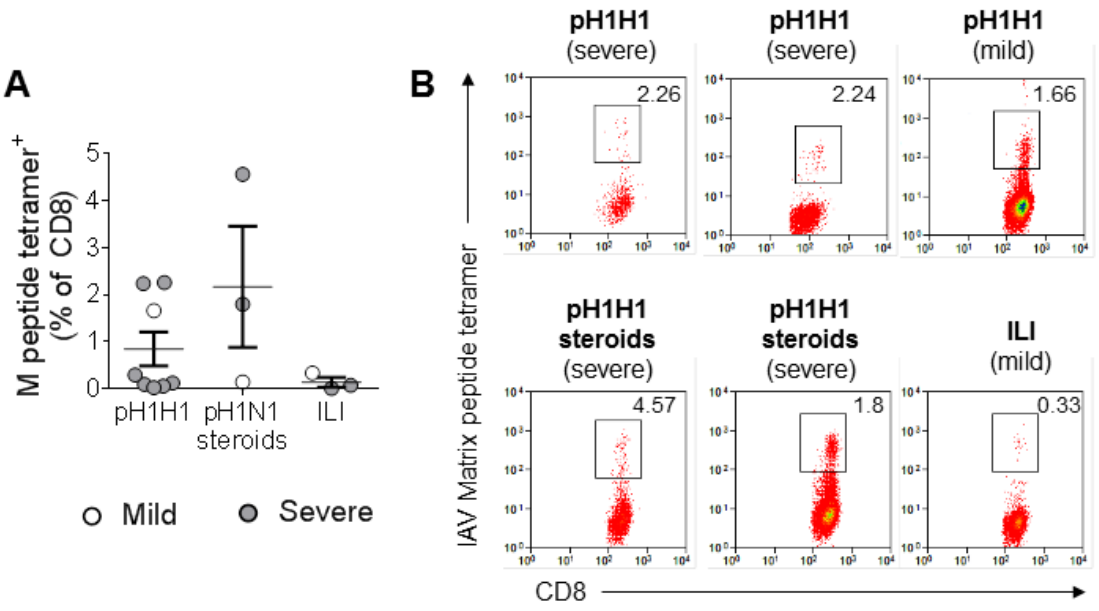

Figure 5.5: Identification of IAV-specific T cells in blood during pH1N1 infection. **(A)** Frequencies of CD8$^+$ T cells specific to H1N1 matrix (M) epitope as detected by MHC-I tetramer loaded with M peptide in pH1N1 (n=8), steroid-treated pH1N1 (n=3) and ILI (n=3) patients. **(B)** Flow cytometry analysis of M1-specific T cells in three pH1N1 patients, two steroid-treated pH1N1 patients and one ILI patient, showing individuals with the highest percentages of M1-specific CD8$^+$ T cells identified in (A).

To examine whether the differences in frequency of M1 tetramer-specific cells could be accounted for by differences in monocyte frequencies, as examined in the previous chapter, correlations were carried out to total monocyte percentage and $CD14^+CD16^+$ inflammatory monocytes as percentage of total monocytes, as both were found to associate with severe disease. There was no correlation between the amount of M1 tetramer-specific $CD8^+$ T cells and total monocyte frequency (Figure 5.6A), or inflammatory monocyte frequency (Figure 5.6B).

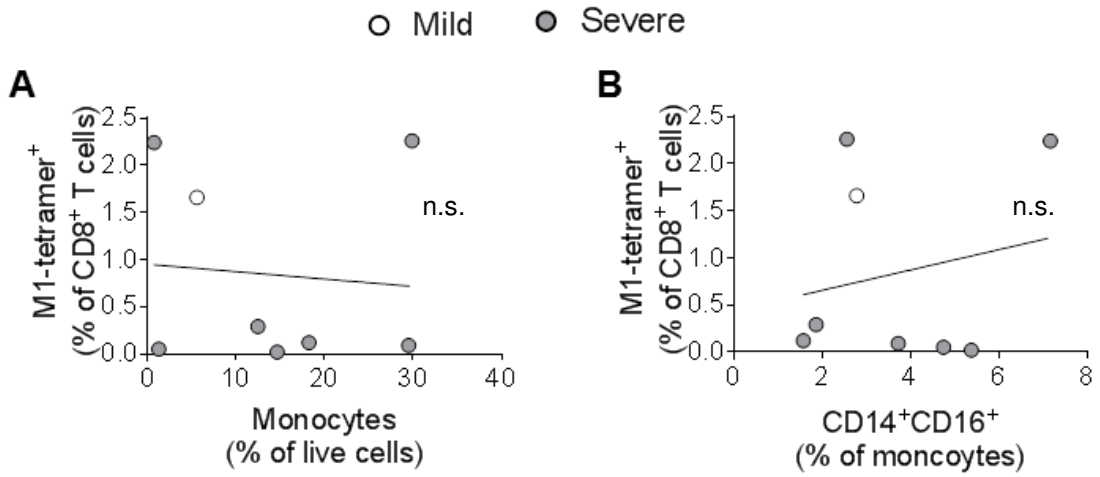

Figure 5.6: No association of IAV-specific T cells with monocyte frequency. Correlation of frequencies of M1-specific $CD8^+$ T cells against **(A)** total monocyte frequency as a percentage of live cells and **(B)** $CD14^+CD16^+$ inflammatory monocytes as a percentage of total monocytes. Correlations examined using Spearman's rank.

T cell responses to overlapping peptides spanning the entire pH1N1 proteome were next examined in an IFNγ ELISpot assay. The number of IAV-specific T cells capable of secreting IFNγ upon activation with peptide pools comprising overlapping peptides to HA, NA, NP, NS1, PA, PB1, PB2 and M1/2 were measured and compared between severe and mild disease for pH1N1 and ILI patients.

Total IAV-specific T cell responses are shown for each individual pH1N1 infected patient in Figure 5.7A. Patients with severe disease had higher IAV-specific T cell responses (median [range] SFU/10^6 PBMC: 1,021 [37-2,020]) than patients with mild disease (123 [5-407]). Four of the severe patients had noticeably low T cell responses compared to the other severe patients, and so confounding factors for these were examined. No common confounding factor was however identified, as duration from first symptom ranged from 8-21 days, monocyte frequency ranged from 0.7% to 29.9% of live cells and neutrophilic MDSC frequency ranged from 1.9% to 18.6% of live cells.

Next, IAV-specific IFNγ responses to individual virus proteins were compared between mild and severe pH1N1 disease (Figure 5.7B). All patients responded to at least one protein. Comparing severe to mild disease, there was a significantly increased response, measured as SFU/10^6 PBMC, to HA (median [range]: 218 [13-848] vs 15 [0-93]), NA (185 [0-355] vs 8 [0-23]), PB1 (15 [0-110] vs 3 [0-13]) and PB2 (18 [0-58] vs 0 [0-13]). No significant differences between severe and mild disease were found for NP (238 [8-943] vs 21 [0-210]), M (70 [0-90] vs 16 [0-148]), NS (38 [0-193] vs 11 [0-60]) or PA (10 [0-53] vs 4 [0-10]).

The most immunodominant responses were to HA and NP, based on the number of responding subjects (16/17, 94% for both) and the magnitude of response as detailed in the previous paragraph. PB-2 and M induced responses in the fewest patients (PB-2: 12/17, 71% M: 13/17, 76%).

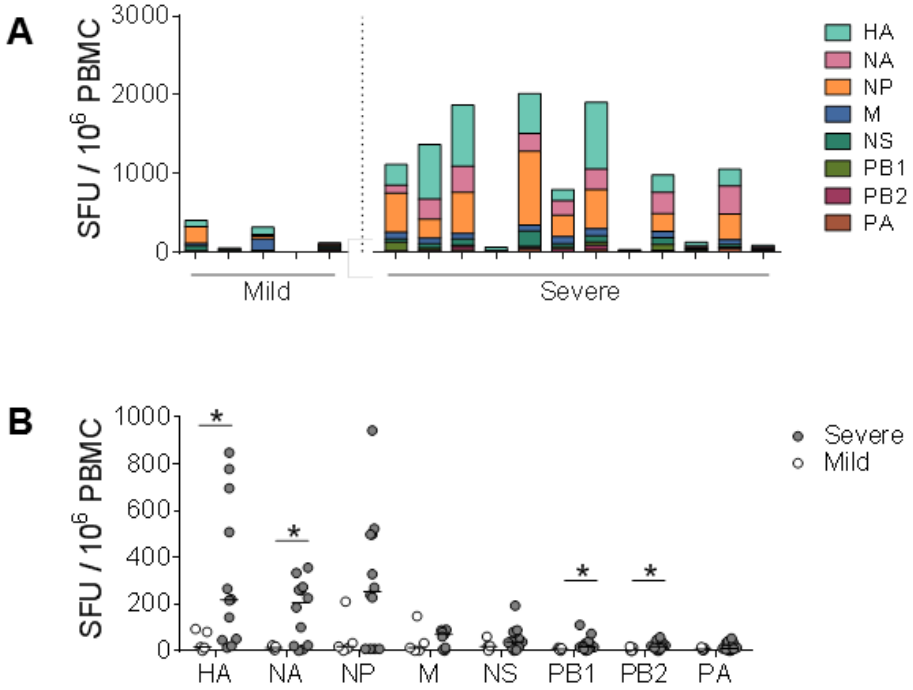

Figure 5.7: IAV-specific IFNγ T cell responses are highest in severely infected pH1N1 infected patients. (A) IAV-specific T cell responses from each patient measuring IFNγ release after stimulation with corresponding peptide pools spanning the entire pH1N1 proteome. Each bar represents the proportion of T cell responses per million PBMCs in one patient, and colours represent the response to each protein. HA, hemagglutinin; NA, neuraminidase; NP, nucleoprotein; M, matrix; NS, nonstructural proteins; PB, polymerase basic; PA, polymerase acidic. **(B)** T cell responses to individual IAV proteins (peptide pools) comparing mild (white) and severe (grey) patients. Lines are drawn at the median. Mann-Whitney U-test used to determine significance between mild and severe disease. *p≤0.05

T cell responses were measured in ILI patients as for pH1N1 patients, and shown in Figure 5.8A for each individual patient. IAV-specific T cell IFNγ responses were low, as expected, and did not differ significantly between severe and mild disease (31 [0-360] vs 213 [10-815]).

IAV-specific IFNγ responses to individual virus proteins were not significantly different between severe and mild disease in ILI patients for any of the IAV proteins: HA (5 [0-185] vs 50 [0-145]), NA (3 [0-35] vs 20 [3-493]), NP (14 [0-55] vs 48 [0-120]), M (5 [0-10] vs 15 [0-155]), NS (4 [0-43] vs 3 [0-120]), PB1 (3 [0-28] vs 13 [0-35]), PB2 (3 [0-43] vs 3 [0-25]) and PA (3 [0-23] vs 8 [0-50]) (Figure 5.8B).

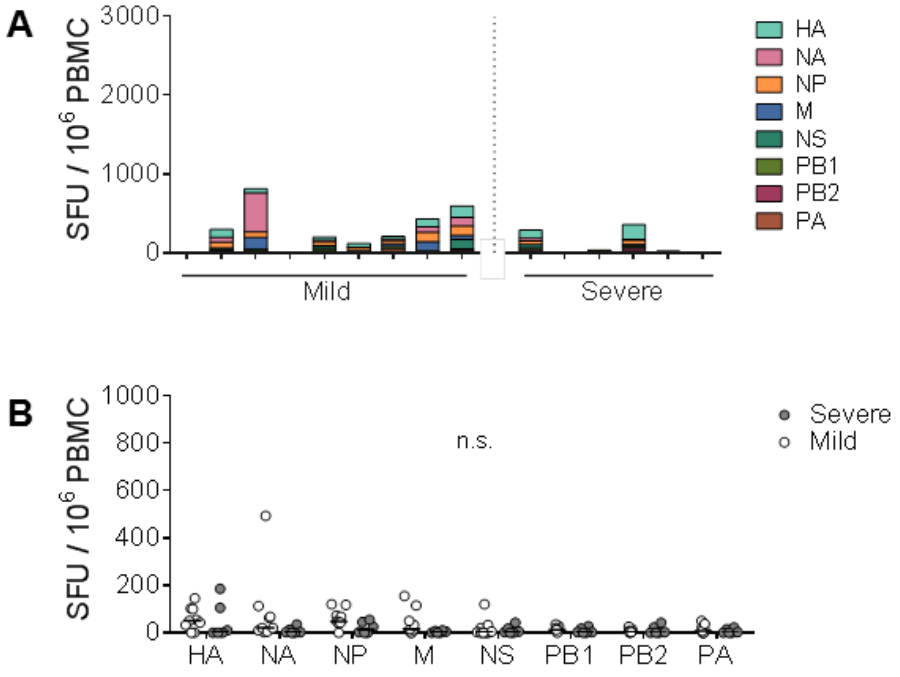

Figure 5.8: IAV-specific IFNγ T cell responses are low in ILI patients. (A) IAV-specific T cell responses from each patient measuring IFNγ release after stimulation with corresponding peptide pools spanning the entire pH1N1 proteome. Each bar represents the proportion of T cell responses per million PBMCs in one patient, and colours represent the response to each protein. HA, hemagglutinin; NA, neuraminidase; NP, nucleoprotein; M, matrix; NS, nonstructural proteins; PB, polymerase basic; PA, polymerase acidic. **(B)** T cell responses to individual IAV proteins (peptide pools) comparing mild (white) and severe (grey) patients. Lines are drawn at the median. Mann-Whitney U-test used to determine significance between mild and severe disease.

5.4.2 Reduced $CD8^+$ T cell differentiation in severe disease is associated with high monocyte frequency

To evaluate differences in the T cell differentiation profile during acute IAV infection based on disease severity, comparisons were made between severe and mild pH1N1 infected patients and healthy controls. The differentiation state of $CD8^+$ and $CD4^+$ T cells was evaluated using CD27, CD28 and CCR7. Figure 5.9A shows the identification of 4 populations of $CD8^+$ T cells based on CD27 and CD28 expression. $CD27^+CD28^+$ cells were then further divided by $CCR7^+$ and $CCR7^-$ expression. T cell differentiation was measured along the following axis: $CD27^+CD28^+CCR7^+$ → $CD27^+CD28^+CCR7^-$ → $CD27^+CD28^-$ or $CD27^-CD28^+$ → $CD27^-CD28^-$.

Pie charts were created, shown in Figure 5.9, using mean values to depict differences in differentiation state of $CD8^+$ T cells in (B) severe pH1N1, (C) mild pH1N1 and (D) HC. $CD8^+$ T cells from severe pH1N1 patients had more T cells in the earliest $CD27^+CD28^+CCR7^+$ differentiation state compared to mild (63.2%±5.85 vs 54%.63±7.04) and less T cells in the most differentiated $CD27^-CD28^-$ state compared to mild (7.4%±1.63 vs 15.8%±4.16). The mean number of T cells in the intermediate differentiation states in severe compared to mild pH1N1 infection were similar for $CD27^+CD28^+CCR7^-$ (15.57%±3.0 vs 14.24%±2.62), $CD27^+CD28^-$ (10.52%±1.42 vs 12.28%±2.04) and $CD27^-CD28^+$ (3.31%±1.03 vs 3.1%±0.62) T cells.

The differentiation profile of $CD8^+$ T cells in healthy controls was similar to that of mild pH1N1 patients at all differentiation stages; $CD27^+CD28^+CCR7^+$ (54.01%±5.26), $CD27^+CD28^+CCR7^-$ (13.38%±1.89), $CD27^+CD28^-$ (12.9%±1.48), $CD27^-CD28^+$ (2.99%± 0.65) and $CD27^-CD28^-$ (16.71%±4.93) Figure 5.9D).

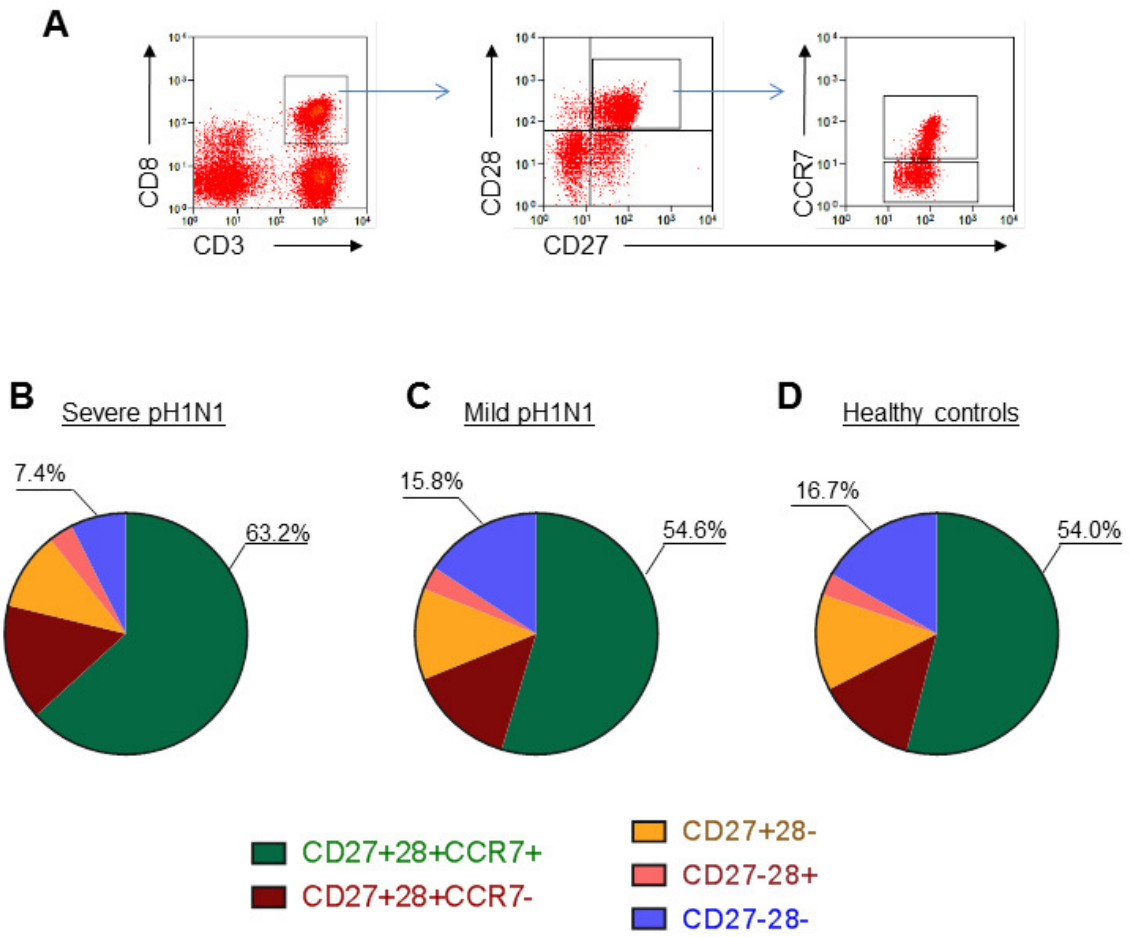

Figure 5.9: Reduced CD8⁺ T cell differentiation in severe pH1N1 infection. (A) Flow cytometry identification of different populations of T cells based on CD27, CD28 and CCR7. **(B)** $CD8^+$ T cell differentiation profiles in severe and mild pH1N1 infection and HC as pie charts. Percentages identify populations that are significantly different in severe and mild disease.

The influence of total monocytes or neutrophilic myeloid-derived suppressor cells (MDSCs) on $CD8^+$T cell differentiation was next assessed, as high frequencies of both were found to be a correlate with severe disease in the previous chapter. Monocyte frequency in PBMCs correlated positively with the proportion of $CD27^+CD28^+CCR7^-$ T cells (Figure 5.10A), and negatively with the proportion of $CD17^-CD28^-$ T cells (Figure 5.10B), linking higher monocyte frequency with less differentiated T cells. Neutrophilic MDSC frequency did not correlate with T cell differentiation state (Figure 5.10C-D).

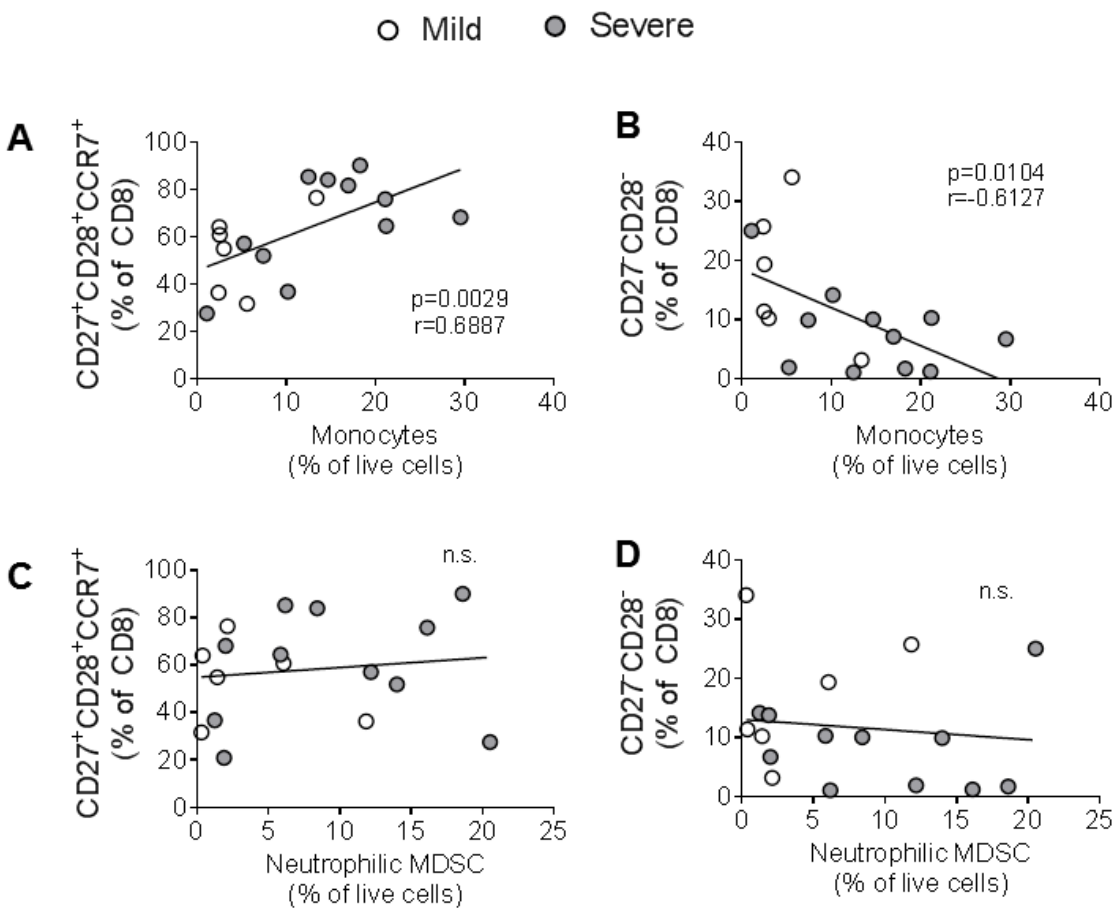

Figure 5.10: Reduced CD8$^+$ T cell differentiation correlates with high monocyte frequency. (A) Positive correlation between monocyte frequency and frequency of the lowest level of T cell differentiation (CD27$^+$CD28$^+$CCR7$^+$) in CD8$^+$ T cells. **(B)** Increased monocyte frequency correlates with low numbers of effector CD8$^+$ T cells (CD27$^-$ CD28$^-$) in blood of pH1N1 infected patients. No correlation between neutrophilic MDSCs and **(C)** CD27$^+$CD28$^+$CCR7$^+$ T cells or **(D)** CD27$^-$CD28$^-$ T cells. Correlations examined using Spearman's rank.

No significant differences were found in the differentiation state of CD4$^+$ T cells comparing severe and mild pH1N1 infection and healthy controls: CD27$^+$CD28$^+$CCR7$^+$ (85.63%±2.22, 79.9%±4.78 and 81.1%±3.16), CD27$^+$CD28$^+$CCR7$^-$ (6.63%±1.0, 7.99%±1.55 and 7.88%±1.36), CD27$^+$CD28$^-$ (0.83%±0.38, 0.70%±0.22 and 1.47%±0.45), CD27$^-$CD28$^+$ (4.48%±0.7, 7.36%±2.83 and 6.47%±1.25) and CD27$^-$ CD28$^-$ (2.43%±1.0, 4.05%±1.72 and 3.09%±1.25) (Figure 11).

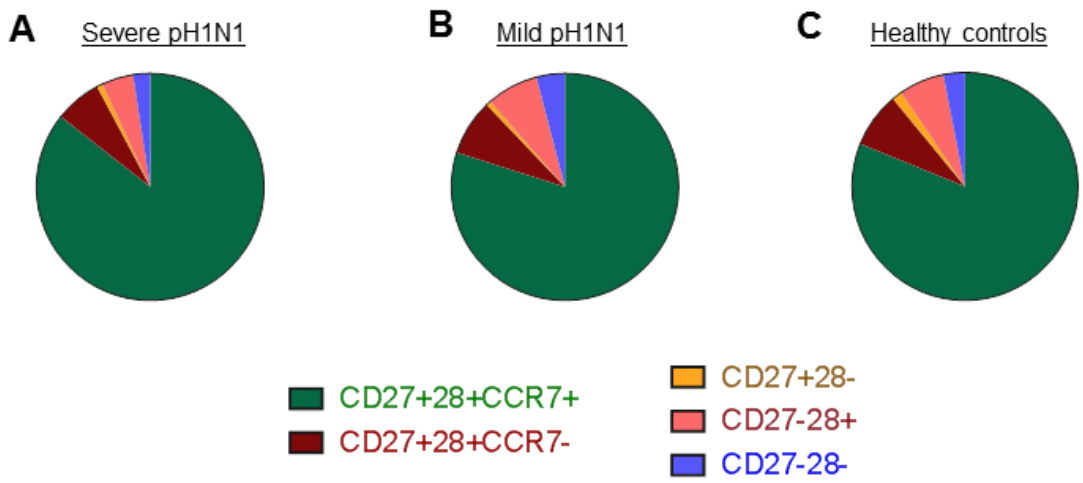

Figure 5.11: CD4$^+$ T cell differentiation in pH1N1 infection does not differ from healthy controls. CD4$^+$ T cell differentiation profiles in severe and mild pH1N1 infection and HC as pie charts show no significant differences between groups.

5.4.3 iNKT cells are lowest in pH1N1 patients with high CD14$^+$CD16$^+$ inflammatory monocytes

Frequency of iNKT cells (as defined in 5.3.3) were examined in the blood of patients with pH1N1 patients, steroid-treated pH1N1 patients, patients with ILI and healthy controls. Absolute numbers of iNKT cells were not significantly different between severe and mild disease in pH1N1 (217.8±66.37 vs 339.2±124.0), steroid-treated pH1N1 (102.1±40.20 vs 365.9±161.6) or ILI (94.48±34.95 vs 215.1±87.17) patients (Figure 5.12A). There was however a reduction in iNKT cells in both mild and severe disease compared to healthy controls (741±111).

iNKT cells as a percentage of lymphocytes were reduced in pH1N1 patients with severe disease compared to mild (0.019±0.004 vs 0.041±0.013) (Figure 5.12B). There were no changes in iNKT cell percentage between severe and mild disease in steroid-treated patients (0.015±0.0052 vs 0.034±0.008) or ILI patients (0.046±0.024 vs 0.023±0.008). The percentage of iNKT cells in severe pH1N1 patients was lower than

healthy controls (0.066±0.007). While this analysis only focused on differences between pH1N1 patients and HC, it is worth noting that low iNKT cells were not unique to pH1N1 infection as they were also reduced in ILI patients, however the differences relating to disease severity were pH1N1 specific.

$CD4^+$ iNKT cell frequency was compared between severe and mild pH1N1 infection and healthy controls to identify if differences in iNKT subsets existed, but no differences were found between severe pH1N1 (47.41±6.03), mild pH1N1 (38.61±7.38) or HC (42.67± 5.45) (Figure 5.12C).

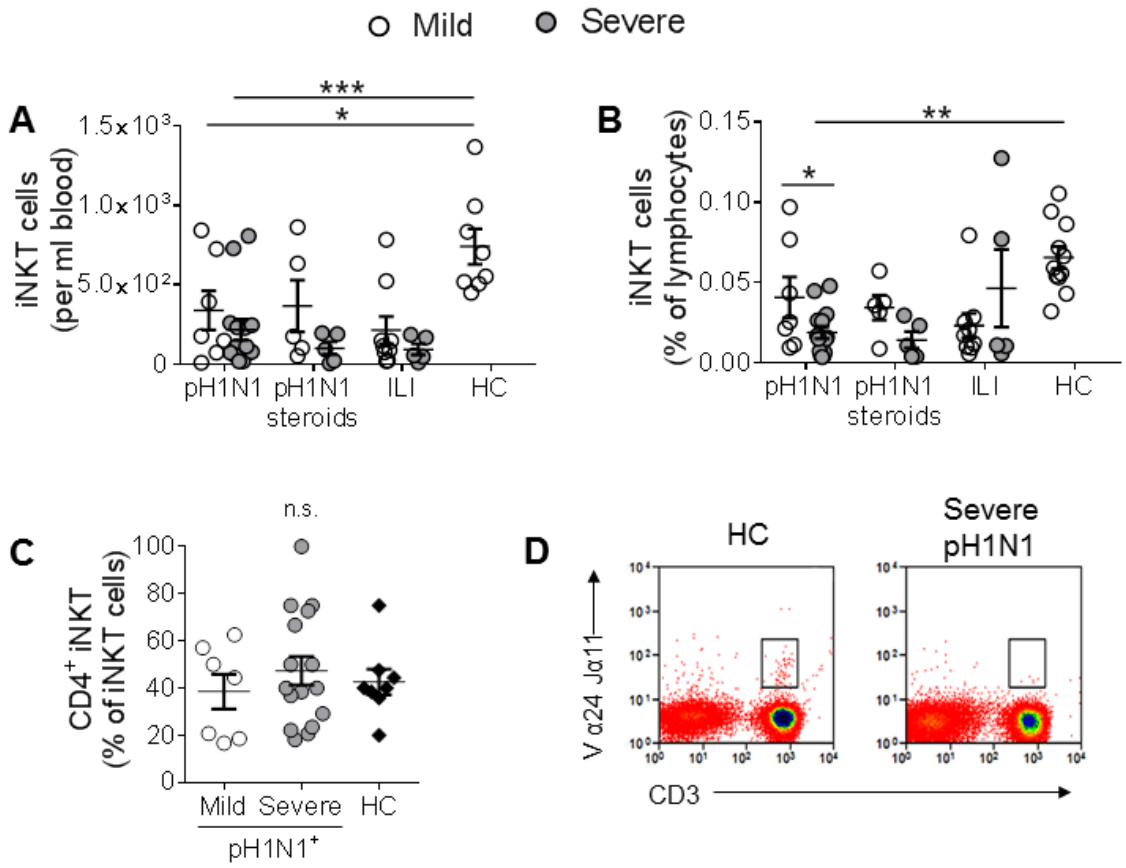

Figure 5.12: Invariant NKT cells are low in IAV infection. iNKT cell frequency as **(A)** absolute count per ml of blood or **(B)** percentage of live cells from flow cytometry analysis in pH1N1 subjects (n=7 mild, n=14 severe), pH1N1 steroid-treated subjects (n=5 mild, n=6 severe), ILI subjects (n=10 mild, n=5 severe) and healthy controls (n=8-11). **(C)** $CD4^+$ iNKT cells as a percentage of total iNKT cells. **(D)** Flow cytometry identification of iNKT cells in a healthy control and absence in a severe pH1N1 patient. Significance determined by t-tests within groups and one-way ANOVA between pH1N1 patients and HC.*p≤0.05, **p≤0.01, ***p≤0.001.

The relationship between iNKT cell numbers and monocytes was next explored by comparing the absolute number of iNKT cells in blood with total monocyte frequency as percentage of live cells and $CD14^+CD16^+$ inflammatory monocytes as a percentage of total monocytes, as both were identified as correlates of severe disease in the previous chapter.

iNKT cells were divided into two groups based on absolute numbers per ml blood; high (>260) and low (≤260), based on the mean absolute value of iNKT cells in both mild and severe disease, which was 260, and plotted against monocyte frequency in the same patient. There was no significant difference in total monocyte frequency as percentage of live cells in the low iNKT cell group compared to the high iNKT cell group (10.73%±2.39 vs 8.85%±2.62) (Figure 5.13A). Inflammatory monocytes were however higher in the low iNKT cell group compared to the high iNKT cell group (5.23%±0.69 vs 2.69%±0.55) (Figure 5.13B), suggesting a link between high levels of inflammatory monocytes and low iNKT cells.

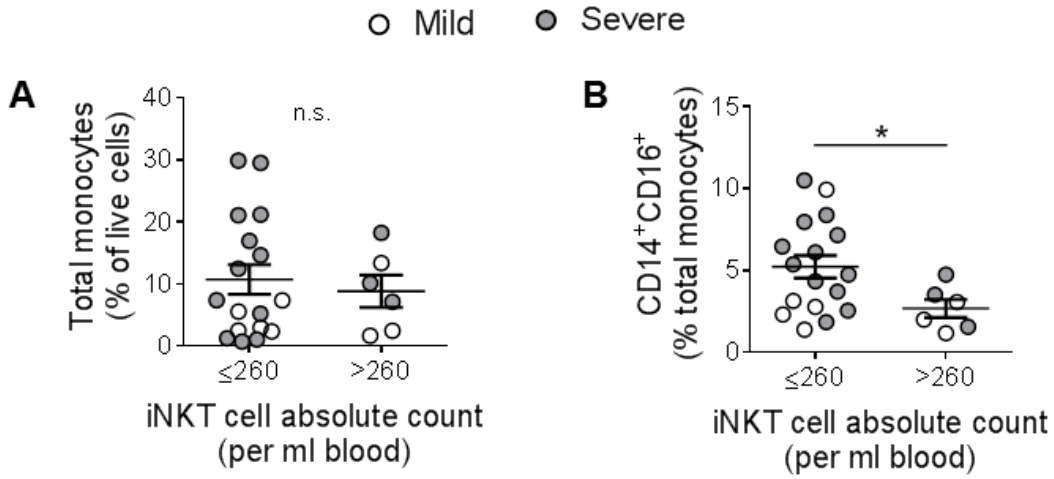

Figure 5.13: Association between low iNKT cells and high $CD14^+CD16^+$ inflammatory monocytes. (A) Total monocyte frequency, as percentage of live cells, is unchanged in individuals with low (≤260) or high (>260) iNKT cell numbers per ml blood. **(B)** Percentage of $CD14^+CD16^+$ monocytes are higher in patients with low iNKT cell numbers. T-test between groups. *p≤0.05.

5.4.4 Magnitude of IAV-specific T cell responses, but not T cell frequency, increases with time from infection

As detailed in Chapter 4.4.4, blood samples were obtained during acute illness which was within 48-72 hours of hospital admission, and 4-6 weeks later. At the time of acute sampling, patients were at different stages of disease, as symptoms had started anywhere from five to 26 days earlier. Correlations to days from first symptoms for iNKT cells (Figure 5.14A), $CD3^+$ T cells (Figure 5.14B), activated effector $CD8^+$ T cells (Figure 5.14C), M1 tetramer-specific $CD8^+$ T cells (Figure 5.14D) and IAV-specific IFNγ T cell responses (Figure 5.14E) identified that only IAV-specific T cell response, which included both $CD4^+$ and $CD8^+$ T cells, increased significantly with time from first symptoms.

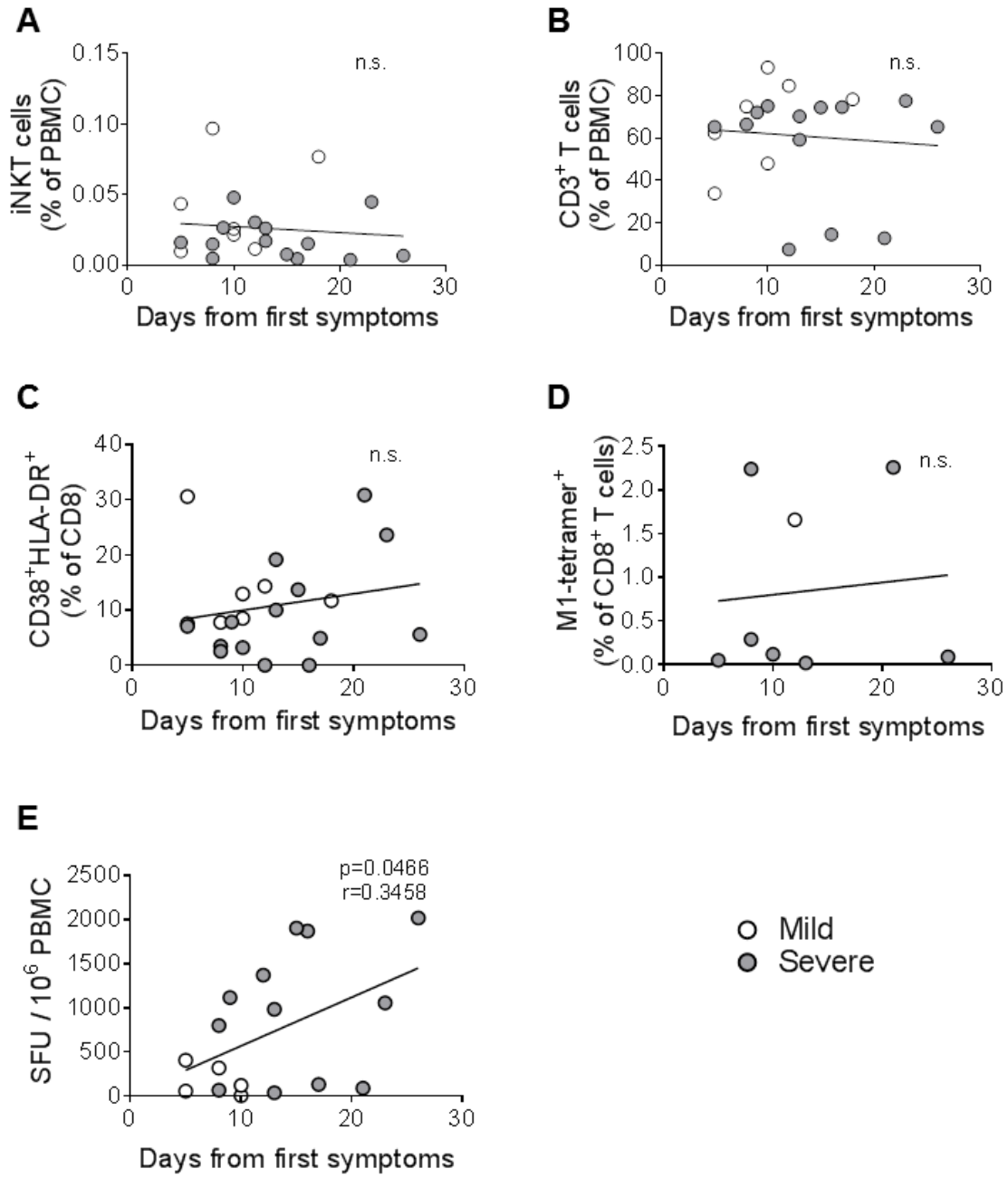

Figure 5.14: IAV-specific T cell responses correlate with symptom duration. No significant correlation of percentage of **(A)** iNKT cells, **(B)** $CD3^+$ T cells, **(C)** activated effector $CD8^+$ T cells or **(D)** Matrix-specific T cells with days from first symptoms. **(E)** IAV-specific IFNγ responses correlate positively with days from first symptoms. While=mild, grey=severe disease. Correlations examined using Spearman's rank.

Next, changes between acute and convalescent disease stages were examined in paired samples. iNKT cell frequency did not change significantly in convalescent compared to acute samples in pH1N1 (0.026±0.011 vs 0.027±0.010), steroid-treated pH1N1 (0.015±0.003 vs 0.228±0.006) or ILI groups (0.045±0.020 vs 0.031±0.016) (Figure 5.15A).

The overall frequency of $CD3^+$ T cells was unchanged in convalescent samples compared to acute illness in pH1N1 (73.12%±405 vs 66.47%±7.38), steroid-treated pH1N1 (65.02%±5.48 vs 44.81%±9.02), and ILI (71.33%±3.29 vs 71.73%±7.79) patients (Figure 5.15B). However, within this subset the frequencies of $CD4^+$ and $CD8^+$ cells were altered in pH1N1 convalescent samples compared to acute illness (Figure 5.15C-D). $CD4^+$ cells were lower (71.46%±4.45 vs 80.96%±3.07) and $CD8^+$ cells were higher (22.01%±3.75 vs 15.0%±2.69) in convalescent samples. No changes comparing convalescent to acute illness were found for $CD4^+$ T cells in steroid-treated pH1N1 (65.94%±7.14 vs 4.38%±7.21) or ILI (73.98%±7.54 vs 78.67%±3.09) patients, or $CD8^+$ T cells in steroid-treated pH1N1 (28.44%±6.83 vs 17.9%±3.46) or ILI (22.79%±6.88 vs 17.97%±3.33) patients.

The frequency of activated effector $CD8^+$ T cells remained high in convalescent samples (Figure 5.15E). No significant differences were found when comparing convalescent samples to acute illness for pH1N1 (28.65%±7.63 vs 12.29%±3.28), steroid-treated pH1N1 (38.41%±9.61 vs 23.32%±5.83), and ILI (16.91%±10.13± 23.77%±10.07) patients.

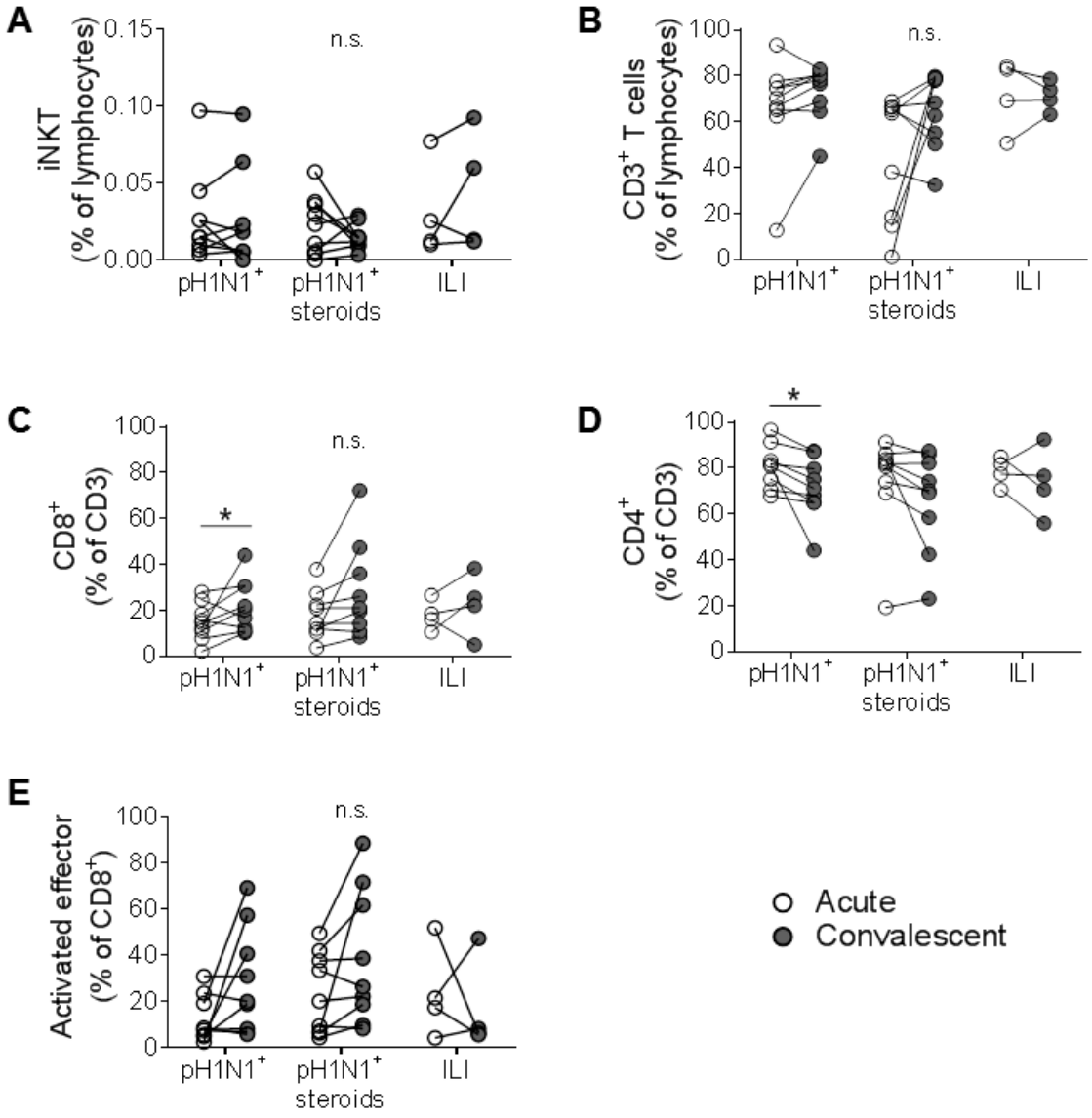

Figure 5.15: T cell subsets in convalescent samples. Percentage of **(A)** iNKT cells, **(B)** $CD3^+$ T cells, **(C)** $CD8^+$ T cells, **(D)** $CD4^+$ T cells and **(E)** activated effector $CD8^+$ T cells in acute and convalescent samples from pH1N1 subjects (n=9), pH1N1 subjects treated with steroids (n=9) or ILI subjects (n=4). Paired t-tests within groups used to determine significance. *p≤0.05.

Paired acute and convalescent samples for ELISPOT analysis of IAV-specific T cell responses were available for 7 pH1N1 patients; 3 mild ('M') and 4 severe ('S'). All 3 mild patients showed increased responses at convalescence, as there was a 6.9-fold increase in IAV-specific IFNγ T cell responses in convalescent samples compared to acute illness (Figure 5.16). In severe infection, two patients (S2 and S3) had increased IAV-specific IFNγ T cell responses at convalescence (10.3-fold higher), while a modest 0.6-fold reduction was observed in the other two severe patients (S1 and S4).

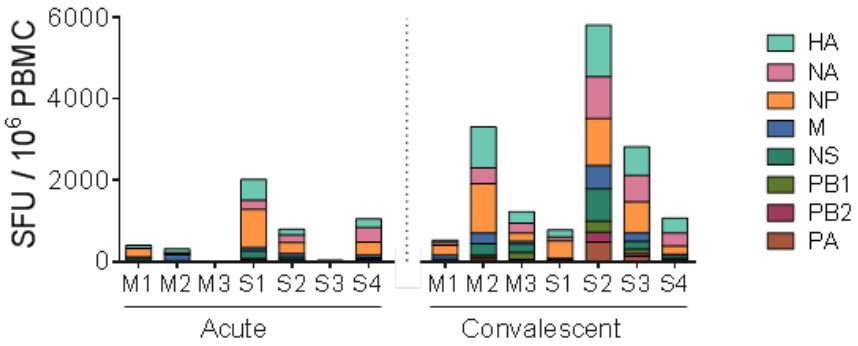

Figure 5.16: Heightened IAV-specific IFNγ responses in convalescent samples. IAV-specific T cell responses from each patient measuring IFNγ release after stimulation with corresponding peptide pools spanning the entire pH1N1 proteome. Each bar represents the proportion of T cell responses per million PBMCs in one patient, and colours represent the response to each protein. Paired samples have the same row ID at acute and convalescent time points. M, mild; S, severe. HA, hemagglutinin; NA, neuraminidase; NP, nucleoprotein; M, matrix; NS, nonstructural proteins; PB, polymerase basic; PA, polymerase acidic.

5.5 Discussion

Analysis of the T cell response in IAV infection revealed that high monocyte frequency, identified in the previous chapter as correlating with severe disease, was associated with lower iNKT cell number and reduced T cell differentiation. IAV-specific T cell responses, comprising both $CD4^+$ and $CD8^+$, were also significantly higher in patients with severe disease during acute infection, and increased with time from infection.

Findings from the previous chapter identified that monocyte phenotype and function were altered in severe pH1N1 infection, but it was not yet clear what the direct consequences of this were on other immune cell subsets. In this chapter reduced T cell differentiation was shown to correlate positively with monocyte frequency. Low frequencies of $CD8^+$ T cells in the most differentiated effector state ($CD27^-CD28^-$) in severe pH1N1 infection compared to mild infection and healthy controls could either suggest that $CD8^+$ T cells during severe acute pH1N1 infection are less differentiated, which may be a result of monocytes halting T cell differentiation at an earlier stage, or it could reflect recruitment of the most differentiated subset to the lungs. Further studies would be needed to identify whether manipulation of monocytes can influence T cell differentiation, as well as analysis of the differentiation state of IAV-specific T cells. As shown by Zhao et al, antigen-specific $CD8^+$ effector T cells were 45-fold higher in lungs than blood following human pH1N1 infection, supporting the hypothesis that these cells reside in the lungs during acute infection (435). In convalescent samples, $CD8^+$ T cell frequency, which was reduced in acute infection, had returned to levels similar as in healthy controls. This supports a transient loss of $CD8^+$ T cells in acute infection, which may have been recruited to the lungs.

IAV-specific T cell responses measured by IFNγ were highest in severely infected patients during acute illness, increased with time from symptoms in acute illness in different patients, and were further increased in convalescent samples in 5/7 patients. Following antigen encounter *in vivo*, virus-specific T cells expand 10^4- to 10^5-fold (521). The increase in IAV-specific T cell responses with time from first symptoms in this study may therefore represent the proliferation and expansion of IAV-specific T cells during acute infection. While differences were not drawn between the $CD4^+$ or $CD8^+$ IAV-specific responses identified by ELISpot, the results in this chapter of higher IAV-specific IFNγ T cell responses in severe compared to mild disease are similar to those found by Zhao et al. who showed that high levels of IAV-specific $CD4^+$ T cells predicted

severe outcome to pH1N1 infection (435). The authors concluded that the higher responses in severe infection were unlikely to be the major cause of severe disease, as none of the proinflammatory cytokines produced by $CD4^+$ T cells were raised in the blood of patients with severe compared to mild disease. Expression of the exhaustion marker PD-1 in this study was upregulated on $CD4^+$, but not $CD8^+$ T cells, and was highest in severe infection. A recent report showed an association between PD-1 expression on IAV-specific $CD8^+$ T cells with worse outcome in high pathogenicity infection due to a dysregulated T cell response induced by the inflamed airway microenvironment, compared to low pathogenicity infection where PD-1 was not upregulated (520). PD-1 upregulation on antigen-specific T cells is known to cause T cell exhaustion during chronic infections such as HIV or LCMV, and blocking PD-1/PD-L1 interactions restored T cell responses (522). Taken together with the findings from Zhao et al. in human pH1N1 infection, it is possible that a dysregulated, exhausted $CD4^+$ T cell response contributed to severe infection, although it would be useful to measure PD-1 expression on virus-specific T cells to confirm this.

High IAV-specific T cell responses were observed in convalescent samples, with only 2/7 subjects showing a small reduction in IFNγ secretion and all others showing an increase at convalescence. This may suggest that the expanded pool of IAV-specific T cells has not contracted yet, as normally occurs following virus clearance, or that the virus has not been efficiently cleared. In *L. monocytogenes* infection, it was discovered that the contraction of antigen-specific T cell responses was not dependent on initial infection dose or magnitude of expansion, but rather is programmed early after infection (523). The high IAV-specific T cell responses at convalescence are supported by the finding that total activated effector $CD8^+$ T cells also remained high in convalescent samples in this study. Others have shown that the IAV-specific $CD8^+$ response is diminished in CD4-depleted mice (524). Taken together with the findings from Zhao et al. of increased $CD4^+$ responses in hospitalised individuals during pH1N1

infection, it is possible that an increased IAV-specific helper $CD4^+$ response is contributing to a longer-lasting total IAV-specific T cell response. Furthermore due to the outline of the current study, where convalescent samples were received 4-6 weeks after acute samples from patients who were unwell enough to be admitted to hospital, it may be possible that some patients have not fully cleared the virus at the convalescent time point, particularly those severely infected. Even the mildly infected patients were ill enough to require hospitalisation, and are therefore not representative of a mild community IAV infected cohort, as has been studied by others, who have found antigen-specific T cell responses to be reduced to baseline 28 days after mild infection (144). This would however require further details regarding the peak of T cell response, as the majority (90 to 95%) of antigen-specific $CD8^+$ T cells are thought to die by apoptosis within 2-3 weeks following the peak of $CD8^+$ T cell expansion (523), and therefore would not be expected to be detectable 4-6 weeks after acute illness.

The high number of circulating monocytes in blood at both acute and convalescent stages in this study (identified in Figure 4.22) provide a means where APCs are readily available to be recruited to lungs and draining lymph nodes for acquisition of antigen and continued presentation to T cells. The induction of a successful effector T cell response was shown to require interaction with DCs bearing antigen at multiple stages following initial priming (525). While purified monocytes infected with IAV *in* vitro have been shown to be poor at presenting viral peptides to T cells, in a tissue setting monocytes infected with IAV effectively stimulated proliferation of IAV-specific $CD4^+$ and $CD8^+$ T cells (526). Tip-DCs, which arose from blood-derived monocytes, were also shown to be necessary for proliferation of IAV-specific $CD8^+$ T cells in the infected lung (270). Therefore the increased frequency of circulating monocytes at acute and convalescent stages of infection in this study may be eliciting virus-specific T cell responses. As BAL samples were not available in this study, it was unfortunately not possible to determine the extent and duration of monocyte recruitment to lungs

following infection. Another caveat is that monocytes from severe patients had low HLA-DR expression (Figure 4.13), and therefore theoretically low antigen presentation capacity. This finding clashes with the correlation between IAV-specific T cell responses and severity, as this infers that IAV-specific T cell responses were highest in patients where monocyte HLA-DR expression was lowest. While it is possible that high HLA-DR expressing monocytes had been recruited to lungs, as discussed in the previous chapter, another potentially contentious suggestion is that the ELISpot assay, which uses peptide pools to virus proteins to stimulate T cells, may represent more a recall response from effector memory T cells rather than an assay to determine the magnitude of T cell response.

The magnitude and frequency of recognition of IAV-specific T cell responses was highest for the IAV proteins HA and NP. High HA-specific responses have not been widely published, as virus-specific CTL responses tend to focus on conserved internal proteins, such as NP, PB-1 and M. Work from the 1980's identified that the CTL response to IAV was directed primarily at NP (527-529). This has recently also been determined in mild human H3N2 infection (144), as well as during severe pH1N1 infection in a Chinese cohort (435), and in cross-recognition of H5N1 T cell responses (530). In all of these recent studies, the matrix protein was also identified as an immunodominant epitope, which was not found in the current study, where M-specific responses were some of the lowest identified. Low M-specific responses identified by ELISpot does however support the flow cytometry findings from this study, where detectable M-specific T cells were only identified in 5/11 HLA-A*0201 pH1N1 infected subjects. The findings by Zhao et al. that $CD8^+$ IAV-specific T cells are found in high quantities in the lungs during severe infection could explain the lack of identification of M1-tetramer specific $CD8^+$ T cells in the blood from some patients in this study, as they may have homed to the lungs. It is not clear however why IAV-specific T cells were identified for some patients and not others, particularly as no correlations were

apparent when comparing with frequency of monocytes (total and $CD14^+CD16^+$), neutrophilic MDSCs or time from first symptoms. Antigen-specific T cells are known to fluctuate during infection however, which could explain the lack of detection in some patients (518). It is also possible that the tetramer is detecting memory $CD8^+$ cells from a previous IAV infection with a different strain of virus, which are circulating in some patients, as the $M1_{58-66}$ epitope is highly conserved between different IAV strains.

High levels of $CD14^+CD16^+$ inflammatory monocytes were also found to be associated with reduced frequencies of iNKT cells during acute infection. This supports previous work from our laboratory where iNKT-deficient mice were shown to have higher numbers of lung-infiltrating monocytes following high pathogenicity IAV infection, leading to a worse outcome (280). Both high frequencies of monocytes and low frequencies of iNKT cell remained unchanged in convalescent samples. The direct interactions between iNKT cells and monocytes were not investigated further here, but are examined later in this thesis.

5.6 Conclusions

The magnitude of the T cell response in acute IAV infection is greatest in severe disease, and remains high 4-6 weeks later. High monocyte frequency is associated with lower iNKT cell numbers and reduced $CD8^+$ T cell differentiation, which were associated with severe disease.

Chapter 6: The role of iNKT cells in regulating monocyte number and function during influenza A virus infection

6.1 Introduction

My studies so far have shown that both monocytes and MDSCs are prominent cellular players during the early phase of influenza A virus (IAV) infection. The concomitant immune landscape suggests that reduction in T cell differentiation and low iNKT cell number may be associated with the changes in myeloid cells. This chapter focuses on the possibility that iNKT cells may alter monocyte number and function in severe IAV infection. Studies in our laboratory have shown that mice lacking iNKT cells ($J\alpha18^{-/-}$) have very high numbers of monocytes and severe lung injury, but it is unclear whether iNKT cells have a direct effect on monocytes. Given this, and the finding of sustained reduction of iNKT cells and increased monocytes over time in severe human IAV infection, I hypothesise that one of the regulators of monocytes is iNKT cells.

The plasticity of monocytes following IAV infection is clear from their differentiation into dendritic cells or macrophages upon reaching the lungs. Monocytes that were recruited to lungs can differentiate into inflammatory dendritic cells (DCs) that cause immune pathology, (279), type I IFN-producing DCs that mediated virus clearance (278), or inflammatory macrophages, which are abundant in post-mortem lungs from fatal cases of human infection with highly pathogenic avian influenza viruses (531).

In our previous study, $J\alpha18^{-/-}$ mice had an increased influx of inflammatory monocytes into the lungs and higher MCP-1 levels in serum and BAL, with more weight loss, mortality and pulmonary inflammation compared to wild-type mice (414). That study did not examine function and phenotype of monocytes so it was unknown how monocytes

caused pathology; whether it was an overwhelming number of monocytes causing injury via release of increased levels of inflammatory mediators, or if their functions were also altered in the absence of iNKT cells.

iNKT cells are capable of rapid production of cytokines and cytolytic mediators upon activation. Direct activation of iNKT cells by monocytes during viral infection can occur via iNKT TCR recognition of endogenous lipid antigen presentation by CD1d on monocytes, co-stimulatory CD40/CD40L interactions, and monocyte production of cytokines such as IL-12 (306, 532). iNKT cells have been shown to constitutively accumulate in microvasculature of mouse lungs, suggesting they are present at the point of monocyte influx following IAV infection, offering possibilities for interaction (533). The frequency of iNKT cells varies by 100-fold in healthy individuals (336), and this variability is likely to have an impact on the immune system, particularly during disease, but it is not known what the consequences are.

In this chapter I question how iNKT cells might regulate monocyte phenotype and function during IAV infection by first examining limited phenotypic and functional changes in lung and blood monocytes after infection of wild-type and Jα18$^{-/-}$ mice, and then widening this to global gene expression profiling of monocytes purified from these mice 3 days after severe IAV infection.

6.2 Aims

The aim of this chapter was to examine the impact of iNKT cells on monocytes during acute IAV infection.

6.3 Methods

6.3.1 Mouse infection and sample preparation

Wild-type C57BL/6 ('WT') and Jα18$^{-/-}$ mice on a C57BL/6 background were infected with a highly pathogenic dose (0.1 HAU) of A/PR/8/34 H1N1 influenza virus ('PR8') (Methods 2.3.2).

Monocytes were purified on day 3 of infection by FACS sorting of Ly6C^{hi} cells from the blood or BAL of WT and Jα18$^{-/-}$ mice and gene expression analysed by Illumina whole genome profiling (Methods 2.1.20.1). From separate mice, immune cell profile was examined on day 3 of infection in blood and BAL (Methods 2.3.3) using multi-colour flow cytometry. Monocyte profile from uninfected mice was also examined in blood, however there was no monocyte influx in lungs of uninfected mice so it was not possible to study monocytes from BAL of uninfected mice. Cellular influx to lungs in PR8 and uninfected mice is displayed in Figure 6.1. Lung perfusion and adoptive transfer methods are described in (Methods 2.3.4 – 2.3.5).

Gating strategy for FACS sorting and flow cytometry analysis of monocytes is shown in Figure 6.1. Following exclusion of doublets and autofluorescent cells, CD3^{+} lymphocytes were gated out, as some CD3^{+} cells express Ly6C, and the remaining cells analysed for Ly6C and Ly6G expression. Ly6C^{hi}Ly6G^{-} cells represent inflammatory monocytes, which are most comparable to human classical CD14^{+} monocytes, although species differences exist, as detailed in the Introduction (1.2.2). Ly6G^{hi}Ly6C^{-} cells are representative of classical neutrophils.

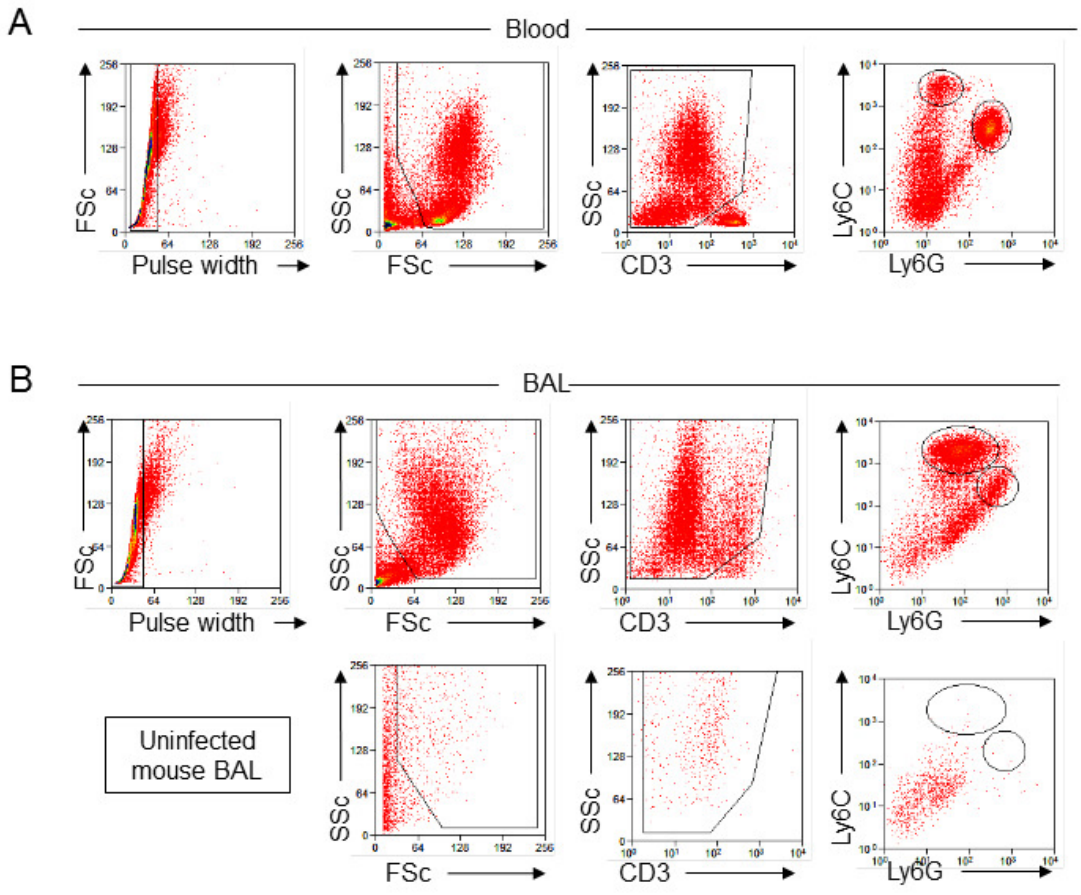

Figure 6.1: Flow cytometry gating strategy for analysis of mouse monocytes. Doublets were excluded by pulse width analysis, and singlets were analysed for size and granularity by FSc/SSc profile. Autofluorescent cells and $CD3^+$ lymphocytes were gated out. The remaining cells were analysed for Ly6C and Ly6G expression. Representative plots for **(A)** Blood and **(B)** BAL are shown. Second row of BAL plots are from uninfected mice showing lack of $CD3^+$, $Ly6C^{hi}$ and $Ly6G^+$ cells.

6.3.2 Microarray analysis

Data from microarrays of purified monocytes from blood and BAL on day 3 of PR8 infection were analysed separately and gene lists compared to each other. Raw data were firstly processed by computing the mean intensity for each probe set. Analysis was carried out using the 'limma' (linear models for microarray analysis) package from Bioconductor. Bayesian moderated t-tests were applied to identify differentially expressed genes between groups, while the Benjamini-Hochberg false discovery rate (FDR) procedure was used to correct for multiple testing. This created lists of genes

significantly differentially expressed between groups with relevant outputs including significance levels (adjusted p value) and log2 fold change (log2FC). The adjusted p value is the p value adjusted for multiple testing. These analyses were carried out with the help of Stephen Taylor at the Computational Biology Research Group, Weatherall Institute of Molecular Medicine.

Biological interpretation of data was carried out using MetaCore^{TM} and GSEA (Methods 2.1.21). MetaCore was used to identify pathways and processes associated with significantly differentially expressed genes. Following this, GSEA was utilised to determine whether pre-defined gene sets were enriched in monocytes from WT or Jα18$^{-/-}$ mice. GSEA interrogates the whole genome of detected genes from the microarray, which for the blood monocytes consisted of 12,503 transcripts and for the BAL monocytes consisted of 11,828 transcripts. Ranked lists of these transcripts were created so that genes highly expressed in Jα18$^{-/-}$ monocytes were at the top of the list and genes highly expressed in WT monocytes were at the bottom. Two lists were created; one for blood monocytes and one for BAL monocytes, which were interrogated for enrichment of genes from pre-defined gene sets of interest. Pre-defined gene sets were derived as described in Chapter 3.3.2.

6.4 Results

6.4.1 Monocyte frequency is higher in the lungs of iNKT deficient mice compared to wild-type

Monocyte numbers in Jα18$^{-/-}$ ('KO') were first determined relative to WT mice in blood and BAL following PR8 infection. In the blood on day 3 of PR8 infection, monocyte frequency (gated as described in 6.3.1) increased in response to infection as absolute number ([cells/ml blood ± SEM] WT: 173,830±45,879 to 516,616±83,277; KO:

139,122±12,571 to 575,956±86,192) (Figure 6.2A) and percentage (WT: 2.33±0.36 to 4.68±0.71; KO: 1.61±0.15 to 5.89±0.36) (Figure 6.2B), although there were no differences between WT and Jα18$^{-/-}$ mice. In the BAL, Jα18$^{-/-}$ mice had more Ly6C^{hi} monocytes infiltrating the lungs than WT, both as absolute numbers (WT: 286,581±36,177; KO 452,088±60,103) (Figure 6.2C) and percentage of live cells (WT: 32.2±2.78; KO 42.82± 3.55) (Figure 6.2D). Ly6C^{hi} monocytes were also increased nearly 2-fold in perfused lung digests from Jα18$^{-/-}$ mice compared to WT, confirming the increase in monocytes in lungs (Figure 6.2E).

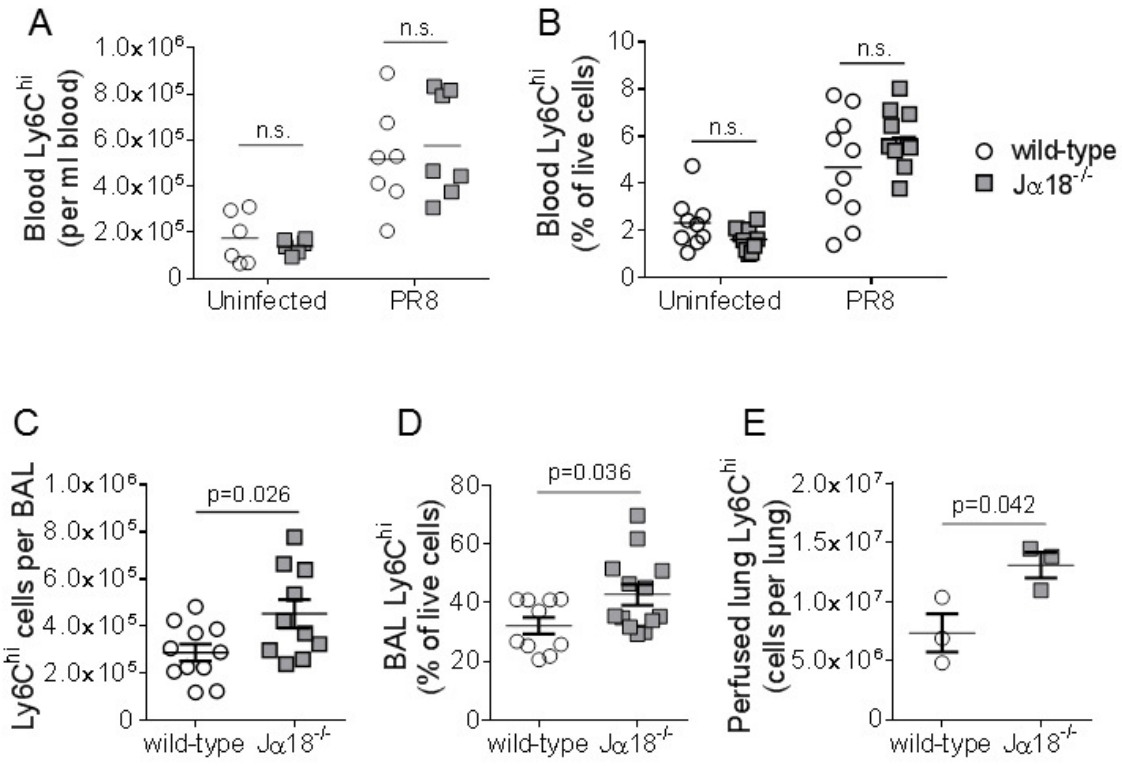

Figure 6.2: Monocyte frequency in wild-type and iNKT deficient mice following IAV infection. Ly6C^{hi} monocyte frequency in blood of uninfected or day 3 PR8-infected WT and Ja18$^{-/-}$ mice as **(A)** absolute counts (n=6-7 mice/group) or **(B)** percentage of live cells (n=11 mice/group). Ly6C^{hi} monocyte frequency in BAL of day 3 PR8 infected WT and Ja18$^{-/-}$ mice as **(C)** absolute counts or **(D)** percentage of live cells. n=10-11 mice/group. **(E)** Absolute number of Ly6C^{hi} monocytes in perfused lung digests from WT or Ja18$^{-/-}$ mice. n=3 mice/group. Statistical analysis performed using two-way ANOVA (A)-(B) or t-tests between groups (C)-(E).

As published, Jα18$^{-/-}$ mice lost more weight than WT mice (Figure 6.3A) (280). iNKT cells were detected on day 3 of PR8 infection in the BAL of WT but not Jα18$^{-/-}$ mice using a PE-labelled αGalCer-loaded CD1d dimer (Figure 6.3B), showing that iNKT cells are recruited to lungs following PR8 infection in WT mice.

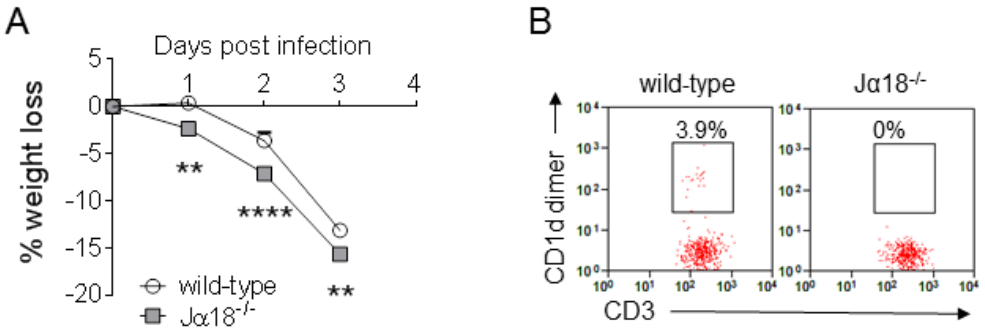

Figure 6.3: iNKT deficient mice lose weight more rapidly than wild-type mice. (A) Weight loss profile of WT and Ja18$^{-/-}$ mice over 3 days of infection with PR8. n=10 mice/group. Difference between groups analysed using two-way ANOVA with repeated measures on different days. **(B)** Detection of iNKT cells in BAL of day 3 PR8 infected WT and Ja18$^{-/-}$ mice by flow cytometry using a PE-labelled αGalCer loaded CD1d dimer showing presence of iNKT cells in BAL of WT and absence in Ja18$^{-/-}$ mice.

6.4.2 Phenotypic and functional profile of monocytes in wild-type and iNKT deficient mice following IAV infection

Having established differences in monocyte frequency upon IAV infection, monocyte phenotype was next evaluated by flow cytometry (gating described in 6.3.1) analysis of surface receptors CD115 and CCR7, and pro-inflammatory cytokines TNFα and IL-12. CD115 is the M-CSF receptor and is expressed on the majority of mononuclear phagocytes. M-CSF controls differentiation, proliferation and survival of these cells, and M-CSFR downregulation is synonymous with activation (534). CCR7 is upregulated upon differentiation into M1 macrophages. Blood from uninfected and day 3 PR8 infected WT and Jα18$^{-/-}$ mice was analysed first in order to determine monocyte

activation and inflammatory state following IAV infection, and examine differences between mouse genotypes.

CD115 expression remained unchanged following IAV infection, however percentage of CD115 expressing monocytes in Jα18$^{-/-}$ mice were 1.4 fold lower than WT (Figure 6.4A). Percentage of CCR7 expressing monocytes increased upon infection in both WT (14.85± 2.23 to 24.87±4.26) and Jα18$^{-/-}$ mice (16.32±1.96 to 22.31±1.59), but no significant differences were found comparing mouse genotypes (Figure 6.4B). TNFα production was upregulated 6-fold and IL-12 was upregulated 4-6 fold upon infection, but no changes were found between WT and Jα18$^{-/-}$ mice (Figure 6.4C-D).

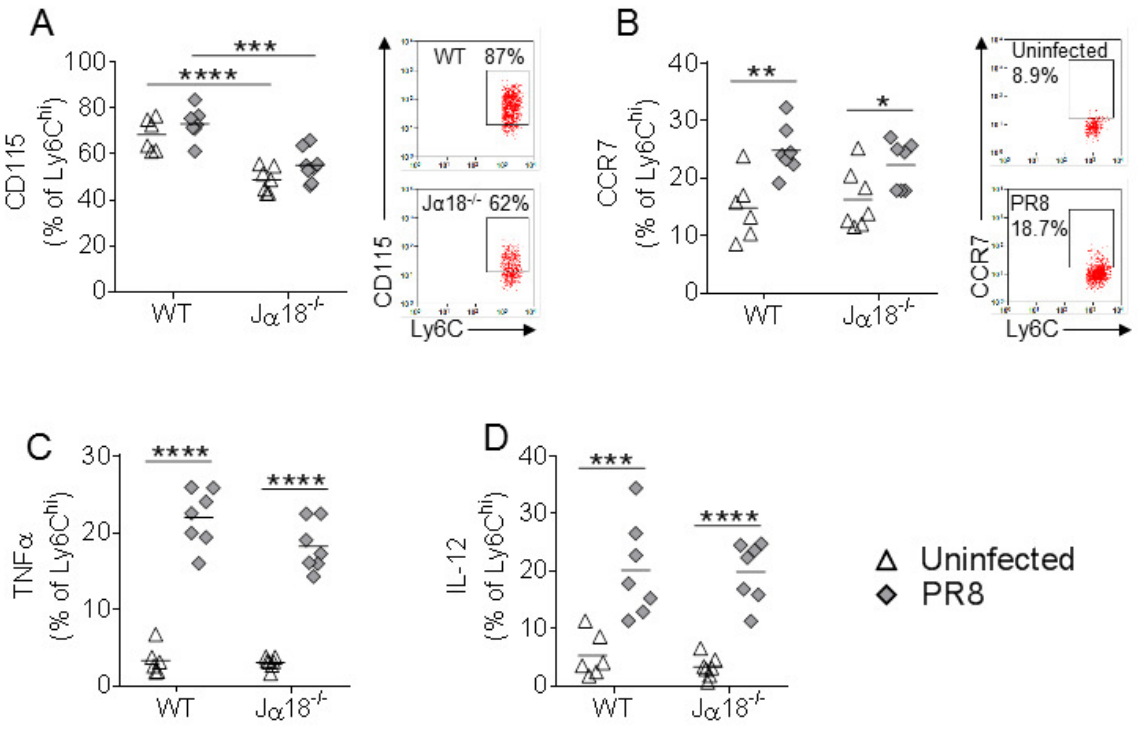

Figure 6.4: Monocyte phenotype and function are altered upon PR8 infection but show little change between wild-type and iNKT deficient mice in blood. Percentage of circulating Ly6C^{hi} monocytes expressing **(A)** CD115 or **(B)** CCR7 and producing **(E)** TNFα or **(F)** IL-12 on day 3 of PR8 infection. White triangles represent uninfected mice (n=6-7/group) and grey diamonds represent PR8 infected mice (n=7-10/group). Two-way ANOVA *p≤0.05, **p≤0.01, ***p≤0.0001, ****p≤0.0001.

Next, expression of CD115 and CCR7 on monocytes from BAL was determined in PR8 infected mice. Monocytes from BAL however showed very low expression of both CD115 (Figure 6.5A) and CCR7 (Figure 6.5B), possibly due to activation and downregulation upon recruitment, and it was therefore not possible to determine differences between WT and Jα18$^{-/-}$ mice using this method. IL-6 levels in BAL fluid were measured, as this cytokine was shown to be associated with a more severe outcome in previous chapters. While it cannot be identified what cells are producing IL-6, monocytes are known to produce high levels of IL-6 upon inflammation, and Jα18$^{-/-}$ mice had higher IL-6 levels in BAL than WT (809.9pg/ml ±84.45 vs 521.2pg/ml±28.69) (Figure 6.5C).

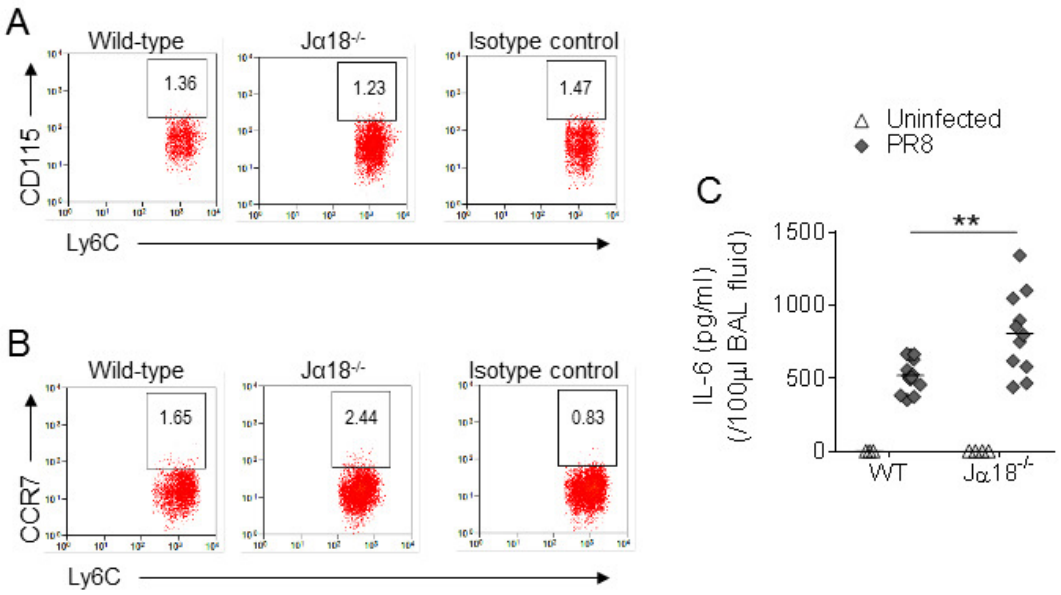

Figure 6.5: Monocyte phenotype in the lungs in wild-type and Ja18$^{-/-}$ mice. Expression of **(A)** CD115 and **(B)** CCR7 on BAL Ly6C^{hi} monocytes from WT and Jα18$^{-/-}$ mice on day 3 of PR8 infection. **(C)** IL-6 levels in BAL fluid of WT or Jα18$^{-/-}$ mice on day 3 of PR8 infection. Two-way ANOVA **p≤0.01.

These data so far showed that monocytes became activated in response to IAV infection and infiltrated the lungs in high numbers, and confirmed that in my hands the IAV infection model reproduced the monocytic changes in Jα18$^{-/-}$ from published

literature (280). Furthermore, the lack of identifiable changes and possible downregulation of monocyte surface receptors identified the need for a transcriptomics approach to investigate changes in monocytes between WT and Jα18$^{-/-}$ mice.

6.4.3 Microarray QC

Prior to hybridisation, RNA sample quality was assessed using an Agilent 2100 Bioanalyser. A RIN number was assigned along a scale of 1-10, with 10 representing highly intact RNA. All samples used in this study had pure, intact RNA (Table 6.1).

	Wild-type			**Jα18$^{-/-}$**		
	(a)	**(b)**	**(c)**	**(a)**	**(b)**	**(c)**
BAL	9.0	8.8	9.1	8.4	9.3	8.6
Blood	8.8	8.7	9.0	8.0	8.4	9.1

Table 6.1: RNA quality for microarray. RIN numbers of RNA from BAL or blood monocytes from WT or Jα18$^{-/-}$ mice. Quality ranked on a scale of 1-10 (1=poor, 10=excellent). (a)-(c) represent biological replicates.

Over 10,000 genes were detected in each sample from both blood (Figure 6.6A) and BAL (Figure 6.6B). Raw data were processed with the VSN (variance-stabilisation and normalisation) algorithm in order to stabilise the variance to better meet the assumptions of the statistical test for differential expression, and also to normalise signal intensities from different samples so they are comparable.

To determine whether there was unintended bias in output data due to experimental procedures or sample quality, distribution of probe intensities of VSN normalised data were evaluated using density plots (Figure 6.6C-D) and box plots (Figure 6.6E-F). For both blood and BAL monocytes, distributions of intensities were consistent across all samples with none showing any distinction in intensity. Therefore the data were considered high quality and suitable for further analysis.

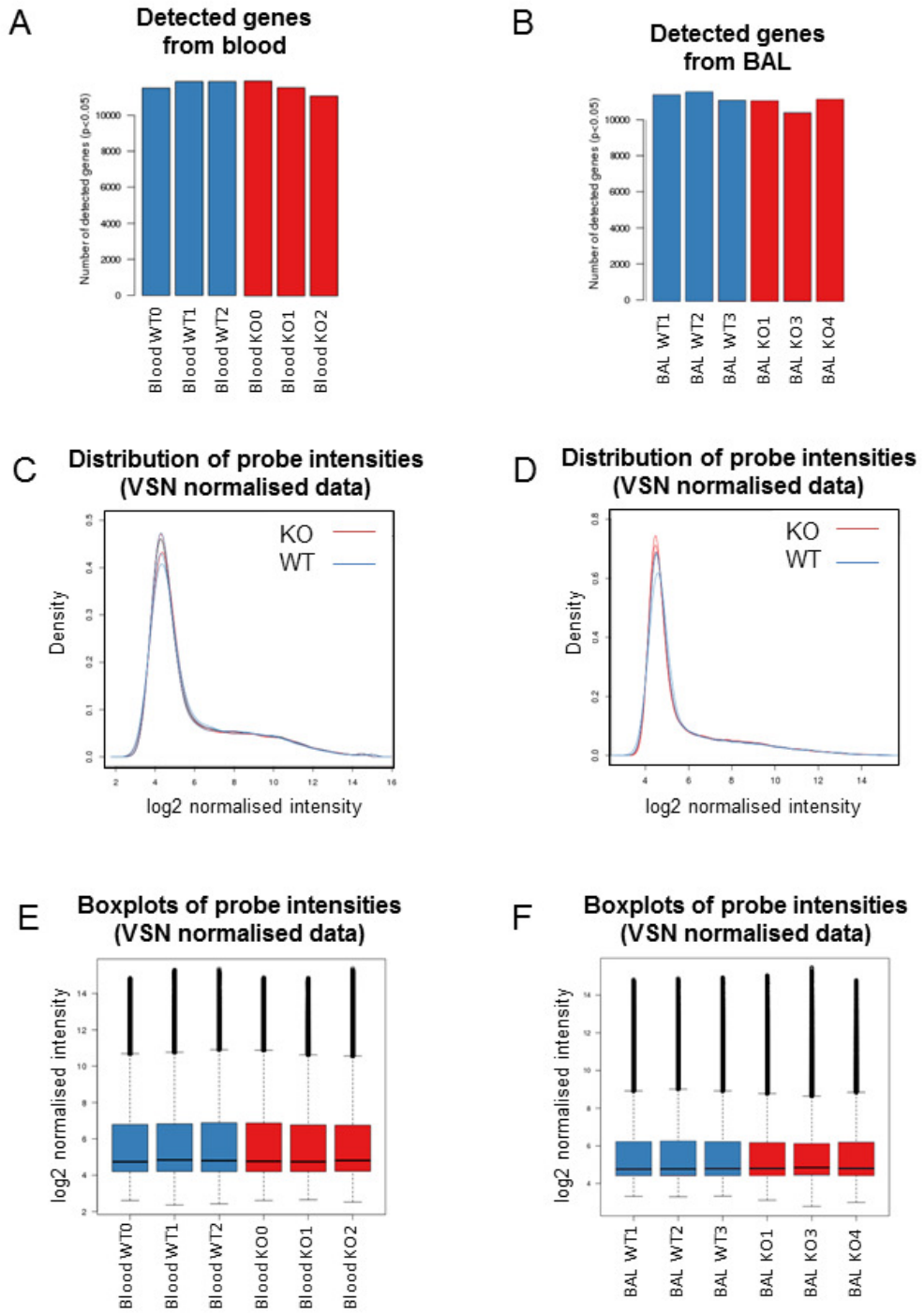

Figure 6.6: Microarray quality control. Number of detected genes in microarray samples from **(A)** blood **(B)** and BAL was high and consistent across samples. Expression of probe intensities of VSN normalised data displayed as density plots for **(C)** blood and **(D)** BAL, and box plots for **(E)** blood and **(F)** BAL demonstrated consistent variance in probe intensities across all samples. Samples coloured by experimental group: wild-type ('WT') – blue; Ja18$^{-/-}$ (knock out, 'KO') – red.

Hierarchical clustering was next utilised to examine the natural grouping of similarities and dissimilarities of the samples. Unsupervised clustering using the 'complete linkage' method was employed, which computed the maximum distance between any two data points in neighbouring sets. For monocytes from blood, samples did not cluster into two experimental groups, but rather formed three clusters of WT/WT, KO/KO and more distantly WT/KO (Figure 6.7A). No factors relating to collection, preparation or processing of the samples could be identified to explain this pattern, and therefore the similarity between samples from different genotypes is likely to be a true biological factor. Monocytes from BAL formed two distinct clusters with clear separation between wild-type and Jα18$^{-/-}$ mice (Figure 6.7B).

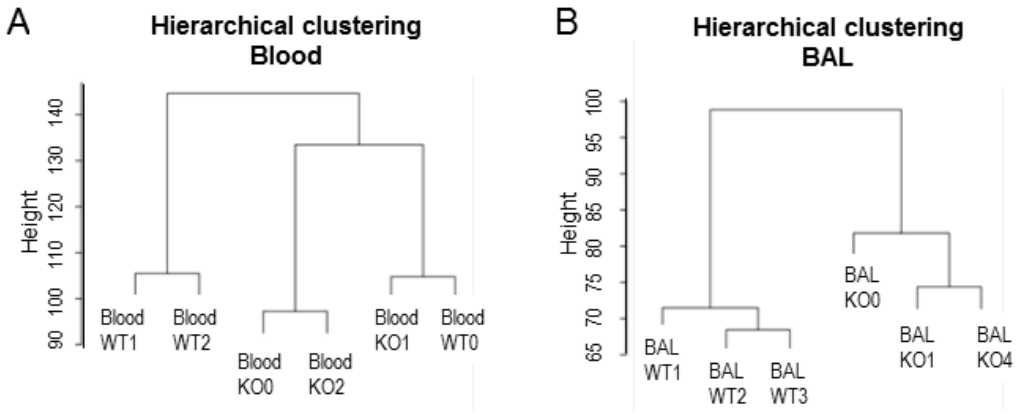

Figure 6.7: Unbiased clustering of Ly6C^{hi} monocytes from wild-type and Ja18$^{-/-}$ mice. Unsupervised hierarchical clustering of **(A)** blood samples and **(B)** BAL samples.

6.4.4 Gene expression of monocytes from iNKT-deficient mice compared to wild-type is more variable in lungs than blood during IAV infection

Monocytes from blood of Jα18$^{-/-}$ mice were first compared to monocytes from blood of WT mice on day 3 after IAV infection; and another comparison made between monocytes from BAL from the two groups of mice.

In the blood, 99 genes were differentially expressed between the two groups of mice on day 3 of IAV infection (adjusted p≤0.05), whereas in the BAL 1,373 genes were differentially expressed. The top 10 upregulated and downregulated genes of known function in monocytes from blood and BAL are shown in Table 6.2. Genes which were differentially expressed in monocytes from both BAL and blood are highlighted in grey.

Blood monocytes		BAL monocytes	
Gene	**Log2FC**	**Gene**	**Log2FC**
ST6GALNAC2	3.80	IFI202B	4.13
CTSE	3.16	CHI3L1	4.12
PVRL2	2.49	ANXA4	2.22
RNASE4	1.91	EAR11	1.66
GPR114	1.80	APOBEC1	1.60
D13ERTD608E	1.71	SLC7A8	1.54
EG384179	1.51	CTSE	1.53
BC018473	1.45	SOAT1	1.41
SOAT1	1.36	SLC38A6	1.38
P2RY14	1.33	PGLYRP1	1.33
PARP2	-1.61	CCL6	-1.82
APOE	-1.66	COPS8	-2.26
SUPT16H	-1.94	MNDA	-2.37
LOC100047132	-1.97	ZFP330	-2.48
COPS8	-2.35	OLFML2B	-2.65
LOC623121 (IFI203)	-2.37	MAN2B1	-2.73
MCM6	-2.47	IFI205	-3.82
MAN2B1	-2.95	APOC2	-4.23
ZFP330	-2.99	APOE	-4.54
FCER1G	-5.71	FCER1G	-6.48

Table 6.2: Top 10 differentially expressed genes in blood and BAL monocytes from iNKT deficient mice. Top 10 upregulated and downregulated genes differentially expressed between monocytes from Jα18$^{-/-}$ mice and WT mice at adjusted p≤0.05. Genes highlighted in grey are differentially expressed in monocytes from both blood and BAL. Full details are in Appendix 4.

To identify all genes that were differentially expressed in monocytes from both blood and BAL, or only one compartment alone, Venn diagrams were created (Figure 6.8A-B). A large proportion of genes that were differentially regulated due to lack of iNKT cells in monocytes from blood were also differentially regulated in monocytes derived from BAL; 26/43 (61%) upregulated genes, 41/56 (73%) downregulated genes. 563 and 743 genes were upregulated and downregulated respectively in BAL alone.

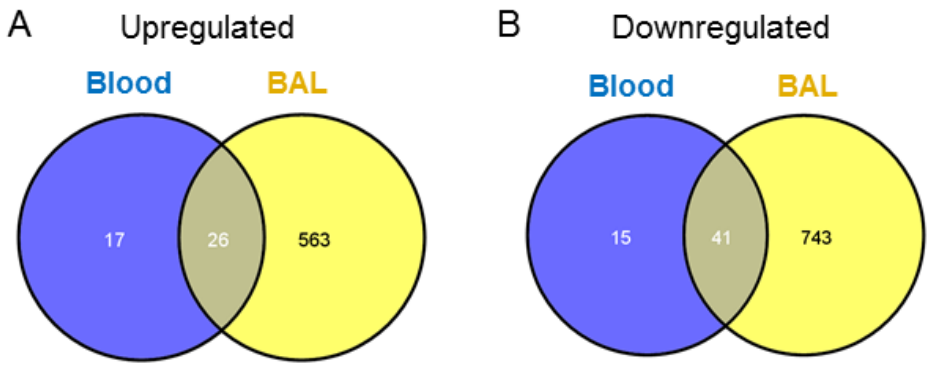

Figure 6.8: Number of differentially expressed genes in Jα18$^{-/-}$ mice between monocytes from blood and BAL. Venn diagrams depicting number of differentially expressed genes either **(A)** upregulated or **(B)** downregulated in Ja18$^{-/-}$ mice compared to WT. Blue circle represents number of differentially expressed genes in blood, and yellow circle represents number of differentially expressed genes in BAL, with common genes differentially expressed in both blood and BAL in the middle.

Therefore, there were a large number of genes unique to monocytes infiltrating the lungs when comparing Jα18$^{-/-}$ and WT mice.

6.4.5 Inflammatory processes are upregulated in monocytes from iNKT deficient mice compared to wild-type

Having established significant differences in monocyte gene expression profiles from PR8 infected WT and Jα18$^{-/-}$ mice, the functional relevance of these differences were evaluated using MetaCore. This identified sets of genes involved in pathways and processes that were either up- or down-regulated in monocytes from blood or BAL in Jα18$^{-/-}$ mice compared to WT. The top 3 processes identified by Metacore using GeneGo and Gene Ontology as being enriched in monocytes from blood or BAL of WT or Jα18$^{-/-}$ mice are displayed in Tables 6.3 to 6.6.

In blood, monocytes from Jα18$^{-/-}$ mice were enriched for inflammatory processes involving interferon signalling, inflammasome signalling, apoptosis-related processes and regulation of defence responses (Table 6.3). Relevant processes downregulated in

blood monocytes from Jα18$^{-/-}$ mice included proteolysis in cell cycle & apoptosis and phagocytosis (Table 6.4).

	P value	FDR
Processes		
Inflammation- Interferon signalling	1.640E-02	1.519E-01
Inflammation- Inflammasome	1.873E-02	1.519E-01
Apoptosis- Death Domain receptors & caspases in apoptosis	2.025E-02	1.519E-01
GO Processes		
Regulation of defense response	6.950E-09	1.189E-05
Regulation of innate immune response	8.359E-07	4.968E-04
Positive regulation of defense response	9.924E-07	4.968E-04

Table 6.3: Upregulated processes in blood of Jα18$^{-/-}$ mice compared to wild-type. P value and FDR (false discovery rate) calculated based on number of input transcripts that were identified in processes defined by Metacore.

	P value	FDR
Processes		
Proteolysis- Proteolysis in cell cycle and apoptosis	2.747E-02	4.052E-01
Response to hypoxia and oxidative stress	4.470E-02	4.052E-01
Immune response- Phagocytosis	7.737E-02	4.052E-01
GO Processes		
Regulation of blood coagulation	3.063E-07	1.962E-04
Regulation of hemostasis	3.063E-07	1.962E-04
Regulation of coagulation	4.148E-07	1.962E-04

Table 6.4: Downregulated processes in blood of Jα18$^{-/-}$ mice compared to wild-type. P value and FDR (false discovery rate) calculated based on number of input transcripts that were identified in processes defined by Metacore.

In BAL, inflammatory processes involving interferon signalling were upregulated in monocytes from Jα18$^{-/-}$ mice (Table 6.5). Downregulated processes in monocytes from BAL showed the most significant results of this entire analysis ($p=7.8x10^{-50}$), by identifying transcripts belonging to viral translation (Table 6.6). IAV translation utilises host cell ribosomes, which was reflected in the identified transcripts as 46/91 ribosomal proteins were downregulated in monocytes from BAL in Jα18$^{-/-}$ mice.

	P value	FDR
Processes		
Inflammation- Interferon signalling	3.064E-04	4.749E-02
Inflammation- IFN-gamma signalling	1.213E-03	9.401E-02
Proliferation- Positive regulation cell proliferation	4.586E-03	1.035E-01
GO Processes		
Regulation of response to stimulus	1.088E-20	5.731E-17
Immune system process	1.758E-17	4.633E-14
Regulation of immune response	5.580E-16	9.800E-13

Table 6.5: Upregulated processes in BAL of Jα18$^{-/-}$ mice compared to wild-type. P value and FDR (false discovery rate) calculated based on number of input transcripts that were identified in processes defined by Metacore.

	P value	FDR
Processes		
Translation- Translation initiation	3.162E-33	3.541E-31
Translation- Elongation-Termination	1.259E-30	4.700E-29
Translation- Translation in mitochondria	2.487E-07	6.964E-06
GO Processes		
Viral transcription	7.856E-50	3.685E-46
Viral gene expression	4.020E-48	9.428E-45
Translational termination	1.550E-46	2.424E-43

Table 6.6: Downregulated processes in BAL of Jα18$^{-/-}$ mice compared to wild-type. P value and FDR (false discovery rate) calculated based on number of input transcripts that were identified in processes defined by Metacore.

Having identified biological processes that the differentially expressed genes in monocytes from WT and Jα18$^{-/-}$ mice were involved in for blood or BAL separately, the analysis was next directed at the set of genes identified in Venn diagrams in Figure 6.8 that were differentially expressed in monocytes from both blood and BAL. As numbers were so low (26 upregulated; 41 downregulated) it was not possible to identify biological processes or pathways that these genes were involved in using Metacore without inducing a large false discovery rate (FDR). As IFN signalling was identified as being upregulated in monocytes from both blood and BAL (Tables 6.3 and 6.5), the overlapping genes from Figure 6.8 were subjected to analysis using the Interferome

v2.01 online database (535). This identified if genes were involved in IFN signalling, and whether this was type I, II or III IFN signalling.

Of the upregulated genes in monocytes from Jα18$^{-/-}$ mice, 7/26 were associated with interferon signalling (26.9%), while 4/41 (9.8%) of the downregulated genes were associated with interferon signalling (Table 6.7).

Upregulated		Downregulated	
Gene	**Interferon type associated with**	**Gene**	**Interferon type associated with**
APOBEC1	I	FCERG1	I
ATF3	I	APOE	II
IFI202B	I, II	MAN2B1	II
IRF1	I, II	MCM6	II
PSMB6	I, II		
NOD1	II		
TGM2	II		

Table 6.7: Interferon regulated genes are upregulated in monocytes from both blood and BAL. IFN regulated genes identified by inputting common gene lists from blood or BAL into the Interferome v2.01 database.

This showed that over ¼ of genes upregulated similarly in monocytes from blood and BAL of Jα18$^{-/-}$ mice were involved in type I and II IFN signalling.

6.4.7 Functional analysis of monocyte gene expression profiles

To further characterise monocytes, analysis was carried out using GSEA, (432) as described in 6.3.2 and 2.1.21, to identify enrichment of custom-designed gene sets in monocytes from either WT or Jα18$^{-/-}$ mice. For this analysis, a ranked list of all filtered, normalised genes was first created where genes highly expressed in Jα18$^{-/-}$ monocytes (and low in WT monocytes) were at the top of the list, while genes highly expressed in WT monocytes (and low in Jα18$^{-/-}$ monocytes) were at the bottom, as per protocol. The gene sets in table 6.8 were tested for enrichment in the ranked gene lists of monocytes from blood and BAL.

Gene set name	Gene set origin	Number of genes
Influenza life cycle	Reactome (MSigDB M4669)	203
Apoptosis induction	(536) (MSigDB M16169)	88
Positive regulation of Inflammasome	Human Inflammasome PCR Array, Qiagen (PAMM-097A). Used in (537)	70
M1/M2 phenotype	GSE51466 (440)	500
M1 vs M2a, M2b, M2c	GSE32690 (538)	500
Severe IAV infection	Chapter 3 (Section 3.4.4)	305

Table 6.8: Pre-defined gene sets used in GSEA. Name, origin and number of genes contained in gene sets that were tested for enrichment in monocytes from WT or Jα18$^{-/-}$ mice.

To begin with, as the most significant pathway identified, the role of ribosomal proteins in viral translation was assessed by testing whether genes involved in the IAV life cycle were enriched in monocytes from WT or Jα18$^{-/-}$ mice. Ribosomal proteins and translation of viral genes are required for IAV replication and are essential components in the viral life cycle. A gene set comprising transcripts involved in the IAV life cycle was significantly enriched in monocytes from WT mice in the BAL ($p=\leq 0.001$), but not blood ($p=0.052$) (Figure 6.9A). This enrichment of transcripts involved in IAV replication in monocytes from WT mice compared to Jα18$^{-/-}$ supports Metacore analysis of reduced viral transcription in Jα18$^{-/-}$ monocytes.

Ly6C^{hi} monocytes from the BAL were next analysed for H1N1 hemagglutinin (HA) expression by flow cytometry in order to identify cells which have been infected and to validate GSEA and Metacore findings of increased viral replication in monocytes from WT BAL. HA was expressed on the surface of Ly6C^{hi} monocytes from BAL on day 3 of infection (Figure 6.9B). A higher percentage of monocytes from WT mice expressed HA than from Jα18$^{-/-}$ mice (49.78±2.67 vs 39.11±1.32) (Figure 6.9C). This suggested that more monocytes in WT mice were directly infected by IAV, which is likely due to the reduced number of monocytes in WT BAL compared to Jα18$^{-/-}$ following infection with the same number of virus particles. IAV however has been reported to replicate

less effectively in monocytes compared to other cells in the lung such as epithelial cells, but to cause apoptotic cell death. Therefore the enhanced replication of IAV in WT monocytes may be inducing programmed cell death.

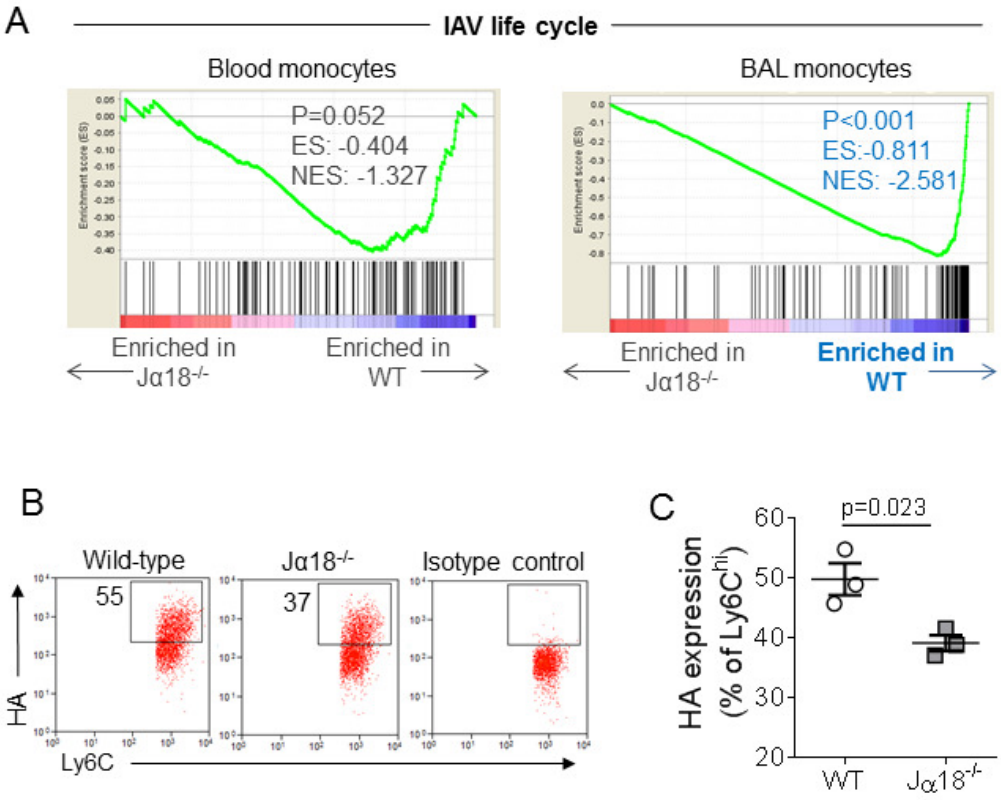

Figure 6.9: Enrichment of influenza virus life cycle in monocytes from wild-type mice. (A) GSEA plots showing highly significant enrichment of genes involved in the influenza virus life cycle in monocytes from WT mice in the BAL. Genes are ranked from high expression in Ja18$^{-/-}$ (left) to high expression in WT (right) in both graphs. Significant enrichment of analysed gene set in WT mice is displayed by blue text. Grey text= no enrichment. ES: enrichment score (scale -1 to 1), NES: nominal enrichment score (ES normalised for gene set size). P value is significance of the ES. **(B)** Flow cytometry staining of viral hemagglutinin (HA) on the surface of Ly6C^{hi} monocyte from the BAL of WT and Ja18$^{-/-}$ mice and isotype control staining. **(C)** Cumulative data from flow cytometry HA staining showing more viral HA on Ly6C^{hi} monocytes from WT mice relative to Ja18$^{-/-}$. n=3 mice per group. T-test between groups.

The involvement of programmed cell death in regulation of monocyte numbers was investigated using a concise list of genes involved in the induction of apoptosis (536) (Figure 6.10). Genes involved in the induction of apoptosis showed no significant enrichment towards either phenotype in blood monocytes (p=0.545) as transcripts in

this gene set were expressed just as densely by both Jα18$^{-/-}$ and WT monocytes. In the BAL however, there was an enrichment in monocytes from WT mice (p=0.003). This highlights that monocyte apoptosis is greater in the presence of iNKT cells, which could be due to the increase in IAV replication identified earlier, or an ability of iNKT cells to directly cause monocyte apoptosis.

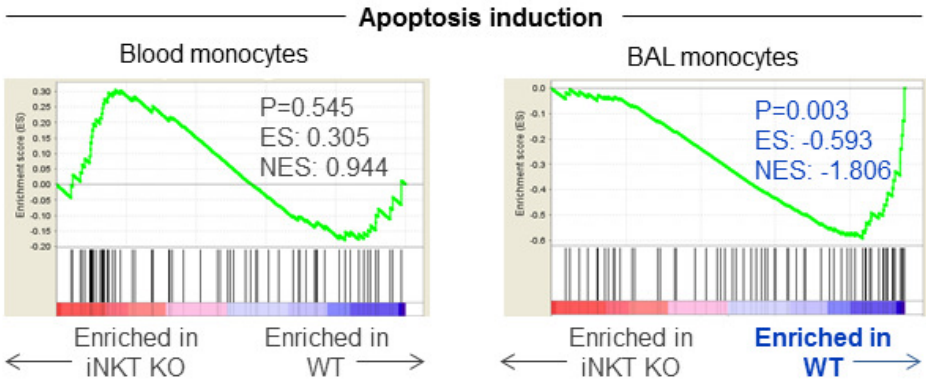

Figure 6.10: Enrichment of apoptosis induction in monocytes from wild-type mice. GSEA plots showing enrichment of genes involved in apoptosis induction in Ly6C^{hi} monocytes from the BAL of WT mice. Genes are ranked from high expression in Ja18$^{-/-}$ (left) to high expression in WT (right) in all graphs. Significant enrichment of analysed gene set in WT mice is displayed by blue text. Grey text= no enrichment. ES: enrichment score (scale -1 to 1), NES: nominal enrichment score (ES normalised for gene set size). P value is significance of the ES.

Metacore analysis identified inflammasome signalling as being upregulated in blood monocytes from Jα18$^{-/-}$ mice due to expression of NOD1, NOD2 and AIM2. These sets of signalling components from Metacore analysis can be sparse and are often not unique to the process implicated. Therefore to test whether other components of inflammasome signalling were also enriched in monocytes from Jα18$^{-/-}$ mice, and also to determine whether this pathway is unique to blood monocytes or is also enriched in monocytes from the BAL, 70 transcripts involved in inflammasome activation (537) were analysed. Inflammasome activation transcripts were found to be upregulated in both blood (p=0.019) and BAL (p=0.018) monocytes from Jα18$^{-/-}$ mice compared to WT (Figure 6.11).

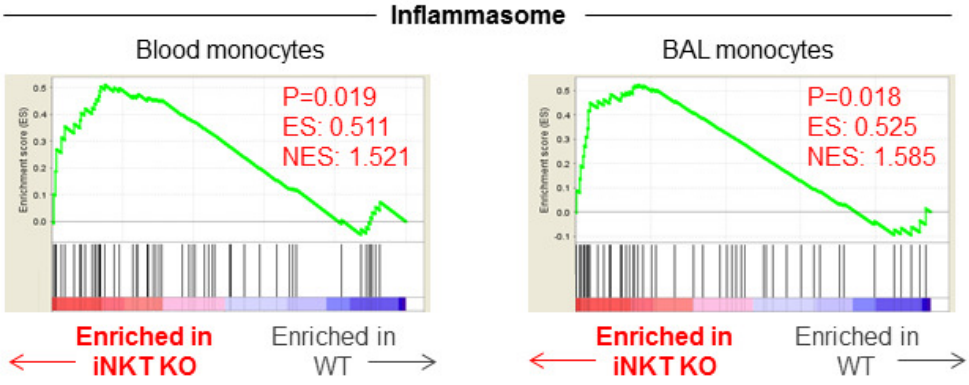

Figure 6.11: Enrichment of inflammasome activation in monocytes from iNKT deficient mice. GSEA plots showing enrichment of genes involved in positive regulation of the inflammasome in Ly6C^{hi} monocytes from the blood and BAL of Ja18$^{-/-}$ mice. Genes are ranked from high expression in Ja18$^{-/-}$ (left) to high expression in WT (right) in all graphs. Significant enrichment of analysed gene set in Jα18$^{-/-}$ mice is displayed by red text. Grey text= no enrichment. ES: enrichment score (scale -1 to 1), NES: nominal enrichment score (ES normalised for gene set size). P value is significance of the ES.

As processes involved in inflammation were highly enriched in Jα18$^{-/-}$ monocytes from both blood and BAL by MetaCore analysis, genes involved in polarisation of monocytes towards an M1 (inflammatory) or M2 (regulatory) macrophage phenotype were investigated. As a continuum exists regarding monocyte-macrophage development, the aim of this analysis was to identify whether monocytes expressed transcripts predisposing them towards M1 or M2 differentiation. Two gene sets were analysed; the first differentiated M1 and M2 macrophages (GSE51466), and the second differentiated M1 from M2a, M2b and M2c subsets (GSE32690). Gene set details can be found in Appendix 2. The M1 phenotype was highly enriched at p≤0.001 in monocytes from Jα18$^{-/-}$ mice in both blood and BAL (Figure 6.12A). The M2 phenotype was significantly enriched in monocytes from WT blood (p=0.035), but not enriched either way in BAL (p=0.414) (Figure 6.12B).

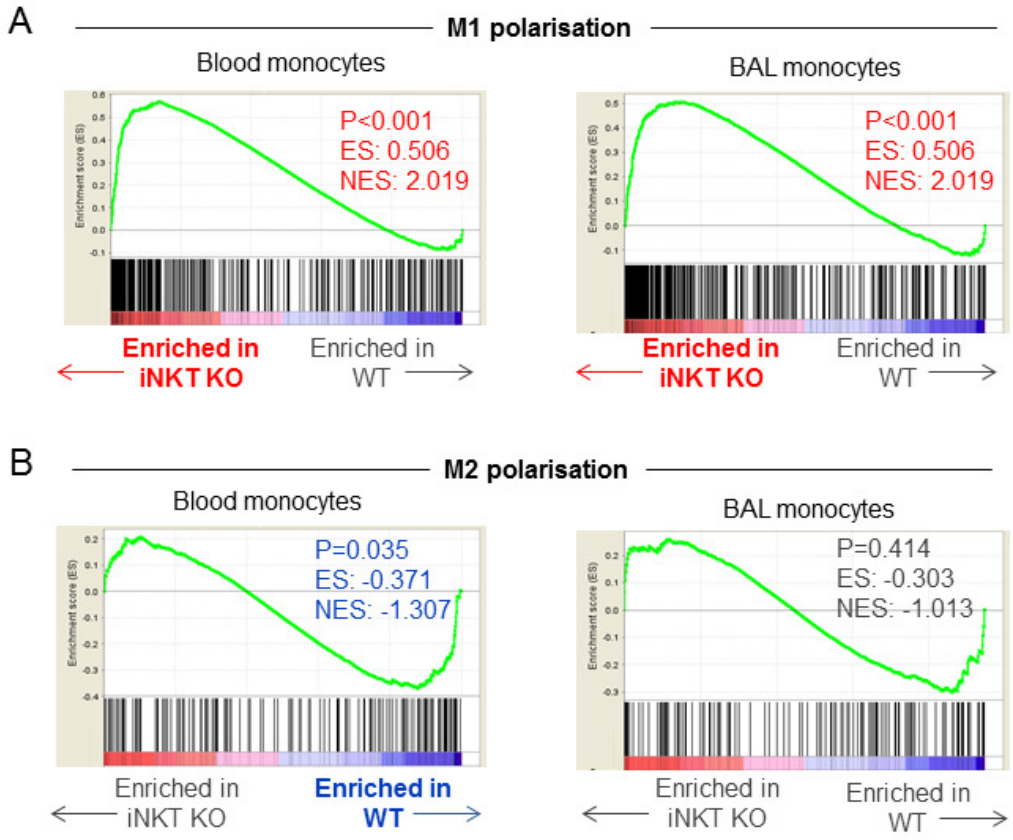

Figure 6.12: M1 polarisation in monocytes from IAV infected iNKT deficient mice. **(A)** GSEA plots showing enrichment of genes involved in M1 polarisation in Ly6C^{hi} monocytes from the blood and BAL of Ja18$^{-/-}$ mice. **(B)** GSEA plots showing enrichment of genes involved in M2 polarisation in Ly6^{hi} monocytes from the blood of WT mice. Genes are ranked from high expression in Ja18$^{-/-}$ (left) to high expression in WT (right) in all graphs. Significant enrichment of analysed gene set in Jα18$^{-/-}$ mice is displayed by red text and significant enrichment in WT mice is displayed in blue text. Grey text= no enrichment. ES: enrichment score (scale -1 to 1), NES: nominal enrichment score (ES normalised for gene set size). P value is significance of the ES.

M2 subset differentiation was further examined by determining enrichment of M2a, M2b or M2c gene sets in monocytes from blood and BAL. The M2a gene set was not enriched in monocytes from either mice in blood (p=0.323) or BAL (p=0.209) (Figure 6.13A). M2b was enriched in monocytes from WT mice in the blood (p=0.015) but not BAL (p=0.279) (Figure 6.13B), while M2c was enriched in monocytes from WT mice in the BAL (p=0.002) but not blood (p=0.332) (Figure 6.13C). Monocytes from Jα18$^{-/-}$ mice

therefore show an inflammatory M1 phenotype in blood and BAL, while monocytes from WT mice display alternatively activated macrophage profiles.

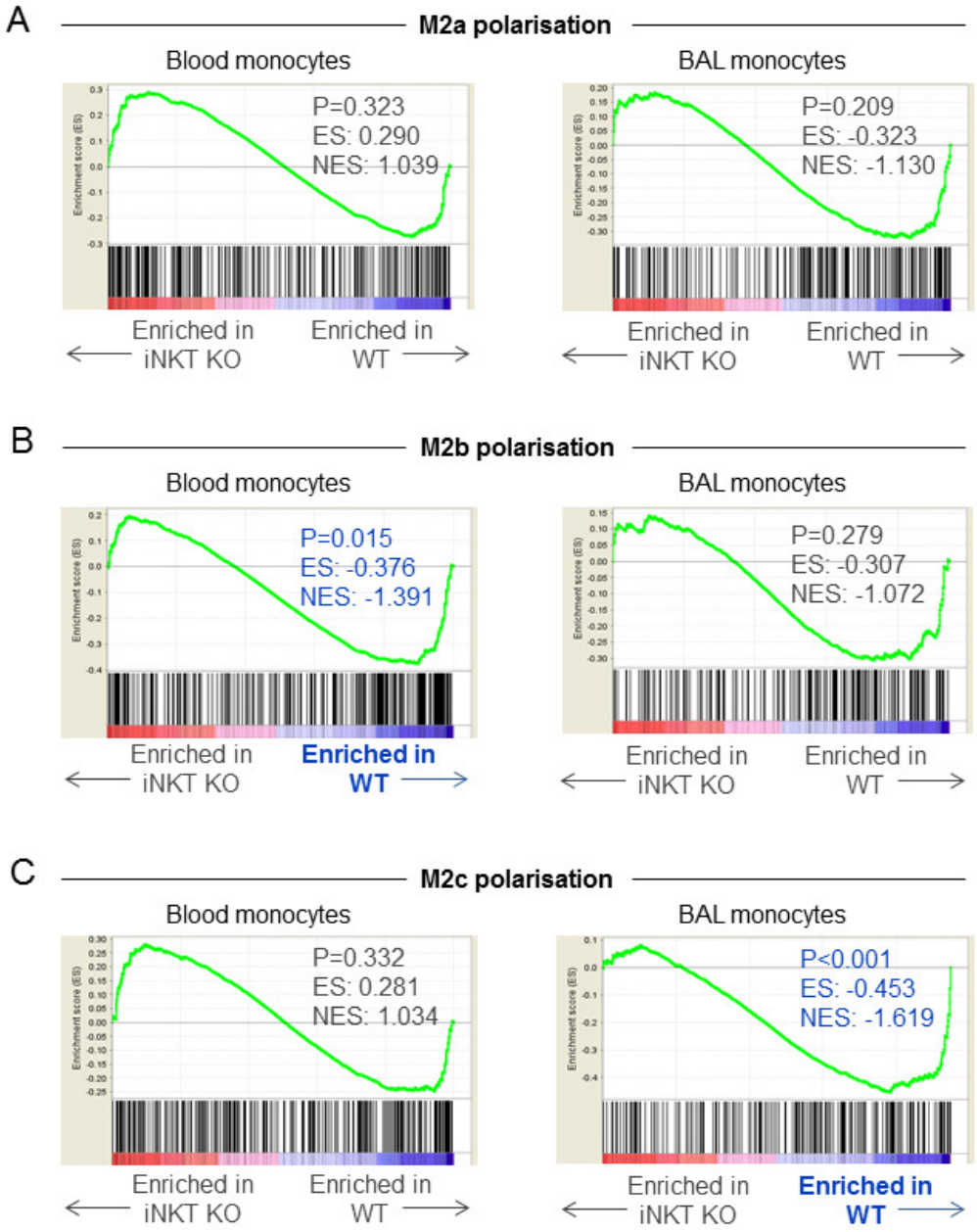

Figure 6.13: M2 polarisation in monocytes from IAV infected wild-type mice. GSEA plots of **(A)** M2a **(B)** M2b or **(C)** M2c polarisation of Ly6C^{hi} monocytes from blood and BAL. M2a was not significantly enriched in either genotype in blood or BAL (A), M2b was enriched in blood monocytes from WT mice (B) and M2c was enriched in BAL monocytes from WT mice (C). Genes are ranked from high expression in Ja18$^{-/-}$ (left) to high expression in WT (right) in all graphs. Significant enrichment of analysed gene set in WT mice is displayed by blue text. Grey text= no enrichment. ES: enrichment score (scale -1 to 1), NES: nominal enrichment score (ES normalised for gene set size). P value is significance of the ES.

Finally, monocytes were tested for enrichment of transcripts identified in chapter 3 as being unique to severe IAV infection caused by H5N1 on day 3. This gene set was highly enriched in monocytes from Jα18$^{-/-}$ mice in both blood and BAL at p≤0.001 (Figure 6.14), indicating that genes upregulated in lungs during severe IAV were also enriched in monocytes from infected Jα18$^{-/-}$ mice when compared to WT .

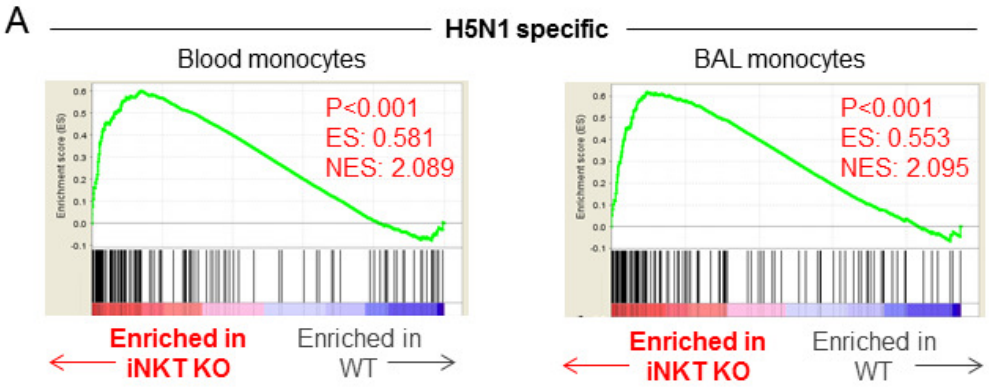

Figure 6.14: Enrichment of genes upregulated specifically to severe IAV in monocytes from iNKT deficient mice. GSEA plots showing enrichment of genes identified to be specific to severe influenza infection in Ly6C^{hi} monocytes from the blood and BAL of Ja18$^{-/-}$ mice. Genes are ranked from high expression in Ja18$^{-/-}$ (left) to high expression in WT (right) in all graphs. Significant enrichment of analysed gene set in Jα18$^{-/-}$ mice is displayed by red text. Grey text= no enrichment. ES: enrichment score (scale -1 to 1), NES: nominal enrichment score (ES normalised for gene set size). P value is significance of the ES.

6.4.8 Characterisation of monocyte apoptosis

Findings from 6.4.7 suggested that iNKT cells had multifarious effects on monocytes during early IAV infection. Of these effects, the changes to how apoptosis is regulated may be a method by which iNKT cells control the number of monocytes. To verify this, monocytes from day 3 IAV infected WT and Jα18$^{-/-}$ mice were analysed for expression of Annexin V and 7AAD by flow cytometry, gated as described in 6.3.1. Annexin V detects phosphatidylserine which becomes externalised and is displayed on the surface of cells undergoing apoptosis, while 7AAD binds to DNA from dead or late apoptosing cells. Figure 6.15A shows gating of apoptosing cells in uninfected or PR8 infected mice; Annexin V^{+}7AAD^{-} cells are in early apoptosis, Annexin V^{+}7AAD^{+} are in late apoptosis and Annexin V^{-}7AAD^{+} are dead cells. In the blood, the majority of monocytes from uninfected mice were in early apoptosis. The frequency of early apoptosing monocytes following IAV infection decreased by an average of 6.96% in WT mice and by an average of 28.8% in Jα18$^{-/-}$ mice, indicating that iNKT cells maintained apoptosis of monocytes following infection (Figure 6.15B). The percentage of monocytes in the late apoptosis phase increased upon infection, but frequencies of cells in this phase were still very low in infected WT (5.54±0.46) and Jα18$^{-/-}$ (5.40±0.46) mice (Figure 6.15C). Hardly any Ly6C^{hi} monocytes were dead in WT (0.75±0.16) or Jα18$^{-/-}$ (1.14±0.19) mice (Figure 6.15D).

In the BAL, the majority of monocytes were again in early apoptosis and did not differ between WT (87.54±1.68) and Jα18$^{-/-}$ (87.4±1.05) mice (Figure 6.15E). Frequencies of late apoptosing and dead cells were unchanged between WT (7.83±1.1 and 0.72±0.25) (Figure 6.15F) and Jα18$^{-/-}$ (7.26±0.81 and 0.99±0.42) (Figure 6.15G) mice.

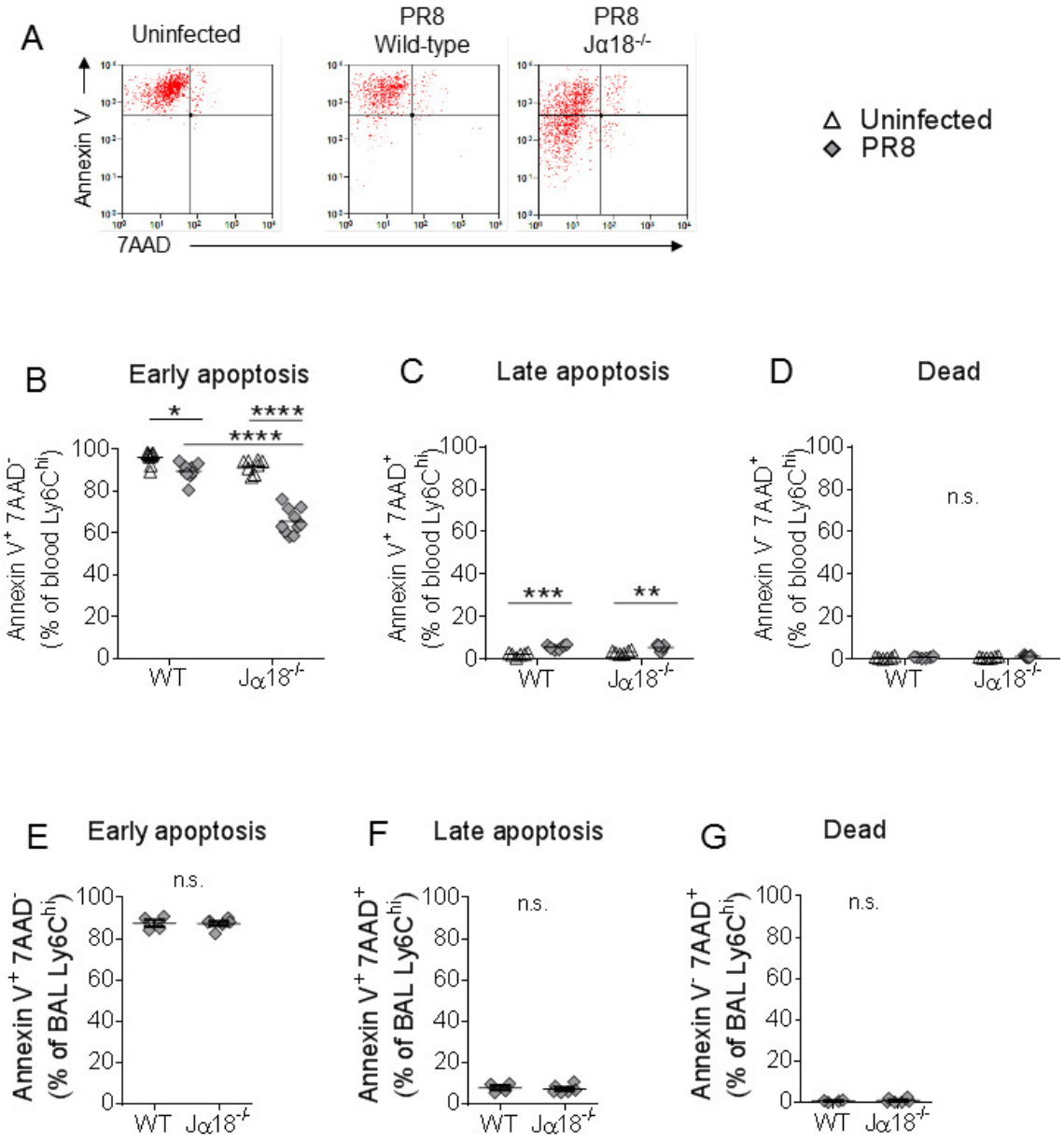

Figure 6.15: Early monocyte apoptosis is reduced in the blood of IAV-infected iNKT deficient mice. (A) Flow cytometry analysis of monocytes in early apoptosis (Annexin V^+ $7AAD^-$), in late apoptosis (Annexin V^+ $7AAD^+$) or dead (Annexin V^- $7AAD^+$) from WT or Jα18$^{-/-}$ mice either uninfected or on day 3 of PR8 infection. Percentage of blood monocytes **(B)** in early apoptosis, **(C)** in late apoptosis or **(D)** dead in WT and Jα18$^{-/-}$ mice uninfected or on day 3 of PR8 infection (n=6-10 mice per group). Percentage of BAL monocytes **(E)** in early apoptosis, **(F)** in late apoptosis or **(G)** dead in WT and Jα18$^{-/-}$ mice on day 3 of PR8 infection (n=4-5 mice per group). Two-way ANOVA in (B)-(D), t-tests in (E)-(G). *p≤0.05, **p≤0.01, ***p≤0.001, ****p≤0.0001.

6.4.9 Adoptive transfer of iNKT cells to iNKT deficient mice reduces BAL monocytes

The findings so far suggest that at the gene and cellular level, regulation of apoptosis may cause the differences in monocyte numbers in Jα18$^{-/-}$ and WT mice following IAV infection. To test whether iNKT cells were able to directly reduce monocytes *in vivo*, iNKT cells were purified from spleen of PR8-infected mice on day 3 and instilled into lungs of Jα18$^{-/-}$ mice, intra-nasally via a large volume (40µl) delivery, at the same point as infection with PR8. Ly6C^{hi} monocyte numbers in BAL on day 3 were determined for these mice, as well as WT mice and Jα18$^{-/-}$ mice which underwent the same procedure but without cells in the nasal instillate. Jα18$^{-/-}$ mice which received iNKT cells had lower numbers of Ly6C^{hi} monocytes (238,780±36,258); similar to WT mice (230,606±43,314) (Figure 6.16). Jα18$^{-/-}$ mice that did not receive iNKT cells had an increased number of inflammatory monocytes, as reported previously (458,084±60,372) (414).

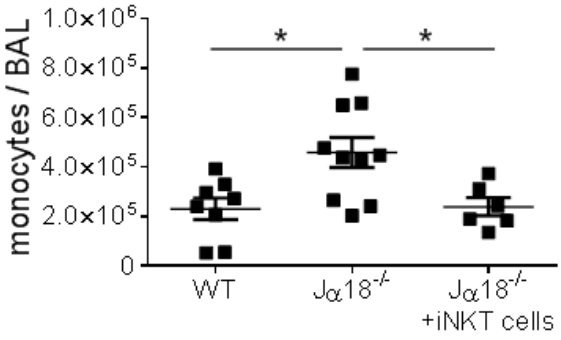

Figure 6.16: Adoptive transfer of iNKT cells to iNKT deficient mice reduces BAL monocyte numbers. Absolute number of Ly6C^{hi} monocytes per ml of BAL fluid on day 3 of PR8 infection from WT mice, Jα18$^{-/-}$ mice or Jα18$^{-/-}$ mice that received adoptively transferred iNKT cells to the lungs. One-way ANOVA *p≤0.05

6.5 Discussion

This chapter questioned how iNKT regulated monocytes during severe IAV infection. As well as an increase in monocyte number in Jα18$^{-/-}$ mice, monocytes from these mice also had a more inflammatory phenotype during IAV infection, upregulating genes for M1 macrophage polarisation and inflammasome activation. More monocytes were apoptosing on day 3 of IAV infection in WT mice compared to Jα18$^{-/-}$ mice, suggesting that iNKT cells may be involved in maintaining monocyte apoptosis, and making this a possible mechanism for regulating numbers during infection. The reduction in monocytes following iNKT cell adoptive transfer to the lungs supports the idea that iNKT cells have a direct effect on reducing monocyte numbers.

Activation of iNKT cells using αGalCer has been shown to improve outcome during IAV infection, supporting a protective role for iNKT cells in the response to IAV (413). iNKT cells were not activated with exogenous lipid antigen in the present study, therefore the results should bear greater physiological relevance to events that occur during human IAV infection. Viral genomes, unlike bacteria, do not encode lipid molecules and therefore iNKT activation either utilises endogenous lipids or is entirely cytokine driven and TCR independent. In a mouse IAV infection model, adoptive transfer of iNKT cells offered protection against severe infection when transferred to Jα18$^{-/-}$ but not CD1d$^{-/-}$ mice, implying that iNKT activation and subsequent protection is CD1d-dependent (306). Viral infection has been shown to alter or increase endogenous lipid presentation by CD1d, which along with TLR-induced production of cytokines such as IL-12 and IL-18 can activate iNKT cells (539, 540).

Gene expression profiling revealed a 15-fold higher detection of differentially expressed genes in BAL than blood when comparing monocytes from WT and Jα18$^{-/-}$ mice, suggesting that iNKT cells may be exerting their influence on monocytes in the lungs. It

has been postulated that iNKT cells are long term residents of the lung microvasculature network (533). A 10-20x enrichment in iNKT cells was observed in blood collected from right and left ventricles of the heart which connect to the pulmonary artery and vein, suggesting that accumulation in the lung microvascular compartment may occur (541). Interaction between iNKT cells and monocytes in lungs is further supported by the flow cytometry findings where the number and phenotypic characteristics of monocytes did not differ between WT and Jα18$^{-/-}$ mice in blood, but monocyte numbers were higher in BAL. The increase in IL-6 in BAL of Jα18$^{-/-}$ mice further supports the theory that iNKT cells exert their regulatory functions in the BAL, although both monocytes and airway epithelial cells have been shown to produce high levels of IL-6 upon IAV infection (542, 543). These differences may also reflect the fact that the lungs are the main site of IAV infection and the destination of recruited monocytes, while the blood simply offers a route for trafficking. However, it was noted that IFN signalling genes were common between monocytes derived from blood and lungs. It is possible that the effect of iNKT deficiency on IFN signalling occurs early and therefore was observed in circulating monocytes. Gene expression changes unique to monocytes derived from the lungs may therefore be downstream to IFN signalling.

The upregulation of IFN signalling in blood and BAL monocytes from Jα18$^{-/-}$ mice that had a worse outcome to IAV infection supports findings from Chapter 3 where IFN-regulated genes were higher in severe infection. Type I IFNs have long been recognised as key antiviral cytokines that function in virus clearance. A recent study however showed that mice with higher levels of IFNαβ had increased morbidity, mortality and lung damage, and that IFNα/β receptor deficiency decreased these factors (158). Worse outcome was due to uncontrolled inflammation due to massive inflammatory cell recruitment mediated by excessive IFN signalling, exacerbating lung damage. A separate study found that low dose IFN treatment protected from lethal IAV challenge, whereas high-dose IFN treatment did not (544). Upregulation of IFN

signalling in circulating monocytes from Jα18$^{-/-}$ mice following IAV infection suggests that IFN-regulated genes may be some of the first changes induced by IAV infection, which are sustained in monocytes from BAL. The consequence of high IFN signalling in severe IAV infection likely induces inflammation and inflammatory cell recruitment, which in a milder infection help to clear the virus, however in severe infection contribute to lung pathology (545). IFN signalling has furthermore been shown to be able to induce macrophage polarisation, as high IRF5 expression promoted M1 polarisation, partly via directly activating transcription of genes encoding IL-12p40 and repressing IL-10 (546).

While Jα18$^{-/-}$ mice showed clear M1 inflammatory gene expression in both blood and BAL, monocytes from WT mice also showed enrichment for regulatory M2 genes. Monocytes from WT mouse blood showed enrichment for the M2b subset, which is not surprising as this is the most closely related M2 subset to inflammatory macrophages as they produce both pro- and anti-inflammatory cytokines (255). Polarisation towards a less inflammatory subset may however be an important factor in the reduced immune pathology observed in WT mice. A very recent study found that alveolar macrophages from naïve mice infected with IAV *in vitro* were polarised towards an M1 phenotype 4 hours after infection and an M2b phenotype 8 hours after infection (547). In BAL, monocytes from WT mice were highly enriched in M2c genes. This has been shown to be the most effective of the M2 subsets in protecting against tissue injury in chronic kidney disease, as a result of their ability to increase Foxp3^{+} T cell frequency in renal draining lymph nodes, thus reducing fibrosis following adoptive transfer and compared to M2a and unpolarised (M0) macrophages (266). Therefore it is possible that the reduced pulmonary injury in WT mice is due to polarisation of monocytes towards M2c macrophages with reparative functions. Mechanisms of macrophage polarisation by iNKT cells are not known, however in *Schistosoma manosi* granuloma, CD4^{+} T cells caused accumulation of M2 macrophages (548). Therefore it is possible that iNKT cells

in this study cause accumulation of M2 macrophages in WT mice in the lungs, which were not enriched in Jα18$^{-/-}$ mice. The findings of M2 polarisation in WT mice, whose outcome is better following IAV infection than Jα18$^{-/-}$ mice, are supported by a study showing that iNKT cells were involved in polarisation towards a regulatory M2 phenotype during IAV infection, and supports a protective role of iNKT cells in the outcome to IAV infection (466).

Frequency of early apoptosing monocytes in blood and BAL from uninfected mice was very high as measured by Annexin V expression. This was not unexpected as circulating monocytes have a short half-life of 20 hours after which they undergo spontaneous apoptosis (206). The reduced Annexin V staining following PR8 infection suggests higher resistance to apoptosis, possibly to allow time for monocytes to home to infected lungs, as has been proposed in other models (235). Reduction in the number of apoptosing monocytes in the blood of Jα18$^{-/-}$ compared to WT mice following IAV infection has however not previously been identified, and offers an explanation for the increased number of monocytes during PR8 infection in the absence of iNKT cells. The ability of adoptively transferred iNKT cells from IAV infected mice to reduce lung monocyte numbers in Jα18$^{-/-}$ mice suggests that activated iNKT cells may be inducing or maintaining apoptosis in monocytes. The mechanisms by which iNKT cells cause apoptosis in monocytes are unknown, although activated iNKT cells have been shown to induce B cell apoptosis via FasL (549) and myeloid leukaemia cell apoptosis via TRAIL (550).

Genes involved in virus transcription and translation were highly enriched in WT BAL monocytes. Further analysis of the genes involved in this enrichment identified ribosomal proteins; constituents of the ribosome. Ribosomal proteins are typically very abundant and expressed constitutively in all cell types, as all living cells utilise

ribosomes to synthesise proteins. IAV hijacks host cell ribosomes for replication, as the virus does not encode its own translation machinery, and has been proposed to alter and enhance ribosome biogenesis, thereby achieving high levels of replication (551, 552). Analysis of complexes used for replication of a number of viruses including IAV, HIV, HCV and Dengue identified ribosomes as being the most significant complexes specific to IAV replication, highlighting their importance for IAV replication (553). Therefore differential expression of ribosomal proteins identified in monocytes may signify altered levels of virus replication. If this is the case, it is likely that the enhanced virus replication observed in monocytes from WT mice is due to the fact that fewer monocytes are present in the BAL when compared to Jα18$^{-/-}$ following infection with a standardised dose of virus, and therefore there are more infectious virus particles on a per cell basis, which could lead to an increased amount of infection. Previous studies have been conflicting in their findings of whether IAV replicates effectively in myeloid cells. Since the 1970's, different groups have found that IAV undergoes abortive infection in monocytes and macrophages and that these cells do not support the effective replication of the virus (554-556). The differential expression of ribosomal proteins in this study however suggests differences in IAV translation, proposing that IAV is able to replicate in monocytes, agreeing with others who found that IAV can replicate in myeloid cells, although most of these studies involve highly pathogenic viruses such as H5N1 or the 1918 H1N1 virus (542, 557, 558). The expression of hemagglutinin on the surface of monocytes in this study further suggests effective infection and viral progeny release from monocytes.

Inflammasome signalling was enriched in monocytes from Jα18$^{-/-}$ in both blood and BAL compartments. IAV has been shown to stimulate the NLRP3 inflammasome via its intracellular M2 ion channel in primed macrophages and dendritic cells (559). Activation of the inflammasome was shown in three separate studies to be required for late stage virus clearance by the adaptive immune system, while early viral clearance

up to 7 days after infection is not altered in inflammasome deficient mice (170, 171, 560). Activation of inflammasome signalling during IAV infection is important for production of chemokines such as MIP-1α and CXCL1 mediating recruitment of monocytes and neutrophils to the lungs, which has been shown to be beneficial in some studies (170). However, when excessive monocyte recruitment to the lungs is associated with higher pathology as in the present study, enrichment of inflammasome signalling in Jα18$^{-/-}$ mice provides a means for further monocyte recruitment to lungs, which in this model of severe infection leads to a worse outcome.

6.6 Conclusions

The high number of inflammatory monocytes in the lungs during severe IAV infection is amplified by the lack of iNKT cells and can be reversed by adoptive transfer of iNKT cells to lungs. These *in vivo* studies suggest that iNKT cells are required to maintain monocyte apoptosis, which may be a mechanism whereby monocyte numbers are regulated during inflammation. Monocytes in IAV infected Jα18$^{-/-}$ mice showed enrichment for genes involved in activation of inflammasome and interferon signalling, and downregulated genes associated with M2 regulatory macrophage polarisation and apoptosis. The impact of iNKT cells on monocytes at the gene level was largely observed for monocytes derived from the lungs, suggesting that iNKT cells interact with monocytes in the lungs.

Chapter 7: iNKT cells and apoptosis of human monocytes

7.1 Introduction

Work from the previous chapter showed that iNKT cells had multifarious effects on the function, differentiation and number of monocytes during influenza A virus (IAV) infection in mice. I was especially interested in the change in apoptosis-inducing genes and reduced frequency of apoptosing monocytes derived from the lungs of iNKT deficient ($J\alpha18^{-/-}$) mice during IAV infection, since this may be a mechanism whereby iNKT cells regulate the number of monocytes. iNKT cells have potent effector and regulatory capabilities and have been shown to induce apoptosis of B cells and myeloid leukaemia cells (549, 550), but their effect on monocyte apoptosis is unknown. This chapter examines this possibility in human cells, *in vitro*.

Apoptosis occurs either via an extrinsic, intrinsic or a perforin/granzyme pathway. Activation of distinct caspases are characteristic for each pathway, but all ultimately lead to activation of executioner caspases, most notably caspase 3, which induces apoptosis. Apoptosis via the extrinsic pathway occurs via receptor-ligand interactions, most notably involving members of the TNF superfamily including TRAIL and FasL. Both of these ligands are expressed by iNKT cells and have been shown to be involved in iNKT cell-mediated killing of $CD1d^+$ tumor cells (374). Induction of perforin-mediated apoptosis by iNKT has also been widely shown, for example perforin-deficient iNKT cells, unlike normal iNKT cells, were unable to cause apoptosis of CD1d-expressing EL4 (T lymphoma) tumor cells in mice (561).

iNKT cells have the ability to regulate other immune cells despite existing at low frequencies of 0.01 to 1% peripheral blood mononuclear cells. This is partly due to their

rapid ability to produce cytokines and cytolytic molecules. iNKT activation occurs via CD1d presented lipids, innate cytokines such as IL-12 and IL-18, or both, offered by antigen presenting cells (APC). The consequences of interaction between iNKT cells and different APCs appear cell-type specific, yet have mostly been studied in dendritic cells (DCs). Different group have shown that following iNKT cell activation, monocytes mature into non-inflammatory DCs that are unable to stimulate T cell proliferation or IFNγ production (562), while immature DCs co-cultured with iNKT cells become highly stimulatory, characterised by sustained IL-12 production, expression of activating ligands CD40 and CD86 and gain the ability to induce T cell IFN production and cytotoxicity (563). Thus, I am interested in examining iNKT cell interaction with $CD14^+$ monocytes in humans, specifically how iNKT cells affect apoptosis of monocytes.

7.2 Aims

The aim of this chapter was to examine the effect of iNKT cell-monocyte interactions in human cells, with specific emphasis on the influence of iNKT cells on monocyte apoptosis.

7.3 Methods

A previously characterised iNKT clone, LH22, was used to represent iNKT cells. LH22 is a human $CD4^+$ iNKT clone with preferential cytokine production (426) (Methods 2.1.8). iNKT clones were co-cultured with $2x10^5$ primary human monocytes isolated from different donors using $CD14^+$ MACS bead positive selection, in 96 well plates in 200µl H10 media (Methods 2.1.9). Unless stated otherwise, a ratio of 1:4 iNKT:monocytes was used. This co-culture set up provided a clean system containing

only iNKT cells and monocytes, and therefore any effects could be confidently related to either of these cells. The well-established exogenous glycolipid antigen, α-galactosylceramide (αGC) was added at 0.4μg/ml as an activation stimulus in the absence of IAV infection to induce CD1d-TCR interactions and to allow further examination of costimulatory molecule interactions. IAV infection of monocytes directly induced rapid cell death, thereby making the study of apoptosis not possible.

The effect of co-culturing monocytes with iNKT cells was first examined by identifying cytokine production by both cell types, and iNKT cell degranulation using CD107a mAb (Methods 2.1.6) at the end point of activation; either 6 or 24 hours.

Apoptosis was measured using Annexin V and 7AAD to identify cells in early apoptosis (Annexin V^+7AAD^-), late apoptosis (Annexin V^+7AAD^+) or dead cells (Annexin V^-7AAD^+) following addition of αGC or a combination of IL-12 (50ng/ml) and IL-18 (100ng/ml) by flow cytometry. As co-cultures consisted of only monocytes and iNKT cells, monocytes were gated as $CD3^-Vα24Jα18^-$ cells, as they begin to downregulate CD14 upon activation, making it a less reliable marker. This, and the gating strategy used are shown in Figure 7.1.

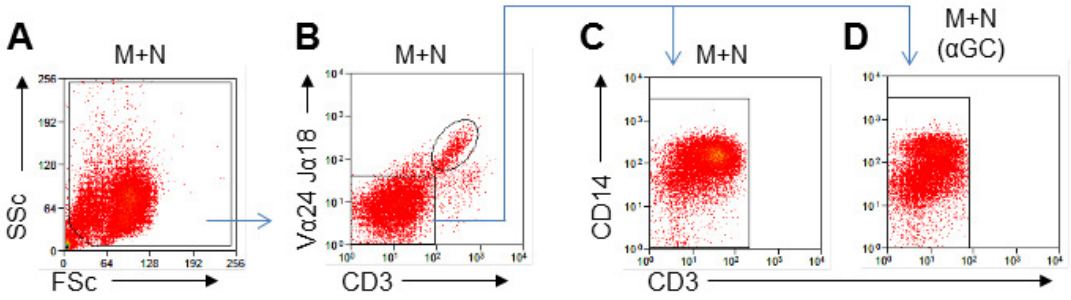

Figure 7.1: Gating strategy for monocyte identification in co-cultures. (A) Autofluorescent cells only were gated out of FSc/SSc profiles. **(B)** All other cells were analysed for CD3 and Vα24Jα18 expression which identified iNKT cells. **(C)** $CD3^-$ $Vα24Jα18^-$ cells were confirmed as monocytes by gating against CD14, which is detectable in M+N co-cultures without activation. **(D)** CD14 becomes downregulated upon αGC activation. M=monocytes, N= iNKT clone.

Finally the involvement of co-stimulatory molecules on monocyte apoptosis was investigated by analysing the expression of molecules identified to be involved in apoptosis and/or survival by flow cytometry (Methods 2.1.6), and the influence on apoptosis was determined as described above and following the addition of blocking antibodies. For experiments involving blocking antibodies, monocytes were pre-treated with optimised doses of blocking antibodies for 30 minutes prior to addition of iNKT cells and αGC. (Methods 2.1.9) Recombinant cytokines were added directly to monocytes alone or to monocytes and iNKT cells.

7.4 Results

7.4.1 iNKT-monocyte co-culture results in bi-directional activation

Following αGC activation in the iNKT-monocyte co-culture system, TNFα, IFNγ and IL-4 were produced by iNKT cells, with levels highest at 6 hours (Figure 7.2A). By 24 hours, the percentage of iNKT cells producing cytokines had declined from [%±SEM] 54.2%±7.0 to 9.2%±1.3 for TNFα, 20.9%±3.4 to 16%±2.5 for IFNγ and 29.1%±3.1 to 17%±2.7 for IL-4. CD107a expression on iNKT cells was measured as a marker of degranulation and was also highly induced upon activation after 24 hours (66.23%±1.07) (Figure 7.2B). Levels of perforin in co-culture supernatants were measured after 24 hours, revealing high perforin production following αGC activation (1,369pg/ml ±270.8) (Figure 7.2C).

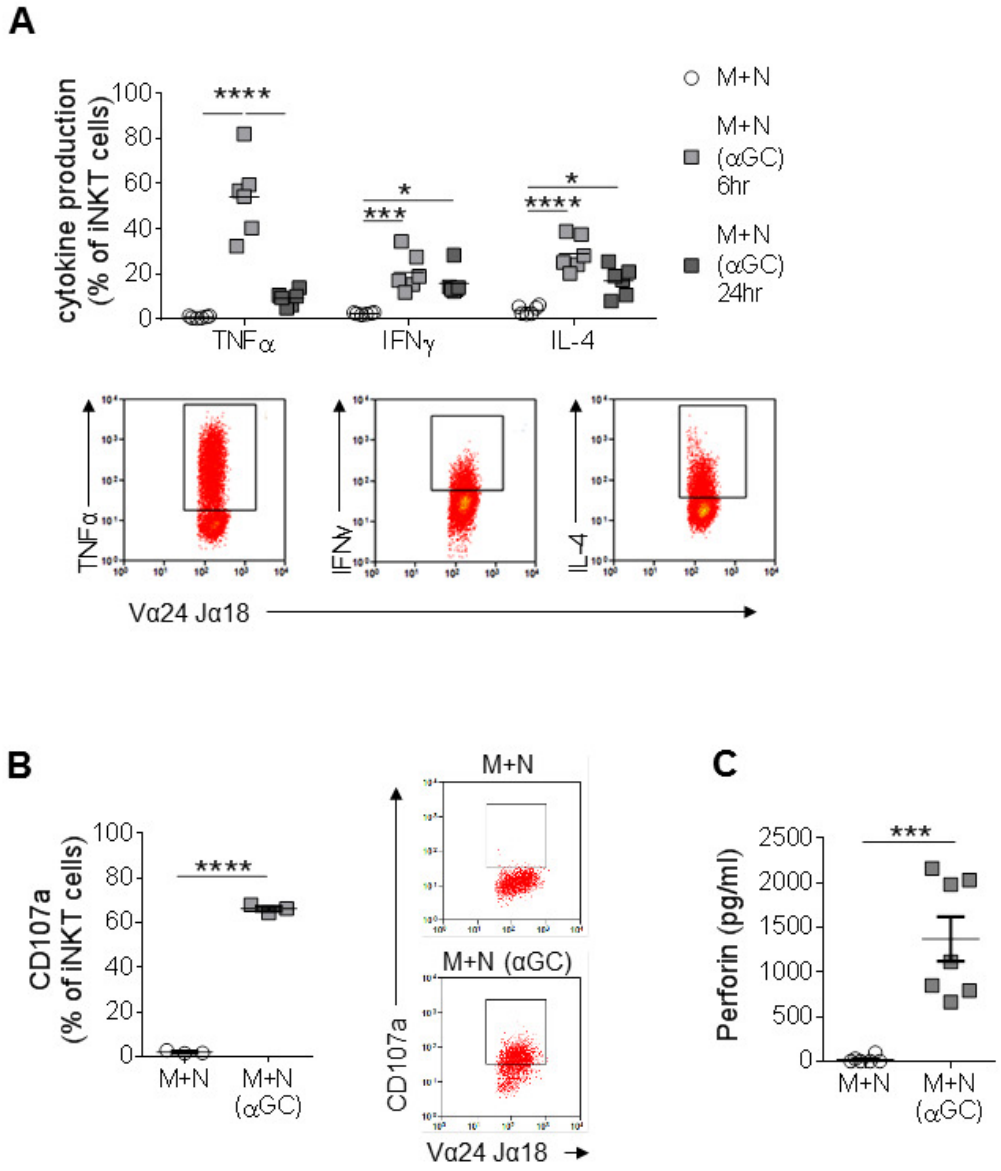

Figure 7.2: Cytokine production and cytotoxicity of αGC activated iNKT clones. **(A)** TNFα, IFNγ or IL-4 production by iNKT cells determined by flow cytometry after 6 or 24 hours of co-culture with monocytes and αGC (Brefeldin A added for the last 4 hours of stimulation.) Representative flow cytometry plots of cytokine staining are shown below the graph. Monocytes from n=6 donors. One-way ANOVA for each cytokine **(B)** CD107a expression by iNKT cells following 6 hour co-culture with monocytes ± αGC. Representative FACS plots of CD107a expression on Vα24Jα18^{+} iNKT cells are shown. **(C)** Perforin production measured by ELISA in supernatant following 24 hours of co-culture. Paired t-tests in (B)-(C). M= monocyte, N= iNKT clone. *p≤0.05, ***p≤0.001, ****p≤0.0001.

Examining monocyte function in this co-culture showed that activation of iNKT cells induced both TNFα (8.9%±0.7) and IL-12 (5.9%±1.4) production by monocytes after 24 hours (Figure 7.3A-B). This suggested that either cytokines produced by iNKT cells were acting on monocytes, or reverse signals were being transmitted to monocytes upon CD1d-TCR ligation to cause their activation. TNFα and IL-12 levels in co-cultures were also measured by ELISA. High levels of TNFα (520.2pg/ml ±50.1) were seen in supernatants from co-cultures following iNKT cell activation by αGC, likely due to production by both monocytes and iNKT cells (Figure 7.3C). Significant levels of IL-12 (16.9pg/ml ±4.0) were also produced in αGC-activated co-cultures (Figure 7.3D). αGC treatment of monocytes alone led to no detectable cytokine production in co-culture supernatants, confirming that αGC alone is not activating monocytes (Figure 7.3C-D). These results show that iNKT-monocyte co-culture results in activation of both cell types following αGC treatment.

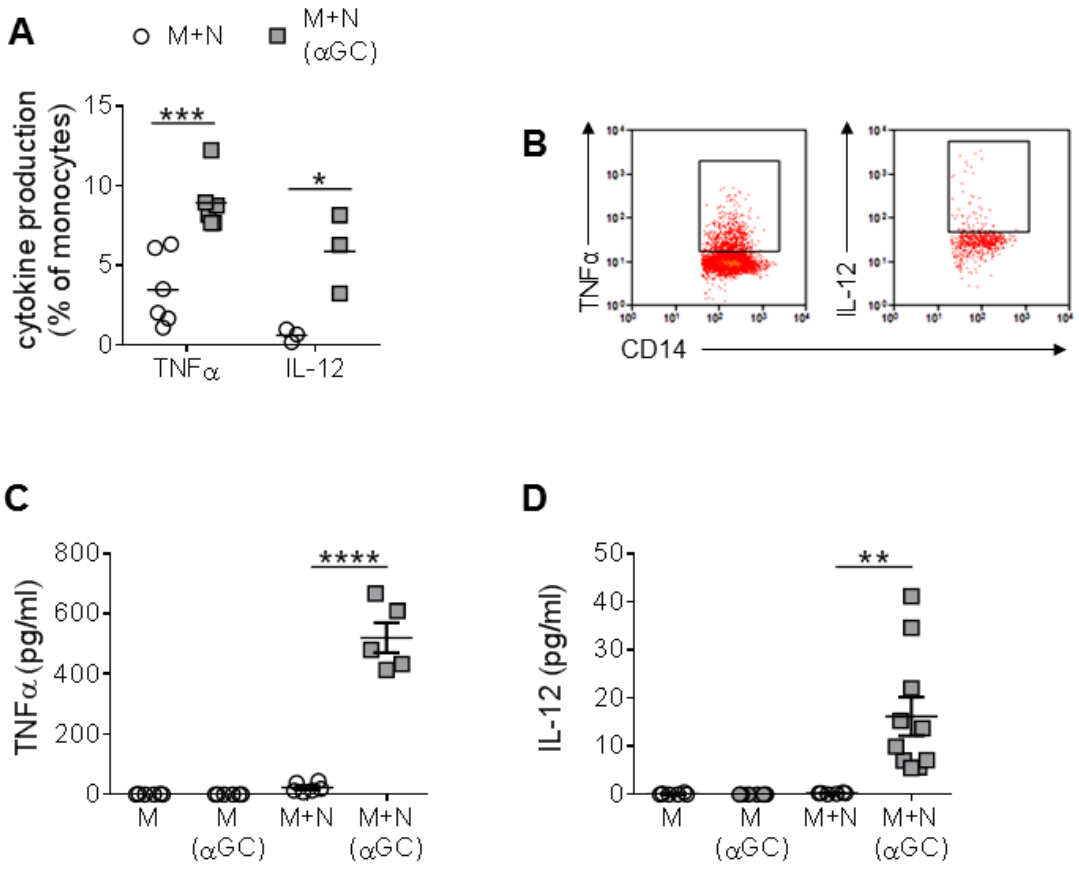

Figure 7.3: Cytokine production by monocytes in αGC activated co-cultures. (A) TNFα or IL-12 production by $CD14^+$ monocytes in co-cultures with or without αGC. Monocytes from n=6 donors. Paired t-test for each cytokine **(B)** Representative FACS plots of monocyte TNFα and IL-12 production following αGC activation. **(C)** ELISA of TNFα in co-culture supernatants. Monocytes from n=5 donors. **(D)** ELISA of IL-12 in co-culture supernatants. Monocytes from n=6-10 donors. One-way ANOVA in (C)-(D). *p≤0.05, **p≤0.01, ***p≤0.001, ****p≤0.0001. M= monocytes, N= iNKT clones.

7.4.2 Activated iNKT cells induce monocyte apoptosis

The consequence of iNKT cell activation on monocyte apoptosis was next determined using Annexin V and 7AAD. Activation of iNKT cells induced rapid monocyte apoptosis after 6 hours of co-culture (apoptosis gating described in 7.3) (Figure 7.4A). This was due to an increase in the percentage of early apoptosing monocytes from 11.25%±1.6 to 53.82%±2.9. Percentage of early apoptosing monocytes were maintained at 24

hours (55.5%±2.5) suggesting that the induction of apoptosis is quick and sustained. The frequency of late apoptosing and dead monocytes were also determined at 24 hours. A significant increase was found in monocytes undergoing late apoptosis following αGC activation (3.7%±0.47 to 8.78%±0.41) although this was 6-fold lower than the frequency of early apoptosing monocytes (Figure 7.4B). There was no difference in dead monocytes in iNKT-monocyte co-cultures following αGC activation (Figure 7.4C). As the greatest change in apoptosis was the increase 'early apoptosing' monocytes, this subset is further investigated later.

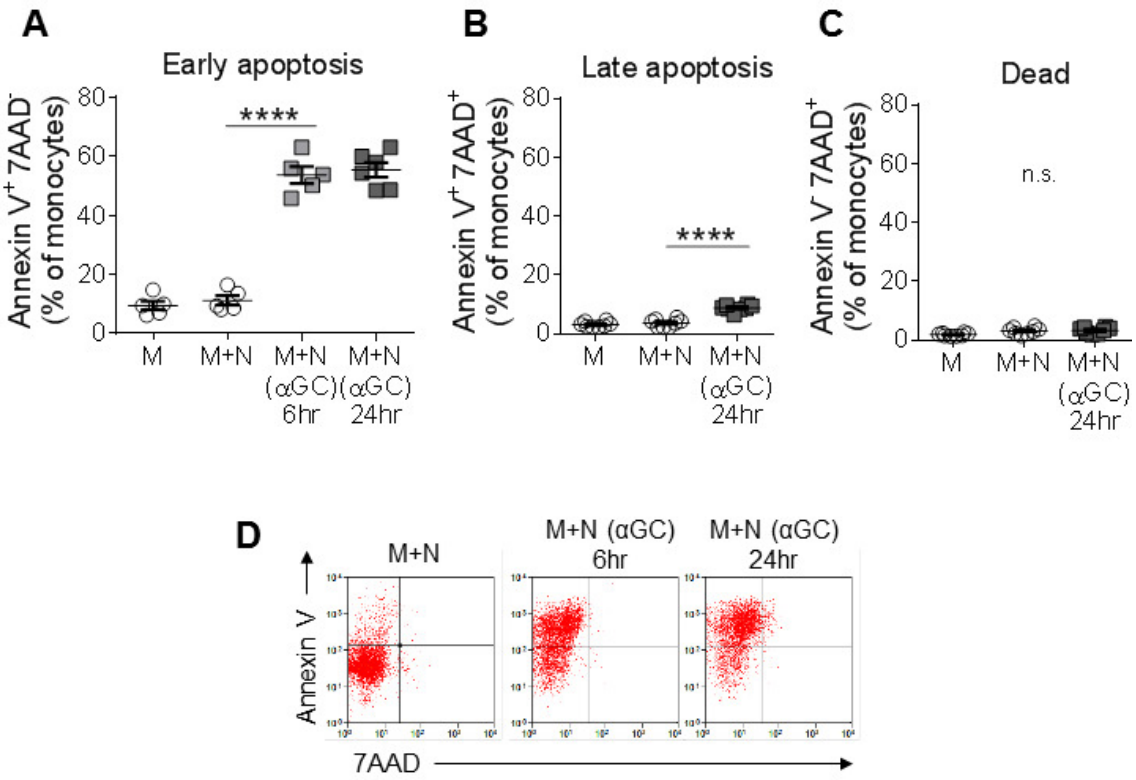

Figure 7.4: Monocyte apoptosis is induced following iNKT cell activation. (A) Percentage of Annexin V^+7AAD^- monocytes gated on $CD3^-Vα24Jα18^-$ cells in monocytes alone, monocytes and iNKT cells for 6 hours or monocytes, iNKT cells and αGC for 6 or 24 hours. Monocytes from n=5-6 donors. **(B)** Percentage of Annexin V^+7AAD^+ monocytes gated as in (A). **(C)** Percentage of Annexin V^-7AAD^+ monocytes gated as in (A). **(D)** Flow cytometry analysis of monocyte apoptosis from co-cultures, gated on $CD3^-Vα24Jα18^-$ cells. One-way ANOVA between groups. ****p≤0.0001. M= monocytes, N= iNKT clones.

The ability of activated CD8$^+$ T cells or NK cells to cause monocyte apoptosis was next investigated and compared to iNKT cells activated with αGC, in order to determine whether induction of monocyte apoptosis was unique to activated iNKT cells. Activation of CD8$^+$ T cell clones (details in Methods 2.1.9) with a specific peptide, or primary NK cells isolated using MACS beads from different donors activated with an α-NKp46 antibody did not induce monocyte apoptosis (Figure 7.5A). Activation of iNKT cells, CD8$^+$ T cells and NK cells was confirmed by TNFα production from effector cells (Figure 7.5B-C).

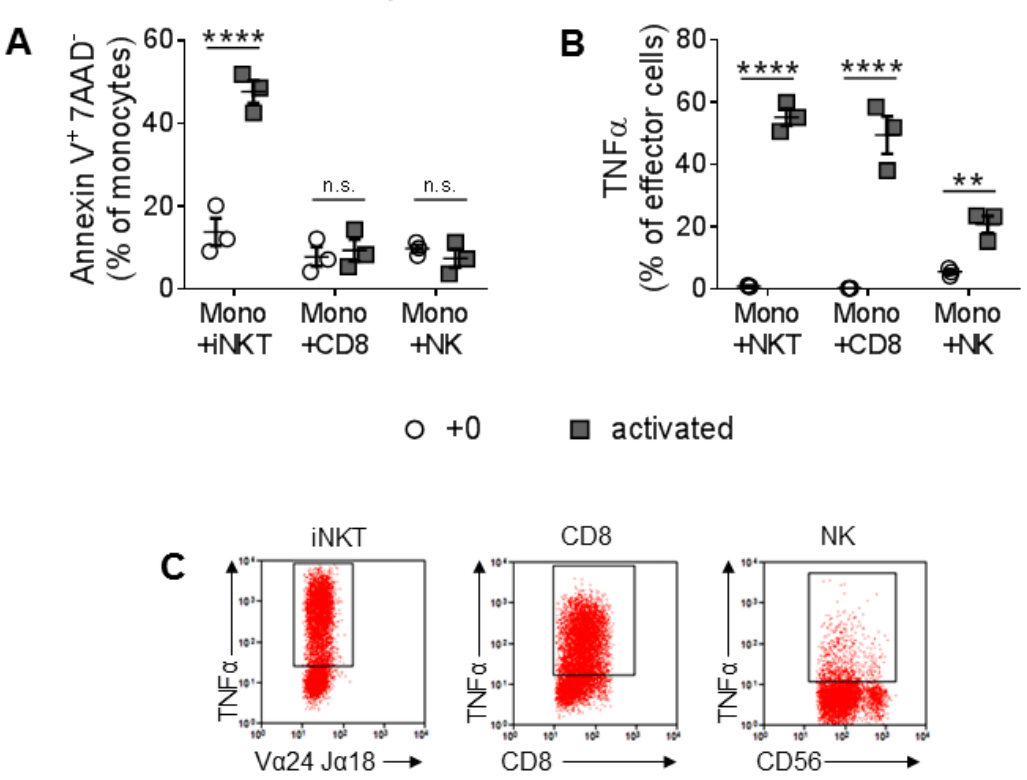

Figure 7.5: Monocyte apoptosis is not induced by activated CD8$^+$ or NK cells. (A) Percentage of early apoptosing monocytes following co-culture with iNKT cells and αGC, CD8$^+$ T cell clones and specific activating peptide, or allogeneic primary isolated NK cells and activating α-NKp46 mAb. **(B)** Percentage of TNFα producing iNKT clones, CD8$^+$ clones or NK cells following activation as in (A). **(C)** Representative FACS plots depicting TNFα staining from activated iNKT clones, CD8$^+$ T cell clones or NK cells. Paired t-tests in (A)-(B). **p≤0.01, ****p≤0.0001. Mono= monocytes.

As it is unlikely that a super-glycolipid antigen like αGC is the natural activator of iNKT cells, the role of a more plausible iNKT cell activation pathway in induction of monocyte apoptosis was investigated. As IL-12 and IL-18 have been shown to activate iNKT cells in the absence of endogenous lipids (363), the role of these cytokines in activating iNKT cells to cause monocyte apoptosis was next investigated. Firstly, the ability of IL-12/IL-18 to activate iNKT cells was examined by measuring IFNγ in co-culture supernatants, compared to activation with αGC. IFNγ was chosen as monocytes do not produce IFNγ, unlike iNKT cells which produce high levels of IFNγ upon activation. IL-12/IL-18-activation (50/100ng/ml) induced substantial IFNγ production (840.9±11.78 pg/ml), confirming the ability of these cytokines to activate iNKT cells, possibly through amplification of CD1d-TCR signalling as suggested by Brenner et al. (363). IFNγ production following IL-12/IL-18 activation was less than was observed with αGC (2,200±57.74 pg/ml) (Figure 7.6A), and blocking CD1d in αGC-activated co-cultures reduced but did not abolish IFNγ production, regardless of dose of blocking antibody (973.3±107.5pg/ml at 10μg/ml α-CD1d; 523.6±85.14pg/ml at 25μg/ml α-CD1d).

The ability of IL-12/IL-18-activated iNKT cells to cause monocyte apoptosis was next investigated. No induction of apoptosis was observed using this method of iNKT cell activation (Figure 7.6B).

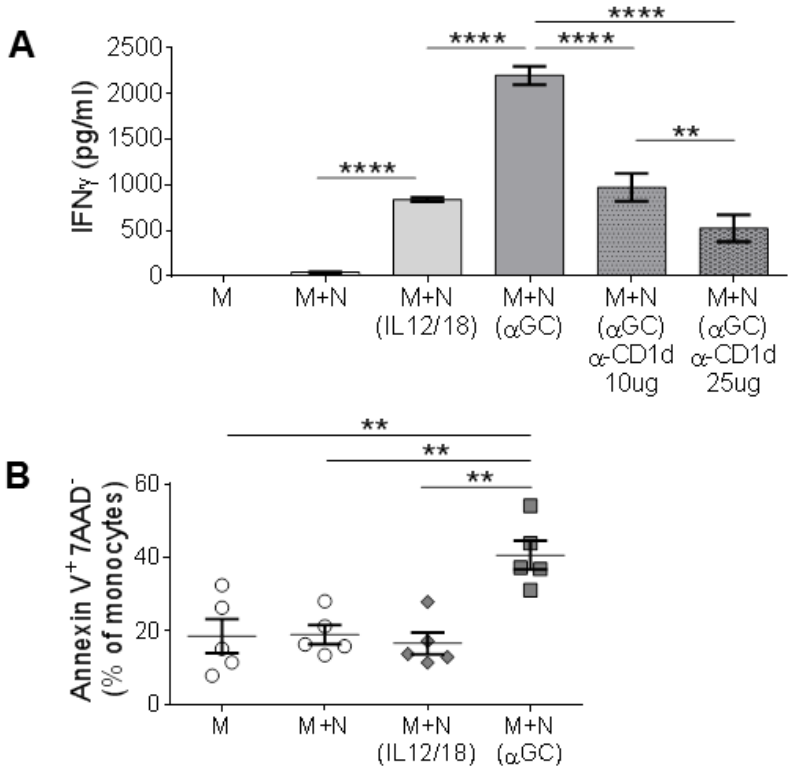

Figure 7.6: IL-12 and IL-18 activate iNKT cells to secrete IFNγ but not to cause monocyte apoptosis. (A) IFNγ in supernatants from monocytes cultured alone for 24 hours, or co-culture of monocytes with iNKT clones and either 50ng/ml IL-12 and 100ng/ml IL-18, αGC, or αGC and CD1d blockade. **(B)** Percentage of early apoptosing monocytes from co-cultures activated with αGC or IL-12/IL-18. Monocytes from n=5 donors. One-way ANOVA in (A)-(B). **p≤0.01, ****p≤0.0001. M= monocytes, N= iNKT clones.

To determine whether the induction of monocyte apoptosis was wholly dependent on CD1d, CD1d blocking antibody was added to co-cultures. Blocking CD1d reduced but did not abolish early monocyte apoptosis from 27.85%±2.47 to 17.6%±2.99 (Figure 7.7).

The effect of CD1d blocking on perforin levels in supernatant were next investigated to determine the extent to which perforin may be involved in monocyte apoptosis induction. Levels of perforin in supernatants of iNKT-monocyte co-cultures were low in non-activated co-cultures (41.55pg/ml±28.69), increased upon αGC activation (767pg/ml±55.3), and reduced back to baseline levels following CD1d blockade (21.02pg/ml±21.02). Therefore CD1d blockade inhibits perforin production, but does not completely abrogate monocyte apoptosis, suggesting involvement of other apoptotic factors.

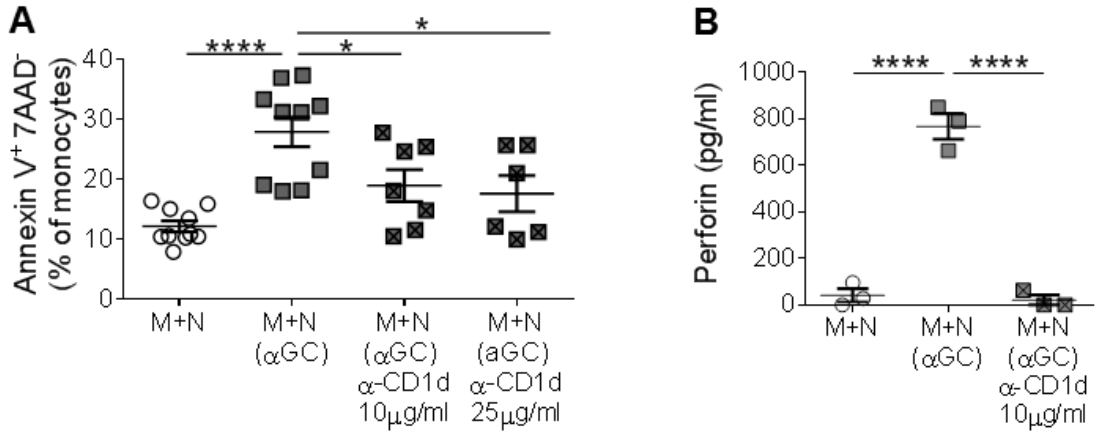

Figure 7.7: CD1d is partially involved in inducing monocyte apoptosis. (A) Percentage of early apoptosing monocytes following 24 hours of co-culture with iNKT cells ±αGC and ±CD1d blockade at 10 or 25μg/ml. Monocytes from 7-10 donors. Gated on $CD3^{-}Vα24Jα18^{-}$ cells. **(B)** Perforin in co-culture supernatants measured by ELISA following 24 hours of iNKT-monocyte co-culture ± αGC and ± CD1d blockade. One-way ANOVA *p≤0.05, ****p≤0.0001. M= monocytes, N= iNKT clones.

Because the induction of apoptosis appeared only partially dependent on direct contact via CD1d, the involvement of soluble factors in contributing towards monocyte apoptosis were next investigated. A Transwell system was set up where monocytes alone were placed in the bottom of the well of a 24-well plate, and the iNKT-monocyte co-culture was set up in the top compartment of the Transwell, with or without αGC (Figure 7.8A). This system allowed soluble factors such as cytokines, but not cells, to pass through the Transwell pores. αGC activation of monocytes and iNKT cells in the top transwell induced monocyte apoptosis in the bottom compartment, suggesting that soluble factors were at least partly responsible for the associated monocyte apoptosis (Figure 7.8B).

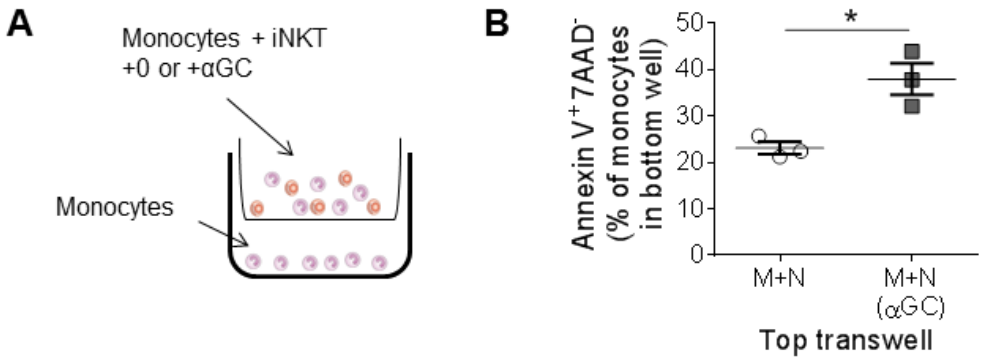

Figure 7.8: Soluble factors induce monocyte apoptosis. (A) Experimental setup of Transwell system with monocytes in the bottom of a 24-well plate and transwell insert containing monocyte and iNKT cells either with or without αGC. **(B)** Percentage of early apoptosing monocytes following activation of cells in transwell insert with αGC or no αGC. Monocytes from n=3 donors. Paired t-test *p≤0.05.

7.4.3 Monocyte apoptosis does not involve TNFα

Having shown that activation of iNKT-monocyte co-cultures resulted in secretion of a soluble factor that caused monocyte apoptosis, I went on to examine potential candidates for this soluble factor. I hypothesised that TNFα could be the pro-apoptotic factor since it induces apoptosis via binding to TNF receptor-1 (TNFR1), leading to recruitment of adapter proteins intracellularly and caspase activation, and was produced at high levels by iNKT cells. Addition of TNFR1 blocking mAb (10μg/ml) to inhibit TNFα signalling in αGC activated co-cultures did however not inhibit apoptosis after 24 hours (Figure 7.9A). Neutralisation of TNFα using 5-500ng/ml of TNFα neutralising antibody did also not reduce monocyte apoptosis following αGC activation of co-cultures after 24 hours (Figure 7.9B). Furthermore, addition of 5-500ng/ml exogenous TNFα to monocytes alone (Figure 7.9C) or monocyte-iNKT co-cultures (Figure 7.9D) did not induce apoptosis after 24 hours.

As a positive control to ensure α-TNFR1 and recombinant TNFα were working, THP-1 cells were stimulated with 10 or 50ng/ml of TNFα, which has been shown to induce IL-8 production (564). TNFα addition to THP-1 cells induced IL-8 production, as could be expected, in a dose-dependent manner (452.8 to 695.7pg/ml) over 24 hours. Addition of TNFR1 blocking antibody to inhibit TNFα signalling reduced IL-8 production by 6-8 fold (Figure 7.9E). This confirmed that recombinant TNFα and TNFR1 induced a response in THP-1 cells, and therefore the lack of effect on apoptosis in monocyte-iNKT co-cultures is due to TNFα not being involved in inducing apoptosis in this system.

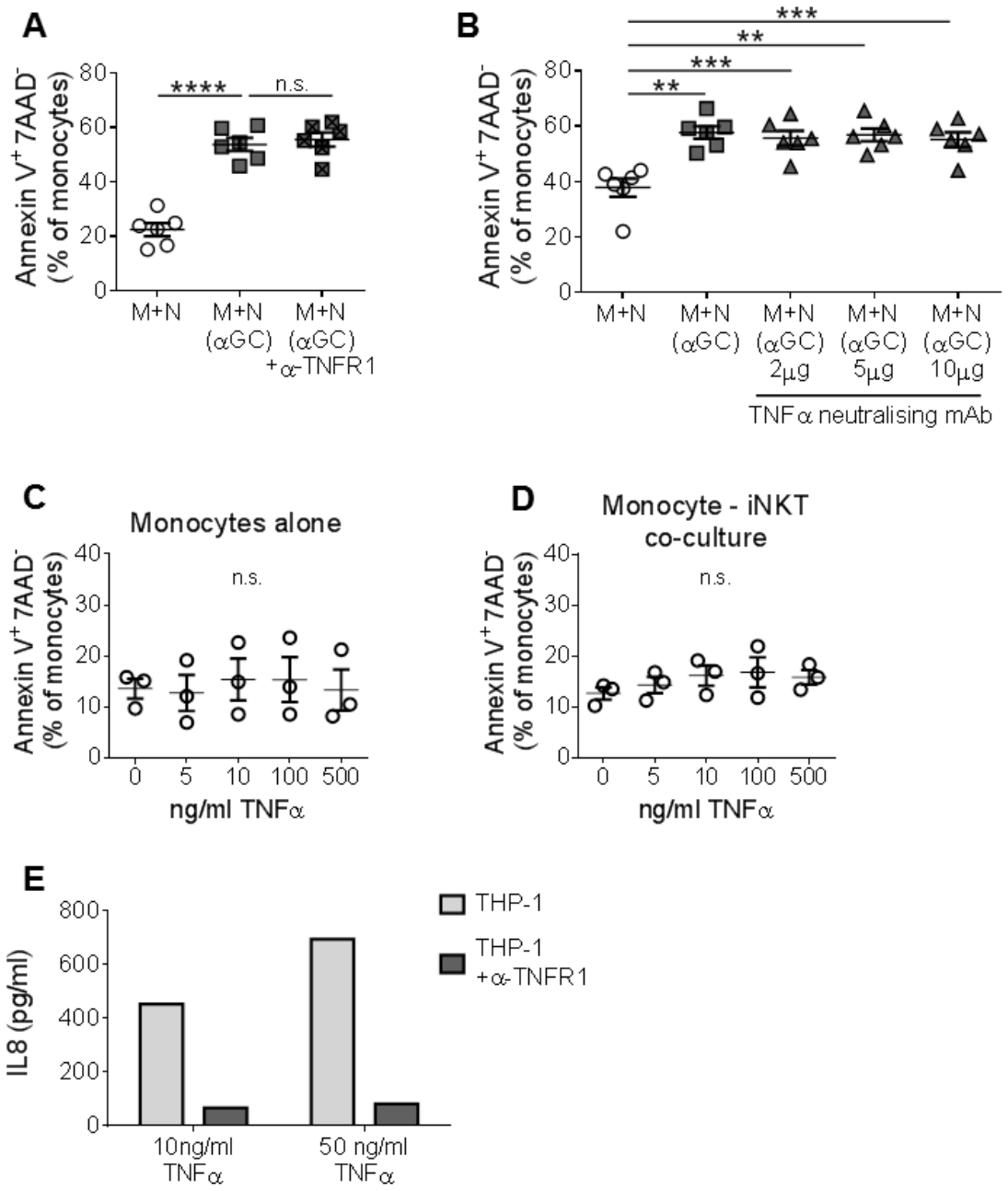

Figure 7.9: Monocyte apoptosis is not caused by TNFα. Percentage of early apoptosing monocytes: **(A)** in co-cultures of monocytes and iNKT cells with or without αGC and 10μg/ml TNFR1 blockade, **(B)** in co-cultures of monocytes and iNKT cells with or without αGC and TNFα neutralising mAb at varying concentrations, **(C)** following addition of TNFα at varying concentrations, or **(D)** in co-cultures following addition of TNFα at varying concentrations. **(E)** IL-8 production in supernatant of THP-1 cell line stimulated with varying concentrations of TNFα and blocked with 10μg/ml α-TNFR1 or left unblocked, measured by ELISA. One-way ANOVA in (A)-(D). **p≤0.01, ***p≤0.001, ****p≤0.0001.

These studies showed that TNFα was not responsible for the increase in monocyte apoptosis induced by iNKT cells. This is further supported by the lack of apoptosis induction by $CD8^+$ clones and NK cells (Figure 7.5) despite high production of TNFα, as well as the fact that monocytes themselves produce TNFα (Figure 7.3).

7.4.4 Expression of TNF receptor superfamily members in iNKT-monocyte co-cultures

At the same time as examining TNFα as a potential soluble factor for induction of apoptosis, I also questioned if expression of co-stimulatory molecules on iNKT cells might be implicated in causing monocyte apoptosis. Expression of TNF-related apoptosis-inducing ligand ('TRAIL'; TNFSF10, CD253), Fas ligand ('FasL'; TNFSF6, CD178), CD40 ligand ('CD40L'; TNFSF5, CD154), 4-1BB (TNFRSF9, CD137) and OX40 (TNFRSF4, CD134) on iNKT cells were determined following 6 hour co-culture with monocytes with or without αGC activation. The 6 hour timepoint was chosen because by this time early apoptosis was induced in αGC-activated co-cultures. The molecules listed above were investigated because TRAIL and FasL are prototypic membrane-expressed apoptosis inducing ligands (565), while optimal iNKT cell activation is strongly dependent on CD40L signals (566), and dual costimulation through 4-1BB and OX40 has been shown to induce $CD4^+$ T cell cytotoxicity (567, 568). Expression was low in un-activated co-cultures, however αGC activation led to upregulation of 4-1BB, TRAIL and CD40L on iNKT cells (Figure 7.10A). FasL and OX40 were not expressed by this iNKT clone (Figure 7.10B).

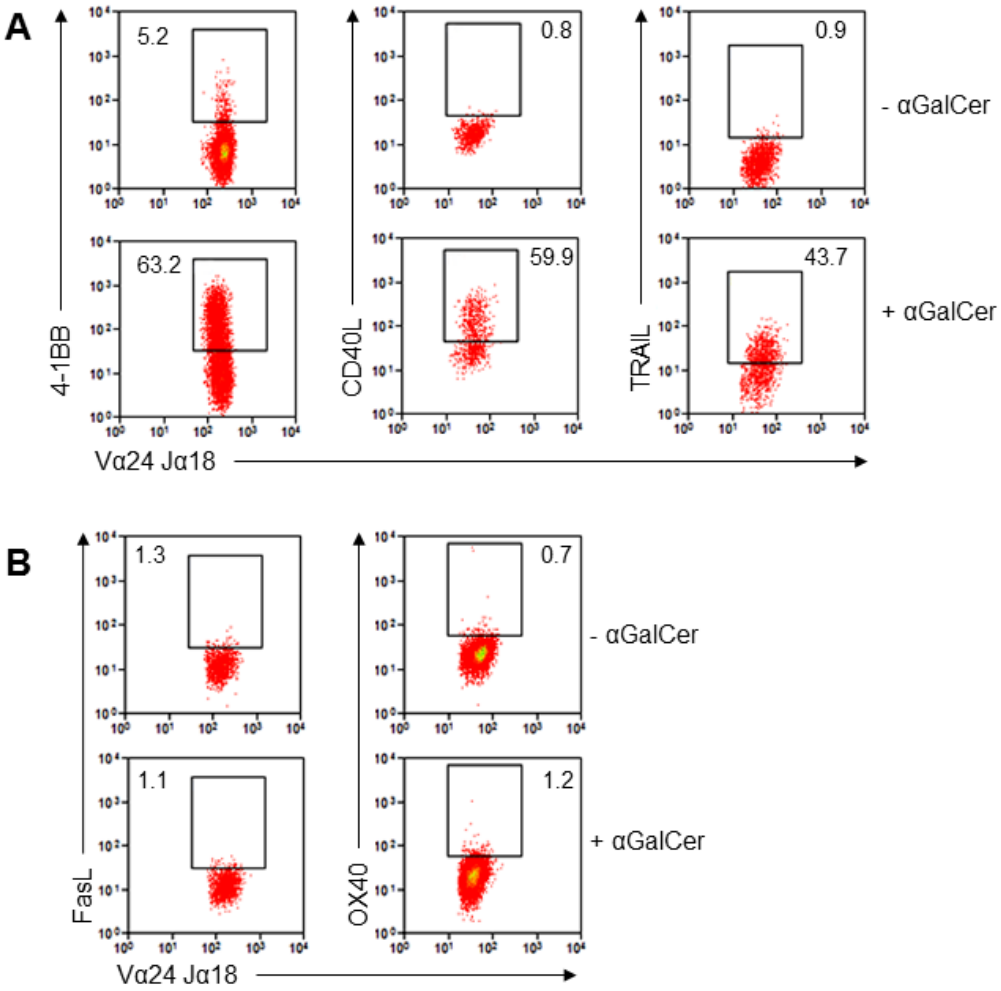

Figure 7.10: Expression of co-stimulatory molecules on iNKT clones. (A) Expression of co-stimulatory molecules 4-1BB, CD40L and TRAIL on iNKT clones following 6 hour co-culture with monocytes ± αGC. **(B)** No expression of FasL or OX40 on iNKT clones following 6 hour co-culture with monocytes ± αGC.

The expression of complementary receptors/ligands for 4-1BB, TRAIL and CD40L on primary human monocytes was next determined following 6 hours of co-culture with iNKT cells ± αGC (Figure 7.11). 4-1BB engages with 4-1BBL, which was the only co-stimulatory molecule analysed that increased on monocytes upon αGC activation of iNKT cells (from 3.2%±0.65 to 12.1%±1.32). TRAIL signals through TRAIL-R1 (DR4) or TRAIL-R2 (DR5) to induce apoptosis of receptor-bearing cells, but neither TRAIL-R1 nor TRAIL-R2 were significantly expressed on primary human monocytes following co-

culture with iNKT clones with or without αGC at this time point. CD40L on iNKT cells binds CD40 on antigen presenting cells (APC), however CD40 was also not expressed on monocytes with or without αGC stimulation at 6 hours. This suggests that 4-1BB/4-1BBL may play a role in early interactions between iNKT cells and monocytes.

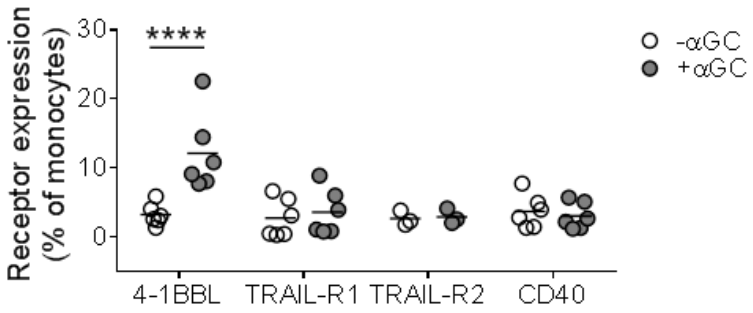

Figure 7.11: Expression of co-stimulatory molecules on monocytes. Expression of 4-1BBL, TRAIL-R1, TRAIL-R2 or CD40 on monocytes following 6 hour co-culture with iNKT cells ± αGC. Monocytes from 6 donors. Paired t-tests ****p≤0.0001.

7.4.5 4-1BB/4-1BBL co-stimulatory pathway maintains monocyte survival and iNKT cell proliferation

4-1BB and 4-1BBL are known to participate in dual co-stimulation where reverse signals from 4-1BB can signal to 4-1BBL-bearing cells to modulate functions such as survival and cytokine production (569). To determine the role played by 4-1BB/4-1BBL interactions between iNKT cells and monocytes, 5μg/ml of each 4-1BB and 4-1BBL blocking antibodies were added to iNKT-monocyte co-cultures to block this interaction, and apoptosis measured at 6 or 24 hours. Blocking 4-1BB/4-1BBL interactions ('4-1BB/L') induced early monocyte apoptosis at 24 hours (42.09%±3.52), but not 6 hours (12.47%±1.34), to a similar level as αGC activation (42.52%±2.0), suggesting that the 4-1BB/L pathway prevented monocyte apoptosis under non-activated conditions (Figure 7.12A). 4-1BB/L blockade following αGC activation further enhanced monocyte apoptosis compared to αGC activation without 4-1BB/L blockade to 54.88%±2.51.

Monocyte IL-12 production was also completely abrogated following 4-1BB/L blockade (Figure 7.12B). This suggests that 4-1BB/L signals are necessary for monocyte survival and IL-12 production.

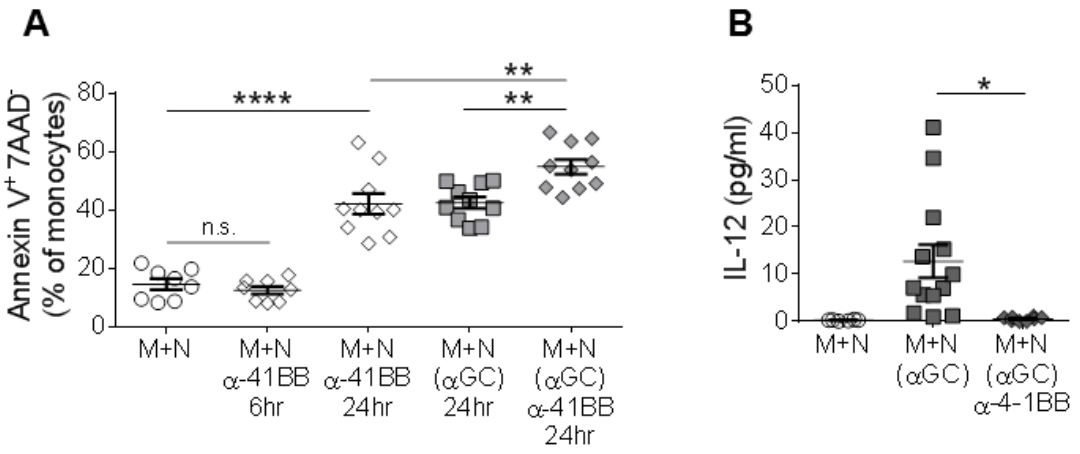

Figure 7.12: Role of 4-1BB/L interactions in maintaining monocyte survival. (A) Percentage of early apoptosing monocytes following co-culture with iNKT cells and α-4-1BB/L mAbs for 6 or 24 hours and/or αGC for 24 hours. **(B)** IL-12 production in co-culture supernatant following αGC activation with or without 4-1BB/L blockade after 24 hours. One-way ANOVA *p≤0.05, **p≤0.001, ****p≤0.0001.

The role of the 4-1BB/4-1BBL pathway on iNKT cell function was next investigated by analysing iNKT cell proliferation, as signals transmitted through 4-1BB in $CD8^+$ T cells have been found to induce their proliferation (570). Furthermore this could identify a way of maintaining the number of iNKT cells, which are not very abundant. In iNKT-monocyte co-cultures stimulated with αGC, 87.15%±4.24 of iNKT cells were proliferating after 5 days, as determined using CFSE (Methods 2.1.10). Proliferating iNKT cells were reduced to 28.17%±9.81 following 4-1BB/L blockade, suggesting that 4-1BB/L interactions between iNKT cells and monocytes are required for efficient proliferation of activated iNKT cells (Figure 7.13A).

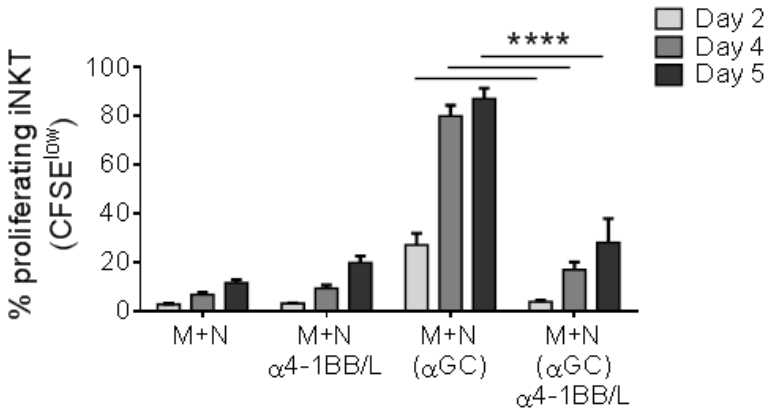

Figure 7.13: 4-1BB/L is required for iNKT proliferation. Proliferation of iNKT cells in co-culture with monocytes in paired samples over 2, 4 or 5 days following 4-1BB/L blockade, αGC activation or αGC activation and 4-1BB/L blockade. Two-way ANOVA *p≤0.05, ****p≤0.0001.

Finally to examine the relevance of 4-1BB/L interactions between iNKT cells and monocytes during IAV infection, expression levels of 4-1BB and 4-1BBL were determined following infection of monocytes with PR8 (Methods 2.1.12). PR8 infection of monocytes enhanced 4-1BBL expression relative to control mock-infected monocytes from 8.1%±2.36 to 16.9%±3.37 (Figure 7.14A). Monocytes that were either mock-infected or PR8-infected were then co-cultured with iNKT cells, and expression of 4-1BB on iNKT cells was measured after 24 hours. Co-culture with PR8-infected monocytes increased iNKT cell 4-1BB expression relative to co-culture with mock-infected monocytes from 10.03%±1.72 to 23.4%±1.90 (Figure 7.14B), suggesting interaction between these cell types following IAV infection with a likely consequence being increased survival.

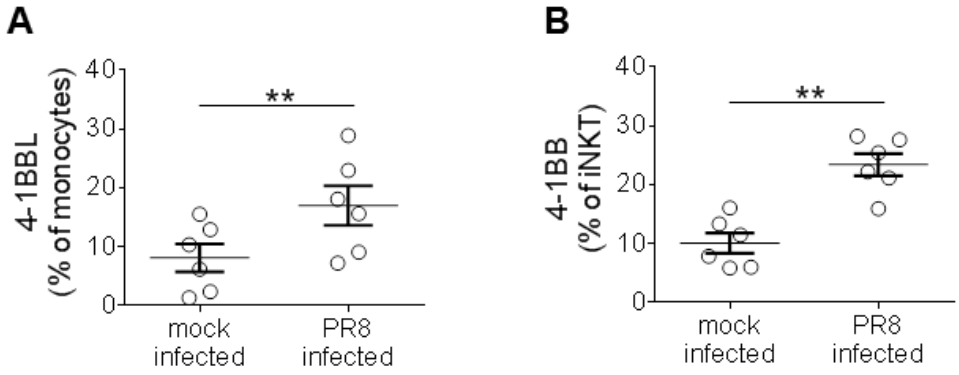

Figure 7.14: 4-1BBL and 4-1BB induction on monocytes and iNKT cells following *in vitro* PR8 infection. (A) 4-1BBL expression on monocytes that were mock infected or infected with PR8 for 24 hours. **(B)** 4-1BB expression on iNKT clones following co-culture with either mock-infected or PR8-infected monocytes for a further 24 hours. T-tests. **p≤0.01.

7.5 Discussion

In this chapter I showed that iNKT cells induced monocyte apoptosis upon TCR-CD1d ligation using αGC as an antigen. Induction of monocyte apoptosis was a unique, novel feature of activated iNKT cells, rather than a consequence of highly activated effector cells, such as $CD8^+$ or NK cells. While high amounts of TNFα were produced by iNKT cells upon activation, TNFα did not appear to play a role in apoptosis induction. On the other hand, 4-1BB/4-1BBL interactions between iNKT cells and monocytes, which were increased upon monocyte PR8 infection, maintained monocyte survival supporting a role for this pathway in maintaining cell viability.

The majority of this work was carried out using cells from healthy controls and without IAV infection, as direct infection of monocytes itself induced high amounts of monocyte cell death, making the study of induction of apoptosis difficult. Direct IAV infection of monocytes did however increase 4-1BBL expression. Findings from this chapter suggest that a likely consequence of this in increased survival. While the co-culture

system is not a natural representation of *in vivo* cell behaviour, it does have the benefit of providing a clean system that only contained iNKT cells and monocytes so that the functions observed could be attributed to one of these cell types. *In vivo*, there are many other factors and cell types contributing to the outcome of interactions between APCs and iNKT cells. The huge range of cytokines and cytolytic factors produced by iNKT cells influence not just monocytes, but also NK cell effector functions such as IFNγ production and T helper cell differentiation, amongst others (327). Apoptosis induction in monocytes by iNKT cells likely involves multiple factors, such as in the killing of IAV-infected lung alveolar epithelial cells by γδ T cells, which required direct cell contact as well as a combination of perforin-granzyme B, TRAIL and Fas-FasL signals to kill IAV-infected alveolar epithelial cells (571).

The induction of monocyte apoptosis by iNKT cells upon TCR ligation using αGC, supports a CD1d-TCR-mediated mechanism as being involved in causing apoptosis, which likely also requires other signalling molecules due to the incomplete reduction in monocyte apoptosis following CD1d blockade. Activated iNKT cells have been reported to produce over 20 different types of cytokines, as well as apoptosis-inducing molecules (352). TNFα was investigated in this study due to its high production by activated iNKT cells at 6 hours; the same time that monocyte apoptosis induction was observed, and its known role as an apoptosis-inducing factor. While being recognised as a major pro-apoptotic cytokine, TNFα has both pro- and anti-apoptotic effects, as ligation results in NFκB activation which regulates survival, or caspase activation which regulates apoptosis induction. NFκB induces transcription of survival genes including caspase inhibitors cFLIP and XIAP (572), and has been shown to promote survival of neutrophils via IL-8 release, which has survival-promoting effects (573). It is possible that TNFα had a similar effect on monocytes in this study, which can also produce IL-8. On the other hand, others found that while low doses of TNFα maintained neutrophil survival, high amounts of TNFα caused apoptosis, partially by inhibiting anti-apoptotic

effects of GM-CSF and IFNγ (574). The inability of TNFα to induce monocyte apoptosis was further supported by the findings that activated NK or $CD8^+$ cells did not induce monocyte apoptosis, despite producing TNFα.

The major mechanisms involved in inducing apoptosis involve either surface receptors, of which Fas/FasL, TNFα/TNF-R and TRAIL/TRAIL-R are the most prominent, or soluble mediators which are mainly perforin and granzymes. Some studies investigating the role of iNKT cells in inducing apoptosis have revealed involvement of FasL and TRAIL (374), however the perforin/granzyme pathway has been the most implicated in cytotoxic and apoptotic activities of iNKT cells (575, 576). It is likely that iNKT cells are equipped with multiple mechanisms to induce cell death, and the choice of which to employ depends on the presence of specific receptors or ligands on target cells. The observation that perforin was highly expressed in supernatants from iNKT-monocyte co-cultures, and that over 60% of iNKT cells expressed the degranulation marker, CD107a, suggest a role for these molecules in apoptosis of monocytes. Perforin and granzymes are normally stored within secretory granules which are released upon immune synapse formation, and play a major role in elimination of virus infected cells (577). $CD4^+$ T cells in the lungs provided protection against IAV by inducing apoptosis of infected cells via perforin-mediated mechanisms (578). As perforin levels in co-culture supernatants were abolished following CD1d blockade, it is likely that activated iNKT cells engage with monocytes via CD1d and induce apoptosis via perforin release.

TCR-independent activation of iNKT cells via IL-12 and IL-18 led to activation as shown by IFNγ production, but did not induce monocyte apoptosis in co-cultures. IL-12/IL-18 stimulation has been shown by others to induce iNKT cell IFNγ production, proliferation and upregulation of FasL (579). IL-12/IL-18 stimulated iNKT cells expressed increased cytotoxic potential against Fas-positive targets in a tumor model (580) suggesting that

FasL is involved in apoptosis following IL-12/IL-18 activation. The lack of FasL expression by the iNKT clone used in this study could therefore explain the lack of monocyte apoptosis following IL-12/IL-18 stimulation of iNKT cells.

4-1BB was the only co-stimulatory molecule expressed whose ligand, 4-1BBL, also increased on monocytes following αGC activation after 6 hours. While pro-apoptotic signals were originally being investigated in this study, I found that bidirectional signalling via 4-1BB/L promoted monocyte survival under homeostatic conditions, and optimal iNKT cell proliferation upon activation. A role for 4-1BB in maintaining iNKT numbers supports findings from Vinnay et al who found reduced iNKT cell numbers in 4-1BB$^{-/-}$ mice (581). The role of 4-1BB signals in mediating optimal proliferation were also shown in an HIV setting, where 4-1BBL expressing dendritic cells enhanced proliferation, functionality, cytokine production and survival of HIV-specific CD8^{+} T cells (582). The apoptosis of monocytes and inhibition of IL-12 production following 4-1BB/L blockade is supported by studies from others showing that 4-1BBL reverse signalling increases viability and cytokine production in murine bone marrow-derived macrophages (583). A specific role for IL-12 production via this pathway has however not been identified by others, and provides a potential link to iNKT cell activation, as myeloid-derived IL-12 augments iNKT cell activation (566). These results provide a potential mechanism whereby engagement of 4-1BB on iNKT cells promotes proliferation of activated effector cells able to control monocyte numbers when found in close vicinity, as in the lungs during IAV infection.

FasL and TRAIL share 25-30% sequence similarity with TNFα, and also have established roles in inducing cell apoptosis by binding to their death-domain containing receptors (584). In glioma cell lines, different sensitivities towards FasL and TRAIL were noted, with some cell lines being completely resistant (565), suggesting that apoptosis via these pathways is partially cell-type dependent. FasL was not expressed

by the iNKT cell clone used in this study and was therefore not accountable for the observed apoptosis. TRAIL was expressed on iNKT cells, but neither of the two receptors that it signals through to impart apoptotic signals were expressed by monocytes after 6 hours of co-culture with or without αGC activation. TRAIL also interacts with two decoy receptors, DcR1 and DcR2 which do not transmit apoptotic signals upon ligand binding due to incomplete death domains (585). Overexpression of decoy receptors could have protected monocytes from apoptosis. While differences in apoptosis-inducing mechanisms may exist in iNKT cells that do express FasL, this study highlights the ability of iNKT cells to induce apoptosis, even in the absence of pro-apoptotic signals from FasL and TRAIL, which appears to be highly specific to CD1d ligation.

CD40L expression on iNKT cells has established functions in signalling to dendritic cells via CD40 and promotes their maturation and IL-12 production (402). CD40L expression on activated iNKT cells was confirmed in this study, but lack of CD40 on monocytes again suggested that this pathway was not involved in early iNKT cell-monocyte signalling at the 6 hour time point. CD40 expression is reported to be upregulated on professional APCs, so it is likely that this pathway plays a role later once monocytes have differentiated, as is the case for CD80, which is upregulated upon DC maturation but is not expressed by primary human monocytes (586).

OX40 expression was analysed because OX40 and 4-1BB dual co-stimulation programmed $CD4^+$ Th1 cells to develop into cytotoxic effector cells (567). High levels of both OX40 and 4-1BB on $CD4^+$ T cells were also associated with perforin production from $OX40^+4\text{-}1BB^+$ cells in patients with acute coronary syndrome (568). Therefore it was plausible that OX40 and 4-1BB dual co-stimulation could be responsible for apoptosing-inducing activities of the $CD4^+$ iNKT clone used in the current study. Lack

of OX40 expression on iNKT clones in co-culture with monocytes and αGC however meant that this was not the case.

It is likely that expression of some co-stimulatory receptors and ligands occurs at a later time point. Another possibility for lack of detectable expression is that receptors have become internalised or soluble receptors have been shed upon activation (587), although some expression would still be expected. As the primary aim was to identify factors leading to early monocyte apoptosis at 6 hours, later time points were not investigated for all molecules. As it turned out, 4-1BB/L interactions did not induce apoptosis, but rather maintained monocyte survival, which was apparent after 24 hours. It is likely that early interactions via 4-1BB/L, which were upregulated 6 hours after activation, initiated this signalling.

7.6 Conclusions

iNKT cells regulate monocyte survival and apoptosis during steady state and following activation. During steady state, 4-1BB/4-1BBL interactions between iNKT cells and monocytes were required for monocyte survival, providing a mechanism for maintenance of monocyte numbers under homeostatic conditions. Expansion of activated iNKT cells relied heavily on 4-1BB co-stimulation, and activated iNKT cells were able to override the 4-1BBL survival signal to induce rapid monocyte apoptosis, which was likely to at least partially involve the perforin/granzyme pathway but not TNFα.

Chapter 8: Final discussion and future directions

8.1 Main findings

The overall aim of this project was to examine the role of monocytes during severe influenza A virus (IAV) infection. Following on from findings that high numbers of monocytes with an altered inflammatory phenotype were associated with worse outcome in both mouse and human IAV infection, their regulation by iNKT cells was examined to reveal that iNKT cells had multifarious influences on monocyte phenotype and number, which appeared to be exerted primarily in the lungs during IAV infection.

The first key finding was that in mice infected with high pathogenicity PR8, severe disease was associated with high Ly6C^{hi} inflammatory monocyte influx to lungs compared to mild infection, in a setting that controlled for host genotype (C57BL/6) and time of inoculation (Figure 3.12). Importantly, although Ly6G^{+} cells, which could represent classical neutrophils or neutrophilic MDSCs, were higher than monocytes in blood, inflammatory monocyte frequency was highest in the lungs. This study underlines the likelihood that in the lungs, immunopathology may more likely be a consequence of monocytes than neutrophils or neutrophilic MDSCs. In addition, in iNKT deficient (Jα18$^{-/-}$) mice, monocytes rather than neutrophils were increased in numbers in the lungs and associated with lung injury (Figure 6.2 and (280)).

Studies in human disease have several limitations, not least that most of what can be inferred is from associations and correlations, but also *in vivo* mechanistic work is very limited. However, they form a very important complement and add relevance to murine studies. The cellular immunology studies in humans were designed so that samples

were processed fresh rather than from frozen stock. This provided the advantage of being able to capture signals across immune cells without differential changes caused by storing of different cell subsets. For example, MDSCs were entirely lost after storage. Thus, this study provides possibly the first accurate analysis of monocytes and MDSCs in acute IAV infection in humans, and their relative association to outcome. By only including patients without confounding factors, as described in Chapter 4.3.1, the number of samples was unfortunately low, which is a limitation due to genetic differences between individuals leading to greater variation than when host genotype is controlled, as in murine studies.

High levels of monocytes were associated with more severe disease in H5N1 mouse infection, pandemic H1N1 2009 ('pH1N1') infection in humans, and high pathogenicity H1N1 infection in mice lacking iNKT cells ($J\alpha18^{-/-}$). The phenotype and function of monocytes in these different models showed similarities, such as upregulation of genes involved in polarisation towards an M1 inflammatory macrophage phenotype in both mouse infections with worse outcome. CCR7, which is expressed by M1 macrophages, was also highest on monocytes from pH1N1 infected patients compared to healthy controls, whereas CD163, which marks M2 macrophages, was not upregulated (267). Excessive inflammatory monocytes/ macrophages during IAV infection induce production of proinflammatory cytokines in the lungs that cause pulmonary damage and respiratory dysfunction (270). It is therefore probable that the polarisation towards an M1 phenotype aggravates lung inflammation in highly pathogenic IAV infection.

The higher upregulation of interferon (IFN)-regulated genes in H5N1 compared to X179A infection (Figure 3.5), and upregulation in monocytes from both blood and BAL of $J\alpha18^{-/-}$ mice compared to WT (Table 6.7), links upregulation of IFN-regulated genes with a worse outcome. As IFN-regulated genes made up a large proportion of upregulated genes in monocyte from both blood and BAL, it is likely that an

upregulation in IFN signalling occurs early, in blood monocytes, and is sustained in monocytes from the BAL. IFN regulatory factors have also been shown to be involved in macrophage polarisation, as IRF5 causes upregulation of M1 specific markers and induces Th1 responses (546). Higher IFNαβ signalling was found to lead to a worse outcome in mice following severe IAV infection, and blocking IFNαβ signalling improved outcome (158), supporting the findings of higher IFN regulated genes in severe infection potentially being involved in pathology in this study. This is likely to only be the case in severe infection when high amounts of IFN are produced, as IFN production has been shown to contribute to virus clearance and improved outcome in mild or season IAV infections due to antiviral properties (278, 545). These findings of IFN contributing to severe disease are notable, as IFN treatment been proposed as a therapeutic measure to combat IAV infection since the 1960s, however it is possible that IFN treatment of severe IAV infections that are associated with an inflammatory immune microenvironment would aggravate, and not improve, outcome (588).

In human acute IAV infection both monocytes and neutrophilic MDSCs were increased in severe compared to mild disease. However, only the increase in monocytes was unique to pH1N1 infection, as patients with influenza-like illness also had increased neutrophilic MDSCs in severe compared to mild disease, albeit at lower levels than pH1N1 patients. The dysregulation in monocyte number was accompanied by phenotypic changes including reduced HLA-DR, CD62L and IL-10 and increased IL-$6^{+}TNF\alpha^{-}$ production. Abnormal function and frequency of monocytes in human IAV infection supports the work from mouse IAV infection where severe disease was associated not only with higher monocyte numbers in lungs, but changes in their gene expression and functional profiles. Monocytes show high plasticity and have been shown to differentiate into different types of macrophages or DCs using different IAV strains and infection models in mice (270, 278, 279). However the contribution of monocytes to disease severity in IAV infection, and association with outcome in human

disease in particular has not been well documented. The distinct downregulation of HLA-DR and near complete loss of IL-10 production by circulating monocytes could be useful predictive biomarkers of severe disease, although expression of these would need to be investigated early after symptom acquisition to determine predictive ability. The influential roles of monocytes during IAV infection was further highlighted by their potential effect on T cells. Monocytes recruited to the lungs have been shown to be necessary for effective priming of T cell responses (270). The lower level of $CD8^+$ T cell differentiation in severe disease and correlation with high monocyte frequency identified a possible novel link between monocytes and T cell differentiation. pH1N1-specific circulating T cell responses measured by IFNγ were however highest in severe disease, suggesting that the reduced pool of circulating differentiated T cells did not affect development and differentiation of pH1N1-specific T cells. It is possible that the increased number of monocytes in severe disease act as antigen presenting cells to induce a greater T cell response, strengthening their importance as biomarkers of severe disease. Reduction in the antigen presenting-molecule HLA-DR on circulating monocytes has been suggested to occur as a protective response to inflammation or as a result of preferential recruitment of high HLA-DR expressing monocytes to the site of infection, and replenishment in the blood by immature monocytes from bone marrow. I propose that the latter is a more probable explanation of reduced HLA-DR in circulating monocytes in this study, since low HLA-DR expression has been associated with reduced T cell stimulation, however pH1N1-specific T cells were found to be high in severe infection.

Patients with higher frequencies of inflammatory monocytes also had the lowest absolute number of circulating iNKT cells, which did not increase upon recovery. This therefore forms a link between severe disease, high monocyte frequency, and low iNKT cells in human IAV infection.

The finding that iNKT cells have the potential to modulate multiple functions of monocytes during IAV infection has not been previously established, although their role as protective, rather than pathogenic, players in the outcome to IAV has been shown by others (280, 306, 413, 415, 417). Findings from mouse monocyte gene expression and human *in vitro* work suggest that one way iNKT cells may be regulating the number of monocytes during IAV infection is via inducing their apoptosis. During steady-state, survival signals are imparted upon iNKT cells and monocytes via 4-1BB/4-1BBL interactions. Upon iNKT cell activation however, these signals are overridden and iNKT cells induce rapid apoptosis of monocytes, while themselves proliferating. Apoptosis of IAV-infected cells has been shown by others to occur via perforin and FasL mediated mechanisms by IAV-specific $CD8^+$ T cells (148). It is possible that iNKT cells target monocytes due to their high CD1d expression, and induce their apoptosis via CD1d-mediated mechanisms. iNKT cells in mouse IAV infection were furthermore found to regulate inflammasome activation in monocytes, as inflammasome signalling components were enriched in monocytes from $J\alpha18^{-/-}$ mice. Inflammasome signalling during IAV infection induces production of chemokines such as MIP-1α, which mediate monocyte recruitment to the lungs (170). Activation of the inflammasome has been shown to be beneficial for late stages of virus clearance (171), however in severe infection where the onslaught of high monocyte numbers induces pulmonary damage within the first few days, it is likely to be detrimental by contributing to monocyte and macrophage recruitment.

Findings from this thesis infer that monocytes and iNKT cells interact *in* vivo, leading to modulation of monocyte functions. The site of this interaction is however not known. Possible sites include but are not limited to lungs, blood, lymph nodes and spleen. As discussed in chapter 6, interaction during IAV infection may occur in the lungs, which is supported by work from others showing that iNKT cells are long term residents of the lung microvasculature network (533). While direct interaction in the bloodstream seems

unlikely due to the high shear force generated by circulating cells, interaction along the endothelium is a possibility. iNKT cells were shown to slowly crawl along sinusoidal endothelial cells, providing a scaffold of slow-moving iNKT cells for monocytes to interact with (332). iNKT cells were also shown to be positioned within interfollicular zones and the medulla of lymph nodes and could actively scan and communicate with macrophages (589), providing another opportunity for interaction. The same groups showed that iNKT cells patrol at low speeds of 6μm per minute around the marginal zone and red pulp of the spleen where they form a net for receipt of circulating monocytes (590). Identifying the site of interaction may influence therapeutic measures. iNKT cells have been targeted for immunotherapeutic treatment in diseases such as cancer, with clinical trials involving direct αGalCer injection, reinfusion of autologous DCs loaded *ex vivo* with αGalCer and autologous transplant of *ex vivo* expanded iNKT cells (591). While safe and well-tolerated by patients, many of these treatments were met with little success in Phase I clinical trials. Further understanding of the interactions between iNKT cells and APCs and their localisation may aid future trials.

8.2 Future work

This study raised further questions relating to both the upstream cause of monocyte accumulation and downstream effects of monocytes during IAV infection. The increase in monocytes in severe disease could be due to an upstream depletion of iNKT cells, but this would require iNKT cells to be low prior to infection, or a genomic variation which affects iNKT cell numbers or responses. It is also possible that certain IAV strains evoke larger monocyte responses, as seemed to be the case in H5N1 and X179A infections where host genotype was controlled. This is however less likely in the human study of pH1N1 infection since, theoretically, the virus is the same but the host

is variable. Therefore, not unexpectedly, both host and virus factor likely play a role in determining the magnitude of monocyte response. For the virus factor, genetic tools are available to systematically silence each of the candidate genetic elements in highly pathogenic viruses, to determine if any genes in particular cause the monocyte response. The readout would be monocyte numbers, differentiation and function in the lungs of IAV infected mice. I will explore this in collaboration with our previous collaborators in Mill Hill. For the host response, one step would be to examine genomic variants of candidate genes like the CCR2 gene, utilising known SNPs such as the CCR2-V64I mutation which is protective in HIV infection, and a large cohort of patients with our collaborators (107).

There are many possible sites of interaction between iNKT cells and monocytes, including lungs, blood, lymph nodes, and more, which I would like to investigate using intravital microscopy to image iNKT cells and monocytes in living mice. Work for this is currently underway, and we have been able to detect iNKT cells in the lungs of uninfected mice by injection of a fluorescently labelled αGC-loaded CD1d dimer. I plan on taking this work further in transgenic mice where CCR2 monocytes are fluorescently labelled, as this would identify Ly6C^{hi} inflammatory monocytes and enable imaging of iNKT cells and monocytes, following injection of the CD1d dimer. This would allow further study on where and how iNKT cells cause apoptosis of monocytes during IAV infection. It is also possible that iNKT cells interact with the Ly6C^{low} subset of monocytes, which have been shown to crawl along and monitor the luminal side of blood vessels, and can be identified in Cx3cr1$^{+/gfp}$ mice (220). While the Ly6C^{hi} subset is primarily involved in the immune response to IAV infection, it is possible that interactions between the Ly6C^{low} subset and iNKT cells occur that alter the disease course in IAV infection, as the patrolling nature of Ly6C^{low} monocytes enables rapid egress to tissues, and iNKT cells can crawl along sinusoidal endothelial cells and arrest following antigen recognition (332). Ly6C^{hi} adoptively transferred monocytes were

shown to transition through a Ly6C^{low} state and adopt patrolling behaviour in vasculature, before being recruited to tissue granulomas in *Schistosoma manosi* infection (548), so it would be interesting to examine Ly6C^{low}, as well as Ly6C^{hi} monocytes.

Since the human studies are necessarily observational, I would first determine if CCR2 blockade, potentially using a drug already available, could attenuate the outcome of severe IAV infection by reducing monocyte influx to lungs. Carrying this work out in a CCR2$^{+/gfp}$ mouse, which is currently being bred in the animal facility, would allow simultaneous examination of monocyte trafficking and differentiation to M1 or M2 macrophage subsets with or without CCR2 blockade. These studies would also enable examination of the effect of monocytes on T cell differentiation by examining IAV-specific T cells both in blood and lungs. The identification of enrichment of genes involved in M1 or M2 macrophage polarisation were of particular interest as they were identified early on in monocytes, on day 3 of infection in mice. This may suggest that monocytes sense signals early on that drive their differentiation down a particular pathway. Different drug treatments have been shown to influence M1 or M2 polarisation in patients. Corticosteroid treatment was shown by others to associate with M2 polarisation in respiratory diseases, with high M2 macrophage activity in the lungs contributing towards fibrosis (592). Rapamycin on the other hand induces an M1 phenotype after 21 days in patients treated before islet transplant, proposing therapeutic strategies for M2-related diseases (593). The ability to modulate macrophage differentiation has the potential to influence outcome to disease, but before this it needs to be established which macrophage subsets are involved in driving pathogenesis and resolution during IAV infection. Monocyte accumulation in lungs during severe IAV infection has largely been associated with a worse outcome due to lung pathology, however the presence of M1 or M2 macrophages, or the effect of polarisation towards either phenotype on outcome to infection, have not been

investigated *in vivo*. I would be interested in determining this in a severe mouse IAV infection model, which would involve analysing macrophages in lungs beyond day 3, both as infiltrating monocytes and part of the lung vasculature network.

Finally, relating to the findings that monocytes were sustained at a high frequency throughout IAV infection and at recovery in humans, I am interested in understanding the signals that lead to this sustained monocyte production in severe IAV infection. I would firstly establish if this is indeed the case in mice by examining myelopoiesis and determining both Ly6C^{hi} and Ly6G^{+} cells in bone marrow, blood and lungs during the acute and resolving phase of severe IAV infection. Understanding the cause of high monocytes in IAV infection and the effect of blocking CCR2 would form a robust platform to investigate the use of CCR2-blockade in humans.

8.3 Final conclusions

My studies show that poor outcome to severe IAV infection is, at least partly, driven by a high number of monocytes with an altered inflammatory phenotype that not only induce inflammation during acute infection, but have the potential to influence the T cell response. Profiling of monocytes from the lungs identified that enrichment of immune signalling components such as interferon-regulated genes and inflammasome signalling, which have been shown to be beneficial in mild infection, may influence the poor outcome to high pathogenicity IAV infection.

Appendix 1: ImmGen RNA extraction protocol

Immunological Genome Project
Immgen.org

RNA extraction with Trizol

For Whole Tissues:
1 – Isolate tissue and snap freeze in liquid nitrogen
2 – Transfer tissue to a 14-ml culture tube and add 2ml of Trizol
3 – Homogenize completely
4 – Transfer 1ml each into two fresh 1.5-ml Epp. tubes
5 – Incubate 5 min @ RT
(Recommended: Freeze in Trizol at least 1 hr @ -80°C after incubating @ RT)
*Potential indefinite stopping point @ -80°C

For Sorted Cells:
1 – Sort cells into 1.5 ml epp. tubes coated in Fetal Calf Serum (FCS) or in 500μl media with 2% FCS
(Recommended: For ≤ 100,000 cells sort directly into 500μl Trizol and proceed to step 5)
2 – Centrifuge 30 sec @ full speed, 4°C (make sure to see a pellet)
3 – Remove supernatant from each sample with a pipette tip
Leave behind a small amount of liquid so as not to disturb the pellet
4 – Add 500 μl Trizol to each sample (mix well by pipetting)
5 – Incubate 5 min @ RT
(Recommended: Freeze in Trizol at least 1 hr @ -80°C after incubating @ RT)
* Potential indefinite stopping point @ -80°C

Thaw Trizol samples at RT
6 – Add the appropriate amount of Chloroform to each sample (work in hood, do not pipette)
- For 500μl Trizol, Add 100μl Chloroform
- For 1ml Trizol, Add 200μl Chloroform

7 – Shake vigorously for approx 15 sec
8 – **Incubate 2-3 min** @ RT
9 – Centrifuge **15 min** @ 12,000 g, 4°C

10 – Transfer aqueous phase CAREFULLY to a fresh tube[1] (work on ice from this point on)
- For 500μl Trizol, Transfer ~250μl
- For 1ml Trizol, Transfer ~500μl

11 – Add 1μl Glycoblue to each sample (flick well but don't pipette to mix, quick spin, on ice)
12 – Add the appropriate amount of Isopropanol to each sample (flick well to mix, do not pipette)
- For 500μl Trizol, Add 250μl Isopropanol
- For 1ml Trizol, Add 500μl Isopropanol

13 – **Incubate 1+ hr @ -80°C**
*Potential indefinite stopping point @ -80°C

14 – Centrifuge **20 min** @ 12,000 g, 4°C
Remove supernatant with a pipette tip
15 – Wash with the appropriate amount of 75% cold ethanol (flick to loosen pellet)
- For 500μl Trizol, Wash with 500μl 75% cold ethanol
- For 1ml Trizol, Wash with 1ml 75% cold ethanol

16 – Centrifuge **15 min** @ 7,400 g, 4°C
Pipette off as much ethanol as possible, air dry 1 hr (pellet will change color)
17 – Resuspend each RNA pellet in 12.5 - 15 μl Nuclease-free water
18 – Incubate @ RT for **2-3 min**, then flick well to mix and place on ice
19 – Quantify total RNA using a Nanodrop
*Store total RNA indefinitely @ -80°C

---

[1] Leave behind a small amount of clear aqueous phase; do NOT pick up any pink phenol-chloroform phase; use pipette tips with a larger hole to prevent this from happening.

Appendix 2: GSE accession details for GSEA analysis

Gene set	GEO ID/ Platform	Experiment design
M1/M2 phenotype	GSE51466/ Agilent-028005 SurePrint G3 Mouse GE Microarray	Bone marrow-derived macrophages generated over 7 days were stimulated for 24 hours with the following reagents to induce differentiation into: M1: LPS & GM-CSF M2: IL-4 and M-CSF
M1 vs M2a, M2b, M2c	GSE32690/ Agilent 014868 Whole Mouse Genome Microarray	$Ly6C^{hi}Ly6G^{-}CD11b^{hi}$ monocytes FACS-sorted from bone marrow and cultured with the following reagents to induce differentiation to the following macrophage subsets: • M1: M-CSF, IFNγ & LPS • M2a: M-CSF & IL-4 • M2b: complexed Ig & IFNγ • M2c: M-CSF & dexamethasone

GSE51466

Gene arrays for M1 differentiated macrophages (n=3) and M2 differentiated macrophages (n=3) were compared against each other using GEO2R (Chapter xx) to identify genes unique to M1 or M2 polarisation

GSE32690

Gene arrays for M1 differentiated macrophages (n=3) were compared to each of M2a (n=3), M2b (n=3) and M2c (n=3) gene arrays using GEO2R to identify genes unique to M2a, M2b or M2c polarisation.

Appendix 3: Descriptions of differentially regulated genes in H5N1 and X179A infection

Gene	Description
Apod	Apolipoprotein D
BC023105	cDNA sequence BC023105
Bcl3	B-cell lymphoma 3-encoded protein
Ccl12	Chemokine (C-C motif) ligand 12 (MCP-5)
Ccl19	C-C motif chemokine 19 (MIP-3-β)
Ccl2	Chemokine (C-C motif) ligand 2 (MCP-1)
Ccl20	Chemokine (C-C motif) ligand 20 (MIP3A)
Ccl3	Chemokine (C-C motif) ligand 3 (MIP1-α)
Ccl4	Chemokine (C-C motif) ligand 4 (MIP1β)
Ccl5	Chemokine (C-C motif) ligand 5 (RANTES)
Ccl7	Chemokine (C-C motif) ligand 7 (MCP-3)
Ccl8	Chemokine (C-C motif) ligand 8 (MCP-2)
Ccl9	Chemokine (C-C motif) ligand 9 (MIP1-γ)
Ccr1	C-C chemokine receptor type 1
Ccr2	C-C chemokine receptor type 2
Ccr5	C-C chemokine receptor type 5
Cxcl10	C-X-C motif chemokine 10 (IP-10)
Cxcl11	Chemokine (C-X-C motif) ligand 11 (IP-9)
Cxcl13	Chemokine (C-X-C motif) ligand 11 (BCL)
Cxcl2	Chemokine (C-X-C motif) ligand 2 (MIP2-α)
Cxcl3	Chemokine (C-X-C motif) ligand 3 (GRO3)
Cxcl5	C-X-C motif chemokine 5 (ENA-78)
Cxcl9	Chemokine (C-X-C motif) ligand 9 (MIG)
Cxcr2	Interleukin 8 receptor, β
Fcgr1	High affinity immunoglobulin gamma Fc receptor I
Fcgr2b	Low affinity immunoglobulin gamma Fc region receptor II-b
Fcgr3	Fcgr3 Fc receptor, IgG, low affinity III
Gm5431	Predicted gene 5431
H2-Q6	Histocompatibility 2, Q region locus 6
H2-Q8	Histocompatibility 2, Q region locus 8
Ido1	Indoleamine-pyrrole 2,3-dioxygenase
Ifi203	Interferon activated gene 203
Ifi204	Interferon activated gene 204
Ifi205	Interferon activated gene 205
Ifi27l2a	Interferon, α-inducible protein 27 like 2A
Ifi35	Interferon-inducible protein 35
Ifi44	Interferon-inducible protein 44
Ifi47	Interferon-inducible protein 47

Gene	Description
Ifih1	MDA5 (Melanoma Differentiation-Associated protein 5)
Ifit1	Interferon-induced protein with tetratricopeptide repeats 1
Ifit2	Interferon-induced protein with tetratricopeptide repeats 2
Ifit3	Interferon-induced protein with tetratricopeptide repeats 3
Ifitm3	Interferon-induced transmembrane protein 3
Iigp1	Interferon inducible GTPase 1
Il15	Interleukin 15
Il18bp	Interleukin-18-binding protein
Il1a	Interleukin-1α
Il1b	Interleukin-1β
Il6	Interleukin 6
Il7r	Interleukin 7 receptor
Irf1	Interferon regulatory factor 1
Irf7	Interferon regulatory factor 7,
Irg1	Immune responsive gene 1
Irgm1	Immunity-related GTPase family M member 1
Irgm2	Immunity-related GTPase family M member 2
Isg15	Interferon-induced 17 kDa protein
Isg20	Interferon-stimulated gene 20 kDa protein
Ly6i	Lymphocyte antigen 6 complex
Ms4a4c	Membrane-spanning 4-domains, subfamily A, member 4C
Mx1	Myxovirus (influenza virus) resistance 1
Mx2	Myxovirus (influenza virus) resistance 2
Myd88	Myeloid differentiation primary response gene (88)
Rsad2	Radical S-adenosyl methionine domain containing 2
Saa1	Serum amyloid A 1
Saa3	Serum amyloid A 3
Samhd1	SAM domain and HD domain-containing protein 1
Slfn4	Schlafen 4
Timp1	TIMP metallopeptidase inhibitor 1
TLR1	Toll-like receptor 1
TLR13	Toll-like receptor 13
TLR3	Toll-like receptor 3
TLR7	Toll-like receptor 7
TLR9	Toll-like receptor 9
Tnf	Tumor necrosis factor
Zbp1	Z-DNA-binding protein 1

Full descriptions of differentially expressed genes from mouse H5N1 or X179A infection identified in Chapter 3, arranged in alphabetical order.

Appendix 4: Differentially regulated genes in Jα18$^{-/-}$ monocytes

Log2FC	Adjusted P	Gene name	Description
Upregulated in blood			
3.802392399	0.000177949	ST6GALNAC2	Alpha-N-acetylgalactosaminide alpha-2,6-sialyltransferase 2
3.164775195	0.001314985	CTSE	Cathepsin E
2.49227143	0.006469193	PVRL2	Poliovirus receptor-related 2
1.906346834	0.020316027	RNASE4	Ribonuclease, RNase A family 4
1.799284071	0.00155536	GPR114	G protein-coupled receptor 114
1.71400143	0.039942847	D13ERTD608E	DNA segment, Chr 13, ERATO Doi 608
1.514089316	0.00254483	EG384179	PREDICTED: Mus musculus predicted gene, EG384179
1.448194268	0.000910334	BC018473	cDNA sequence BC018473, non-coding RNA
1.363490466	0.048862412	SOAT1	Sterol O-acyltransferase 1
1.330228936	0.047645192	P2RY14	Purinergic receptor P2Y, G-protein coupled, 14
Downregulated in blood			
-1.612082273	0.0043596	PARP2	Poly (ADP-ribose) polymerase family, member 2
-1.663223124	0.004603043	APOE	Apolipoprotein E
-1.969845153	0.0043596	SUPT16H	Suppressor of Ty 16 homolog
-1.938924773	0.001269754	LOC100047132	PREDICTED: Mus musculus similar to monoclonal antibody 17-1A, light chain
-2.354296574	0.000228314	COPS8	COP9 (constitutive photomorphogenic) homolog, subunit 8
-2.367517314	0.006986488	LOC623121	PREDICTED: Mus musculus similar to Interferon-activatable protein 203 (Ifi-203)
-2.468860561	0.000413269	MCM6	Minichromosome maintenance deficient 6
-2.950523977	0.000876225	MAN2B1	Mannosidase 2, alpha B1
-2.989487484	0.001314985	ZFP330	Zinc finger protein 330
-5.705197531	0.000876225	FCER1G	Fc fragment of IgE, high affinity I, receptor for γ polypeptide
Upregulated in BAL			
4.128517	1.17E-06	IFI202B	Interferon activated gene 202B
4.116614	3.25E-06	CHI3L1	Chitinase 3-like 1
2.22226	0.000295	ANXA4	Annexin A4
1.661789	0.011495	EAR11	Eosinophil-associated, ribonuclease A family, member 11
1.596281	0.000969	APOBEC1	Apolipoprotein B mRNA editing enzyme, catalytic polypeptide 1
1.543947	0.000852	SLC7A8	Solute carrier family 7 (cationic amino acid transporter light chain, L system), member 8
1.526761	0.0000517	CTSE	Cathepsin E
1.408671	0.001165	SOAT1	Sterol O-acyltransferase 1
1.377549	0.000204	SLC38A6	PREDICTED: Mus musculus solute carrier family 38, member 6
1.32726	0.0033	PGLYRP1	Peptidoglycan recognition protein
Downregulated in BAL			
-1.81781	0.00437	CCL6	Chemokine (C-C motif) ligand 6
-2.26162	9.36E-06	COPS8	COP9 (constitutive photomorphogenic) homolog, subunit 8
-2.36471	9.14E-05	MNDA	Myeloid cell nuclear differentiation antigen (Mnda)
-2.47555	1.17E-06	ZFP330	Zinc finger protein 330
-2.65329	0.000275	OLFML2B	Olfactomedin-like 2B
-2.72508	1.38E-05	MAN2B1	Mannosidase 2, alpha B1
-3.82327	2.15E-05	IFI205	Interferon activated gene 205
-4.2289	3.64E-07	APOC2	Apolipoprotein C-II
-4.54449	3.25E-06	APOE	Apolipoprotein E
-6.47671	6.16E-07	FCER1G	Fc fragment of IgE, high affinity I, receptor for γ polypeptide

Details of the 10 most upregulated and downregulated genes in monocytes from blood and BAL of Jα18$^{-/-}$ mice compared to WT, arranged in order of Log2FC.

References

1. WHO. 2014. Influenza fact sheet.
2. Reid, A. H., and J. K. Taubenberger. 2003. The origin of the 1918 pandemic influenza virus: a continuing enigma. *Journal of General Virology* 84: 2285-2292.
3. Palese, P., and M. L. Shaw. 2007. Orthomyxoviridae: the viruses and their replication. In *Fields Virology*. D. M. Knipe, and P. M. Howley, eds. Lippincott Williams & Wilkins, Philadelphia, PA. 1647-1689.
4. Noda, T., and Y. Kawaoka. 2010. Structure of influenza virus ribonucleoprotein complexes and their packaging into virions. *Rev Med Virol* 20: 380-391.
5. Obenauer, J. C., J. Denson, P. K. Mehta, X. Su, S. Mukatira, D. B. Finkelstein, X. Xu, J. Wang, J. Ma, Y. Fan, K. M. Rakestraw, R. G. Webster, E. Hoffmann, S. Krauss, J. Zheng, Z. Zhang, and C. W. Naeve. 2006. Large-scale sequence analysis of avian influenza isolates. *Science* 311: 1576-1580.
6. Munster, V. J., C. Baas, P. Lexmond, J. Waldenstrom, A. Wallensten, T. Fransson, G. F. Rimmelzwaan, W. E. Beyer, M. Schutten, B. Olsen, A. D. Osterhaus, and R. A. Fouchier. 2007. Spatial, temporal, and species variation in prevalence of influenza A viruses in wild migratory birds. *PLoS Pathog* 3: e61.
7. Tong, S., Y. Li, P. Rivailler, C. Conrardy, D. A. Castillo, L. M. Chen, S. Recuenco, J. A. Ellison, C. T. Davis, I. A. York, A. S. Turmelle, D. Moran, S. Rogers, M. Shi, Y. Tao, M. R. Weil, K. Tang, L. A. Rowe, S. Sammons, X. Xu, M. Frace, K. A. Lindblade, N. J. Cox, L. J. Anderson, C. E. Rupprecht, and R. O. Donis. 2012. A distinct lineage of influenza A virus from bats. *Proc Natl Acad Sci U S A* 109: 4269-4274.
8. Tong, S., X. Zhu, Y. Li, M. Shi, J. Zhang, M. Bourgeois, H. Yang, X. Chen, S. Recuenco, J. Gomez, L. M. Chen, A. Johnson, Y. Tao, C. Dreyfus, W. Yu, R. McBride, P. J. Carney, A. T. Gilbert, J. Chang, Z. Guo, C. T. Davis, J. C. Paulson, J. Stevens, C. E. Rupprecht, E. C. Holmes, I. A. Wilson, and R. O. Donis. 2013. New world bats harbor diverse influenza A viruses. *PLoS Pathog* 9: e1003657.
9. Wu, Y., B. Tefsen, Y. Shi, and G. F. Gao. 2014. Bat-derived influenza-like viruses H17N10 and H18N11. *Trends Microbiol* 22: 183-191.
10. Landolt, G. A., and C. W. Olsen. 2007. Up to new tricks - a review of cross-species transmission of influenza A viruses. *Anim Health Res Rev* 8: 1-21.
11. Chen, R., and E. C. Holmes. 2006. Avian influenza virus exhibits rapid evolutionary dynamics. *Mol Biol Evol* 23: 2336-2341.
12. Taubenberger, J. K., and D. M. Morens. 2008. The pathology of influenza virus infections. *Annu Rev Pathol* 3: 499-522.
13. Cox, N. J., and K. Subbarao. 2000. Global epidemiology of influenza: past and present. *Annu Rev Med* 51: 407-421.
14. Webster, R. G., W. J. Bean, O. T. Gorman, T. M. Chambers, and Y. Kawaoka. 1992. Evolution and ecology of influenza A viruses. *Microbiology and Molecular Biology Reviews* 56: 152-179.
15. Kilbourne, E. D. 2006. Influenza pandemics of the 20th century. *Emerg Infect Dis* 12: 9-14.
16. Johnson, N. P., and J. Mueller. 2002. Updating the accounts: global mortality of the 1918-1920 "Spanish" influenza pandemic. *Bull Hist Med* 76: 105-115.
17. Scholtissek, C., W. Rohde, V. Von Hoyningen, and R. Rott. 1978. On the origin of the human influenza virus subtypes H2N2 and H3N2. *Virology* 87: 13-20.
18. Kawaoka, Y., S. Krauss, and R. G. Webster. 1989. Avian-to-human transmission of the PB1 gene of influenza A viruses in the 1957 and 1968 pandemics. *J Virol* 63: 4603-4608.

19. Morens, D. M., J. K. Taubenberger, and A. S. Fauci. 2009. The persistent legacy of the 1918 influenza virus. *N Engl J Med* 361: 225-229.
20. Simonsen, L., M. J. Clarke, L. B. Schonberger, N. H. Arden, N. J. Cox, and K. Fukuda. 1998. Pandemic versus epidemic influenza mortality: a pattern of changing age distribution. *J Infect Dis* 178: 53-60.
21. Finckh, E. S., and L. Bader. 1974. Pulmonary damage from Hong Kong influenza. *Aust N Z J Med* 4: 16-22.
22. Guarner, J., W. J. Shieh, J. Dawson, K. Subbarao, M. Shaw, T. Ferebee, T. Morken, K. B. Nolte, A. Freifeld, N. Cox, and S. R. Zaki. 2000. Immunohistochemical and in situ hybridization studies of influenza A virus infection in human lungs. *Am J Clin Pathol* 114: 227-233.
23. Louria, D. B., H. L. Blumenfeld, J. T. Ellis, E. D. Kilbourne, and D. E. Rogers. 1959. Studies on influenza in the pandemic of 1957-1958. II. Pulmonary complications of influenza. *J Clin Invest* 38: 213-265.
24. Guarner, J., C. D. Paddock, W. J. Shieh, M. M. Packard, M. Patel, J. L. Montague, T. M. Uyeki, N. Bhat, A. Balish, S. Lindstrom, A. Klimov, and S. R. Zaki. 2006. Histopathologic and immunohistochemical features of fatal influenza virus infection in children during the 2003-2004 season. *Clin Infect Dis* 43: 132-140.
25. Opie, E. L., F. G. Blake, and T. M. Rivers. 1921. The pathology and bacteriology of pneumonia following influenza. In *Epidemic Respiratory Disease: The Pneumonias and Other Infections of the Respiratory Tract Accompanying Influenza and Measles*. E. L. Opie, F. G. Blake, J. C. Small, and T. M. Rivers, eds. C.V. Mosby Co., St. Louis. 107-281.
26. MacCallum, W. G. 1921. Pathological anatomy of pneumonia associated with influenza. In *Johns Hopkins Hospital Reports*. The Johns Hopkins Press, Baltimore. 149-249.
27. Hers, J. F. P., N. Masurel, and J. Mulder. 1958. Bacteriology and histopathology of the respiratory tract and lungs in fatal Asian Influenza. *The Lancet* 272: 1141-1143.
28. Cowling, B. J., L. M. Jin, E. H. Y. Lau, Q. H. Liao, P. Wu, H. Jiang, T. K. Tsang, J. D. Zheng, V. J. Fang, Z. R. Chang, M. Y. Ni, Q. Zhang, D. K. M. Ip, J. X. Yu, Y. Li, L. P. Wang, W. X. Tu, L. Meng, J. T. Wu, H. M. Luo, Q. Li, Y. L. Shu, Z. J. Li, Z. J. Feng, W. Z. Yang, Y. Wang, G. M. Leung, and H. J. Yu. 2013. Comparative epidemiology of human infections with avian influenza A H7N9 and H5N1 viruses in China: a population-based study of laboratory-confirmed cases. *Lancet* 382: 129-137.
29. Gao, H. N., H. Z. Lu, B. Cao, B. Du, H. Shang, J. H. Gan, S. H. Lu, Y. D. Yang, Q. Fang, Y. Z. Shen, X. M. Xi, Q. Gu, X. M. Zhou, H. P. Qu, Z. Yan, F. M. Li, W. Zhao, Z. C. Gao, G. F. Wang, L. X. Ruan, W. H. Wang, J. Ye, H. F. Cao, X. W. Li, W. H. Zhang, X. C. Fang, J. He, W. F. Liang, J. Xie, M. Zeng, X. Z. Wu, J. Li, Q. Xia, Z. C. Jin, Q. Chen, C. Tang, Z. Y. Zhang, B. M. Hou, Z. X. Feng, J. F. Sheng, N. S. Zhong, and L. J. Li. 2013. Clinical Findings in 111 Cases of Influenza A (H7N9) Virus Infection. *New England Journal of Medicine* 368: 2277-2285.
30. Claas, E. C. J., A. Osterhaus, R. van Beek, J. C. De Jong, G. F. Rimmelzwaan, D. A. Senne, S. Krauss, K. F. Shortridge, and R. G. Webster. 1998. Human influenza A H5N1 virus related to a highly pathogenic avian influenza virus. *Lancet* 351: 472-477.
31. WHO. 2014. Cumulative number of confirmed human cases for avian influenza A (H5N1) reported to WHO, 2003-2014.
32. Powell, T. J., A. Fox, Y. Peng, T. Quynh Mai le, V. T. Lien, N. L. Hang, L. Wang, L. Y. Lee, C. P. Simmons, A. J. McMichael, J. J. Farrar, B. A. Askonas, T. N. Duong, P. Q. Thai, N. T. Thu Yen, S. L. Rowland-Jones, N. T. Hien, P. Horby, and T. Dong. 2012. Identification of H5N1-specific T-cell responses in a high-

risk cohort in vietnam indicates the existence of potential asymptomatic infections. *J Infect Dis* 205: 20-27.

33. Wang, T. T., M. K. Parides, and P. Palese. 2012. Seroevidence for H5N1 influenza infections in humans: meta-analysis. *Science* 335: 1463.
34. Lin, Y. P., M. Shaw, V. Gregory, K. Cameron, W. Lim, A. Klimov, K. Subbarao, Y. Guan, S. Krauss, K. Shortridge, R. Webster, N. Cox, and A. Hay. 2000. Avian-to-human transmission of H9N2 subtype influenza A viruses: Relationship between H9N2 and H5N1 human isolates. *Proc. Natl. Acad. Sci. U. S. A.* 97: 9654-9658.
35. Herfst, S., E. J. Schrauwen, M. Linster, S. Chutinimitkul, E. de Wit, V. J. Munster, E. M. Sorrell, T. M. Bestebroer, D. F. Burke, D. J. Smith, G. F. Rimmelzwaan, A. D. Osterhaus, and R. A. Fouchier. 2012. Airborne transmission of influenza A/H5N1 virus between ferrets. *Science* 336: 1534-1541.
36. Imai, M., T. Watanabe, M. Hatta, S. C. Das, M. Ozawa, K. Shinya, G. Zhong, A. Hanson, H. Katsura, S. Watanabe, C. Li, E. Kawakami, S. Yamada, M. Kiso, Y. Suzuki, E. A. Maher, G. Neumann, and Y. Kawaoka. 2012. Experimental adaptation of an influenza H5 HA confers respiratory droplet transmission to a reassortant H5 HA/H1N1 virus in ferrets. *Nature* 486: 420-428.
37. Biosecurity, T. N. S. A. B. f. 2011. Press Statement on the NSABB Review of H5N1 Research.
38. Ellebedy, A. H., and R. J. Webby. 2009. Influenza vaccines. *Vaccine* 27 Suppl 4: D65-68.
39. Fiers, W., M. De Filette, K. E. Bakkouri, B. Schepens, K. Roose, M. Schotsaert, A. Birkett, and X. Saelens. 2009. M2e-based universal influenza A vaccine. *Vaccine* 27: 6280-6283.
40. Steel, J., A. C. Lowen, T. T. Wang, M. Yondola, Q. Gao, K. Haye, A. Garcia-Sastre, and P. Palese. 2010. Influenza virus vaccine based on the conserved hemagglutinin stalk domain. *MBio* 1.
41. Pleguezuelos, O., S. Robinson, G. A. Stoloff, and W. Caparrós-Wanderley. 2012. Synthetic Influenza vaccine (FLU-v) stimulates cell mediated immunity in a double-blind, randomised, placebo-controlled Phase I trial. *Vaccine* 30: 4655-4660.
42. Palese, P. 2004. Influenza: old and new threats. *Nature Medicine* 10: S82 - S87.
43. Monto, A. S., and N. H. Arden. 1992. Implications of viral resistance to amantadine in control of influenza A. *Clin Infect Dis* 15: 362-367; discussion 368-369.
44. Kiso, M., K. Mitamura, Y. Sakai-Tagawa, K. Shiraishi, C. Kawakami, K. Kimura, F. G. Hayden, N. Sugaya, and Y. Kawaoka. 2004. Resistant influenza A viruses in children treated with oseltamivir: descriptive study. *Lancet* 364: 759-765.
45. Morrison, J., L. Josset, N. Tchitchek, J. Chang, J. A. Belser, D. E. Swayne, M. J. Pantin-Jackwood, T. M. Tumpey, and M. G. Katze. 2014. H7N9 and Other Pathogenic Avian Influenza Viruses Elicit a Three-Pronged Transcriptomic Signature That Is Reminiscent of 1918 Influenza Virus and Is Associated with Lethal Outcome in Mice. *J Virol* 88: 10556-10568.
46. Wise, H. M., A. Foeglein, J. Sun, R. M. Dalton, S. Patel, W. Howard, E. C. Anderson, W. S. Barclay, and P. Digard. 2009. A complicated message: Identification of a novel PB1-related protein translated from influenza A virus segment 2 mRNA. *J Virol* 83: 8021-8031.
47. Backström Winquist, E., S. Abdurahman, A. Tranell, S. Lindström, S. Tingsborg, and S. Schwartz. 2012. Inefficient splicing of segment 7 and 8 mRNAs is an inherent property of influenza virus A/Brevig Mission/1918/1 (H1N1) that causes elevated expression of NS1 protein. *Virology* 422: 46-58.

48. Vreede, F. T., A. K. Ng, P. C. Shaw, and E. Fodor. 2011. Stabilization of influenza virus replication intermediates is dependent on the RNA-binding but not the homo-oligomerization activity of the viral nucleoprotein. *J Virol* 85: 12073-12078.
49. Das, K., J. M. Aramini, L. C. Ma, R. M. Krug, and E. Arnold. 2010. Structures of influenza A proteins and insights into antiviral drug targets. *Nat Struct Mol Biol* 17: 530-538.
50. Wiley, D. C., and J. J. Skehel. 1987. The structure and function of the hemagglutinin membrane glycoprotein of influenza virus. *Annu Rev Biochem* 56: 365-394.
51. Ward, C. W. 1981. Structure of the Influenza-virus hemagglutinin. *Current Topics in Microbiology and Immunology* 94-5: 1-74.
52. Wiley, D. C., J. J. Skehel, and M. Waterfield. 1977. Evidence from studies with a cross-linking reagent that hemagglutinin of Influenza-virus is a trimer. *Virology* 79: 446-448.
53. Huang, R. T. C., R. Rott, and H. D. Klenk. 1981. Influenza viruses cause hemolysis and fusion of cells. *Virology* 110: 243-247.
54. Durrer, P., C. Galli, S. Hoenke, C. Corti, R. Glück, T. Vorherr, and J. Brunner. 1996. H+-induced membrane insertion of influenza virus hemagglutinin involves the HA2 amino-terminal fusion peptide but not the coiled coil region. *J. Biol. Chem.* 271: 13417-13421.
55. Pinto, L. H., L. J. Holsinger, and R. A. Lamb. 1992. Influenza virus M2 protein has ion channel activity. *Cell* 69: 517-528.
56. Neumann, G., T. Noda, and Y. Kawaoka. 2009. Emergence and pandemic potential of swine-origin H1N1 influenza virus. *Nature* 459: 931-939.
57. Wu, W. W., Y. H. Sun, and N. Pante. 2007. Nuclear import of influenza A viral ribonucleoprotein complexes is mediated by two nuclear localization sequences on viral nucleoprotein. *Virol J* 4: 49.
58. O'Neill, R. E., R. Jaskunas, G. Blobel, P. Palese, and J. Moroianu. 1995. Nuclear import of influenza virus RNA can be mediated by viral nucleoprotein and transport factors required for protein import. *J Biol Chem* 270: 22701-22704.
59. Babcock, H. P., C. Chen, and X. Zhuang. 2004. Using single-particle tracking to study nuclear trafficking of viral genes. *Biophys J* 87: 2749-2758.
60. Gorlich, D., F. Vogel, A. D. Mills, E. Hartmann, and R. A. Laskey. 1995. Distinct functions for the two importin subunits in nuclear protein import. *Nature* 377: 246-248.
61. Baudin, F., C. Bach, S. Cusack, and R. W. Ruigrok. 1994. Structure of influenza virus RNP. I. Influenza virus nucleoprotein melts secondary structure in panhandle RNA and exposes the bases to the solvent. *EMBO J* 13: 3158-3165.
62. Crow, M., T. Deng, M. Addley, and G. G. Brownlee. 2004. Mutational analysis of the influenza virus cRNA promoter and identification of nucleotides critical for replication. *Journal of Virology* 78: 6263-6270.
63. Plotch, S. J., M. Bouloy, I. Ulmanen, and R. M. Krug. 1981. A unique cap(m7GpppXm)-dependent influenza virion endonuclease cleaves capped RNAs to generate the primers that initiate viral RNA transcription. *Cell* 23: 847-858.
64. Ulmanen, I., B. A. Broni, and R. M. Krug. 1981. Role of two of the influenza virus core P proteins in recognizing cap 1 structures (m7GpppNm) on RNAs and in initiating viral RNA transcription. *Proc Natl Acad Sci U S A* 78: 7355-7359.
65. Li, M. L., P. Rao, and R. M. Krug. 2001. The active sites of the influenza cap-dependent endonuclease are on different polymerase subunits. *EMBO J* 20: 2078-2086.

66. Newcomb, L. L., R. L. Kuo, Q. Ye, Y. Jiang, Y. J. Tao, and R. M. Krug. 2009. Interaction of the influenza a virus nucleocapsid protein with the viral RNA polymerase potentiates unprimed viral RNA replication. *J Virol* 83: 29-36.
67. Burgui, I., E. Yanguez, N. Sonenberg, and A. Nieto. 2007. Influenza virus mRNA translation revisited: is the eIF4E cap-binding factor required for viral mRNA translation? *J Virol* 81: 12427-12438.
68. Shimizu, T., N. Takizawa, K. Watanabe, K. Nagata, and N. Kobayashi. 2011. Crucial role of the influenza virus NS2 (NEP) C-terminal domain in M1 binding and nuclear export of vRNP. *FEBS Lett* 585: 41-46.
69. Neumann, G., M. T. Hughes, and Y. Kawaoka. 2000. Influenza A virus NS2 protein mediates vRNP nuclear export through NES-independent interaction with hCRM1. *EMBO J* 19: 6751-6758.
70. Nemeroff, M. E., S. M. Barabino, Y. Li, W. Keller, and R. M. Krug. 1998. Influenza virus NS1 protein interacts with the cellular 30 kDa subunit of CPSF and inhibits 3'end formation of cellular pre-mRNAs. *Mol Cell* 1: 991-1000.
71. Shimizu, K., A. Iguchi, R. Gomyou, and Y. Ono. 1999. Influenza virus inhibits cleavage of the HSP70 pre-mRNAs at the polyadenylation site. *Virology* 254: 213-219.
72. Scheiffele, P., A. Rietveld, T. Wilk, and K. Simons. 1999. Influenza viruses select ordered lipid domains during budding from the plasma membrane. *J Biol Chem* 274: 2038-2044.
73. Nayak, D. P., T. M. Chambers, and R. K. Akkina. 1985. Defective-interfering (DI) RNAs of influenza viruses: origin, structure, expression, and interference. *Curr Top Microbiol Immunol* 114: 103-151.
74. Fujii, Y., H. Goto, T. Watanabe, T. Yoshida, and Y. Kawaoka. 2003. Selective incorporation of influenza virus RNA segments into virions. *Proc Natl Acad Sci U S A* 100: 2002-2007.
75. Muramoto, Y., A. Takada, K. Fujii, T. Noda, K. Iwatsuki-Horimoto, S. Watanabe, T. Horimoto, H. Kida, and Y. Kawaoka. 2006. Hierarchy among viral RNA (vRNA) segments in their role in vRNA incorporation into influenza A virions. *J Virol* 80: 2318-2325.
76. Nayak, D. P., E. K.-W. Hui, and S. Barman. 2004. Assembly and budding of influenza virus. *Virus Research* 106: 147-165.
77. Bourmakina, S. V., and A. Garcia-Sastre. 2003. Reverse genetics studies on the filamentous morphology of influenza A virus. *J Gen Virol* 84: 517-527.
78. Varghese, J. N., and P. M. Colman. 1991. Three-dimensional structure of the neuraminidase of influenza virus A/Tokyo/3/67 at 2.2 A resolution. *J Mol Biol* 221: 473-486.
79. Matrosovich, M. N., T. Y. Matrosovich, T. Gray, N. A. Roberts, and H. D. Klenk. 2004. Neuraminidase is important for the initiation of influenza virus infection in human airway epithelium. *J Virol* 78: 12665-12667.
80. Dawood, F. S., S. Jain, L. Finelli, M. W. Shaw, S. Lindstrom, R. J. Garten, L. V. Gubareva, X. Xu, C. B. Bridges, and T. M. Uyeki. 2009. Emergence of a novel swine-origin influenza A (H1N1) virus in humans. *N Engl J Med* 360: 2605-2615.
81. Webby, R. J., S. L. Swenson, S. L. Krauss, P. J. Gerrish, S. M. Goyal, and R. G. Webster. 2000. Evolution of swine H3N2 influenza viruses in the United States. *J Virol* 74: 8243-8251.
82. Zhou, N. N., D. A. Senne, J. S. Landgraf, S. L. Swenson, G. Erickson, K. Rossow, L. Liu, K. Yoon, S. Krauss, and R. G. Webster. 1999. Genetic reassortment of avian, swine, and human influenza A viruses in American pigs. *J Virol* 73: 8851-8856.
83. Vincent, A. L., K. M. Lager, W. J. Ma, P. Lekcharoensuk, M. R. Gramer, C. Loiacono, and J. A. Richt. 2006. Evaluation of hemagglutinin subtype 1 swine influenza viruses from the United States. *Veterinary Microbiology* 118: 212-222.

84. Dunham, E. J., V. G. Dugan, E. K. Kaser, S. E. Perkins, I. H. Brown, E. C. Holmes, and J. K. Taubenberger. 2009. Different evolutionary trajectories of European avian-like and classical swine H1N1 influenza A viruses. *J Virol* 83: 5485-5494.
85. Tscherne, D. M., and A. Garcia-Sastre. 2011. Virulence determinants of pandemic influenza viruses. *J Clin Invest* 121: 6-13.
86. Smith, G. J. D., D. Vijaykrishna, J. Bahl, S. J. Lycett, M. Worobey, O. G. Pybus, S. K. Ma, C. L. Cheung, J. Raghwani, S. Bhatt, J. S. M. Peiris, Y. Guan, and A. Rambaut. 2009. Origins and evolutionary genomics of the 2009 swine-origin H1N1 influenza A epidemic. *Nature* 459: 1122-U1107.
87. 1919. Public Health Weekly Reports for AUGUST 15, 1919. *Public Health Rep* 34: 1823-1926.
88. Brundage, J. F. 2006. Cases and deaths during influenza pandemics in the United States. *Am J Prev Med* 31: 252-256.
89. Kelly, H., H. A. Peck, K. L. Laurie, P. Wu, H. Nishiura, and B. J. Cowling. 2011. The age-specific cumulative incidence of infection with pandemic influenza H1N1 2009 was similar in various countries prior to vaccination. *PLoS ONE* 6: e21828.
90. Miller, E., K. Hoschler, P. Hardelid, E. Stanford, N. Andrews, and M. Zambon. 2010. Incidence of 2009 pandemic influenza A H1N1 infection in England: a cross-sectional serological study. *Lancet* 375: 1100-1108.
91. Gras, S., L. Kedzierski, S. A. Valkenburg, K. Laurie, Y. C. Liu, J. T. Denholm, M. J. Richards, G. F. Rimmelzwaan, A. Kelso, P. C. Doherty, S. J. Turner, J. Rossjohn, and K. Kedzierska. 2010. Cross-reactive CD8+ T-cell immunity between the pandemic H1N1-2009 and H1N1-1918 influenza A viruses. *Proc Natl Acad Sci U S A* 107: 12599-12604.
92. Xu, R., D. C. Ekiert, J. C. Krause, R. Hai, J. E. Crowe, Jr., and I. A. Wilson. 2010. Structural basis of preexisting immunity to the 2009 H1N1 pandemic influenza virus. *Science* 328: 357-360.
93. Sridhar, S., S. Begom, A. Bermingham, K. Hoschler, W. Adamson, W. Carman, T. Bean, W. Barclay, J. J. Deeks, and A. Lalvani. 2013. Cellular immune correlates of protection against symptomatic pandemic influenza. *Nat Med* 19: 1305-1312.
94. Tu, W., H. Mao, J. Zheng, Y. Liu, S. S. Chiu, G. Qin, P. L. Chan, K. T. Lam, J. Guan, L. Zhang, Y. Guan, K. Y. Yuen, J. S. Peiris, and Y. L. Lau. 2010. Cytotoxic T lymphocytes established by seasonal human influenza cross-react against 2009 pandemic H1N1 influenza virus. *J Virol* 84: 6527-6535.
95. Epstein, S. L. 2006. Prior H1N1 influenza infection and susceptibility of Cleveland Family Study participants during the H2N2 pandemic of 1957: an experiment of nature. *J Infect Dis* 193: 49-53.
96. Slepushkin, A. N. 1959. The effect of a previous attack of A1 influenza on susceptibility to A2 virus during the 1957 outbreak. *Bull World Health Organ* 20: 297-301.
97. Chi, C. Y., C. C. Liu, C. C. Lin, H. C. Wang, Y. T. Cheng, C. M. Chang, and J. R. Wang. 2010. Preexisting antibody response against 2009 pandemic influenza H1N1 viruses in the Taiwanese population. *Clin Vaccine Immunol* 17: 1958-1962.
98. Rizzo, C., M. C. Rota, A. Bella, V. Alfonsi, S. Declich, M. G. Caporali, A. Ranghiasci, G. Lapini, S. Piccirella, S. Salmaso, and E. Montomoli. 2010. Cross-reactive antibody responses to the 2009 A/H1N1v influenza virus in the Italian population in the pre-pandemic period. *Vaccine* 28: 3558-3562.
99. Ikonen, N., M. Strengell, L. Kinnunen, P. Osterlund, J. Pirhonen, M. Broman, I. Davidkin, T. Ziegler, and I. Julkunen. 2010. High frequency of cross-reacting antibodies against 2009 pandemic influenza A(H1N1) virus among the elderly in Finland. *Euro Surveill* 15.

100. Hancock, K., V. Veguilla, X. H. Lu, W. M. Zhong, E. N. Butler, H. Sun, F. Liu, L. B. Dong, J. R. DeVos, P. M. Gargiullo, T. L. Brammer, N. J. Cox, T. M. Tumpey, and J. M. Katz. 2009. Cross-Reactive Antibody Responses to the 2009 Pandemic H1N1 Influenza Virus. *New England Journal of Medicine* 361: 1945-1952.
101. Zarychanski, R., T. L. Stuart, A. Kumar, S. Doucette, L. Elliott, J. Kettner, and F. Plummer. 2010. Correlates of severe disease in patients with 2009 pandemic influenza (H1N1) virus infection. *CMAJ* 182: 257-264.
102. Nguyen-Van-Tam, J. S., P. J. M. Openshaw, A. Hashim, E. M. Gadd, W. S. Lim, M. G. Semple, R. C. Read, B. L. Taylor, S. J. Brett, J. McMenamin, J. E. Enstone, C. Armstrong, and K. G. Nicholson. 2010. Risk factors for hospitalisation and poor outcome with pandemic A/H1N1 influenza: United Kingdom first wave (May–September 2009). *Thorax* 65: 645-651.
103. Horby, P., H. Sudoyo, V. Viprakasit, A. Fox, P. Q. Thai, H. Yu, S. Davila, M. Hibberd, S. J. Dunstan, Y. Monteerarat, J. J. Farrar, S. Marzuki, and N. T. Hien. 2010. What is the evidence of a role for host genetics in susceptibility to influenza A/H5N1? *Epidemiol Infect* 138: 1550-1558.
104. Juno, J., K. R. Fowke, and Y. Keynan. 2012. Immunogenetic factors associated with severe respiratory illness caused by zoonotic H1N1 and H5N1 influenza viruses. *Clin Dev Immunol* 2012: 797180.
105. Antonopoulou, A., F. Baziaka, T. Tsaganos, M. Raftogiannis, P. Koutoukas, A. Spyridaki, M. Mouktaroudi, A. Kotsaki, A. Savva, M. Georgitsi, and E. J. Giamarellos-Bourboulis. 2012. Role of tumor necrosis factor gene single nucleotide polymorphisms in the natural course of 2009 influenza A H1N1 virus infection. *Int J Infect Dis* 16: e204-208.
106. Everitt, A. R., S. Clare, T. Pertel, S. P. John, R. S. Wash, S. E. Smith, C. R. Chin, E. M. Feeley, J. S. Sims, D. J. Adams, H. M. Wise, L. Kane, D. Goulding, P. Digard, V. Anttila, J. K. Baillie, T. S. Walsh, D. A. Hume, A. Palotie, Y. Xue, V. Colonna, C. Tyler-Smith, J. Dunning, S. B. Gordon, R. L. Smyth, P. J. Openshaw, G. Dougan, A. L. Brass, and P. Kellam. 2012. IFITM3 restricts the morbidity and mortality associated with influenza. *Nature* 484: 519-523.
107. Zhang, Y. H., Y. Zhao, N. Li, Y. C. Peng, E. Giannoulatou, R. H. Jin, H. P. Yan, H. Wu, J. H. Liu, N. Liu, D. Y. Wang, Y. L. Shu, L. P. Ho, P. Kellam, A. McMichael, and T. Dong. 2013. Interferon-induced transmembrane protein-3 genetic variant rs12252-C is associated with severe influenza in Chinese individuals. *Nat Commun* 4: 1418.
108. Keynan, Y., J. Juno, A. Meyers, T. B. Ball, A. Kumar, E. Rubinstein, and K. R. Fowke. 2010. Chemokine receptor 5 big up tri, open32 allele in patients with severe pandemic (H1N1) 2009. *Emerg Infect Dis* 16: 1621-1622.
109. To, K. K., J. Zhou, Y. Q. Song, I. F. Hung, W. C. Ip, Z. S. Cheng, A. S. Chan, R. Y. Kao, A. K. Wu, S. Chau, W. K. Luk, M. S. Ip, K. H. Chan, and K. Y. Yuen. 2014. Surfactant protein B gene polymorphism is associated with severe influenza. *Chest* 145: 1237-1243.
110. Lindenmann, J. 1962. Resistance of mice to mouse-adapted influenza A virus. *Virology* 16: 203-204.
111. Dittmann, J., S. Stertz, D. Grimm, J. Steel, A. Garcia-Sastre, O. Haller, and G. Kochs. 2008. Influenza A virus strains differ in sensitivity to the antiviral action of Mx-GTPase. *J Virol* 82: 3624-3631.
112. McMichael, A. J., A. Ting, H. J. Zweerink, and B. A. Askonas. 1977. HLA restriction of cell-mediated lysis of influenza virus-infected human cells. *Nature* 270: 524-526.
113. Hertz, T., C. M. Oshansky, P. L. Roddam, J. P. DeVincenzo, M. A. Caniza, N. Jojic, S. Mallal, E. Phillips, I. James, M. E. Halloran, P. G. Thomas, and L. Corey. 2013. HLA targeting efficiency correlates with human T-cell response

magnitude and with mortality from influenza A infection. *Proc Natl Acad Sci U S A* 110: 13492-13497.
114. Imai, M., and Y. Kawaoka. 2012. The role of receptor binding specificity in interspecies transmission of influenza viruses. *Curr Opin Virol* 2: 160-167.
115. Nicholls, J. M., R. W. Chan, R. J. Russell, G. M. Air, and J. S. Peiris. 2008. Evolving complexities of influenza virus and its receptors. *Trends Microbiol* 16: 149-157.
116. Harduin-Lepers, A., R. Mollicone, P. Delannoy, and R. Oriol. 2005. The animal sialyltransferases and sialyltransferase-related genes: a phylogenetic approach. *Glycobiology* 15: 805-817.
117. Rogers, G. N., and B. L. D'Souza. 1989. Receptor binding properties of human and animal H1 influenza virus isolates. *Virology* 173: 317-322.
118. Shinya, K., M. Ebina, S. Yamada, M. Ono, N. Kasai, and Y. Kawaoka. 2006. Avian flu: influenza virus receptors in the human airway. *Nature* 440: 435-436.
119. Uiprasertkul, M., P. Puthavathana, K. Sangsiriwut, P. Pooruk, K. Srisook, M. Peiris, J. M. Nicholls, K. Chokephaibulkit, N. Vanprapar, and P. Auewarakul. 2005. Influenza A H5N1 replication sites in humans. *Emerg Infect Dis* 11: 1036-1041.
120. van Riel, D., L. M. Leijten, M. de Graaf, J. Y. Siegers, K. R. Short, M. I. Spronken, E. J. Schrauwen, R. A. Fouchier, A. D. Osterhaus, and T. Kuiken. 2013. Novel avian-origin influenza A (H7N9) virus attaches to epithelium in both upper and lower respiratory tract of humans. *Am J Pathol* 183: 1137-1143.
121. Matrosovich, M., A. Tuzikov, N. Bovin, A. Gambaryan, A. Klimov, M. R. Castrucci, I. Donatelli, and Y. Kawaoka. 2000. Early alterations of the receptor-binding properties of H1, H2, and H3 avian influenza virus hemagglutinins after their introduction into mammals. *J Virol* 74: 8502-8512.
122. Glaser, L., J. Stevens, D. Zamarin, I. A. Wilson, A. Garcia-Sastre, T. M. Tumpey, C. F. Basler, J. K. Taubenberger, and P. Palese. 2005. A single amino acid substitution in 1918 influenza virus hemagglutinin changes receptor binding specificity. *J Virol* 79: 11533-11536.
123. Nelli, R. K., S. V. Kuchipudi, G. A. White, B. B. Perez, S. P. Dunham, and K. C. Chang. 2010. Comparative distribution of human and avian type sialic acid influenza receptors in the pig. *BMC Vet Res* 6: 4.
124. Ito, T., J. N. Couceiro, S. Kelm, L. G. Baum, S. Krauss, M. R. Castrucci, I. Donatelli, H. Kida, J. C. Paulson, R. G. Webster, and Y. Kawaoka. 1998. Molecular basis for the generation in pigs of influenza A viruses with pandemic potential. *J Virol* 72: 7367-7373.
125. Boon, A. C., D. Finkelstein, M. Zheng, G. Liao, J. Allard, K. Klumpp, R. Webster, G. Peltz, and R. J. Webby. 2011. H5N1 influenza virus pathogenesis in genetically diverse mice is mediated at the level of viral load. *MBio* 2.
126. Hatta, Y., K. Hershberger, K. Shinya, S. C. Proll, R. R. Dubielzig, M. Hatta, M. G. Katze, Y. Kawaoka, and M. Suresh. 2010. Viral replication rate regulates clinical outcome and CD8 T cell responses during highly pathogenic H5N1 influenza virus infection in mice. *PLoS Pathog* 6: e1001139.
127. Lee, C. K., H. K. Lee, T. P. Loh, F. Y. Lai, P. A. Tambyah, L. Chiu, E. S. Koay, and J. W. Tang. 2011. Comparison of pandemic (H1N1) 2009 and seasonal influenza viral loads, Singapore. *Emerg Infect Dis* 17: 287-291.
128. Pan, W., Z. Dong, F. Li, W. Meng, L. Feng, X. Niu, C. Li, Q. Luo, Z. Li, C. Sun, and L. Chen. 2013. Visualizing influenza virus infection in living mice. *Nat Commun* 4.
129. Chen, W., P. A. Calvo, D. Malide, J. Gibbs, U. Schubert, I. Bacik, S. Basta, R. O'Neill, J. Schickli, P. Palese, P. Henklein, J. R. Bennink, and J. W. Yewdell. 2001. A novel influenza A virus mitochondrial protein that induces cell death. *Nat Med* 7: 1306-1312.

130. Jaworska, J., F. Coulombe, J. Downey, F. Tzelepis, K. Shalaby, I. Tattoli, J. Berube, S. Rousseau, J. G. Martin, S. E. Girardin, J. A. McCullers, and M. Divangahi. 2014. NLRX1 prevents mitochondrial induced apoptosis and enhances macrophage antiviral immunity by interacting with influenza virus PB1-F2 protein. *Proc Natl Acad Sci U S A* 111: E2110-2119.
131. McAuley, J. L., F. Hornung, K. L. Boyd, A. M. Smith, R. McKeon, J. Bennink, J. W. Yewdell, and J. A. McCullers. 2007. Expression of the 1918 influenza A virus PB1-F2 enhances the pathogenesis of viral and secondary bacterial pneumonia. *Cell Host Microbe* 2: 240-249.
132. Conenello, G. M., D. Zamarin, L. A. Perrone, T. Tumpey, and P. Palese. 2007. A single mutation in the PB1-F2 of H5N1 (HK/97) and 1918 influenza A viruses contributes to increased virulence. *PLoS Pathog* 3: 1414-1421.
133. Wang, T. T., and P. Palese. 2009. Unraveling the mystery of swine influenza virus. *Cell* 137: 983-985.
134. Hai, R., M. Schmolke, Z. T. Varga, B. Manicassamy, T. T. Wang, J. A. Belser, M. B. Pearce, A. Garcia-Sastre, T. M. Tumpey, and P. Palese. 2010. PB1-F2 expression by the 2009 pandemic H1N1 influenza virus has minimal impact on virulence in animal models. *J Virol* 84: 4442-4450.
135. Pena, L., A. L. Vincent, C. L. Loving, J. N. Henningson, K. M. Lager, A. Lorusso, and D. R. Perez. 2012. Restored PB1-F2 in the 2009 pandemic H1N1 influenza virus has minimal effects in swine. *J Virol* 86: 5523-5532.
136. Kilander, A., R. Rykkvin, S. G. Dudman, and O. Hungnes. 2010. Observed association between the HA1 mutation D222G in the 2009 pandemic influenza A(H1N1) virus and severe clinical outcome, Norway 2009-2010. *Euro Surveill* 15.
137. Chutinimitkul, S., S. Herfst, J. Steel, A. C. Lowen, J. Ye, D. van Riel, E. J. Schrauwen, T. M. Bestebroer, B. Koel, D. F. Burke, K. H. Sutherland-Cash, C. S. Whittleston, C. A. Russell, D. J. Wales, D. J. Smith, M. Jonges, A. Meijer, M. Koopmans, G. F. Rimmelzwaan, T. Kuiken, A. D. Osterhaus, A. Garcia-Sastre, D. R. Perez, and R. A. Fouchier. 2010. Virulence-associated substitution D222G in the hemagglutinin of 2009 pandemic influenza A(H1N1) virus affects receptor binding. *J Virol* 84: 11802-11813.
138. Li, S., J. Schulman, S. Itamura, and P. Palese. 1993. Glycosylation of neuraminidase determines the neurovirulence of influenza A/WSN/33 virus. *J Virol* 67: 6667-6673.
139. Geiss, G. K., M. Salvatore, T. M. Tumpey, V. S. Carter, X. Wang, C. F. Basler, J. K. Taubenberger, R. E. Bumgarner, P. Palese, M. G. Katze, and A. Garcia-Sastre. 2002. Cellular transcriptional profiling in influenza A virus-infected lung epithelial cells: the role of the nonstructural NS1 protein in the evasion of the host innate defense and its potential contribution to pandemic influenza. *Proc Natl Acad Sci U S A* 99: 10736-10741.
140. Iwasaki, A., and P. S. Pillai. 2014. Innate immunity to influenza virus infection. *Nat Rev Immunol* 14: 315-328.
141. Kim, T. S., and T. J. Braciale. 2009. Respiratory dendritic cell subsets differ in their capacity to support the induction of virus-specific cytotoxic CD8+ T cell responses. *PLoS ONE* 4: e4204.
142. Tamura, S., and T. Kurata. 2004. Defense mechanisms against influenza virus infection in the respiratory tract mucosa. *Jpn J Infect Dis* 57: 236-247.
143. Lawrence, C. W., and T. J. Braciale. 2004. Activation, differentiation, and migration of naive virus-specific CD8+ T cells during pulmonary influenza virus infection. *J Immunol* 173: 1209-1218.
144. Wilkinson, T. M., C. K. F. Li, C. S. C. Chui, A. K. Y. Huang, M. Perkins, J. C. Liebner, R. Lambkin-Williams, A. Gilbert, J. Oxford, B. Nicholas, K. J. Staples, T. Dong, D. C. Douek, A. J. McMichael, and X.-N. Xu. 2012. Preexisting

influenza-specific CD4+ T cells correlate with disease protection against influenza challenge in humans. *Nat Med* 18: 274-280.
145. Zhu, J., and W. E. Paul. 2010. Peripheral CD4+ T-cell differentiation regulated by networks of cytokines and transcription factors. *Immunol Rev* 238: 247-262.
146. Kamperschroer, C., J. P. Dibble, D. L. Meents, P. L. Schwartzberg, and S. L. Swain. 2006. SAP is required for Th cell function and for immunity to influenza. *J Immunol* 177: 5317-5327.
147. Brown, D. M., A. M. Dilzer, D. L. Meents, and S. L. Swain. 2006. CD4 T cell-mediated protection from lethal influenza: perforin and antibody-mediated mechanisms give a one-two punch. *J Immunol* 177: 2888-2898.
148. Moffat, J. M., T. Gebhardt, P. C. Doherty, S. J. Turner, and J. D. Mintern. 2009. Granzyme A expression reveals distinct cytolytic CTL subsets following influenza A virus infection. *Eur J Immunol* 39: 1203-1210.
149. La Gruta, N. L., S. J. Turner, and P. C. Doherty. 2004. Hierarchies in cytokine expression profiles for acute and resolving influenza virus-specific CD8+ T cell responses: correlation of cytokine profile and TCR avidity. *J Immunol* 172: 5553-5560.
150. Assarsson, E., H. H. Bui, J. Sidney, Q. Zhang, J. Glenn, C. Oseroff, I. N. Mbawuike, J. Alexander, M. J. Newman, H. Grey, and A. Sette. 2008. Immunomic analysis of the repertoire of T-cell specificities for influenza A virus in humans. *J Virol* 82: 12241-12251.
151. La Gruta, N. L., K. Kedzierska, J. Stambas, and P. C. Doherty. 2007. A question of self-preservation: immunopathology in influenza virus infection. *Immunol Cell Biol* 85: 85-92.
152. Waffarn, E. E., and N. Baumgarth. 2011. Protective B cell responses to flu--no fluke! *J Immunol* 186: 3823-3829.
153. de Jong, J. C., A. M. Palache, W. E. Beyer, G. F. Rimmelzwaan, A. C. Boon, and A. D. Osterhaus. 2003. Haemagglutination-inhibiting antibody to influenza virus. *Dev Biol (Basel)* 115: 63-73.
154. Johansson, B. E., D. J. Bucher, and E. D. Kilbourne. 1989. Purified influenza virus hemagglutinin and neuraminidase are equivalent in stimulation of antibody response but induce contrasting types of immunity to infection. *J Virol* 63: 1239-1246.
155. Schmolke, M., and A. García-Sastre. 2010. Evasion of innate and adaptive immune responses by influenza A virus. *Cellular Microbiology* 12: 873-880.
156. Miao, H., J. A. Hollenbaugh, M. S. Zand, J. Holden-Wiltse, T. R. Mosmann, A. S. Perelson, H. Wu, and D. J. Topham. 2010. Quantifying the early immune response and adaptive immune response kinetics in mice infected with influenza A virus. *J Virol* 84: 6687-6698.
157. Ronni, T., T. Sareneva, J. Pirhonen, and I. Julkunen. 1995. Activation of IFN-alpha, IFN-gamma, MxA, and IFN regulatory factor 1 genes in influenza A virus-infected human peripheral blood mononuclear cells. *J Immunol* 154: 2764-2774.
158. Davidson, S., S. Crotta, T. M. McCabe, and A. Wack. 2014. Pathogenic potential of interferon αβ in acute influenza infection. *Nat Commun* 5.
159. Julkunen, I., K. Melén, M. Nyqvist, J. Pirhonen, T. Sareneva, and S. Matikainen. 2000. Inflammatory responses in influenza A virus infection. *Vaccine* 19: S32-S37.
160. Tripathi, S., M. R. White, and K. L. Hartshorn. 2013. The amazing innate immune response to influenza A virus infection. *Innate Immun*.
161. Pichlmair, A., O. Schulz, C. P. Tan, T. I. Naslund, P. Liljestrom, F. Weber, and C. Reis e Sousa. 2006. RIG-I-mediated antiviral responses to single-stranded RNA bearing 5'-phosphates. *Science* 314: 997-1001.
162. Takeuchi, O., and S. Akira. 2008. MDA5/RIG-I and virus recognition. *Curr Opin Immunol* 20: 17-22.

163. Le Goffic, R., J. Pothlichet, D. Vitour, T. Fujita, E. Meurs, M. Chignard, and M. Si-Tahar. 2007. Cutting Edge: Influenza A virus activates TLR3-dependent inflammatory and RIG-I-dependent antiviral responses in human lung epithelial cells. *J Immunol* 178: 3368-3372.
164. Diebold, S. S., T. Kaisho, H. Hemmi, S. Akira, and C. Reis e Sousa. 2004. Innate antiviral responses by means of TLR7-mediated recognition of single-stranded RNA. *Science* 303: 1529-1531.
165. Wang, J. P., P. Liu, E. Latz, D. T. Golenbock, R. W. Finberg, and D. H. Libraty. 2006. Flavivirus activation of plasmacytoid dendritic cells delineates key elements of TLR7 signaling beyond endosomal recognition. *J Immunol* 177: 7114-7121.
166. Schulz, O., S. S. Diebold, M. Chen, T. I. Naslund, M. A. Nolte, L. Alexopoulou, Y.-T. Azuma, R. A. Flavell, P. Liljestrom, and C. Reis e Sousa. 2005. Toll-like receptor 3 promotes cross-priming to virus-infected cells. *Nature* 433: 887-892.
167. Le Goffic, R., V. Balloy, M. Lagranderie, L. Alexopoulou, N. Escriou, R. Flavell, M. Chignard, and M. Si-Tahar. 2006. Detrimental contribution of the Toll-like receptor (TLR)3 to influenza A virus-induced acute pneumonia. *PLoS Pathog* 2: e53.
168. Imai, Y., K. Kuba, G. G. Neely, R. Yaghubian-Malhami, T. Perkmann, G. van Loo, M. Ermolaeva, R. Veldhuizen, Y. H. Leung, H. Wang, H. Liu, Y. Sun, M. Pasparakis, M. Kopf, C. Mech, S. Bavari, J. S. Peiris, A. S. Slutsky, S. Akira, M. Hultqvist, R. Holmdahl, J. Nicholls, C. Jiang, C. J. Binder, and J. M. Penninger. 2008. Identification of oxidative stress and Toll-like receptor 4 signaling as a key pathway of acute lung injury. *Cell* 133: 235-249.
169. Pang, I. K., and A. Iwasaki. 2011. Inflammasomes as mediators of immunity against influenza virus. *Trends Immunol* 32: 34-41.
170. Thomas, P. G., P. Dash, J. R. Aldridge, Jr., A. H. Ellebedy, C. Reynolds, A. J. Funk, W. J. Martin, M. Lamkanfi, R. J. Webby, K. L. Boyd, P. C. Doherty, and T. D. Kanneganti. 2009. The intracellular sensor NLRP3 mediates key innate and healing responses to influenza A virus via the regulation of caspase-1. *Immunity* 30: 566-575.
171. Ichinohe, T., H. K. Lee, Y. Ogura, R. Flavell, and A. Iwasaki. 2009. Inflammasome recognition of influenza virus is essential for adaptive immune responses. *Journal of Experimental Medicine* 206: 79-87.
172. Brydon, E. W., H. Smith, and C. Sweet. 2003. Influenza A virus-induced apoptosis in bronchiolar epithelial (NCI-H292) cells limits pro-inflammatory cytokine release. *J Gen Virol* 84: 2389-2400.
173. Tsuru, S., H. Fujisawa, M. Taniguchi, Y. Zinnaka, and K. Nomoto. 1987. Mechanism of protection during the early phase of a generalized viral infection. II. Contribution of polymorphonuclear leukocytes to protection against intravenous infection with influenza virus. *J Gen Virol* 68 (Pt 2): 419-424.
174. Wareing, M. D., A. L. Shea, C. A. Inglis, P. B. Dias, and S. R. Sarawar. 2007. CXCR2 is required for neutrophil recruitment to the lung during influenza virus infection, but is not essential for viral clearance. *Viral Immunol* 20: 369-378.
175. Winternitz, M. C., I. M. Wason, and F. P. McNamara. 1920. *The Pathology of Influenza*. Yale Univ. Press, New Haven.
176. Skoner, D. P., D. A. Gentile, A. Patel, and W. J. Doyle. 1999. Evidence for cytokine mediation of disease expression in adults experimentally infected with influenza A virus. *J Infect Dis* 180: 10-14.
177. Virelizier, J. L., A. C. Allison, and G. C. Schild. 1979. Immune responses to influenza virus in the mouse, and their role in control of the infection. *Br Med Bull* 35: 65-68.
178. Matsukura, S., F. Kokubu, H. Noda, H. Tokunaga, and M. Adachi. 1996. Expression of IL-6, IL-8, and RANTES on human bronchial epithelial cells, NCI-H292, induced by influenza virus A. *J Allergy Clin Immunol* 98: 1080-1087.

179. Adachi, M., S. Matsukura, H. Tokunaga, and F. Kokubu. 1997. Expression of cytokines on human bronchial epithelial cells induced by influenza virus A. *Int Arch Allergy Immunol* 113: 307-311.
180. Sprenger, H., R. G. Meyer, A. Kaufmann, D. Bussfeld, E. Rischkowsky, and D. Gemsa. 1996. Selective induction of monocyte and not neutrophil-attracting chemokines after influenza A virus infection. *J Exp Med* 184: 1191-1196.
181. Hashimoto, Y., T. Moki, T. Takizawa, A. Shiratsuchi, and Y. Nakanishi. 2007. Evidence for phagocytosis of influenza virus-infected, apoptotic cells by neutrophils and macrophages in mice. *J Immunol* 178: 2448-2457.
182. Watanabe, Y., Y. Hashimoto, A. Shiratsuchi, T. Takizawa, and Y. Nakanishi. 2005. Augmentation of fatality of influenza in mice by inhibition of phagocytosis. *Biochem Biophys Res Commun* 337: 881-886.
183. Wang, J., M. P. Nikrad, E. A. Travanty, B. Zhou, T. Phang, B. Gao, T. Alford, Y. Ito, P. Nahreini, K. Hartshorn, D. Wentworth, C. A. Dinarello, and R. J. Mason. 2012. Innate Immune Response of Human Alveolar Macrophages during Influenza A Infection. *PLoS ONE* 7: e29879.
184. Tumpey, T. M., A. Garcia-Sastre, J. K. Taubenberger, P. Palese, D. E. Swayne, M. J. Pantin-Jackwood, S. Schultz-Cherry, A. Solorzano, N. Van Rooijen, J. M. Katz, and C. F. Basler. 2005. Pathogenicity of influenza viruses with genes from the 1918 pandemic virus: functional roles of alveolar macrophages and neutrophils in limiting virus replication and mortality in mice. *J Virol* 79: 14933-14944.
185. Fujisawa, H., S. Tsuru, M. Taniguchi, Y. Zinnaka, and K. Nomoto. 1987. Protective mechanisms against pulmonary infection with influenza virus. I. Relative contribution of polymorphonuclear leukocytes and of alveolar macrophages to protection during the early phase of intranasal infection. *J Gen Virol* 68 (Pt 2): 425-432.
186. Kim, H. M., Y. W. Lee, K. J. Lee, H. S. Kim, S. W. Cho, N. van Rooijen, Y. Guan, and S. H. Seo. 2008. Alveolar macrophages are indispensable for controlling influenza viruses in lungs of pigs. *J Virol* 82: 4265-4274.
187. Grayson, M. H. 2006. Lung dendritic cells and the inflammatory response. *Annals of Allergy, Asthma & Immunology* 96: 643-652.
188. Barchet, W., A. Blasius, M. Cella, and M. Colonna. 2005. Plasmacytoid dendritic cells: in search of their niche in immune responses. *Immunol Res* 32: 75-83.
189. Diacovo, T. G., A. L. Blasius, T. W. Mak, M. Cella, and M. Colonna. 2005. Adhesive mechanisms governing interferon-producing cell recruitment into lymph nodes. *J Exp Med* 202: 687-696.
190. Piqueras, B., J. Connolly, H. Freitas, A. K. Palucka, and J. Banchereau. 2006. Upon viral exposure, myeloid and plasmacytoid dendritic cells produce 3 waves of distinct chemokines to recruit immune effectors. *Blood* 107: 2613-2618.
191. Teijaro, John R., Kevin B. Walsh, S. Cahalan, Daniel M. Fremgen, E. Roberts, F. Scott, E. Martinborough, R. Peach, Michael B. A. Oldstone, and H. Rosen. 2011. Endothelial Cells Are Central Orchestrators of Cytokine Amplification during Influenza Virus Infection. *Cell* 146: 980-991.
192. Iwasaki, A., and R. Medzhitov. 2011. A new shield for a cytokine storm. *Cell* 146: 861-862.
193. Abdul-Careem, M. F., M. F. Mian, G. Yue, A. Gillgrass, M. J. Chenoweth, N. G. Barra, M. V. Chew, T. Chan, A. A. Al-Garawi, M. Jordana, and A. A. Ashkar. 2012. Critical role of natural killer cells in lung immunopathology during influenza infection in mice. *J Infect Dis* 206: 167-177.
194. Stein-Streilein, J., J. Guffee, and W. Fan. 1988. Locally and systemically derived natural killer cells participate in defense against intranasally inoculated influenza virus. *Reg Immunol* 1: 100-105.

195. Narni-Mancinelli, E., B. N. Jaeger, C. Bernat, A. Fenis, S. Kung, A. De Gassart, S. Mahmood, M. Gut, S. C. Heath, J. Estelle, E. Bertosio, F. Vely, L. N. Gastinel, B. Beutler, B. Malissen, M. Malissen, I. G. Gut, E. Vivier, and S. Ugolini. 2012. Tuning of natural killer cell reactivity by NKp46 and Helios calibrates T cell responses. *Science* 335: 344-348.
196. Hashimoto, G., P. F. Wright, and D. T. Karzon. 1983. Antibody-dependent cell-mediated cytotoxicity against influenza virus-infected cells. *J Infect Dis* 148: 785-794.
197. Medzhitov, R., D. S. Schneider, and M. P. Soares. 2012. Disease Tolerance as a Defense Strategy. *Science* 335: 936-941.
198. van Furth, R., and Z. A. Cohn. 1968. The origin and kinetics of mononuclear phagocytes. *J Exp Med* 128: 415-435.
199. Ingersoll, M. A., R. Spanbroek, C. Lottaz, E. L. Gautier, M. Frankenberger, R. Hoffmann, R. Lang, M. Haniffa, M. Collin, F. Tacke, A. J. Habenicht, L. Ziegler-Heitbrock, and G. J. Randolph. 2010. Comparison of gene expression profiles between human and mouse monocyte subsets. *Blood* 115: e10-19.
200. Etzrodt, M., V. Cortez-Retamozo, A. Newton, J. Zhao, A. Ng, M. Wildgruber, P. Romero, T. Wurdinger, R. Xavier, F. Geissmann, E. Meylan, M. Nahrendorf, F. K. Swirski, D. Baltimore, R. Weissleder, and M. J. Pittet. 2012. Regulation of monocyte functional heterogeneity by miR-146a and Relb. *Cell Rep* 1: 317-324.
201. Swirski, F. K., M. Nahrendorf, M. Etzrodt, M. Wildgruber, V. Cortez-Retamozo, P. Panizzi, J. L. Figueiredo, R. H. Kohler, A. Chudnovskiy, P. Waterman, E. Aikawa, T. R. Mempel, P. Libby, R. Weissleder, and M. J. Pittet. 2009. Identification of splenic reservoir monocytes and their deployment to inflammatory sites. *Science* 325: 612-616.
202. van Furth, R., and W. Sluiter. 1986. Distribution of blood monocytes between a marginating and a circulating pool. *J Exp Med* 163: 474-479.
203. Van Furth, R. 1985. Monocyte production during inflammation. *Comparative Immunology, Microbiology and Infectious Diseases* 8: 205-211.
204. Crane, M. J., K. L. Hokeness-Antonelli, and T. P. Salazar-Mather. 2009. Regulation of inflammatory monocyte/macrophage recruitment from the bone marrow during murine cytomegalovirus infection: role for type I interferons in localized induction of CCR2 ligands. *J Immunol* 183: 2810-2817.
205. Yona, S., K. W. Kim, Y. Wolf, A. Mildner, D. Varol, M. Breker, D. Strauss-Ayali, S. Viukov, M. Guilliams, A. Misharin, D. A. Hume, H. Perlman, B. Malissen, E. Zelzer, and S. Jung. 2013. Fate mapping reveals origins and dynamics of monocytes and tissue macrophages under homeostasis. *Immunity* 38: 79-91.
206. Parihar, A., T. D. Eubank, and A. I. Doseff. 2010. Monocytes and macrophages regulate immunity through dynamic networks of survival and cell death. *J Innate Immun* 2: 204-215.
207. Fahy, R. J., A. I. Doseff, and M. D. Wewers. 1999. Spontaneous human monocyte apoptosis utilizes a caspase-3-dependent pathway that is blocked by endotoxin and is independent of caspase-1. *J Immunol* 163: 1755-1762.
208. Schulz, C., E. Gomez Perdiguero, L. Chorro, H. Szabo-Rogers, N. Cagnard, K. Kierdorf, M. Prinz, B. Wu, S. E. Jacobsen, J. W. Pollard, J. Frampton, K. J. Liu, and F. Geissmann. 2012. A lineage of myeloid cells independent of Myb and hematopoietic stem cells. *Science* 336: 86-90.
209. Cecchini, M. G., M. G. Dominguez, S. Mocci, A. Wetterwald, R. Felix, H. Fleisch, O. Chisholm, W. Hofstetter, J. W. Pollard, and E. R. Stanley. 1994. Role of colony stimulating factor-1 in the establishment and regulation of tissue macrophages during postnatal development of the mouse. *Development* 120: 1357-1372.
210. Dai, X. M., G. R. Ryan, A. J. Hapel, M. G. Dominguez, R. G. Russell, S. Kapp, V. Sylvestre, and E. R. Stanley. 2002. Targeted disruption of the mouse colony-stimulating factor 1 receptor gene results in osteopetrosis, mononuclear

phagocyte deficiency, increased primitive progenitor cell frequencies, and reproductive defects. *Blood* 99: 111-120.
211. Varol, C., L. Landsman, D. K. Fogg, L. Greenshtein, B. Gildor, R. Margalit, V. Kalchenko, F. Geissmann, and S. Jung. 2007. Monocytes give rise to mucosal, but not splenic, conventional dendritic cells. *J Exp Med* 204: 171-180.
212. Hettinger, J., D. M. Richards, J. Hansson, M. M. Barra, A. C. Joschko, J. Krijgsveld, and M. Feuerer. 2013. Origin of monocytes and macrophages in a committed progenitor. *Nat Immunol* 14: 821-830.
213. Ginhoux, F., and S. Jung. 2014. Monocytes and macrophages: developmental pathways and tissue homeostasis. *Nat Rev Immunol* 14: 392-404.
214. Geissmann, F., S. Jung, and D. R. Littman. 2003. Blood monocytes consist of two principal subsets with distinct migratory properties. *Immunity* 19: 71-82.
215. Jakubzick, C., E. L. Gautier, S. L. Gibbings, D. K. Sojka, A. Schlitzer, T. E. Johnson, S. Ivanov, Q. Duan, S. Bala, T. Condon, N. van Rooijen, J. R. Grainger, Y. Belkaid, A. Ma'ayan, D. W. Riches, W. M. Yokoyama, F. Ginhoux, P. M. Henson, and G. J. Randolph. 2013. Minimal differentiation of classical monocytes as they survey steady-state tissues and transport antigen to lymph nodes. *Immunity* 39: 599-610.
216. Sunderkotter, C., T. Nikolic, M. J. Dillon, N. Van Rooijen, M. Stehling, D. A. Drevets, and P. J. Leenen. 2004. Subpopulations of mouse blood monocytes differ in maturation stage and inflammatory response. *J Immunol* 172: 4410-4417.
217. Passlick, B., D. Flieger, and H. W. Ziegler-Heitbrock. 1989. Identification and characterization of a novel monocyte subpopulation in human peripheral blood. *Blood* 74: 2527-2534.
218. Ziegler-Heitbrock, L., and T. P. Hofer. 2013. Toward a refined definition of monocyte subsets. *Front Immunol* 4: 23.
219. Strauss-Ayali, D., S. M. Conrad, and D. M. Mosser. 2007. Monocyte subpopulations and their differentiation patterns during infection. *J Leukoc Biol* 82: 244-252.
220. Carlin, L. M., E. G. Stamatiades, C. Auffray, R. N. Hanna, L. Glover, G. Vizcay-Barrena, C. C. Hedrick, H. T. Cook, S. Diebold, and F. Geissmann. 2013. Nr4a1-dependent Ly6C(low) monocytes monitor endothelial cells and orchestrate their disposal. *Cell* 153: 362-375.
221. Auffray, C., D. Fogg, M. Garfa, G. Elain, O. Join-Lambert, S. Kayal, S. Sarnacki, A. Cumano, G. Lauvau, and F. Geissmann. 2007. Monitoring of blood vessels and tissues by a population of monocytes with patrolling behavior. *Science* 317: 666-670.
222. Belge, K. U., F. Dayyani, A. Horelt, M. Siedlar, M. Frankenberger, B. Frankenberger, T. Espevik, and L. Ziegler-Heitbrock. 2002. The proinflammatory CD14+CD16+DR++ monocytes are a major source of TNF. *J Immunol* 168: 3536-3542.
223. Kawanaka, N., M. Yamamura, T. Aita, Y. Morita, A. Okamoto, M. Kawashima, M. Iwahashi, A. Ueno, Y. Ohmoto, and H. Makino. 2002. CD14+,CD16+ blood monocytes and joint inflammation in rheumatoid arthritis. *Arthritis Rheum* 46: 2578-2586.
224. Patino, R., J. Ibarra, A. Rodriguez, M. R. Yague, E. Pintor, A. Fernandez-Cruz, and A. Figueredo. 2000. Circulating monocytes in patients with diabetes mellitus, arterial disease, and increased CD14 expression. *Am J Cardiol* 85: 1288-1291.
225. Fingerle, G., A. Pforte, B. Passlick, M. Blumenstein, M. Strobel, and H. W. Ziegler-Heitbrock. 1993. The novel subset of CD14+/CD16+ blood monocytes is expanded in sepsis patients. *Blood* 82: 3170-3176.
226. Locher, C., G. Vanham, L. Kestens, M. Kruger, J. L. Ceuppens, J. Vingerhoets, and P. Gigase. 1994. Expression patterns of Fc gamma receptors, HLA-DR and

selected adhesion molecules on monocytes from normal and HIV-infected individuals. *Clin Exp Immunol* 98: 115-122.

227. Cros, J., N. Cagnard, K. Woollard, N. Patey, S. Y. Zhang, B. Senechal, A. Puel, S. K. Biswas, D. Moshous, C. Picard, J. P. Jais, D. D'Cruz, J. L. Casanova, C. Trouillet, and F. Geissmann. 2010. Human CD14dim monocytes patrol and sense nucleic acids and viruses via TLR7 and TLR8 receptors. *Immunity* 33: 375-386.
228. Hashimoto, D., A. Chow, C. Noizat, P. Teo, M. B. Beasley, M. Leboeuf, C. D. Becker, P. See, J. Price, D. Lucas, M. Greter, A. Mortha, S. W. Boyer, E. C. Forsberg, M. Tanaka, N. van Rooijen, A. Garcia-Sastre, E. R. Stanley, F. Ginhoux, P. S. Frenette, and M. Merad. 2013. Tissue-resident macrophages self-maintain locally throughout adult life with minimal contribution from circulating monocytes. *Immunity* 38: 792-804.
229. Hoeffel, G., Y. Wang, M. Greter, P. See, P. Teo, B. Malleret, M. Leboeuf, D. Low, G. Oller, F. Almeida, S. H. Choy, M. Grisotto, L. Renia, S. J. Conway, E. R. Stanley, J. K. Chan, L. G. Ng, I. M. Samokhvalov, M. Merad, and F. Ginhoux. 2012. Adult Langerhans cells derive predominantly from embryonic fetal liver monocytes with a minor contribution of yolk sac-derived macrophages. *J Exp Med* 209: 1167-1181.
230. Epelman, S., K. J. Lavine, A. E. Beaudin, D. K. Sojka, J. A. Carrero, B. Calderon, T. Brija, E. L. Gautier, S. Ivanov, A. T. Satpathy, J. D. Schilling, R. Schwendener, I. Sergin, B. Razani, E. C. Forsberg, W. M. Yokoyama, E. R. Unanue, M. Colonna, G. J. Randolph, and D. L. Mann. 2014. Embryonic and adult-derived resident cardiac macrophages are maintained through distinct mechanisms at steady state and during inflammation. *Immunity* 40: 91-104.
231. Guilliams, M., I. De Kleer, S. Henri, S. Post, L. Vanhoutte, S. De Prijck, K. Deswarte, B. Malissen, H. Hammad, and B. N. Lambrecht. 2013. Alveolar macrophages develop from fetal monocytes that differentiate into long-lived cells in the first week of life via GM-CSF. *J Exp Med* 210: 1977-1992.
232. Tagliani, E., C. Shi, P. Nancy, C. S. Tay, E. G. Pamer, and A. Erlebacher. 2011. Coordinate regulation of tissue macrophage and dendritic cell population dynamics by CSF-1. *J Exp Med* 208: 1901-1916.
233. Meuret, G., J. Bammert, and G. Hoffmann. 1974. Kinetics of human monocytopoiesis. *Blood* 44: 801-816.
234. Tsou, C. L., W. Peters, Y. Si, S. Slaymaker, A. M. Aslanian, S. P. Weisberg, M. Mack, and I. F. Charo. 2007. Critical roles for CCR2 and MCP-3 in monocyte mobilization from bone marrow and recruitment to inflammatory sites. *J Clin Invest* 117: 902-909.
235. Perera, L. P., and T. A. Waldmann. 1998. Activation of human monocytes induces differential resistance to apoptosis with rapid down regulation of caspase-8/FLICE. *Proceedings of the National Academy of Sciences* 95: 14308-14313.
236. Iliodromiti, Z., A. Anastasiadis, M. Varras, K. I. Pappa, C. Siristatidis, V. Bakoulas, G. Mastorakos, and N. Vrachnis. 2013. Monocyte Function in the Fetus and the Preterm Neonate: Immaturity Combined with Functional Impairment. *Mediat. Inflamm.*
237. Luster, A. D. 1998. Chemokines--chemotactic cytokines that mediate inflammation. *N Engl J Med* 338: 436-445.
238. Struyf, S., E. Van Collie, L. Paemen, W. Put, J. P. Lenaerts, P. Proost, G. Opdenakker, and J. Van Damme. 1998. Synergistic induction of MCP-1 and -2 by IL-1beta and interferons in fibroblasts and epithelial cells. *J Leukoc Biol* 63: 364-372.
239. Rollins, B. J., and J. S. Pober. 1991. Interleukin-4 induces the synthesis and secretion of MCP-1/JE by human endothelial cells. *Am J Pathol* 138: 1315-1319.

240. Jia, T., N. V. Serbina, K. Brandl, M. X. Zhong, I. M. Leiner, I. F. Charo, and E. G. Pamer. 2008. Additive roles for MCP-1 and MCP-3 in CCR2-mediated recruitment of inflammatory monocytes during Listeria monocytogenes infection. *J Immunol* 180: 6846-6853.
241. Shi, C., T. Jia, S. Mendez-Ferrer, T. M. Hohl, N. V. Serbina, L. Lipuma, I. Leiner, M. O. Li, P. S. Frenette, and E. G. Pamer. 2011. Bone marrow mesenchymal stem and progenitor cells induce monocyte emigration in response to circulating toll-like receptor ligands. *Immunity* 34: 590-601.
242. Jia, T., I. Leiner, G. Dorothee, K. Brandl, and E. G. Pamer. 2009. MyD88 and Type I interferon receptor-mediated chemokine induction and monocyte recruitment during Listeria monocytogenes infection. *J Immunol* 183: 1271-1278.
243. Kaufmann, A., R. Salentin, D. Gemsa, and H. Sprenger. 2001. Increase of CCR1 and CCR5 expression and enhanced functional response to MIP-1 alpha during differentiation of human monocytes to macrophages. *J Leukoc Biol* 69: 248-252.
244. Weber, C., K. S. Weber, C. Klier, S. Gu, R. Wank, R. Horuk, and P. J. Nelson. 2001. Specialized roles of the chemokine receptors CCR1 and CCR5 in the recruitment of monocytes and T(H)1-like/CD45RO(+) T cells. *Blood* 97: 1144-1146.
245. Landsman, L., L. Bar-On, A. Zernecke, K. W. Kim, R. Krauthgamer, E. Shagdarsuren, S. A. Lira, I. L. Weissman, C. Weber, and S. Jung. 2009. CX3CR1 is required for monocyte homeostasis and atherogenesis by promoting cell survival. *Blood* 113: 963-972.
246. Ley, K., C. Laudanna, M. I. Cybulsky, and S. Nourshargh. 2007. Getting to the site of inflammation: the leukocyte adhesion cascade updated. *Nat Rev Immunol* 7: 678-689.
247. Tedder, T. F., D. A. Steeber, and P. Pizcueta. 1995. L-selectin-deficient mice have impaired leukocyte recruitment into inflammatory sites. *J Exp Med* 181: 2259-2264.
248. Sumagin, R., H. Prizant, E. Lomakina, R. E. Waugh, and I. H. Sarelius. 2010. LFA-1 and Mac-1 define characteristically different intralumenal crawling and emigration patterns for monocytes and neutrophils in situ. *J Immunol* 185: 7057-7066.
249. Henderson, R. B., J. A. Hobbs, M. Mathies, and N. Hogg. 2003. Rapid recruitment of inflammatory monocytes is independent of neutrophil migration. *Blood* 102: 328-335.
250. Galkina, E., and K. Ley. 2007. Vascular adhesion molecules in atherosclerosis. *Arterioscler Thromb Vasc Biol* 27: 2292-2301.
251. Blankenberg, S., S. Barbaux, and L. Tiret. 2003. Adhesion molecules and atherosclerosis. *Atherosclerosis* 170: 191-203.
252. Mantovani, A., A. Sica, S. Sozzani, P. Allavena, A. Vecchi, and M. Locati. 2004. The chemokine system in diverse forms of macrophage activation and polarization. *Trends in Immunology* 25: 677-686.
253. Mantovani, A., A. Sica, and M. Locati. 2005. Macrophage Polarization Comes of Age. *Immunity* 23: 344-346.
254. Sica, A., and A. Mantovani. 2012. Macrophage plasticity and polarization: in vivo veritas. *Journal of Clinical Investigation* 122: 787-795.
255. Martinez, F. O., A. Sica, A. Mantovani, and M. Locati. 2008. Macrophage activation and polarization. *Frontiers in Bioscience-Landmark* 13: 453-461.
256. Tatano, Y., T. Shimizu, and H. Tomioka. 2014. Unique macrophages different from M1/M2 macrophages inhibit T cell mitogenesis while upregulating Th17 polarization. *Sci Rep* 4: 4146.
257. Verreck, F. A., T. de Boer, D. M. Langenberg, M. A. Hoeve, M. Kramer, E. Vaisberg, R. Kastelein, A. Kolk, R. de Waal-Malefyt, and T. H. Ottenhoff. 2004.

Human IL-23-producing type 1 macrophages promote but IL-10-producing type 2 macrophages subvert immunity to (myco)bacteria. *Proc Natl Acad Sci U S A* 101: 4560-4565.

258. Shaughnessy, L. M., and J. A. Swanson. 2007. The role of the activated macrophage in clearing Listeria monocytogenes infection. *Front Biosci* 12: 2683-2692.
259. Martinez, F. O., L. Helming, and S. Gordon. 2009. Alternative activation of macrophages: an immunologic functional perspective. *Annu Rev Immunol* 27: 451-483.
260. Shirey, K. A., L. M. Pletneva, A. C. Puche, A. D. Keegan, G. A. Prince, J. C. Blanco, and S. N. Vogel. 2010. Control of RSV-induced lung injury by alternatively activated macrophages is IL-4R alpha-, TLR4-, and IFN-beta-dependent. *Mucosal Immunol* 3: 291-300.
261. Page, C., L. Goicochea, K. Matthews, Y. Zhang, P. Klover, M. J. Holtzman, L. Hennighausen, and M. Frieman. 2012. Induction of Alternatively Activated Macrophages Enhances Pathogenesis during Severe Acute Respiratory Syndrome Coronavirus Infection. *Journal of Virology* 86: 13334-13349.
262. Jensen, K. D., Y. Wang, E. D. Wojno, A. J. Shastri, K. Hu, L. Cornel, E. Boedec, Y. C. Ong, Y. H. Chien, C. A. Hunter, J. C. Boothroyd, and J. P. Saeij. 2011. Toxoplasma polymorphic effectors determine macrophage polarization and intestinal inflammation. *Cell Host Microbe* 9: 472-483.
263. Denney, L., W. L. Kok, S. L. Cole, S. Sanderson, A. J. McMichael, and L.-P. Ho. 2012. Activation of Invariant NKT Cells in Early Phase of Experimental Autoimmune Encephalomyelitis Resuls in Differentiation of Ly6Chi Inflammatory Monocyte to M2 Macrophages and Improved Outcome. *Journal of Immunology*.
264. Peiser, L., and S. Gordon. 2001. The function of scavenger receptors expressed by macrophages and their role in the regulation of inflammation. *Microbes Infect* 3: 149-159.
265. Raes, G., P. De Baetselier, W. Noel, A. Beschin, F. Brombacher, and G. Hassanzadeh Gh. 2002. Differential expression of FIZZ1 and Ym1 in alternatively versus classically activated macrophages. *J Leukoc Biol* 71: 597-602.
266. Lu, J., Q. Cao, D. Zheng, Y. Sun, C. Wang, X. Yu, Y. Wang, V. W. S. Lee, G. Zheng, T. K. Tan, X. Wang, S. I. Alexander, D. C. H. Harris, and Y. Wang. 2013. Discrete functions of M2a and M2c macrophage subsets determine their relative efficacy in treating chronic kidney disease. *Kidney Int* 84: 745-755.
267. Martinez, F. O., S. Gordon, M. Locati, and A. Mantovani. 2006. Transcriptional profiling of the human monocyte-to-macrophage differentiation and polarization: new molecules and patterns of gene expression. *J Immunol* 177: 7303-7311.
268. Mantovani, A., S. Sozzani, M. Locati, P. Allavena, and A. Sica. 2002. Macrophage polarization: tumor-associated macrophages as a paradigm for polarized M2 mononuclear phagocytes. *Trends Immunol* 23: 549-555.
269. Dinarello, C. A. 1991. Interleukin-1 and interleukin-1 antagonism. *Blood* 77: 1627-1652.
270. Aldridge, J. R., Jr., C. E. Moseley, D. A. Boltz, N. J. Negovetich, C. Reynolds, J. Franks, S. A. Brown, P. C. Doherty, R. G. Webster, and P. G. Thomas. 2009. TNF/iNOS-producing dendritic cells are the necessary evil of lethal influenza virus infection. *Proc Natl Acad Sci U S A* 106: 5306-5311.
271. Serbina, N. V., T. P. Salazar-Mather, C. A. Biron, W. A. Kuziel, and E. G. Pamer. 2003. TNF/iNOS-producing dendritic cells mediate innate immune defense against bacterial infection. *Immunity* 19: 59-70.
272. Copin, R., P. De Baetselier, Y. Carlier, J. J. Letesson, and E. Muraille. 2007. MyD88-dependent activation of B220-CD11b+LY-6C+ dendritic cells during Brucella melitensis infection. *J Immunol* 178: 5182-5191.

273. Rydstrom, A., and M. J. Wick. 2007. Monocyte recruitment, activation, and function in the gut-associated lymphoid tissue during oral Salmonella infection. *J Immunol* 178: 5789-5801.
274. Bosschaerts, T., M. Guilliams, B. Stijlemans, Y. Morias, D. Engel, F. Tacke, M. Herin, P. De Baetselier, and A. Beschin. 2010. Tip-DC development during parasitic infection is regulated by IL-10 and requires CCL2/CCR2, IFN-gamma and MyD88 signaling. *PLoS Pathog* 6: e1001045.
275. De Trez, C., S. Magez, S. Akira, B. Ryffel, Y. Carlier, and E. Muraille. 2009. iNOS-producing inflammatory dendritic cells constitute the major infected cell type during the chronic Leishmania major infection phase of C57BL/6 resistant mice. *PLoS Pathog* 5: e1000494.
276. Dunay, I. R., R. A. Damatta, B. Fux, R. Presti, S. Greco, M. Colonna, and L. D. Sibley. 2008. Gr1(+) inflammatory monocytes are required for mucosal resistance to the pathogen Toxoplasma gondii. *Immunity* 29: 306-317.
277. Rivollier, A., J. He, A. Kole, V. Valatas, and B. L. Kelsall. 2012. Inflammation switches the differentiation program of Ly6Chi monocytes from antiinflammatory macrophages to inflammatory dendritic cells in the colon. *J Exp Med* 209: 139-155.
278. Cao, W., A. K. Taylor, R. E. Biber, W. G. Davis, J. H. Kim, A. J. Reber, T. Chirkova, J. A. De La Cruz, A. Pandey, P. Ranjan, J. M. Katz, S. Gangappa, and S. Sambhara. 2012. Rapid differentiation of monocytes into type I IFN-producing myeloid dendritic cells as an antiviral strategy against influenza virus infection. *J Immunol* 189: 2257-2265.
279. Lin, K. L., Y. Suzuki, H. Nakano, E. Ramsburg, and M. D. Gunn. 2008. CCR2+ monocyte-derived dendritic cells and exudate macrophages produce influenza-induced pulmonary immune pathology and mortality. *J Immunol* 180: 2562-2572.
280. Kok, W. L., L. Denney, K. Benam, S. Cole, C. Clelland, A. J. McMichael, and L.-P. Ho. 2012. Invariant NKT cells reduce accumulation of inflammatory monocytes in the lungs and decrease immune-pathology during severe influenza A virus infection. *Journal of Leukocyte Biology* 91: 357-368.
281. Susanne Herold, W. v. W., Mirko Steinmueller, Stephan Pleschka, William A. Kuziel, Matthias Mack, Mrigank Srivastava, Werner Seeger, Ulrich A. Maus, and Juergen Lohmeyer. 2006. Alveolar Epithelial Cells Direct Monocyte Transepithelial Migration upon Influenza Virus Infection: Impact of Chemokines and Adhesion Molecules. *The Journal of Immunology* 177: 1817-1824.
282. Dawson, T. C., M. A. Beck, W. A. Kuziel, F. Henderson, and N. Maeda. 2000. Contrasting Effects of CCR5 and CCR2 Deficiency in the Pulmonary Inflammatory Response to Influenza A Virus. *The American Journal of Pathology* 156: 1951-1959.
283. Cook, D. N., M. A. Beck, T. M. Coffman, S. L. Kirby, J. F. Sheridan, I. B. Pragnell, and O. Smithies. 1995. Requirement of MIP-1 alpha for an inflammatory response to viral infection. *Science* 269: 1583-1585.
284. Nakano, H., K. L. Lin, M. Yanagita, C. Charbonneau, D. N. Cook, T. Kakiuchi, and M. D. Gunn. 2009. Blood-derived inflammatory dendritic cells in lymph nodes stimulate acute T helper type 1 immune responses. *Nat Immunol* 10: 394-402.
285. Cline, T. D., E. A. Karlsson, B. J. Seufzer, and S. Schultz-Cherry. 2013. The hemagglutinin protein of highly pathogenic H5N1 influenza viruses overcomes an early block in the replication cycle to promote productive replication in macrophages. *J Virol* 87: 1411-1419.
286. Cheung, C. Y., L. L. M. Poon, A. S. Lau, W. Luk, Y. L. Lau, K. F. Shortridge, S. Gordon, Y. Guan, and J. S. M. Peiris. 2002. Induction of proinflammatory cytokines in human macrophages by influenza A (H5N1) viruses: a mechanism for the unusual severity of human disease? *The Lancet* 360: 1831-1837.

287. Gabrilovich, D. I., and S. Nagaraj. 2009. Myeloid-derived suppressor cells as regulators of the immune system. *Nat Rev Immunol* 9: 162-174.
288. Luyckx, A., E. Schouppe, O. Rutgeerts, C. Lenaerts, S. Fevery, T. Devos, D. Dierickx, M. Waer, J. A. Van Ginderachter, and A. D. Billiau. 2012. G-CSF stem cell mobilization in human donors induces polymorphonuclear and mononuclear myeloid-derived suppressor cells. *Clin Immunol* 143: 83-87.
289. Marigo, I., E. Bosio, S. Solito, C. Mesa, A. Fernandez, L. Dolcetti, S. Ugel, N. Sonda, S. Bicciato, E. Falisi, F. Calabrese, G. Basso, P. Zanovello, E. Cozzi, S. Mandruzzato, and V. Bronte. 2010. Tumor-induced tolerance and immune suppression depend on the C/EBPbeta transcription factor. *Immunity* 32: 790-802.
290. Youn, J. I., M. Collazo, I. N. Shalova, S. K. Biswas, and D. I. Gabrilovich. 2012. Characterization of the nature of granulocytic myeloid-derived suppressor cells in tumor-bearing mice. *J Leukoc Biol* 91: 167-181.
291. Poschke, I., and R. Kiessling. 2012. On the armament and appearances of human myeloid-derived suppressor cells. *Clinical Immunology* 144: 250-268.
292. De Santo, C., P. Serafini, I. Marigo, L. Dolcetti, M. Bolla, P. Del Soldato, C. Melani, C. Guiducci, M. P. Colombo, M. Iezzi, P. Musiani, P. Zanovello, and V. Bronte. 2005. Nitroaspirin corrects immune dysfunction in tumor-bearing hosts and promotes tumor eradication by cancer vaccination. *Proc Natl Acad Sci U S A* 102: 4185-4190.
293. Serafini, P., K. Meckel, M. Kelso, K. Noonan, J. Califano, W. Koch, L. Dolcetti, V. Bronte, and I. Borrello. 2006. Phosphodiesterase-5 inhibition augments endogenous antitumor immunity by reducing myeloid-derived suppressor cell function. *J Exp Med* 203: 2691-2702.
294. Rodriguez, P. C., D. G. Quiceno, and A. C. Ochoa. 2007. L-arginine availability regulates T-lymphocyte cell-cycle progression. *Blood* 109: 1568-1573.
295. Bingisser, R. M., P. A. Tilbrook, P. G. Holt, and U. R. Kees. 1998. Macrophage-derived nitric oxide regulates T cell activation via reversible disruption of the Jak3/STAT5 signaling pathway. *J Immunol* 160: 5729-5734.
296. Rivoltini, L., M. Carrabba, V. Huber, C. Castelli, L. Novellino, P. Dalerba, R. Mortarini, G. Arancia, A. Anichini, S. Fais, and G. Parmiani. 2002. Immunity to cancer: attack and escape in T lymphocyte–tumor cell interaction. *Immunological Reviews* 188: 97-113.
297. Kusmartsev, S., Y. Nefedova, D. Yoder, and D. I. Gabrilovich. 2004. Antigen-specific inhibition of CD8+ T cell response by immature myeloid cells in cancer is mediated by reactive oxygen species. *J Immunol* 172: 989-999.
298. Szuster-Ciesielska, A., E. Hryciuk-Umer, A. Stepulak, K. Kupisz, and M. Kandefer-Szerszen. 2004. Reactive oxygen species production by blood neutrophils of patients with laryngeal carcinoma and antioxidative enzyme activity in their blood. *Acta Oncol* 43: 252-258.
299. Youn, J. I., S. Nagaraj, M. Collazo, and D. I. Gabrilovich. 2008. Subsets of myeloid-derived suppressor cells in tumor-bearing mice. *J Immunol* 181: 5791-5802.
300. Movahedi, K., M. Guilliams, J. Van den Bossche, R. Van den Bergh, C. Gysemans, A. Beschin, P. De Baetselier, and J. A. Van Ginderachter. 2008. *Identification of discrete tumor-induced myeloid-derived suppressor cell subpopulations with distinct T cell–suppressive activity*.
301. Almand, B., J. I. Clark, E. Nikitina, J. van Beynen, N. R. English, S. C. Knight, D. P. Carbone, and D. I. Gabrilovich. 2001. Increased production of immature myeloid cells in cancer patients: a mechanism of immunosuppression in cancer. *J Immunol* 166: 678-689.
302. Diaz-Montero, C. M., M. L. Salem, M. I. Nishimura, E. Garrett-Mayer, D. J. Cole, and A. J. Montero. 2009. Increased circulating myeloid-derived suppressor cells

correlate with clinical cancer stage, metastatic tumor burden, and doxorubicin-cyclophosphamide chemotherapy. *Cancer Immunol Immunother* 58: 49-59.

303. Gabitass, R. F., N. E. Annels, D. D. Stocken, H. A. Pandha, and G. W. Middleton. 2011. Elevated myeloid-derived suppressor cells in pancreatic, esophageal and gastric cancer are an independent prognostic factor and are associated with significant elevation of the Th2 cytokine interleukin-13. *Cancer Immunol Immunother* 60: 1419-1430.
304. Cortez-Retamozo, V., M. Etzrodt, A. Newton, R. Ryan, F. Pucci, S. W. Sio, W. Kuswanto, P. J. Rauch, A. Chudnovskiy, Y. Iwamoto, R. Kohler, B. Marinelli, R. Gorbatov, G. Wojtkiewicz, P. Panizzi, M. Mino-Kenudson, R. Forghani, J. L. Figueiredo, J. W. Chen, R. Xavier, F. K. Swirski, M. Nahrendorf, R. Weissleder, and M. J. Pittet. 2013. Angiotensin II drives the production of tumor-promoting macrophages. *Immunity* 38: 296-308.
305. Ugel, S., E. Peranzoni, G. Desantis, M. Chioda, S. Walter, T. Weinschenk, J. C. Ochando, A. Cabrelle, S. Mandruzzato, and V. Bronte. 2012. Immune tolerance to tumor antigens occurs in a specialized environment of the spleen. *Cell Rep* 2: 628-639.
306. De Santo, C., M. Salio, S. H. Masri, L. Y. Lee, T. Dong, A. O. Speak, S. Porubsky, S. Booth, N. Veerapen, G. S. Besra, H. J. Grone, F. M. Platt, M. Zambon, and V. Cerundolo. 2008. Invariant NKT cells reduce the immunosuppressive activity of influenza A virus-induced myeloid-derived suppressor cells in mice and humans. *J Clin Invest* 118: 4036-4048.
307. Jeisy-Scott, V., W. G. Davis, J. R. Patel, J. B. Bowzard, W. J. Shieh, S. R. Zaki, J. M. Katz, and S. Sambhara. 2011. Increased MDSC accumulation and Th2 biased response to influenza A virus infection in the absence of TLR7 in mice. *PLoS ONE* 6: e25242.
308. Chen, S., S. M. Akbar, M. Abe, Y. Hiasa, and M. Onji. 2011. Immunosuppressive functions of hepatic myeloid-derived suppressor cells of normal mice and in a murine model of chronic hepatitis B virus. *Clin Exp Immunol* 166: 134-142.
309. Willmon, C., R. M. Diaz, P. Wongthida, F. Galivo, T. Kottke, J. Thompson, S. Albelda, K. Harrington, A. Melcher, and R. Vile. 2011. Vesicular stomatitis virus-induced immune suppressor cells generate antagonism between intratumoral oncolytic virus and cyclophosphamide. *Mol Ther* 19: 140-149.
310. Zhu, B., Y. Bando, S. Xiao, K. Yang, A. C. Anderson, V. K. Kuchroo, and S. J. Khoury. 2007. CD11b+Ly-6C(hi) suppressive monocytes in experimental autoimmune encephalomyelitis. *J Immunol* 179: 5228-5237.
311. Brandau, S., S. Trellakis, K. Bruderek, D. Schmaltz, G. Steller, M. Elian, H. Suttmann, M. Schenck, J. Welling, P. Zabel, and S. Lang. 2011. Myeloid-derived suppressor cells in the peripheral blood of cancer patients contain a subset of immature neutrophils with impaired migratory properties. *J Leukoc Biol* 89: 311-317.
312. Bowers, N. L., E. S. Helton, R. P. Huijbregts, P. A. Goepfert, S. L. Heath, and Z. Hel. 2014. Immune suppression by neutrophils in HIV-1 infection: role of PD-L1/PD-1 pathway. *PLoS Pathog* 10: e1003993.
313. Denny, M. F., S. Yalavarthi, W. Zhao, S. G. Thacker, M. Anderson, A. R. Sandy, W. J. McCune, and M. J. Kaplan. 2010. A distinct subset of proinflammatory neutrophils isolated from patients with systemic lupus erythematosus induces vascular damage and synthesizes type I IFNs. *J Immunol* 184: 3284-3297.
314. Fowlkes, B. J., A. M. Kruisbeek, H. Ton-That, M. A. Weston, J. E. Coligan, R. H. Schwartz, and D. M. Pardoll. 1987. A novel population of T-cell receptor alpha beta-bearing thymocytes which predominantly expresses a single V beta gene family. *Nature* 329: 251-254.

315. Sykes, M. 1990. Unusual T cell populations in adult murine bone marrow. Prevalence of CD3+CD4-CD8- and alpha beta TCR+NK1.1+ cells. *J Immunol* 145: 3209-3215.
316. Zlotnik, A., D. I. Godfrey, M. Fischer, and T. Suda. 1992. Cytokine production by mature and immature CD4-CD8- T cells. Alpha beta-T cell receptor+ CD4-CD8- T cells produce IL-4. *J Immunol* 149: 1211-1215.
317. Bendelac, A., P. B. Savage, and L. Teyton. 2007. The biology of NKT cells. *Annu Rev Immunol* 25: 297-336.
318. Kawano, T., J. Cui, Y. Koezuka, I. Toura, Y. Kaneko, K. Motoki, H. Ueno, R. Nakagawa, H. Sato, E. Kondo, H. Koseki, and M. Taniguchi. 1997. CD1d-restricted and TCR-mediated activation of valpha14 NKT cells by glycosylceramides. *Science* 278: 1626-1629.
319. Sriram, V., W. Du, J. Gervay-Hague, and R. R. Brutkiewicz. 2005. Cell wall glycosphingolipids of Sphingomonas paucimobilis are CD1d-specific ligands for NKT cells. *Eur J Immunol* 35: 1692-1701.
320. Kinjo, Y., E. Tupin, D. Wu, M. Fujio, R. Garcia-Navarro, M. R. Benhnia, D. M. Zajonc, G. Ben-Menachem, G. D. Ainge, G. F. Painter, A. Khurana, K. Hoebe, S. M. Behar, B. Beutler, I. A. Wilson, M. Tsuji, T. J. Sellati, C. H. Wong, and M. Kronenberg. 2006. Natural killer T cells recognize diacylglycerol antigens from pathogenic bacteria. *Nat Immunol* 7: 978-986.
321. Zhou, D., J. Mattner, C. Cantu, 3rd, N. Schrantz, N. Yin, Y. Gao, Y. Sagiv, K. Hudspeth, Y. P. Wu, T. Yamashita, S. Teneberg, D. Wang, R. L. Proia, S. B. Levery, P. B. Savage, L. Teyton, and A. Bendelac. 2004. Lysosomal glycosphingolipid recognition by NKT cells. *Science* 306: 1786-1789.
322. Ortaldo, J. R., H. A. Young, R. T. Winkler-Pickett, E. W. Bere, Jr., W. J. Murphy, and R. H. Wiltrout. 2004. Dissociation of NKT stimulation, cytokine induction, and NK activation in vivo by the use of distinct TCR-binding ceramides. *J Immunol* 172: 943-953.
323. Parekh, V. V., A. K. Singh, M. T. Wilson, D. Olivares-Villagomez, J. S. Bezbradica, H. Inazawa, H. Ehara, T. Sakai, I. Serizawa, L. Wu, C. R. Wang, S. Joyce, and L. Van Kaer. 2004. Quantitative and qualitative differences in the in vivo response of NKT cells to distinct alpha- and beta-anomeric glycolipids. *J Immunol* 173: 3693-3706.
324. Wu, D. Y., N. H. Segal, S. Sidobre, M. Kronenberg, and P. B. Chapman. 2003. Cross-presentation of disialoganglioside GD3 to natural killer T cells. *J Exp Med* 198: 173-181.
325. Stetson, D. B., M. Mohrs, R. L. Reinhardt, J. L. Baron, Z. E. Wang, L. Gapin, M. Kronenberg, and R. M. Locksley. 2003. Constitutive cytokine mRNAs mark natural killer (NK) and NK T cells poised for rapid effector function. *J Exp Med* 198: 1069-1076.
326. Tahir, S. M., O. Cheng, A. Shaulov, Y. Koezuka, G. J. Bubley, S. B. Wilson, S. P. Balk, and M. A. Exley. 2001. Loss of IFN-gamma production by invariant NK T cells in advanced cancer. *J Immunol* 167: 4046-4050.
327. Juno, J. A., Y. Keynan, and K. R. Fowke. 2012. Invariant NKT Cells: Regulation and Function during Viral Infection. *PLoS Pathog* 8: e1002838.
328. Lisbonne, M., S. Diem, A. de Castro Keller, J. Lefort, L. M. Araujo, P. Hachem, J. M. Fourneau, S. Sidobre, M. Kronenberg, M. Taniguchi, P. Van Endert, M. Dy, P. Askenase, M. Russo, B. B. Vargaftig, A. Herbelin, and M. C. Leite-de-Moraes. 2003. Cutting edge: invariant V alpha 14 NKT cells are required for allergen-induced airway inflammation and hyperreactivity in an experimental asthma model. *J Immunol* 171: 1637-1641.
329. Wilson, S. B., S. C. Kent, K. T. Patton, T. Orban, R. A. Jackson, M. Exley, S. Porcelli, D. A. Schatz, M. A. Atkinson, S. P. Balk, J. L. Strominger, and D. A. Hafler. 1998. Extreme Th1 bias of invariant Valpha24JalphaQ T cells in type 1 diabetes. *Nature* 391: 177-181.

330. Taniguchi, M., K. Seino, and T. Nakayama. 2003. The NKT cell system: bridging innate and acquired immunity. *Nat Immunol* 4: 1164-1165.
331. Wong, C. H., and P. Kubes. 2013. Imaging natural killer T cells in action. *Immunol Cell Biol* 91: 304-310.
332. Geissmann, F., T. O. Cameron, S. Sidobre, N. Manlongat, M. Kronenberg, M. J. Briskin, M. L. Dustin, and D. R. Littman. 2005. Intravascular immune surveillance by CXCR6+ NKT cells patrolling liver sinusoids. *PLoS Biol* 3: e113.
333. Jahng, A., I. Maricic, C. Aguilera, S. Cardell, R. C. Halder, and V. Kumar. 2004. Prevention of autoimmunity by targeting a distinct, noninvariant CD1d-reactive T cell population reactive to sulfatide. *J Exp Med* 199: 947-957.
334. Van Rhijn, I., D. C. Young, J. S. Im, S. B. Levery, P. A. Illarionov, G. S. Besra, S. A. Porcelli, J. Gumperz, T. Y. Cheng, and D. B. Moody. 2004. CD1d-restricted T cell activation by nonlipidic small molecules. *Proc Natl Acad Sci U S A* 101: 13578-13583.
335. Terabe, M., J. Swann, E. Ambrosino, P. Sinha, S. Takaku, Y. Hayakawa, D. I. Godfrey, S. Ostrand-Rosenberg, M. J. Smyth, and J. A. Berzofsky. 2005. A nonclassical non-Valpha14Jalpha18 CD1d-restricted (type II) NKT cell is sufficient for down-regulation of tumor immunosurveillance. *J Exp Med* 202: 1627-1633.
336. Montoya, C. J., D. Pollard, J. Martinson, K. Kumari, C. Wasserfall, C. B. Mulder, M. T. Rugeles, M. A. Atkinson, A. L. Landay, and S. B. Wilson. 2007. Characterization of human invariant natural killer T subsets in health and disease using a novel invariant natural killer T cell-clonotypic monoclonal antibody, 6B11. *Immunology* 122: 1-14.
337. Bienemann, K., K. Iouannidou, K. Schoenberg, F. Krux, S. Reuther, O. Feyen, F. Schuster, M. Uhrberg, H. J. Laws, and A. Borkhardt. 2011. iNKT cell frequency in peripheral blood of Caucasian children and adolescent: the absolute iNKT cell count is stable from birth to adulthood. *Scand J Immunol* 74: 406-411.
338. Fereidouni, M., R. Farid Hosseini, F. Jabbari Azad, J. Schenkel, A. Varasteh, and M. Mahmoudi. 2010. Frequency of circulating iNKT cells among Iranian healthy adults. *Cytometry B Clin Cytom* 78: 65-69.
339. Bezbradica, J. S., T. Hill, A. K. Stanic, L. Van Kaer, and S. Joyce. 2005. Commitment toward the natural T (iNKT) cell lineage occurs at the CD4+8+ stage of thymic ontogeny. *Proc Natl Acad Sci U S A* 102: 5114-5119.
340. Bendelac, A. 1995. Positive selection of mouse NK1+ T cells by CD1-expressing cortical thymocytes. *J Exp Med* 182: 2091-2096.
341. Gadue, P., N. Morton, and P. L. Stein. 1999. The Src family tyrosine kinase Fyn regulates natural killer T cell development. *J Exp Med* 190: 1189-1196.
342. Pasquier, B., L. Yin, M. C. Fondaneche, F. Relouzat, C. Bloch-Queyrat, N. Lambert, A. Fischer, G. de Saint-Basile, and S. Latour. 2005. Defective NKT cell development in mice and humans lacking the adapter SAP, the X-linked lymphoproliferative syndrome gene product. *J Exp Med* 201: 695-701.
343. Gumperz, J. E., S. Miyake, T. Yamamura, and M. B. Brenner. 2002. Functionally distinct subsets of CD1d-restricted natural killer T cells revealed by CD1d tetramer staining. *J Exp Med* 195: 625-636.
344. Godfrey, D. I., S. Stankovic, and A. G. Baxter. 2010. Raising the NKT cell family. *Nat Immunol* 11: 197-206.
345. Benlagha, K., D. G. Wei, J. Veiga, L. Teyton, and A. Bendelac. 2005. Characterization of the early stages of thymic NKT cell development. *J Exp Med* 202: 485-492.
346. Benlagha, K., T. Kyin, A. Beavis, L. Teyton, and A. Bendelac. 2002. A thymic precursor to the NK T cell lineage. *Science* 296: 553-555.
347. Pellicci, D. G., K. J. Hammond, A. P. Uldrich, A. G. Baxter, M. J. Smyth, and D. I. Godfrey. 2002. A natural killer T (NKT) cell developmental pathway iInvolving

a thymus-dependent NK1.1(-)CD4(+) CD1d-dependent precursor stage. *J Exp Med* 195: 835-844.

348. Gadue, P., and P. L. Stein. 2002. NK T cell precursors exhibit differential cytokine regulation and require Itk for efficient maturation. *J Immunol* 169: 2397-2406.
349. McNab, F. W., S. P. Berzins, D. G. Pellicci, K. Kyparissoudis, K. Field, M. J. Smyth, and D. I. Godfrey. 2005. The influence of CD1d in postselection NKT cell maturation and homeostasis. *J Immunol* 175: 3762-3768.
350. Franki, A. S., K. Van Beneden, P. Dewint, K. J. Hammond, S. Lambrecht, G. Leclercq, M. Kronenberg, D. Deforce, and D. Elewaut. 2006. A unique lymphotoxin {alpha}beta-dependent pathway regulates thymic emigration of V{alpha}14 invariant natural killer T cells. *Proc Natl Acad Sci U S A* 103: 9160-9165.
351. Baev, D. V., X. H. Peng, L. Song, J. R. Barnhart, G. M. Crooks, K. I. Weinberg, and L. S. Metelitsa. 2004. Distinct homeostatic requirements of CD4+ and CD4- subsets of Valpha24-invariant natural killer T cells in humans. *Blood* 104: 4150-4156.
352. Coquet, J. M., S. Chakravarti, K. Kyparissoudis, F. W. McNab, L. A. Pitt, B. S. McKenzie, S. P. Berzins, M. J. Smyth, and D. I. Godfrey. 2008. Diverse cytokine production by NKT cell subsets and identification of an IL-17-producing CD4-NK1.1- NKT cell population. *Proc Natl Acad Sci U S A* 105: 11287-11292.
353. Kronenberg, M. 2005. Toward an understanding of NKT cell biology: progress and paradoxes. *Annu Rev Immunol* 23: 877-900.
354. Lazarevic, V., A. J. Zullo, M. N. Schweitzer, T. L. Staton, E. M. Gallo, G. R. Crabtree, and L. H. Glimcher. 2009. The gene encoding early growth response 2, a target of the transcription factor NFAT, is required for the development and maturation of natural killer T cells. *Nat Immunol* 10: 306-313.
355. Mycko, M. P., I. Ferrero, A. Wilson, W. Jiang, T. Bianchi, A. Trumpp, and H. R. MacDonald. 2009. Selective requirement for c-Myc at an early stage of V(alpha)14i NKT cell development. *J Immunol* 182: 4641-4648.
356. Monticelli, L. A., Y. Yang, J. Knell, L. M. D'Cruz, M. A. Cannarile, I. Engel, M. Kronenberg, and A. W. Goldrath. 2009. Transcriptional regulator Id2 controls survival of hepatic NKT cells. *Proc Natl Acad Sci U S A* 106: 19461-19466.
357. Doisne, J. M., L. Bartholin, K. P. Yan, C. N. Garcia, N. Duarte, J. B. Le Luduec, D. Vincent, F. Cyprian, B. Horvat, S. Martel, R. Rimokh, R. Losson, K. Benlagha, and J. C. Marie. 2009. iNKT cell development is orchestrated by different branches of TGF-beta signaling. *J Exp Med* 206: 1365-1378.
358. Zheng, X., H. Zhang, L. Yin, C. R. Wang, Y. Liu, and P. Zheng. 2008. Modulation of NKT cell development by B7-CD28 interaction: an expanding horizon for costimulation. *PLoS ONE* 3: e2703.
359. Tupin, E., Y. Kinjo, and M. Kronenberg. 2007. The unique role of natural killer T cells in the response to microorganisms. *Nat Rev Micro* 5: 405-417.
360. Mattner, J., K. L. Debord, N. Ismail, R. D. Goff, C. Cantu, 3rd, D. Zhou, P. Saint-Mezard, V. Wang, Y. Gao, N. Yin, K. Hoebe, O. Schneewind, D. Walker, B. Beutler, L. Teyton, P. B. Savage, and A. Bendelac. 2005. Exogenous and endogenous glycolipid antigens activate NKT cells during microbial infections. *Nature* 434: 525-529.
361. Wingender, G., P. Rogers, G. Batzer, M. S. Lee, D. Bai, B. Pei, A. Khurana, M. Kronenberg, and A. A. Horner. 2011. Invariant NKT cells are required for airway inflammation induced by environmental antigens. *J Exp Med* 208: 1151-1162.
362. Agea, E., A. Russano, O. Bistoni, R. Mannucci, I. Nicoletti, L. Corazzi, A. D. Postle, G. De Libero, S. A. Porcelli, and F. Spinozzi. 2005. Human CD1-restricted T cell recognition of lipids from pollens. *J Exp Med* 202: 295-308.

363. Brigl, M., L. Bry, S. C. Kent, J. E. Gumperz, and M. B. Brenner. 2003. Mechanism of CD1d-restricted natural killer T cell activation during microbial infection. *Nat Immunol* 4: 1230-1237.
364. Berntman, E., J. Rolf, C. Johansson, P. Anderson, and S. L. Cardell. 2005. The role of CD1d-restricted NK T lymphocytes in the immune response to oral infection with Salmonella typhimurium. *Eur J Immunol* 35: 2100-2109.
365. Skold, M., X. Xiong, P. A. Illarionov, G. S. Besra, and S. M. Behar. 2005. Interplay of cytokines and microbial signals in regulation of CD1d expression and NKT cell activation. *J Immunol* 175: 3584-3593.
366. Raghuraman, G., Y. Geng, and C. R. Wang. 2006. IFN-beta-mediated up-regulation of CD1d in bacteria-infected APCs. *J Immunol* 177: 7841-7848.
367. Faveeuw, C., V. Angeli, J. Fontaine, C. Maliszewski, A. Capron, L. Van Kaer, M. Moser, M. Capron, and F. Trottein. 2002. Antigen presentation by CD1d contributes to the amplification of Th2 responses to Schistosoma mansoni glycoconjugates in mice. *J Immunol* 169: 906-912.
368. Nagarajan, N. A., and M. Kronenberg. 2007. Invariant NKT cells amplify the innate immune response to lipopolysaccharide. *J Immunol* 178: 2706-2713.
369. Onoe, K., Y. Yanagawa, K. Minami, N. Iijima, and K. Iwabuchi. 2007. Th1 or Th2 balance regulated by interaction between dendritic cells and NKT cells. *Immunol Res* 38: 319-332.
370. Im, J. S., P. Arora, G. Bricard, A. Molano, M. M. Venkataswamy, I. Baine, E. S. Jerud, M. F. Goldberg, A. Baena, K. O. Yu, R. M. Ndonye, A. R. Howell, W. Yuan, P. Cresswell, Y. T. Chang, P. A. Illarionov, G. S. Besra, and S. A. Porcelli. 2009. Kinetics and cellular site of glycolipid loading control the outcome of natural killer T cell activation. *Immunity* 30: 888-898.
371. Sakuishi, K., S. Oki, M. Araki, S. A. Porcelli, S. Miyake, and T. Yamamura. 2007. Invariant NKT cells biased for IL-5 production act as crucial regulators of inflammation. *J Immunol* 179: 3452-3462.
372. Coquet, J. M., K. Kyparissoudis, D. G. Pellicci, G. Besra, S. P. Berzins, M. J. Smyth, and D. I. Godfrey. 2007. IL-21 is produced by NKT cells and modulates NKT cell activation and cytokine production. *J Immunol* 178: 2827-2834.
373. Watarai, H., E. Sekine-Kondo, T. Shigeura, Y. Motomura, T. Yasuda, R. Satoh, H. Yoshida, M. Kubo, H. Kawamoto, H. Koseki, and M. Taniguchi. 2012. Development and Function of Invariant Natural Killer T Cells Producing T_H2- and T_H17-Cytokines. *PLoS Biol* 10: e1001255.
374. Wingender, G., P. Krebs, B. Beutler, and M. Kronenberg. 2010. Antigen-specific cytotoxicity by invariant NKT cells in vivo is CD95/CD178-dependent and is correlated with antigenic potency. *J Immunol* 185: 2721-2729.
375. Takahashi, T., S. Chiba, M. Nieda, T. Azuma, S. Ishihara, Y. Shibata, T. Juji, and H. Hirai. 2002. Cutting edge: analysis of human V alpha 24+CD8+ NK T cells activated by alpha-galactosylceramide-pulsed monocyte-derived dendritic cells. *J Immunol* 168: 3140-3144.
376. Ho, L. P., B. C. Urban, L. Jones, G. S. Ogg, and A. J. McMichael. 2004. CD4(-)CD8alphaalpha subset of CD1d-restricted NKT cells controls T cell expansion. *J Immunol* 172: 7350-7358.
377. Kim, C. H., E. C. Butcher, and B. Johnston. 2002. Distinct subsets of human Valpha24-invariant NKT cells: cytokine responses and chemokine receptor expression. *Trends Immunol* 23: 516-519.
378. Hayakawa, Y., K. Takeda, H. Yagita, L. Van Kaer, I. Saiki, and K. Okumura. 2001. Differential regulation of Th1 and Th2 functions of NKT cells by CD28 and CD40 costimulatory pathways. *J Immunol* 166: 6012-6018.
379. Akbari, O., P. Stock, A. K. Singh, V. Lombardi, W. L. Lee, G. J. Freeman, A. H. Sharpe, D. T. Umetsu, and R. H. Dekruyff. 2010. PD-L1 and PD-L2 modulate airway inflammation and iNKT-cell-dependent airway hyperreactivity in opposing directions. *Mucosal Immunol* 3: 81-91.

380. Gabriel, B., M. V. Manjunatha, O. A. Y. Karl, S. I. Jin, M. N. Rachel, R. H. Amy, V. Natacha, A. I. Petr, S. B. Gurdyal, L. Qian, C. Young-Tae, and A. P. Steven. 2010. α-Galactosylceramide Analogs with Weak Agonist Activity for Human iNKT Cells Define New Candidate Anti-Inflammatory Agents. *PLoS ONE* 5.
381. Lawson, V. 2012. Turned on by danger: activation of CD1d-restricted invariant natural killer T cells. *Immunology* 137: 20-27.
382. Goff, R. D., Y. Gao, J. Mattner, D. Zhou, N. Yin, C. Cantu, 3rd, L. Teyton, A. Bendelac, and P. B. Savage. 2004. Effects of lipid chain lengths in alpha-galactosylceramides on cytokine release by natural killer T cells. *J Am Chem Soc* 126: 13602-13603.
383. Miyamoto, K., S. Miyake, and T. Yamamura. 2001. A synthetic glycolipid prevents autoimmune encephalomyelitis by inducing TH2 bias of natural killer T cells. *Nature* 413: 531-534.
384. Forestier, C., T. Takaki, A. Molano, J. S. Im, I. Baine, E. S. Jerud, P. Illarionov, R. Ndonye, A. R. Howell, P. Santamaria, G. S. Besra, T. P. Dilorenzo, and S. A. Porcelli. 2007. Improved outcomes in NOD mice treated with a novel Th2 cytokine-biasing NKT cell activator. *J Immunol* 178: 1415-1425.
385. Sullivan, B. A., N. A. Nagarajan, G. Wingender, J. Wang, I. Scott, M. Tsuji, R. W. Franck, S. A. Porcelli, D. M. Zajonc, and M. Kronenberg. 2010. Mechanisms for glycolipid antigen-driven cytokine polarization by Valpha14i NKT cells. *J Immunol* 184: 141-153.
386. Schmieg, J., G. Yang, R. W. Franck, and M. Tsuji. 2003. Superior protection against malaria and melanoma metastases by a C-glycoside analogue of the natural killer T cell ligand alpha-Galactosylceramide. *J Exp Med* 198: 1631-1641.
387. Fujii, S.-i., K. Shimizu, H. Hemmi, M. Fukui, A. J. Bonito, G. Chen, R. W. Franck, M. Tsuji, and R. M. Steinman. 2006. Glycolipid α-C-galactosylceramide is a distinct inducer of dendritic cell function during innate and adaptive immune responses of mice. *Proceedings of the National Academy of Sciences* 103: 11252-11257.
388. Bai, L., M. G. Constantinides, S. Y. Thomas, R. Reboulet, F. Meng, F. Koentgen, L. Teyton, P. B. Savage, and A. Bendelac. 2012. Distinct APCs explain the cytokine bias of alpha-galactosylceramide variants in vivo. *J Immunol* 188: 3053-3061.
389. Bendelac, A., M. N. Rivera, S. H. Park, and J. H. Roark. 1997. Mouse CD1-specific NK1 T cells: development, specificity, and function. *Annu Rev Immunol* 15: 535-562.
390. Mueller, D. L., M. K. Jenkins, and R. H. Schwartz. 1989. Clonal expansion versus functional clonal inactivation: a costimulatory signalling pathway determines the outcome of T cell antigen receptor occupancy. *Annu Rev Immunol* 7: 445-480.
391. Chen, L., and D. B. Flies. 2013. Molecular mechanisms of T cell co-stimulation and co-inhibition. *Nat Rev Immunol* 13: 227-242.
392. Peggs, K. S., and J. P. Allison. 2005. Co-stimulatory pathways in lymphocyte regulation: the immunoglobulin superfamily. *British Journal of Haematology* 130: 809-824.
393. van den Heuvel, M. J., N. Garg, L. Van Kaer, and S. M. M. Haeryfar. 2011. NKT cell costimulation: experimental progress and therapeutic promise. *Trends in Molecular Medicine* 17: 65-77.
394. Wang, J., L. Cheng, Z. Wondimu, M. Swain, P. Santamaria, and Y. Yang. 2009. Cutting edge: CD28 engagement releases antigen-activated invariant NKT cells from the inhibitory effects of PD-1. *J Immunol* 182: 6644-6647.
395. Williams, J. A., J. M. Lumsden, X. Yu, L. Feigenbaum, J. Zhang, S. M. Steinberg, and R. J. Hodes. 2008. Regulation of thymic NKT cell development by the B7-CD28 costimulatory pathway. *J Immunol* 181: 907-917.

396. Parekh, V. V., M. T. Wilson, D. Olivares-Villagomez, A. K. Singh, L. Wu, C. R. Wang, S. Joyce, and L. Van Kaer. 2005. Glycolipid antigen induces long-term natural killer T cell anergy in mice. *J Clin Invest* 115: 2572-2583.
397. Chang, W. S., J. Y. Kim, Y. J. Kim, Y. S. Kim, J. M. Lee, M. Azuma, H. Yagita, and C. Y. Kang. 2008. Cutting edge: Programmed death-1/programmed death ligand 1 interaction regulates the induction and maintenance of invariant NKT cell anergy. *J Immunol* 181: 6707-6710.
398. Parekh, V. V., S. Lalani, S. Kim, R. Halder, M. Azuma, H. Yagita, V. Kumar, L. Wu, and L. V. Kaer. 2009. PD-1/PD-L blockade prevents anergy induction and enhances the anti-tumor activities of glycolipid-activated invariant NKT cells. *J Immunol* 182: 2816-2826.
399. Schwartz, R. H. 2003. T cell anergy. *Annu Rev Immunol* 21: 305-334.
400. Akbari, O., P. Stock, E. H. Meyer, G. J. Freeman, A. H. Sharpe, D. T. Umetsu, and R. H. DeKruyff. 2008. ICOS/ICOSL interaction is required for CD4+ invariant NKT cell function and homeostatic survival. *J Immunol* 180: 5448-5456.
401. Miller, M. L., Y. Sun, and Y. X. Fu. 2009. Cutting edge: B and T lymphocyte attenuator signaling on NKT cells inhibits cytokine release and tissue injury in early immune responses. *J Immunol* 183: 32-36.
402. Kitamura, H., K. Iwakabe, T. Yahata, S. Nishimura, A. Ohta, Y. Ohmi, M. Sato, K. Takeda, K. Okumura, L. Van Kaer, T. Kawano, M. Taniguchi, and T. Nishimura. 1999. The natural killer T (NKT) cell ligand alpha-galactosylceramide demonstrates its immunopotentiating effect by inducing interleukin (IL)-12 production by dendritic cells and IL-12 receptor expression on NKT cells. *J Exp Med* 189: 1121-1128.
403. Pal, E., T. Tabira, T. Kawano, M. Taniguchi, S. Miyake, and T. Yamamura. 2001. Costimulation-dependent modulation of experimental autoimmune encephalomyelitis by ligand stimulation of V alpha 14 NK T cells. *J Immunol* 166: 662-668.
404. Fujii, S., K. Liu, C. Smith, A. J. Bonito, and R. M. Steinman. 2004. The linkage of innate to adaptive immunity via maturing dendritic cells in vivo requires CD40 ligation in addition to antigen presentation and CD80/86 costimulation. *J Exp Med* 199: 1607-1618.
405. Diana, J., T. Griseri, S. Lagaye, L. Beaudoin, E. Autrusseau, A. S. Gautron, C. Tomkiewicz, A. Herbelin, R. Barouki, M. von Herrath, M. Dalod, and A. Lehuen. 2009. NKT cell-plasmacytoid dendritic cell cooperation via OX40 controls viral infection in a tissue-specific manner. *Immunity* 30: 289-299.
406. Damayanti, T., T. Kikuchi, J. Zaini, H. Daito, M. Kanehira, K. Kohu, N. Ishii, M. Satake, K. Sugamura, and T. Nukiwa. 2010. Serial OX40 engagement on CD4+ T cells and natural killer T cells causes allergic airway inflammation. *Am J Respir Crit Care Med* 181: 688-698.
407. Vinay DS, C. B., Bae JS, Kim WY, Gebhardt BM, Kwon BS. 2004. CD137-deficient mice have reduced NK/NKT cell numbers and function, are resistant to lipopolysaccharide-induced shock syndromes, and have lower IL-4 responses. *Journal of Immunology* 173: 4218.
408. Kim, D. H., W. S. Chang, Y. S. Lee, K. A. Lee, Y. K. Kim, B. S. Kwon, and C. Y. Kang. 2008. 4-1BB engagement costimulates NKT cell activation and exacerbates NKT cell ligand-induced airway hyperresponsiveness and inflammation. *Journal of Immunology* 180: 2062-2068.
409. Teng, M. W. L., J. A. Westwood, P. K. Darcy, J. Sharkey, M. Tsuji, R. W. Franck, S. A. Porcelli, G. S. Besra, K. Takeda, H. Yagita, M. H. Kershaw, and M. Smyth. 2007. Combined natural killer T-cell-based immunotherapy eradicates established tumors in mice. *Cancer Research* 67: 7495-7504.

410. Kim, H. J., H. Y. Kim, B. K. Kim, S. Kim, and D. H. Chung. 2006. Engagement of glucocorticoid-induced TNF receptor costimulates NKT cell activation in vitro and in vivo. *J Immunol* 176: 3507-3515.
411. Berzofsky, J. A., and M. Terabe. 2008. NKT cells in tumor immunity: opposing subsets define a new immunoregulatory axis. *J Immunol* 180: 3627-3635.
412. Tessmer, M. S., A. Fatima, C. Paget, F. Trottein, and L. Brossay. 2009. NKT cell immune responses to viral infection. *Expert Opinion on Therapeutic Targets* 13: 153-162.
413. Ho, L. P., L. Denney, K. Luhn, D. Teoh, C. Clelland, and A. J. McMichael. 2008. Activation of invariant NKT cells enhances the innate immune response and improves the disease course in influenza A virus infection. *Eur J Immunol* 38: 1913-1922.
414. Kok, W. L., L. Denney, K. Benam, S. Cole, C. Clelland, A. J. McMichael, and L. P. Ho. 2012. Pivotal Advance: Invariant NKT cells reduce accumulation of inflammatory monocytes in the lungs and decrease immune-pathology during severe influenza A virus infection. *J Leukoc Biol* 91: 357-368.
415. Ishikawa, H., K. Tanaka, E. Kutsukake, T. Fukui, H. Sasaki, A. Hata, S. Noda, and T. Matsumoto. 2010. IFN-gamma production downstream of NKT cell activation in mice infected with influenza virus enhances the cytolytic activities of both NK cells and viral antigen-specific CD8(+) T cells. *Virology* 407: 325-332.
416. Paget, C., S. Ivanov, J. Fontaine, F. Blanc, M. Pichavant, J. Renneson, E. Bialecki, J. Pothlichet, C. Vendeville, G. Barba-Spaeth, M. R. Huerre, C. Faveeuw, M. Si-Tahar, and F. Trottein. 2011. Potential role of invariant NKT cells in the control of pulmonary inflammation and CD8+ T cell response during acute influenza A virus H3N2 pneumonia. *J Immunol* 186: 5590-5602.
417. Paget, C., S. Ivanov, J. Fontaine, J. Renneson, F. Blanc, M. Pichavant, L. Dumoutier, B. Ryffel, J. C. Renauld, P. Gosset, M. Si-Tahar, C. Faveeuw, and F. Trottein. 2012. Interleukin-22 Is Produced by Invariant Natural Killer T Lymphocytes during Influenza A Virus Infection POTENTIAL ROLE IN PROTECTION AGAINST LUNG EPITHELIAL DAMAGES. *J. Biol. Chem.* 287: 8816-8829.
418. Kopecky-Bromberg, S. A., K. A. Fraser, N. Pica, E. Carnero, T. M. Moran, R. W. Franck, M. Tsuji, and P. Palese. 2009. Alpha-C-galactosylceramide as an adjuvant for a live attenuated influenza virus vaccine. *Vaccine* 27: 3766-3774.
419. Guillonneau, C., J. D. Mintern, F. X. Hubert, A. C. Hurt, G. S. Besra, S. Porcelli, I. G. Barr, P. C. Doherty, D. I. Godfrey, and S. J. Turner. 2009. Combined NKT cell activation and influenza virus vaccination boosts memory CTL generation and protective immunity. *Proc Natl Acad Sci U S A* 106: 3330-3335.
420. Youn, H. J., S. Y. Ko, K. A. Lee, H. J. Ko, Y. S. Lee, K. Fujihashi, P. N. Boyaka, S. H. Kim, T. Horimoto, M. N. Kweon, and C. Y. Kang. 2007. A single intranasal immunization with inactivated influenza virus and alpha-galactosylceramide induces long-term protective immunity without redirecting antigen to the central nervous system. *Vaccine* 25: 5189-5198.
421. Kamijuku, H., Y. Nagata, X. Jiang, T. Ichinohe, T. Tashiro, K. Mori, M. Taniguchi, K. Hase, H. Ohno, T. Shimaoka, S. Yonehara, T. Odagiri, M. Tashiro, T. Sata, H. Hasegawa, and K. I. Seino. 2008. Mechanism of NKT cell activation by intranasal coadministration of alpha-galactosylceramide, which can induce cross-protection against influenza viruses. *Mucosal Immunol* 1: 208-218.
422. Benton, K. A., J. A. Misplon, C. Y. Lo, R. R. Brutkiewicz, S. A. Prasad, and S. L. Epstein. 2001. Heterosubtypic immunity to influenza A virus in mice lacking IgA, all Ig, NKT cells, or gamma delta T cells. *Journal of Immunology* 166: 7437-7445.

423. Maazi, H., A. K. Singh, A. O. Speak, V. Lombardi, J. Lam, B. Khoo, K. S. Inn, A. H. Sharpe, J. U. Jung, and O. Akbari. 2013. Lack of PD-L1 Expression by iNKT Cells Improves the Course of Influenza A Infection. *PLoS ONE* 8.
424. Altman, J. D., P. A. Moss, P. J. Goulder, D. H. Barouch, M. G. McHeyzer-Williams, J. I. Bell, A. J. McMichael, and M. M. Davis. 1996. Phenotypic analysis of antigen-specific T lymphocytes. *Science* 274: 94-96.
425. Lehner, P. J., E. C. Wang, P. A. Moss, S. Williams, K. Platt, S. M. Friedman, J. I. Bell, and L. K. Borysiewicz. 1995. Human HLA-A0201-restricted cytotoxic T lymphocyte recognition of influenza A is dominated by T cells bearing the V beta 17 gene segment. *J Exp Med* 181: 79-91.
426. Ho, L.-P., B. C. Urban, L. Jones, G. S. Ogg, and A. J. McMichael. 2004. CD4−CD8αα Subset of CD1d-Restricted NKT Cells Controls T Cell Expansion. *Journal of Immunology* 172: 7350-7358.
427. Fernández Do Porto, D. A., J. O. Jurado, V. Pasquinelli, I. B. Alvarez, R. H. Aspera, R. M. Musella, and V. E. García. 2012. CD137 differentially regulates innate and adaptive immunity against Mycobacterium tuberculosis. *Immunol. Cell Biol.* 90: 449-456.
428. Dong, T., G. Stewart-Jones, N. Chen, P. Easterbrook, X. Xu, L. Papagno, V. Appay, M. Weekes, C. Conlon, C. Spina, S. Little, G. Screaton, A. van der Merwe, D. D. Richman, A. J. McMichael, E. Y. Jones, and S. L. Rowland-Jones. 2004. HIV-specific cytotoxic T cells from long-term survivors select a unique T cell receptor. *J Exp Med* 200: 1547-1557.
429. Powell, T. J., Y. Peng, T. K. Berthoud, M. E. Blais, P. J. Lillie, A. V. Hill, S. L. Rowland-Jones, A. J. McMichael, S. C. Gilbert, and T. Dong. 2013. Examination of influenza specific T cell responses after influenza virus challenge in individuals vaccinated with MVA-NP+M1 vaccine. *PLoS ONE* 8: e62778.
430. Huang da, W., B. T. Sherman, and R. A. Lempicki. 2009. Systematic and integrative analysis of large gene lists using DAVID bioinformatics resources. *Nat Protoc* 4: 44-57.
431. Huang da, W., B. T. Sherman, and R. A. Lempicki. 2009. Bioinformatics enrichment tools: paths toward the comprehensive functional analysis of large gene lists. *Nucleic Acids Res* 37: 1-13.
432. Subramanian, A., P. Tamayo, V. K. Mootha, S. Mukherjee, B. L. Ebert, M. A. Gillette, A. Paulovich, S. L. Pomeroy, T. R. Golub, E. S. Lander, and J. P. Mesirov. 2005. Gene set enrichment analysis: a knowledge-based approach for interpreting genome-wide expression profiles. *Proc Natl Acad Sci U S A* 102: 15545-15550.
433. Nguyen-Van-Tam, J. S., P. J. Openshaw, A. Hashim, E. M. Gadd, W. S. Lim, M. G. Semple, R. C. Read, B. L. Taylor, S. J. Brett, J. McMenamin, J. E. Enstone, C. Armstrong, and K. G. Nicholson. 2010. Risk factors for hospitalisation and poor outcome with pandemic A/H1N1 influenza: United Kingdom first wave (May-September 2009). *Thorax* 65: 645-651.
434. Muramoto, Y., J. E. Shoemaker, M. Q. Le, Y. Itoh, D. Tamura, Y. Sakai-Tagawa, H. Imai, R. Uraki, R. Takano, E. Kawakami, M. Ito, K. Okamoto, H. Ishigaki, H. Mimuro, C. Sasakawa, Y. Matsuoka, T. Noda, S. Fukuyama, K. Ogasawara, H. Kitano, and Y. Kawaoka. 2014. Disease Severity Is Associated with Differential Gene Expression at the Early and Late Phases of Infection in Nonhuman Primates Infected with Different H5N1 Highly Pathogenic Avian Influenza Viruses. *J Virol* 88: 8981-8997.
435. Zhao, Y., Y. H. Zhang, L. Denney, D. Young, T. J. Powell, Y. C. Peng, N. Li, H. P. Yan, D. Y. Wang, Y. L. Shu, Y. Kendrick, A. J. McMichael, L. P. Ho, and T. Dong. 2012. High levels of virus-specific CD4+ T cells predict severe pandemic influenza A virus infection. *Am J Respir Crit Care Med* 186: 1292-1297.
436. Butler, D. 2012. Death-rate row blurs mutant flu debate. *Nature* 482: 289.

437. Meunier, I., S. Pillet, J. N. Simonsen, and V. von Messling. 2010. Influenza pathogenesis: lessons learned from animal studies with H5N1, H1N1 Spanish, and pandemic H1N1 2009 influenza. *Crit Care Med* 38: e21-29.
438. Gao, W., A. C. Soloff, X. Lu, A. Montecalvo, D. C. Nguyen, Y. Matsuoka, P. D. Robbins, D. E. Swayne, R. O. Donis, J. M. Katz, S. M. Barratt-Boyes, and A. Gambotto. 2006. Protection of mice and poultry from lethal H5N1 avian influenza virus through adenovirus-based immunization. *J Virol* 80: 1959-1964.
439. Ringner, M. 2008. What is principal component analysis? *Nat Biotech* 26: 303-304.
440. Taguchi, K., A. Okada, H. Kitamura, T. Yasui, T. Naiki, S. Hamamoto, R. Ando, K. Mizuno, N. Kawai, K. Tozawa, K. Asano, M. Tanaka, I. Miyoshi, and K. Kohri. 2014. Colony-stimulating factor-1 signaling suppresses renal crystal formation. *J Am Soc Nephrol* 25: 1680-1697.
441. Badylak, S. F., J. E. Valentin, A. K. Ravindra, G. P. McCabe, and A. M. Stewart-Akers. 2008. Macrophage phenotype as a determinant of biologic scaffold remodeling. *Tissue Eng Part A* 14: 1835-1842.
442. Gu, J., Z. Xie, Z. Gao, J. Liu, C. Korteweg, J. Ye, L. T. Lau, J. Lu, B. Zhang, M. A. McNutt, M. Lu, V. M. Anderson, E. Gong, A. C. Yu, and W. I. Lipkin. 2007. H5N1 infection of the respiratory tract and beyond: a molecular pathology study. *Lancet* 370: 1137-1145.
443. Chutinimitkul, S., P. Bhattarakosol, S. Srisuratanon, A. Eiamudomkan, K. Kongsomboon, S. Damrongwatanapokin, A. Chaisingh, K. Suwannakarn, T. Chieochansin, A. Theamboonlers, and Y. Poovorawan. 2006. H5N1 influenza A virus and infected human plasma. *Emerg Infect Dis* 12: 1041-1043.
444. de Jong, M. D., C. P. Simmons, T. T. Thanh, V. M. Hien, G. J. Smith, T. N. Chau, D. M. Hoang, N. V. Chau, T. H. Khanh, V. C. Dong, P. T. Qui, B. V. Cam, Q. Ha do, Y. Guan, J. S. Peiris, N. T. Chinh, T. T. Hien, and J. Farrar. 2006. Fatal outcome of human influenza A (H5N1) is associated with high viral load and hypercytokinemia. *Nat Med* 12: 1203-1207.
445. Horimoto, T., and Y. Kawaoka. 1994. Reverse genetics provides direct evidence for a correlation of hemagglutinin cleavability and virulence of an avian influenza A virus. *J Virol* 68: 3120-3128.
446. Le, Q. M., M. Kiso, K. Someya, Y. T. Sakai, T. H. Nguyen, K. H. Nguyen, N. D. Pham, H. H. Ngyen, S. Yamada, Y. Muramoto, T. Horimoto, A. Takada, H. Goto, T. Suzuki, Y. Suzuki, and Y. Kawaoka. 2005. Avian flu: isolation of drug-resistant H5N1 virus. *Nature* 437: 1108.
447. Korteweg, C., and J. Gu. 2008. Pathology, molecular biology, and pathogenesis of avian influenza A (H5N1) infection in humans. *Am J Pathol* 172: 1155-1170.
448. Seo, S. H., E. Hoffmann, and R. G. Webster. 2002. Lethal H5N1 influenza viruses escape host anti-viral cytokine responses. *Nat Med* 8: 950-954.
449. Paquette, S. G., D. Banner, Z. Zhao, Y. Fang, S. S. H. Huang, A. J. León, D. C. K. Ng, R. Almansa, I. Martin-Loeches, P. Ramirez, L. Socias, A. Loza, J. Blanco, P. Sansonetti, J. Rello, D. Andaluz, B. Shum, S. Rubino, R. O. de Lejarazu, D. Tran, G. Delogu, G. Fadda, S. Krajden, B. B. Rubin, J. F. Bermejo-Martin, A. A. Kelvin, and D. J. Kelvin. 2012. Interleukin-6 Is a Potential Biomarker for Severe Pandemic H1N1 Influenza A Infection. *PLoS ONE* 7: e38214.
450. Gentile, D., W. Doyle, T. Whiteside, P. Fireman, F. G. Hayden, and D. Skoner. 1998. Increased interleukin-6 levels in nasal lavage samples following experimental influenza a virus infection. *Clinical and Diagnostic Laboratory Immunology* 5: 604-608.
451. Lauder, S. N., E. Jones, K. Smart, A. Bloom, A. S. Williams, J. P. Hindley, B. Ondondo, P. R. Taylor, M. Clement, C. Fielding, A. J. Godkin, S. A. Jones, and A. M. Gallimore. 2013. Interleukin-6 limits influenza-induced inflammation and

protects against fatal lung pathology. *European Journal of Immunology* 43: 2613-2625.
452. Dienz, O., J. G. Rud, S. M. Eaton, P. A. Lanthier, E. Burg, A. Drew, J. Bunn, B. T. Suratt, L. Haynes, and M. Rincon. 2012. Essential role of IL-6 in protection against H1N1 influenza virus by promoting neutrophil survival in the lung. *Mucosal Immunol* 5: 258-266.
453. Kimura, A., and T. Kishimoto. 2010. IL-6: regulator of Treg/Th17 balance. *Eur J Immunol* 40: 1830-1835.
454. Longhi, M. P., K. Wright, S. N. Lauder, M. A. Nowell, G. W. Jones, A. J. Godkin, S. A. Jones, and A. M. Gallimore. 2008. Interleukin-6 Is Crucial for Recall of Influenza-Specific Memory CD4⁺ T Cells. *PLoS Pathog* 4: e1000006.
455. Antunes, I., and G. Kassiotis. 2010. Suppression of innate immune pathology by regulatory T cells during Influenza A virus infection of immunodeficient mice. *J Virol* 84: 12564-12575.
456. Uguccioni, M., M. D'Apuzzo, M. Loetscher, B. Dewald, and M. Baggiolini. 1995. Actions of the chemotactic cytokines MCP-1, MCP-2, MCP-3, RANTES, MIP-1 alpha and MIP-1 beta on human monocytes. *Eur J Immunol* 25: 64-68.
457. Nakayama, T., S. Sonoda, T. Urano, T. Yamada, and M. Okada. 1993. Monitoring both Serum Amyloid Protein-A and C-Reactive Protein as inflamamtory markers in infectious diseases. *Clinical Chemistry* 39: 293-297.
458. Ioannidis, I., B. McNally, M. Willette, M. E. Peeples, D. Chaussabel, J. E. Durbin, O. Ramilo, A. Mejias, and E. Flano. 2012. Plasticity and virus specificity of the airway epithelial cell immune response during respiratory virus infection. *J Virol* 86: 5422-5436.
459. Wang, X., E. R. Hinson, and P. Cresswell. 2007. The interferon-inducible protein viperin inhibits influenza virus release by perturbing lipid rafts. *Cell Host Microbe* 2: 96-105.
460. Verhelst, J., E. Parthoens, B. Schepens, W. Fiers, and X. Saelens. 2012. Interferon-inducible protein Mx1 inhibits influenza virus by interfering with functional viral ribonucleoprotein complex assembly. *J Virol* 86: 13445-13455.
461. Svitek, N., P. A. Rudd, K. Obojes, S. Pillet, and V. von Messling. 2008. Severe seasonal influenza in ferrets correlates with reduced interferon and increased IL-6 induction. *Virology* 376: 53-59.
462. Dufour, J. H., M. Dziejman, M. T. Liu, J. H. Leung, T. E. Lane, and A. D. Luster. 2002. IFN-gamma-inducible protein 10 (IP-10; CXCL10)-deficient mice reveal a role for IP-10 in effector T cell generation and trafficking. *J Immunol* 168: 3195-3204.
463. Wang, W., P. Yang, Y. Zhong, Z. Zhao, L. Xing, Y. Zhao, Z. Zou, Y. Zhang, C. Li, T. Li, C. Wang, Z. Wang, X. Yu, B. Cao, X. Gao, J. M. Penninger, X. Wang, and C. Jiang. 2013. Monoclonal antibody against CXCL-10/IP-10 ameliorates influenza A (H1N1) virus induced acute lung injury. *Cell Res* 23: 577-580.
464. Yoshimura, T., E. A. Robinson, S. Tanaka, E. Appella, and E. J. Leonard. 1989. Purification and amino acid analysis of two human monocyte chemoattractants produced by phytohemagglutinin-stimulated human blood mononuclear leukocytes. *J Immunol* 142: 1956-1962.
465. Dessinga, M. C., K. F. van der Sluijsa, S. Florquine, and T. van der Polla. 2007. Monocyte chemoattractant protein 1 contributes to an adequate immune response in influenza pneumonia *Clinical Immunology* 125: 328-336.
466. Wang, J., F. Li, R. Sun, X. Gao, H. Wei, L.-J. Li, and Z. Tian. 2013. Bacterial colonization dampens influenza-mediated acute lung injury via induction of M2 alveolar macrophages. *Nat Commun* 4.
467. Beigel, J. H., J. Farrar, A. M. Han, F. G. Hayden, R. Hyer, M. D. de Jong, S. Lochindarat, T. K. Nguyen, T. H. Nguyen, T. H. Tran, A. Nicoll, S. Touch, and K.

Y. Yuen. 2005. Avian influenza A (H5N1) infection in humans. *N Engl J Med* 353: 1374-1385.

468. Schroeder, B. W., C. Verhaeghe, S. W. Park, L. T. Nguyenvu, X. Huang, G. Zhen, and D. J. Erle. 2012. AGR2 is induced in asthma and promotes allergen-induced mucin overproduction. *Am J Respir Cell Mol Biol* 47: 178-185.
469. Wang, G., Z. Xu, R. Wang, M. Al-Hijji, J. Salit, Y. Strulovici-Barel, A. E. Tilley, J. G. Mezey, and R. G. Crystal. 2012. Genes associated with MUC5AC expression in small airway epithelium of human smokers and non-smokers. *BMC Med Genomics* 5: 21.
470. Gill, J. R., Z.-M. Sheng, S. F. Ely, D. G. Guinee, M. B. Beasley, J. Suh, C. Deshpande, D. J. Mollura, D. M. Morens, M. Bray, W. D. Travis, and J. K. Taubenberger. 2010. Pulmonary Pathologic Findings of Fatal 2009 Pandemic Influenza A/H1N1 Viral Infections. *Archives of Pathology & Laboratory Medicine* 134: 235-243.
471. Purnama, C., S. L. Ng, P. Tetlak, Y. A. Setiagani, M. Kandasamy, S. Baalasubramanian, K. Karjalainen, and C. Ruedl. 2014. Transient ablation of alveolar macrophages leads to massive pathology of influenza infection without affecting cellular adaptive immunity. *Eur J Immunol* 44: 2003-2012.
472. Everitt, A. R., S. Clare, T. Pertel, S. P. John, R. S. Wash, S. E. Smith, C. R. Chin, E. M. Feeley, J. S. Sims, D. J. Adams, H. M. Wise, L. Kane, D. Goulding, P. Digard, V. Anttila, J. K. Baillie, T. S. Walsh, D. A. Hume, A. Palotie, Y. L. Xue, V. Colonna, C. Tyler-Smith, J. Dunning, S. B. Gordon, R. L. Smyth, P. J. Openshaw, G. Dougan, A. L. Brass, P. Kellam, I. I. Gen, and M. Investigators. 2012. IFITM3 restricts the morbidity and mortality associated with influenza. *Nature* 484: 519-U146.
473. Venables, W. N., and B. D. Ripley. 2002. *Modern Applied Statistics with S*. Springer, New York.
474. Geissmann, F., M. G. Manz, S. Jung, M. H. Sieweke, M. Merad, and K. Ley. 2010. Development of Monocytes, Macrophages, and Dendritic Cells. *Science* 327: 656-661.
475. Carmona-Rivera, C., and M. J. Kaplan. 2013. Low-density granulocytes: a distinct class of neutrophils in systemic autoimmunity. *Semin Immunopathol* 35: 455-463.
476. Abeles, R. D., M. J. McPhail, D. Sowter, C. G. Antoniades, N. Vergis, G. K. Vijay, E. Xystrakis, W. Khamri, D. L. Shawcross, Y. Ma, J. A. Wendon, and D. Vergani. 2012. CD14, CD16 and HLA-DR reliably identifies human monocytes and their subsets in the context of pathologically reduced HLA-DR expression by CD14(hi) /CD16(neg) monocytes: Expansion of CD14(hi) /CD16(pos) and contraction of CD14(lo) /CD16(pos) monocytes in acute liver failure. *Cytometry A* 81: 823-834.
477. Crawshaw, A., Y. R. Kendrick, A. J. McMichael, and L. P. Ho. 2014. Abnormalities in iNKT cells are associated with impaired ability of monocytes to produce IL-10 and suppress T-cell proliferation in sarcoidosis. *Eur J Immunol* 44: 2165-2174.
478. Seo, S. H., and R. G. Webster. 2002. Tumor necrosis factor alpha exerts powerful anti-influenza virus effects in lung epithelial cells. *J Virol* 76: 1071-1076.
479. Ziegler-Heitbrock, L. 2007. The CD14+ CD16+ blood monocytes: their role in infection and inflammation. *Journal of Leukocyte Biology* 81: 584-592.
480. Mizuno, K., T. Toma, H. Tsukiji, H. Okamoto, H. Yamazaki, K. Ohta, Y. Kasahara, S. Koizumi, and A. Yachie. 2005. Selective expansion of CD16highCCR2- subpopulation of circulating monocytes with preferential production of haem oxygenase (HO)-1 in response to acute inflammation. *Clin Exp Immunol* 142: 461-470.

481. Ziegler-Heitbrock, H. W. L., G. Fingerle, M. Ströbel, W. Schraut, F. Stelter, C. Schütt, B. Passlick, and A. Pforte. 1993. The novel subset of CD14+/CD16+ blood monocytes exhibits features of tissue macrophages. *European Journal of Immunology* 23: 2053-2058.
482. Feng, A. L., J. K. Zhu, J. T. Sun, M. X. Yang, M. R. Neckenig, X. W. Wang, Q. Q. Shao, B. F. Song, Q. F. Yang, B. H. Kong, and X. Qu. 2011. CD16+ monocytes in breast cancer patients: expanded by monocyte chemoattractant protein-1 and may be useful for early diagnosis. *Clin Exp Immunol* 164: 57-65.
483. van Furth, R., J. A. Raeburn, and T. L. van Zwet. 1979. Characteristics of human mononuclear phagocytes. *Blood* 54: 485-500.
484. Burdo, T. H., C. Soulas, K. Orzechowski, J. Button, A. Krishnan, C. Sugimoto, X. Alvarez, M. J. Kuroda, and K. C. Williams. 2010. Increased Monocyte Turnover from Bone Marrow Correlates with Severity of SIV Encephalitis and CD163 Levels in Plasma. *PLoS Pathog* 6: e1000842.
485. Serbina, N. V., and E. G. Pamer. 2006. Monocyte emigration from bone marrow during bacterial infection requires signals mediated by chemokine receptor CCR2. *Nat Immunol* 7: 311-317.
486. Seo, S.-U., H.-J. Kwon, H.-J. Ko, Y.-H. Byun, B. L. Seong, S. Uematsu, S. Akira, and M.-N. Kweon. 2011. Type I Interferon Signaling Regulates Ly6C^{hi} Monocytes and Neutrophils during Acute Viral Pneumonia in Mice. *PLoS Pathog* 7: e1001304.
487. Schurch, C. M., C. Riether, and A. F. Ochsenbein. 2014. Cytotoxic CD8+ T cells stimulate hematopoietic progenitors by promoting cytokine release from bone marrow mesenchymal stromal cells. *Cell Stem Cell* 14: 460-472.
488. Palojarvi, A., J. Petaja, S. Siitonen, C. Janer, and S. Andersson. 2013. Low monocyte HLA-DR expression as an indicator of immunodepression in very low birth weight infants. *Pediatr Res* 73: 469-475.
489. Antoniades, C. G., P. A. Berry, E. T. Davies, M. Hussain, W. Bernal, D. Vergani, and J. Wendon. 2006. Reduced monocyte HLA-DR expression: a novel biomarker of disease severity and outcome in acetaminophen-induced acute liver failure. *Hepatology* 44: 34-43.
490. Haveman, J. W., A. P. van den Berg, J. M. van den Berk, G. Mesander, M. J. Slooff, L. H. de Leij, and T. H. The. 1999. Low HLA-DR expression on peripheral blood monocytes predicts bacterial sepsis after liver transplantation: relation with prednisolone intake. *Transpl Infect Dis* 1: 146-152.
491. Hershman, M. J., W. G. Cheadle, S. R. Wellhausen, P. F. Davidson, and H. C. Polk, Jr. 1990. Monocyte HLA-DR antigen expression characterizes clinical outcome in the trauma patient. *Br J Surg* 77: 204-207.
492. Wakefield, C. H., P. D. Carey, S. Foulds, J. R. Monson, and P. J. Guillou. 1993. Changes in major histocompatibility complex class II expression in monocytes and T cells of patients developing infection after surgery. *Br J Surg* 80: 205-209.
493. Hegde, N. R., R. A. Tomazin, T. W. Wisner, C. Dunn, J. M. Boname, D. M. Lewinsohn, and D. C. Johnson. 2002. Inhibition of HLA-DR assembly, transport, and loading by human cytomegalovirus glycoprotein US3: a novel mechanism for evading major histocompatibility complex class II antigen presentation. *J Virol* 76: 10929-10941.
494. Diao, H., G. Cui, Y. Wei, J. Chen, J. Zuo, H. Cao, Y. Chen, H. Yao, Z. Tian, and L. Li. 2014. Severe H7N9 Infection Is Associated with Decreased Antigen-Presenting Capacity of CD14⁺ Cells. *PLoS ONE* 9: e92823.
495. Carrasco, M., L. Munoz, M. Bellido, S. Bernat, E. Rubiol, J. Ubeda, J. Sierra, and J. F. Nomdedeu. 2000. CD66 expression in acute leukaemia. *Ann Hematol* 79: 299-303.
496. Choi, J., B. Suh, Y. O. Ahn, T. M. Kim, J. O. Lee, S. H. Lee, and D. S. Heo. 2012. CD15+/CD16low human granulocytes from terminal cancer patients:

granulocytic myeloid-derived suppressor cells that have suppressive function. *Tumour Biol* 33: 121-129.
497. Cloke, T., M. Munder, G. Taylor, I. Muller, and P. Kropf. 2012. Characterization of a novel population of low-density granulocytes associated with disease severity in HIV-1 infection. *PLoS ONE* 7: e48939.
498. Pillay, J., V. M. Kamp, E. van Hoffen, T. Visser, T. Tak, J. W. Lammers, L. H. Ulfman, L. P. Leenen, P. Pickkers, and L. Koenderman. 2012. A subset of neutrophils in human systemic inflammation inhibits T cell responses through Mac-1. *J Clin Invest* 122: 327-336.
499. Slaney, C. Y., A. Toker, A. La Flamme, B. T. Backstrom, and J. L. Harper. 2011. Naive blood monocytes suppress T-cell function. A possible mechanism for protection from autoimmunity. *Immunol Cell Biol* 89: 7-13.
500. McKinstry, K. K., T. M. Strutt, A. Buck, J. D. Curtis, J. P. Dibble, G. Huston, M. Tighe, H. Hamada, S. Sell, R. W. Dutton, and S. L. Swain. 2009. IL-10 deficiency unleashes an influenza-specific Th17 response and enhances survival against high-dose challenge. *J Immunol* 182: 7353-7363.
501. Yu, X., X. Zhang, B. Zhao, J. Wang, Z. Zhu, Z. Teng, J. Shao, J. Shen, Y. Gao, Z. Yuan, and F. Wu. 2011. Intensive Cytokine induction in Pandemic H1N1 Influenza Virus Infection Accompanied by Robust Production of IL-10 and IL-6. *PLoS ONE* 6: e28680.
502. Cunningham, L. 2009. Influenza infection: the origin and role of IL10. *Thorax* 64: 805.
503. Leghmari, K., Y. Bennasser, and E. Bahraoui. 2008. HIV-1 Tat protein induces IL-10 production in monocytes by classical and alternative NF-kappaB pathways. *Eur J Cell Biol* 87: 947-962.
504. Kuhweide, R., J. Van Damme, and J. L. Ceuppens. 1990. Tumor necrosis factor-alpha and interleukin 6 synergistically induce T cell growth. *Eur J Immunol* 20: 1019-1025.
505. Tate, M. D., L. J. Ioannidis, B. Croker, L. E. Brown, A. G. Brooks, and P. C. Reading. 2011. The Role of Neutrophils during Mild and Severe Influenza Virus Infections of Mice. *PLoS ONE* 6: e17618.
506. Kowal, K., M. Moniuszko, and A. Bodzenta-Lukaszyk. 2014. The effect of inhaled corticosteroids on the concentration of soluble CD163 in induced sputum of allergic asthma patients. *J Investig Allergol Clin Immunol* 24: 49-55.
507. Ford, A. Q., P. Dasgupta, I. Mikhailenko, E. M. Smith, N. Noben-Trauth, and A. D. Keegan. 2012. Adoptive transfer of IL-4Ralpha+ macrophages is sufficient to enhance eosinophilic inflammation in a mouse model of allergic lung inflammation. *BMC Immunol* 13: 6.
508. Li, C., P. Yang, Y. Zhang, Y. Sun, W. Wang, Z. Zou, L. Xing, Z. Chen, C. Tang, F. Guo, J. Deng, Y. Zhao, Y. Yan, J. Tang, X. Wang, and C. Jiang. 2012. Corticosteroid Treatment Ameliorates Acute Lung Injury Induced by 2009 Swine Origin Influenza A (H1N1) Virus in Mice. *PLoS ONE* 7: e44110.
509. Couch, R. B., and J. A. Kasel. 1983. Immunity to influenza in man. *Annu Rev Microbiol* 37: 529-549.
510. McGill, J., J. W. Heusel, and K. L. Legge. 2009. Innate immune control and regulation of influenza virus infections. *J Leukoc Biol* 86: 803-812.
511. Hohl, T. M., A. Rivera, L. Lipuma, A. Gallegos, C. Shi, M. Mack, and E. G. Pamer. Inflammatory Monocytes Facilitate Adaptive CD4 T Cell Responses during Respiratory Fungal Infection. *Cell Host & Microbe* 6: 470-481.
512. Castellino, F., and R. N. Germain. 2006. Cooperation between CD4+ and CD8+ T cells: when, where, and how. *Annu Rev Immunol* 24: 519-540.
513. Topham, D. J., R. A. Tripp, and P. C. Doherty. 1997. CD8+ T cells clear influenza virus by perforin or Fas-dependent processes. *J Immunol* 159: 5197-5200.

514. Moskophidis, D., and D. Kioussis. 1998. Contribution of virus-specific CD8+ cytotoxic T cells to virus clearance or pathologic manifestations of influenza virus infection in a T cell receptor transgenic mouse model. *J Exp Med* 188: 223-232.
515. Chong, S. Z., K. L. Wong, G. Lin, C. M. Yang, S.-C. Wong, V. Angeli, P. A. MacAry, and D. M. Kemeny. 2011. Human CD8+ T cells drive Th1 responses through the differentiation of TNF/iNOS-producing dendritic cells. *European Journal of Immunology* 41: 1639-1651.
516. Allan, W., Z. Tabi, A. Cleary, and P. C. Doherty. 1990. Cellular events in the lymph node and lung of mice with influenza. Consequences of depleting CD4+ T cells. *J Immunol* 144: 3980-3986.
517. Hua, L., S. Yao, D. Pham, L. Jiang, J. Wright, D. Sawant, A. L. Dent, T. J. Braciale, M. H. Kaplan, and J. Sun. 2013. Cytokine-dependent induction of CD4+ T cells with cytotoxic potential during influenza virus infection. *J Virol* 87: 11884-11893.
518. Miller, J. D., R. G. van der Most, R. S. Akondy, J. T. Glidewell, S. Albott, D. Masopust, K. Murali-Krishna, P. L. Mahar, S. Edupuganti, S. Lalor, S. Germon, C. Del Rio, M. J. Mulligan, S. I. Staprans, J. D. Altman, M. B. Feinberg, and R. Ahmed. 2008. Human effector and memory CD8+ T cell responses to smallpox and yellow fever vaccines. *Immunity* 28: 710-722.
519. Denney, L., C. Aitken, C. Li, E. Wilson-Davies, W. Kok, C. Clelland, K. Rooney, D. Young, T. Dong, A. McMichael, W. Carman, and L. Ho. 2010. Reduction of Natural Killer but Not Effector CD8 T Lymphocytes in Three Consecutive Cases of Severe/Lethal H1N1/09 Influenza A Virus Infection. *PLoS ONE* 5: 1-9.
520. Rutigliano, J. A., S. Sharma, M. Y. Morris, T. H. Oguin, 3rd, J. L. McClaren, P. C. Doherty, and P. G. Thomas. 2014. Highly pathological influenza A virus infection is associated with augmented expression of PD-1 by functionally compromised virus-specific CD8+ T cells. *J Virol* 88: 1636-1651.
521. Murali-Krishna, K., J. D. Altman, M. Suresh, D. J. Sourdive, A. J. Zajac, J. D. Miller, J. Slansky, and R. Ahmed. 1998. Counting antigen-specific CD8 T cells: a reevaluation of bystander activation during viral infection. *Immunity* 8: 177-187.
522. Barber, D. L., E. J. Wherry, D. Masopust, B. Zhu, J. P. Allison, A. H. Sharpe, G. J. Freeman, and R. Ahmed. 2006. Restoring function in exhausted CD8 T cells during chronic viral infection. *Nature* 439: 682-687.
523. Badovinac, V. P., B. B. Porter, and J. T. Harty. 2002. Programmed contraction of CD8(+) T cells after infection. *Nat Immunol* 3: 619-626.
524. Riberdy, J. M., J. P. Christensen, K. Branum, and P. C. Doherty. 2000. Diminished primary and secondary influenza virus-specific CD8(+) T-cell responses in CD4-depleted Ig(-/-) mice. *J Virol* 74: 9762-9765.
525. Celli, S., Z. Garcia, and P. Bousso. 2005. CD4 T cells integrate signals delivered during successive DC encounters in vivo. *J Exp Med* 202: 1271-1278.
526. Qu, C., T. M. Moran, and G. J. Randolph. 2003. Autocrine type I IFN and contact with endothelium promote the presentation of influenza A virus by monocyte-derived APC. *J Immunol* 170: 1010-1018.
527. Townsend, A. R. M., A. J. McMichael, N. P. Carter, J. A. Huddleston, and G. G. Brownlee. 1984. Cytotoxic T cell recognition of the influenza nucleoprotein and hemagglutinin expressed in transfected mouse L cells. *Cell* 39: 13-25.
528. Yewdell, J. W., J. R. Bennink, G. L. Smith, and B. Moss. 1985. Influenza A virus nucleoprotein is a major target antigen for cross-reactive anti-influenza A virus cytotoxic T lymphocytes. *Proceedings of the National Academy of Sciences* 82: 1785-1789.
529. McMichael, A. J., C. A. Michie, F. M. Gotch, G. L. Smith, and B. Moss. 1986. Recognition of influenza A virus nucleoprotein by human cytotoxic T lymphocytes. *J Gen Virol* 67 (Pt 4): 719-726.

530. Lee, L. Y., L. A. Ha do, C. Simmons, M. D. de Jong, N. V. Chau, R. Schumacher, Y. C. Peng, A. J. McMichael, J. J. Farrar, G. L. Smith, A. R. Townsend, B. A. Askonas, S. Rowland-Jones, and T. Dong. 2008. Memory T cells established by seasonal human influenza A infection cross-react with avian influenza A (H5N1) in healthy individuals. *J Clin Invest* 118: 3478-3490.
531. Lee, S. M., I. Dutry, and J. S. Peiris. 2012. Editorial: macrophage heterogeneity and responses to influenza virus infection. *J Leukoc Biol* 92: 1-4.
532. Hamza, T., J. B. Barnett, and B. Li. 2010. Interleukin 12 a key immunoregulatory cytokine in infection applications. *Int J Mol Sci* 11: 789-806.
533. Scanlon, S. T., S. Y. Thomas, C. M. Ferreira, L. Bai, T. Krausz, P. B. Savage, and A. Bendelac. 2011. Airborne lipid antigens mobilize resident intravascular NKT cells to induce allergic airway inflammation. *J Exp Med* 208: 2113-2124.
534. Delneste, Y., P. Charbonnier, N. Herbault, G. Magistrelli, G. Caron, J.-Y. Bonnefoy, and P. Jeannin. 2003. *Interferon-γ switches monocyte differentiation from dendritic cells to macrophages*.
535. Rusinova, I., S. Forster, S. Yu, A. Kannan, M. Masse, H. Cumming, R. Chapman, and P. J. Hertzog. 2013. Interferome v2.0: an updated database of annotated interferon-regulated genes. *Nucleic Acids Res* 41: D1040-1046.
536. Alcala, S., M. Klee, J. Fernandez, A. Fleischer, and F. X. Pimentel-Muinos. 2008. A high-throughput screening for mammalian cell death effectors identifies the mitochondrial phosphate carrier as a regulator of cytochrome c release. *Oncogene* 27: 44-54.
537. Tran, H. B., M. D. Lewis, L. W. Tan, S. E. Lester, L. M. Baker, J. Ng, M. A. Hamilton-Bruce, C. L. Hill, S. A. Koblar, M. Rischmueller, R. E. Ruffin, P. J. Wormald, P. D. Zalewski, and C. J. Lang. 2012. Immunolocalization of NLRP3 Inflammasome in Normal Murine Airway Epithelium and Changes following Induction of Ovalbumin-Induced Airway Inflammation. *J Allergy (Cairo)* 2012: 819176.
538. Riquelme, P., S. Tomiuk, A. Kammler, F. Fandrich, H. J. Schlitt, E. K. Geissler, and J. A. Hutchinson. 2013. IFN-gamma-induced iNOS expression in mouse regulatory macrophages prolongs allograft survival in fully immunocompetent recipients. *Mol Ther* 21: 409-422.
539. Brigl, M., R. V. Tatituri, G. F. Watts, V. Bhowruth, E. A. Leadbetter, N. Barton, N. R. Cohen, F. F. Hsu, G. S. Besra, and M. B. Brenner. 2011. Innate and cytokine-driven signals, rather than microbial antigens, dominate in natural killer T cell activation during microbial infection. *J Exp Med* 208: 1163-1177.
540. Holzapfel, K. L., A. J. Tyznik, M. Kronenberg, and K. A. Hogquist. 2014. Antigen-dependent versus -independent activation of invariant NKT cells during infection. *J Immunol* 192: 5490-5498.
541. Thomas, S. Y., S. T. Scanlon, K. G. Griewank, M. G. Constantinides, A. K. Savage, K. A. Barr, F. Meng, A. D. Luster, and A. Bendelac. 2011. PLZF induces an intravascular surveillance program mediated by long-lived LFA-1-ICAM-1 interactions. *J Exp Med* 208: 1179-1188.
542. Hoeve, M. A., A. A. Nash, D. Jackson, R. E. Randall, and I. Dransfield. 2012. Influenza virus A infection of human monocyte and macrophage subpopulations reveals increased susceptibility associated with cell differentiation. *PLoS ONE* 7: e29443.
543. Chan, M. C., C. Y. Cheung, W. H. Chui, S. W. Tsao, J. M. Nicholls, Y. O. Chan, R. W. Chan, H. T. Long, L. L. Poon, Y. Guan, and J. S. Peiris. 2005. Proinflammatory cytokine responses induced by influenza A (H5N1) viruses in primary human alveolar and bronchial epithelial cells. *Respir Res* 6: 135.
544. Beilharz, M. W., J. M. Cummins, and A. L. Bennett. 2007. Protection from lethal influenza virus challenge by oral type 1 interferon. *Biochem Biophys Res Commun* 355: 740-744.

545. Durbin, J. E., A. Fernandez-Sesma, C. K. Lee, T. D. Rao, A. B. Frey, T. M. Moran, S. Vukmanovic, A. Garcia-Sastre, and D. E. Levy. 2000. Type I IFN modulates innate and specific antiviral immunity. *J Immunol* 164: 4220-4228.
546. Krausgruber, T., K. Blazek, T. Smallie, S. Alzabin, H. Lockstone, N. Sahgal, T. Hussell, M. Feldmann, and I. A. Udalova. 2011. IRF5 promotes inflammatory macrophage polarization and TH1-TH17 responses. *Nat Immunol* 12: 231-238.
547. Zhao, X., J. Dai, X. Xiao, L. Wu, J. Zeng, J. Sheng, J. Su, X. Chen, G. Wang, and K. Li. 2014. PI3K/Akt signaling pathway modulates influenza virus induced mouse alveolar macrophage polarization to M1/M2b. *PLoS ONE* 9: e104506.
548. Girgis, N. M., U. M. Gundra, L. N. Ward, M. Cabrera, U. Frevert, and P. n. Loke. 2014. Ly6Chigh Monocytes Become Alternatively Activated Macrophages in Schistosome Granulomas with Help from CD4+ Cells. *PLoS Pathog* 10: e1004080.
549. Nowak, M., F. Kopp, K. Roelofs-Haarhuis, X. Wu, and E. Gleichmann. 2006. Oral nickel tolerance: Fas ligand-expressing invariant NK T cells promote tolerance induction by eliciting apoptotic death of antigen-carrying, effete B cells. *J Immunol* 176: 4581-4589.
550. Nieda, M., A. Nicol, Y. Koezuka, A. Kikuchi, N. Lapteva, Y. Tanaka, K. Tokunaga, K. Suzuki, N. Kayagaki, H. Yagita, H. Hirai, and T. Juji. 2001. TRAIL expression by activated human CD4(+)V alpha 24NKT cells induces in vitro and in vivo apoptosis of human acute myeloid leukemia cells. *Blood* 97: 2067-2074.
551. Kash, J. C., A. G. Goodman, M. J. Korth, and M. G. Katze. 2006. Hijacking of the host-cell response and translational control during influenza virus infection. *Virus Research* 119: 111-120.
552. Terrier, O., V. Moules, C. Carron, G. Cartet, E. Frobert, M. Yver, A. Traversier, T. Wolff, B. Riteau, N. Naffakh, B. Lina, J.-J. Diaz, and M. Rosa-Calatrava. 2012. The influenza fingerprints: NS1 and M1 proteins contribute to specific host cell ultrastructure signatures upon infection by different influenza A viruses. *Virology* 432: 204-218.
553. Konig, R., S. Stertz, Y. Zhou, A. Inoue, H. H. Hoffmann, S. Bhattacharyya, J. G. Alamares, D. M. Tscherne, M. B. Ortigoza, Y. Liang, Q. Gao, S. E. Andrews, S. Bandyopadhyay, P. De Jesus, B. P. Tu, L. Pache, C. Shih, A. Orth, G. Bonamy, L. Miraglia, T. Ideker, A. Garcia-Sastre, J. A. Young, P. Palese, M. L. Shaw, and S. K. Chanda. 2010. Human host factors required for influenza virus replication. *Nature* 463: 813-817.
554. Wells, M. A., P. Albrecht, S. Daniel, and F. A. Ennis. 1978. Host defense mechanisms against influenza virus: interaction of influenza virus with murine macrophages in vitro. *Infect Immun* 22: 758-762.
555. Rodgers, B. C., and C. A. Mims. 1982. Influenza virus replication in human alveolar macrophages. *J Med Virol* 9: 177-184.
556. Tate, M. D., D. L. Pickett, N. van Rooijen, A. G. Brooks, and P. C. Reading. 2010. Critical role of airway macrophages in modulating disease severity during influenza virus infection of mice. *J Virol* 84: 7569-7580.
557. Perrone, L. A., J. K. Plowden, A. Garcia-Sastre, J. M. Katz, and T. M. Tumpey. 2008. H5N1 and 1918 pandemic influenza virus infection results in early and excessive infiltration of macrophages and neutrophils in the lungs of mice. *PLoS Pathog* 4: e1000115.
558. Yu, W. C., R. W. Chan, J. Wang, E. A. Travanty, J. M. Nicholls, J. S. Peiris, R. J. Mason, and M. C. Chan. 2011. Viral replication and innate host responses in primary human alveolar epithelial cells and alveolar macrophages infected with influenza H5N1 and H1N1 viruses. *J Virol* 85: 6844-6855.
559. Ichinohe, T., I. K. Pang, and A. Iwasaki. 2010. Influenza virus activates inflammasomes via its intracellular M2 ion channel. *Nat Immunol* 11: 404-410.
560. Allen, I. C., M. A. Scull, C. B. Moore, E. K. Holl, E. McElvania-TeKippe, D. J. Taxman, E. H. Guthrie, R. J. Pickles, and J. P. Ting. 2009. The NLRP3

inflammasome mediates in vivo innate immunity to influenza A virus through recognition of viral RNA. *Immunity* 30: 556-565.
561. Bassiri, H., R. Das, and K. E. Nichols. 2013. Invariant NKT cells: Killers and conspirators against cancer. *Oncoimmunology* 2: e27440.
562. Subramanya Hegde, X. C., Jason M. Keaton, Faye Reddington, Gurdyal S. Besra and Jenny E. Gumperz. 2007. NKT cells direct monocytes into a DC differentiation pathway. *Journal of Leukocyte Biology* 81: 1224-1235.
563. Vincent, M. S., D. S. Leslie, J. E. Gumperz, X. Xiong, E. P. Grant, and M. B. Brenner. 2002. CD1-dependent dendritic cell instruction. *Nat Immunol* 3: 1163-1168.
564. Nukada, Y., M. Miyazawa, N. Kosaka, Y. Ito, H. Sakaguchi, and N. Nishiyama. 2008. Production of IL-8 in THP-1 cells following contact allergen stimulation via mitogen-activated protein kinase activation or tumor necrosis factor-alpha production. *J Toxicol Sci* 33: 175-185.
565. Knight, M. J., C. D. Riffkin, A. M. Muscat, D. M. Ashley, and C. J. Hawkins. 2001. Analysis of FasL and TRAIL induced apoptosis pathways in glioma cells. *Oncogene* 20: 5789-5798.
566. Godfrey, D. I., and J. Rossjohn. 2011. New ways to turn on NKT cells. *J Exp Med* 208: 1121-1125.
567. Qui, H. Z., A. T. Hagymasi, S. Bandyopadhyay, M. C. St Rose, R. Ramanarasimhaiah, A. Menoret, R. S. Mittler, S. M. Gordon, S. L. Reiner, A. T. Vella, and A. J. Adler. 2011. CD134 plus CD137 dual costimulation induces Eomesodermin in CD4 T cells to program cytotoxic Th1 differentiation. *J Immunol* 187: 3555-3564.
568. Dumitriu, I. E., P. Baruah, C. J. Finlayson, I. M. Loftus, R. F. Antunes, P. Lim, N. Bunce, and J. C. Kaski. 2012. High levels of costimulatory receptors OX40 and 4-1BB characterize CD4+CD28null T cells in patients with acute coronary syndrome. *Circ Res* 110: 857-869.
569. Sun, M., and P. J. Fink. 2007. A New Class of Reverse Signaling Costimulators Belongs to the TNF Family. *Journal of Immunology* 179: 4307-4312.
570. Shuford, W. W., K. Klussman, D. D. Tritchler, D. T. Loo, J. Chalupny, A. W. Siadak, T. J. Brown, J. Emswiler, H. Raecho, C. P. Larsen, T. C. Pearson, J. A. Ledbetter, A. Aruffo, and R. S. Mittler. 1997. 4-1BB costimulatory signals preferentially induce CD8+ T cell proliferation and lead to the amplification in vivo of cytotoxic T cell responses. *J Exp Med* 186: 47-55.
571. Li, H., Z. Xiang, T. Feng, J. Li, Y. Liu, Y. Fan, Q. Lu, Z. Yin, M. Yu, C. Shen, and W. Tu. 2013. Human V[gamma]9V[delta]2-T cells efficiently kill influenza virus-infected lung alveolar epithelial cells. *Cell Mol Immunol* 10: 159-164.
572. Karin, M., and A. Lin. 2002. NF-kappaB at the crossroads of life and death. *Nat Immunol* 3: 221-227.
573. Cowburn, A. S., J. Deighton, S. R. Walmsley, and E. R. Chilvers. 2004. The survival effect of TNF-alpha in human neutrophils is mediated via NF-kappa B-dependent IL-8 release. *Eur J Immunol* 34: 1733-1743.
574. van den Berg, J. M., S. Weyer, J. J. Weening, D. Roos, and T. W. Kuijpers. 2001. Divergent effects of tumor necrosis factor alpha on apoptosis of human neutrophils. *J Leukoc Biol* 69: 467-473.
575. Kawano, T., J. Cui, Y. Koezuka, I. Toura, Y. Kaneko, H. Sato, E. Kondo, M. Harada, H. Koseki, T. Nakayama, Y. Tanaka, and M. Taniguchi. 1998. Natural killer-like nonspecific tumor cell lysis mediated by specific ligand-activated Valpha14 NKT cells. *Proc Natl Acad Sci U S A* 95: 5690-5693.
576. Nicol, A., M. Nieda, Y. Koezuka, S. Porcelli, K. Suzuki, K. Tadokoro, S. Durrant, and T. Juji. 2000. Human invariant valpha24+ natural killer T cells activated by alpha-galactosylceramide (KRN7000) have cytotoxic anti-tumour activity through mechanisms distinct from T cells and natural killer cells. *Immunology* 99: 229-234.

577. Hoves, S., J. A. Trapani, and I. Voskoboinik. 2010. The battlefield of perforin/granzyme cell death pathways. *J Leukoc Biol* 87: 237-243.
578. Brown, D. M., S. Lee, L. Garcia-Hernandez Mde, and S. L. Swain. 2012. Multifunctional CD4 cells expressing gamma interferon and perforin mediate protection against lethal influenza virus infection. *J Virol* 86: 6792-6803.
579. Leite-de-Moraes, M. C., A. Herbelin, C. Gouarin, Y. Koezuka, E. Schneider, and M. Dy. 2000. Fas/Fas ligand interactions promote activation-induced cell death of NK T lymphocytes. *J Immunol* 165: 4367-4371.
580. Leite-De-Moraes, M. C., A. Hameg, A. Arnould, F. Machavoine, Y. Koezuka, E. Schneider, A. Herbelin, and M. Dy. 1999. A distinct IL-18-induced pathway to fully activate NK T lymphocytes independently from TCR engagement. *J Immunol* 163: 5871-5876.
581. Vinay, D. S., B. K. Choi, J. S. Bae, W. Y. Kim, B. M. Gebhardt, and B. S. Kwon. 2004. CD137-deficient mice have reduced NK/NKT cell numbers and function, are resistant to lipopolysaccharide-induced shock syndromes, and have lower IL-4 responses. *J Immunol* 173: 4218-4229.
582. De Keersmaecker, B., C. Heirman, J. Corthals, C. Empsen, L. A. van Grunsven, S. D. Allard, J. Pen, P. Lacor, K. Thielemans, and J. L. Aerts. 2011. The combination of 4-1BBL and CD40L strongly enhances the capacity of dendritic cells to stimulate HIV-specific T cell responses. *J Leukoc Biol* 89: 989-999.
583. Kim, D. K., S. C. Lee, and H. W. Lee. 2009. CD137 ligand-mediated reverse signals increase cell viability and cytokine expression in murine myeloid cells: involvement of mTOR/p70S6 kinase and Akt. *Eur J Immunol* 39: 2617-2628.
584. Guicciardi, M. E., and G. J. Gores. 2009. Life and death by death receptors. *FASEB J* 23: 1625-1637.
585. LeBlanc, H. N., and A. Ashkenazi. 0000. Apo2L//TRAIL and its death and decoy receptors. *Cell Death Differ* 10: 66-75.
586. Fleischer, J., E. Soeth, N. Reiling, E. Grage-Griebenow, H. D. Flad, and M. Ernst. 1996. Differential expression and function of CD80 (B7-1) and CD86 (B7-2) on human peripheral blood monocytes. *Immunology* 89: 592-598.
587. Sharma, R. K., R. H. Schabowsky, A. K. Srivastava, K. G. Elpek, S. Madireddi, H. Zhao, Z. Zhong, R. W. Miller, K. J. Macleod, E. S. Yolcu, and H. Shirwan. 2010. 4-1BB ligand as an effective multifunctional immunomodulator and antigen delivery vehicle for the development of therapeutic cancer vaccines. *Cancer Res* 70: 3945-3954.
588. Solov'ev, V. D. 1969. The results of controlled observations on the prophylaxis of influenza with interferon. *Bull World Health Organ* 41: 683-688.
589. Barral, P., P. Polzella, A. Bruckbauer, N. van Rooijen, G. S. Besra, V. Cerundolo, and F. D. Batista. 2010. CD169(+) macrophages present lipid antigens to mediate early activation of iNKT cells in lymph nodes. *Nat Immunol* 11: 303-312.
590. Barral, P., M. D. Sanchez-Nino, N. van Rooijen, V. Cerundolo, and F. D. Batista. 2012. The location of splenic NKT cells favours their rapid activation by blood-borne antigen. *EMBO J* 31: 2378-2390.
591. Pilones, K. A., J. Aryankalayil, and S. Demaria. 2012. Invariant NKT cells as novel targets for immunotherapy in solid tumors. *Clin Dev Immunol* 2012: 720803.
592. Boorsma, C. E., C. Draijer, and B. N. Melgert. 2013. Macrophage heterogeneity in respiratory diseases. *Mediators Inflamm* 2013: 769214.
593. Mercalli, A., I. Calavita, E. Dugnani, A. Citro, E. Cantarelli, R. Nano, R. Melzi, P. Maffi, A. Secchi, V. Sordi, and L. Piemonti. 2013. Rapamycin unbalances the polarization of human macrophages to M1. *Immunology* 140: 179-190.